Coronaries,
X - ray imaged,
clinical development

Corstiaan Johannes Storm

De promotiecommissie:

voorzitter en secretaris:

Prof.dr.ir. A.J. Mouthaan	Universiteit Twente

promotor:

Prof.dr.ir. C.H. Slump	Universiteit Twente

leden:

Prof.dr.ir. P.H. Veltink	Universiteit Twente
Prof.dr. E. Marani	Universiteit Twente
Prof.dr.ir. M. Breeuwer	TU Eindhoven & Philips Medical Systems
Prof.dr. E.E. van der Wall	Universiteit Leiden
Prof.dr. L. Schultze Kool	Radboud Universiteit, Nijmegen

Signals & Systems group, Enschede, the Netherlands

Printed by Gildeprint B.V., Enschede, The Netherlands
Typesetting: LaTeX2e
Cover design by Dirk-Jan Kroon

ISBN 978-90-365-3034-7
DOI 10.39901.9789036530347

CORONARIES,
X - RAY IMAGED,
CLINICAL DEVELOPMENT

PROEFSCHRIFT

ter verkrijging van
de graad van doctor aan de Universiteit Twente,
op gezag van de rector magnificus,
prof.dr. H. Brinksma,
volgens besluit van het College voor Promoties
in het openbaar te verdedigen
op donderdag 28 oktober 2010 om 16.45 uur

door

Corstiaan Johannes Storm
geboren op 29 augustus 1942
te Monster

Dit proefschrift is goedgekeurd door de promotor:

Prof.dr.ir. C.H. Slump

Nec scire fas est omnia

Contents

Chapter 1

Preface

The first part of this thesis (*i.e.* Chapters 1 - 8) describes the history of the imaging of coronary arteries, including technical developments in X-ray diagnostic imaging equipment, contrast agents and the possibility of introducing catheters in living persons without serious complications. This thesis has its origins in the clinical practice of my work as a cardiologist and has started many years ago. At that time coronary angiography consisted of filming the coronary arteries on 35 mm cine film at 25 images per second. The diagnosis of the state of the patient's coronary arteries was then performed by viewing the developed film in a film projector. In a discussion with Dr. Reiber, at that time head of the cardiac imaging laboratory at Erasmus University in Rotterdam, who happened to be my tablemate during a dinner at a conference, we analyzed the clinical problem of evaluating the seriousness of a stenose in a coronary artery as seen on analogue film (coronary angiogram) and the clinical impact of such a stenose. This discussion led to a series of experiments concerning cardiac (coronary) imaging that are described in the second part of this thesis.

As time progressed, it became possible to digitize the projected film images. The first question that needed answering was: is it possible, after digitizing the coronary images, to obtain a more reliable calculation (less humanly dependent and thus more objective) of the stenose as viewed and of its impact? Commercial software became available, and experiments were set up (reported in Chapter 8). These involved using digital images after digitizing the analogue film and later on utilizing these images to make calculations (Philips Medical Systems in Best). After the introduction by Philips of Digital Cardiac Imaging (DCI) it was technically possible to have direct access to X-ray images in digital format. This led to a series of experiments with a flow model to imitate laminar and pulsatile (physiologic) flow, mimicking the first part of a left coronary artery. The reproducibility of frequent calculations of the mimicked artery under different X-ray conditions is described

in Chapter 7. The conclusion is that computer-assisted measurement of the stenose parameters (percentage area occlusion and length of the stenose) is not fully reliable but still better than human observation. The answer to the first part of the research question is thus somewhat negative. In Chapter 9 the investigation is continued, aiming at the three-dimensional reconstruction of stenosed coronary artery segments. From the 3D-shape obtained the flow impedance can be computed. So the intention was to calculate the flow impedance based on the reconstructed geometry, to get a better measure of the real flow state of the artery than the stenose parameters provide.

To get more useful information regarding the clinical significance of a stenose, many of the experiments in this thesis required customized software or newly developed image processing software. At first the experiments were performed on models of coronary arteries. Later on, they also involved testing of clinical patient image data. The results of the calculations based on digital images were always compared in clinical settings to the results acquired by other accepted methods, such as intravascular Doppler measurements or nuclear medicine calculations. However, these latter methods are always more time-consuming and more expensive. All experiments and clinical testing were done in a normal catheterization laboratory.

Flow in the coronaries is regulated by the pre-arterioles. As such, the coronary flow reserve is clinically much more relevant than the flow resistance of a mild stenose. Only when the pre-arterioles are fully open (as during physical exertion) will the flow be limited by the stenose. The following chapter investigates if it is possible to measure the elasticity of the coronary vessels from standard coronary angiograms. A healthy vessel expands slightly due to the pressure wave generated by the contracting left ventricle. The dilation is small and cannot be visually assessed, also due to the motion of the arteries. The idea (described in Chapter 10) was to discriminate between dilating and non-dilating vessels, thus between those that are healthy and those possibly stiff due to arteriosclerosis. It turned out that vessel distensibility was also hard to measure by computer means.

The research goal became in fact to obtain information about the coronary flow reserve. The approach reported in the literature by Vogel et al. was too complicated and time-consuming for application in clinical routine, since the patient would have to be paced and ECG-triggered X-ray acquisition would be required due to the image subtraction technique. However, sometimes there is a need for information provided by the flow reserve, especially when no major vessel anomalies are observed. This has been the research drive in the years that followed, as revealed in Chapters 11 - 14. Several calculation models, some imitating the physiologic coronary flow patterns, are described to gain a better understanding of the physiologic importance of a coronary stenose. Various programs compute densitometric flow distribution, pulse

propagation and relative flow distribution. Some of these programs are used in a clinical setting and are compared with intracoronary Doppler measurements and/or nuclear medicine imaging techniques.

Chapters 15 and 16 describe, firstly, the clinical relevance of densitometric calculations of myocardial perfusion when the nurturing coronary artery has a mild stenose and, secondly, the possibility to use an automatic region detection program to calculate flow reserve in that area. Lastly, Chapter 17 presents some thoughts on possible directions in the diagnostics of coronary artery disease and on invasive therapies of this clinical syndrome, with special attention to the radiation burden.

Chapter 2

Introduction

Angina pectoris, the Greek - Latin expression for chest discomfort and or chest pain often caused by physical exercise, is a clinical diagnosis known since more than two centuries and has turned out to be based on coronary vascular imbalance. This symptom of ischemic heart disease, a multifactorial cause, as shown in Figure 2.1, has an enormous impact on the human existence. Ischaemic heart disease is to this day the leading cause of mor-

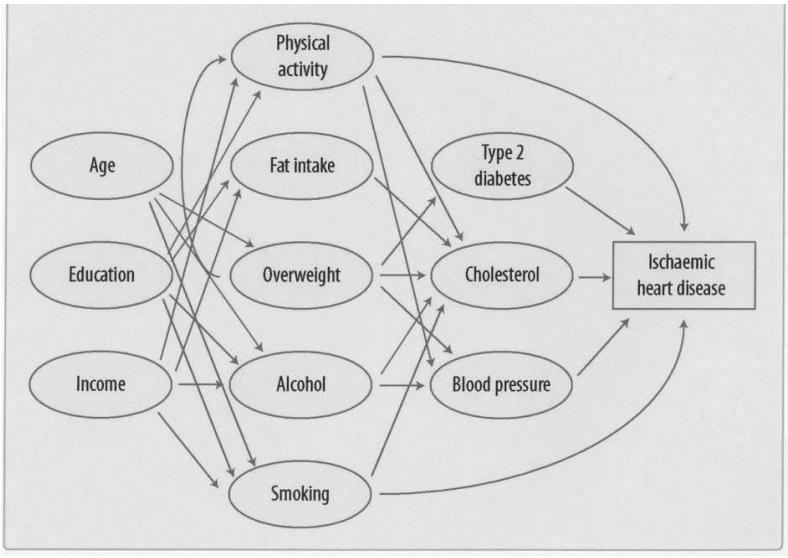

Figure 2.1: Causes of ischaemic heart disease from Global Health Risks (WHO 2009 [1]).

bidity and mortality in the Western world, with major consequences, both social and economic. Worldwide more than $54 billion was spent on cardiac care therapeutics in 1999, with an expected 10% annual increase for the ensuing 10 to 15 years [2]. At the moment coronary heart disease and its

consequences are still the most frequent cause of morbidity and mortality worldwide, accounting for almost 30% of a total of 58 million deaths [3] per year. Remarkable in the statistics for deaths due to coronary heart disease are the differences in socio-economic status of the individual countries in terms of income: for countries with high, middle and low incomes the numbers are 10.8%, 13.4% and 17.1% respectively. In 2004, 7.2 million persons [4] died of coronary heart disease. Although there is some decline in percentage terms, the numbers of cardiac deaths and hospital admissions are still very impressive. In the Netherlands in 2005, more than 40,000 people, or 35% of the total number of deaths, died of a cardiovascular cause, and more than 300,000 people were admitted to hospitals because of infarction and/or heart failure (Dutch Heart Foundation, 2005).

The term angina pectoris was introduced in medicine by William Heberden [5] in 1772.

William Heberden was born in London in 1710 and died in 1801 in Windsor. He commenced his studies in Cambridge and London. After qualification as a Doctor of Physics he worked as a physician and lecturer on materia medica in Cambridge for ten years before moving to London in 1748. Heberden became a fellow of the Royal College of Physicians and the Royal Society of London. Throughout his life as a physician he maintained his habit of taking down notes in Latin of anamnesis and status findings in connection with his examinations of patients. At the end of every month he analysed his observations in an attempt to draw conclusions from his recorded clinical observations. He spent the last twenty years of his life putting his notes in order and editing them for his "Commentaries on the History and Cure of Diseases", written in Latin and later translated into English by his son William Heberden the Younger (1767-1845). The first edition of this book was published in 1772 when Heberden was already 62. His most important contributions are his delineations of several disorders that are well recognised today, including angina pectoris and night blindness.
From: `www.whonamedit.com`

The definition Heberden gave to this clinical entity was: "*There is a disorder of the breast marked with strong and peculiar symptoms considerable for the kind of danger belonging to it, and not extremely rare, of which I do not recollect any mention among medical authors. The seat of it, and sense of strangling and anxiety, with which it is attended, may make it not improperly be called angina pectoris. Those, who are affected with it, are seized while they are walking, and most particularly when they walk soon after eating, with a painful and most disagreeable sensation in the breast, which seems as if it would take their lives away, if it were to increase or to continue; the moment they stand still, all this uneasiness vanishes.*" The description of this clinical entity is still correct at the present time. In 1799 Parry [6] described the pathological substrate of this clinical entity as an imbalance between supply and demand of oxygen in the heart.

Caleb Hillier Parry was born in 1755 in Gloucestershire and died in 1822 in Bath. In 1773 he went to Edinburgh to study medicine. In 1778 he obtained his medical doctorate with a thesis on rabies. The same year he became a licentiate of the College of Physicians of London. In 1779 he commenced a general practice in Bath. As a physician Parry excelled as physiologist and skilled experimenter. His major contribution to medicine was the recognition of the cause of angina pectoris. He conducted a series of experiments on sheep to investigate the circulation and the effects of impairment of the vascular supply. He was the first to suggest the correct mechanism although his explanation was ignored for more than a century. His book "An Inquiry into the Symptoms and Causes of Syncope Anginosa" was based in part upon lectures he had given to the Gloucestershire Medical Society. In it he expounded the concept that ischaemic heart disease resulted from energy demands of the myocardium, which the vascular system was unable to supply. In 1816 Parry suffered a stroke, which left him with aphasia and progressive paralysis.
From: `www.whonamedit.com`

His description was as follows: "*The rigidity of the coronary arteries may act, proportionally to the extent of the ossification, as a mechanical impediment to the free motion of the heart; and though a quantity of blood may circulate through the arteries, sufficient to nourish the heart, yet there may probably be less than what is requisite for ready and vigorous action. Hence, though a heart so diseased may be fit for the purpose of common circulation, during a state of bodily and mental tranquillity, and of health otherwise good, yet when any unusual exertion is required, its powers fail, under new and extraordinary demand*." After the Parry publication it took a long time before a new publication appeared that dealt with the symptom of angina pectoris, probably because of the rarity of this clinical entity at that time. In 1892 Osler [7] described this clinical entity in his textbook as a disease state leading to death.

Sir William Osler was born in 1849 in Bond Head, Tecumseh, West Canada, and died in 1919 in Oxford, England. William was intended for the church like his father. However, he started to study arts, entered medical school in 1868 and took his degree in 1872. During the following two years he visited medical centers in London, Berlin and Vienna. Osler returned to Canada and started a general practices. Soon, however, he was appointed lecturer at McGill University, becoming professor there in 1875. There he taught physiology, pathology and medicine. In 1888 Osler accepted an invitation to be the first professor of medicine at the new Johns Hopkins University Medical School in Baltimore, where he established himself as the most outstanding medical educator of his time. In Baltimore he transformed, together with three other doctors, the medical organization and the teaching curriculum. At that time he wrote "The Principles and Practice of Medicine", which was first published in 1892, soon becoming the most popular textbook of that time. In 1905 Osler he was invited to the Regius Chair of Medicine at Oxford University, at that time the most prestigious medical appointment in the English-speaking world. William Osler died following bronchopneumonia and empyema on December 29, 1919.
From: `www.medicalarchives.jhmi.edu/osler/biography.htm`

White [8] investigated this topic in the early 1900s, although at that time this clinical entity was quite rare or not often recognised.

Paul Dudley White was born in 1886 in Roxbury, Massachusetts and died in 1973. He studied medicine at Harvard University and graduated in 1911. The death of his sister from rheumatic fever determined his interest in cardiology. He spent a year at the University College of London to study electrocardiography with Thomas Lewis. In 1919 he returned to the Massachusetts General Hospital to establish a cardiac unit. There he became professor of medicine and wrote his classical monograph "Heart Diseases", first published in 1931. White emphasized the importance of prevention of coronary disease, strongly advocating fitness and exercise (cycling) in aiding its prevention. The 17-mile Dr. Paul Dudley White Bike Path in the Boston-Brookline area is named after him.
From: `www.whonamedit.com`

Joseph Treloar Wearn, American physician (1893-1984) [9] was the first in 1923 in describing a disease state called instable angina pectoris as a stadium which could result in heart attack. The rapid extension of knowledge in the first half of the past century about heart function and disease gave birth to a new specialism: cardiology. This specialization resulted in an extra acceleration of knowledge in recognizing cardiac symptoms as important and life-threatening. The key factor in this acceleration of knowledge was the discovery and introduction of new diagnostic clinical tools, firstly the discovery of the electrocardiogram by Einthoven [10] in 1903, and led to the rapid development of non-invasive diagnosis of heart disease such as infarctions and rhythm disturbances.

Willem Einthoven, who lived from 1860 (Semarang, Indonesia) until 1927 (Leiden), studied medicine at Utrecht University. There he was influenced by the physicist Buys-Ballot, the anatomist Koster and the ophthalmologists Snellen and Donders. In 1885 he was appointed professor at Leiden University. In 1895 Einthoven saw the work of Waller, the first to succeed in the registration of electrical currents of the heart. Einthoven repeated these investigations in 1895 using a capillary electrometer. After the development of photographic equipment, he made graphic reproductions of the electric charges induced by the contractions of the heart and sounds. Einthoven defined the constants and calculated the true curve: the electrocardiogram. In 1901 he invented a new galvanometer for producing electrocardiograms using a fine quartz string: the string galvanometer. This was an improvement over the capillary galvanometer because of the possibility to regulate the meter within broad limits; this meter was much more sensitive. In 1902 Einthoven published the first electrocardiogram made with the string galvanometer. In 1912 he developed the scheme of the equilateral triangle, considering the extremities as elongations of the electrodes. With simultaneous registration of the three contacts, the size and the direction of the resultant of the potential differences in the heart could be calculated directly. In 1924 Einthoven was awarded the Nobel Prize for physiology or medicine for his discovery of the mechanism of the electrocardiogram.
From: `www.nobelprize.org/nobel_prizes/medicine/laureates/1924`

A second major breakthrough was the discovery of X-rays by Röntgen in 1895. This technique made it possible to image organs and organ systems in living persons to diagnose disorders. The combination of these two important discoveries - the electrocardiogram (ECG) and X-rays - and their recognition as useful clinical tools made cardiology develop fast into an important new specialism, stimulating the development of new diagnostics and therapies.

Wilhelm Conrad Röntgen, born in 1845 in Lennep and died in 1923 in Munich, was educated as physicist at Utrecht University and in Zurich. He was appointed professor at Würzburg University, where he made his most important contribution: the discovery of the X (which stands for unknown) rays on November 8, 1895. Because of this important discovery he was awarded the first Nobel prize in physics.
From: `www.wikipedia.org`

The introduction in medicine in the 1960s of digital computers (making use of transistors, integrated circuits and microprocessors) was another enormous impulse in extending diagnostics in cardiology. It led to the possibility to compute all kinds of functions, including (physiological) function calculations and images of the heart, both invasive catheterisation and non-invasive cardiac functions. Technical improvements of diagnostic vascular imaging devices, resulting in sharper pictures of heart vessels, made cardiology grow into an important specialism, opening the possibility to intervene in living persons to solve intravascular and other cardiac problems that cause angina pectoris. Intervention started initially by applying bypass surgery techniques, but since the 1980s less invasive intervention methods are applied such the balloon catheter, which was introduced in medicine by Dotter. This technique was later also introduced in cardiology by the Swiss cardiologist Andreas Grüntzig. Today it is the most common intervention technique to solve coronary problems causing angina pectoris or infarction.

Charles Theodore Dotter, who lived from 1920 until 1985, attended medical school at Cornell. In 1952 he took the position of professor and chairman of the Department of Radiology at the University of Oregon Medical School, where he remained for 32 years. During those years he developed an entirely new medical specialism, namely intervention radiology, which provided an alternative to surgery. In 1964 Dotter introduced transluminal angioplasty and also intravascular coils, the forerunner of the modern expandable stents. In 1978 Dotter was nominated for the Nobel Prize in Medicine. From: `www.pubmedcentral.nih.gov`.

Nowadays it is often easy for a physician to establish the diagnosis of angina pectoris by means of angiography, with little risk for the patient. However, it took a long period of time starting in the early 1900s and much effort to reach this point. This thesis analyzes the history of the development of invasive diagnostics of the clinical syndrome angina pectoris, based on pathological vessel problems (intravascular stenosis of the coronary arteries), via the evolution of technical possibilities in diagnostics, including contrast agents, to the way invasive cardiac problem handling is carried out at present. Anatomical X-ray images of the coronary arteries reveal only to some extent the cause of the clinical problem, because these images do not give functional or metabolic information about the myocardium in the area supplied by that specific, sometimes anatomic, abnormal coronary artery. This may lead to a wrong decision as to the kind of intervention that should be performed to relieve the cause of the clinical problem experienced as angina pectoris. Using modern possibilities, especially in the field of com-

puter technology, we have tried to develop algorithms to calculate, from a standard coronary angiogram, the real intra-coronary and extra-coronary (functional) myocardial tissue blood flow without the use of specially developed equipment, such as Doppler catheters. By using these newly developed and or adapted algorithms, it should be possible to make a more reliable and realistic decision in solving the clinical problem. That problem is: how important are stenoses or abnormal coronary arteries as seen on a coronary angiogram functionally, and what to propose in terms of intervention (Coronary Bypass Grafting or Percutaneous Coronary Intervention), or wait and see. All with the goal of achieving a better outcome for the patient and enhancing the patient's quality of life.

References

[1] *Global Health Risks. Mortality and burden of diseases attributable to selected major risks,* WHO 2009.

[2] *Trends in the Early Diagnosis of Cardiovascular Disease: Worldwide Market Opportunities*, Kalorama Information, KL1450532, October 1, 2001.

[3] *Preventing chronic diseases: a vital investment*, World Health Organization, Geneva, 2005.

[4] *Cardiovascular Disease, Fact sheet no. 317*, World Health Organization, Geneva, September 2009

[5] W. Heberden, "Some account of a disorder of the breast," *Med. Trans. Coll. Physicians (London)* 2, p. 59, 1772.

[6] C.H. Parry, *An inquiry into symptoms and causes of the syncope anginosa, commonly called angina pectoris, illustrated by dissections*, London, Cadwell and Davis, 1799.

[7] W. Osler, *The Principles and Practice of Medicine*, Appleton, New York, 1892.

[8] P.D. White, "The Prevalence of Coronary Heart Disease," in *Symposion on Coronary Heart Disease*, H.I. Blumgart, ed., American Heart Association, New York, 1968.

[9] J.T. Wearn, "Thrombosis of the coronary arteries, with infarction of the heart," *American Journal of the Medical Sciences* 165, p. 250, 1923.

[10] W. Einthoven, "Ein neues Galvanometer," *Annalen der Physik* 12, p. 1059, 1903.

Chapter 3

Coronary system: anatomy and coronary angiography

The coronary arteries are developed in an early embryonic phase: 42 days [1] after conception by anastomosis of the plexus arteriosus and two buds of the truncus arteriosus in the foetus to form the right and left coronary artery [2], see Figure 3.1.

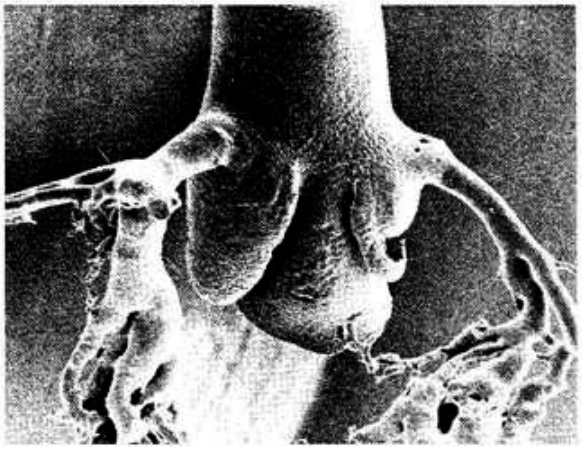

Figure 3.1: Cast of the embryonic aorta, showing the coronary arteries sprouting from the aortic sinuses. From: [3].

The right coronary artery normally has its origin in the right sinus Valsalva. The dimension of the ostium in the adult human is 2.4 $\pm$ 0.9 mm $\times$ 3.7 $\pm$ 1.1 mm.

Antonio Maria Valsalva, who born in 1666 in Imola and died in 1723 in Bologna, was an Italian anatomist with an interest in the anatomy of the ears, but he had described the sinuses of the aorta in his writings, which were published posthumously in 1740. Valsalva was educated in humanities, mathematics and natural sciences before he started to study medicine and philosophy in Bologna. He graduated in 1687 from the medical school and he was appointed professor of anatomy at Bologna in 1705. Valsalva taught in the fields of science, surgery, anatomy, physiology and psychiatry. His complete writings were published in 1740 by Giovanni Battista Morgagni. From: `www.en.wikipedia.org/wiki/Antonio_Maria_Valsalva`

The left coronary artery has its origin in the left sinus Valsalva. Because of the oblique plane of the aortic valves, the ostium is situated slightly above the plane of the right coronary artery ostium. The dimension of this ostium is 4.7 ± 1.2 mm $\times$ 3.2 ± 1.1 mm. The supply area of each artery can differ among humans and is named by the dominant artery: right dominant when the right coronary artery supplies the ramus descendens posterior, left dominant when the left coronary artery supplies the ramus descendens posterior and balanced when both arteries supply the ramus descendens posterior. This artery supplies the lower part of the interventricular septum and the diaphragmatic part of the left ventricle. This subdivision is based on radiological appearance by angiography, see Figure 3.2, introduced by Schlesinger in 1940 [5]. In his original series the right coronary artery was dominant in

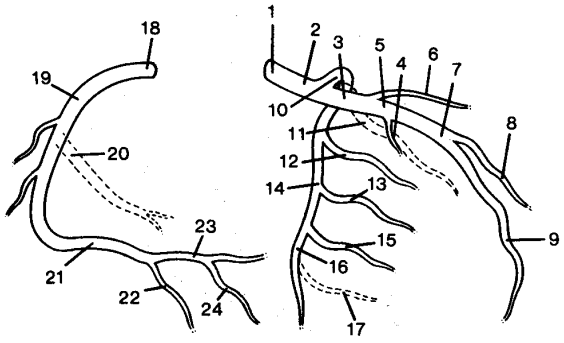

Figure 3.2: Diagram of the coronary circulation. 1, 2 left main; 3, 5, 7, 9 left descending artery; 6, 8 diagonal branches; 4 septal branch; 10, 14, 16 circumflex artery; 11 ramus intermedius; 12, 13, 15 posterolateral branches; 18, 19, 20, 21, 23 right coronary artery; 20 right ventricular branch; 22 posterior descending branch of the right coronary artery; 24 left ventricular branch of the right coronary artery. From: [4].

45% of all cases, right and left were balanced in 34% and left was dominant in 18%. In other newer series the right coronary artery is dominant in 80-90% of the cases, in half to two third of the remaining part (10-20%) the left coronary artery is dominant, *i.e.* the ramus descendens posterior artery arises from the

circumflex artery. A balanced system is a system in which both the right coronary artery and the circumflex artery supply the inferior part of the septum, and where the diaphragmatic part of the left ventricle is seen in half to one third of the cases. Normally, the left coronary artery is the largest artery. This artery is subdivided into three parts: left main, no side branches, with an average length of 6-15 mm. Sometimes, however, there is no left main because of a double ostium based upon a separate ostium of the LAD and the RCX. In two third of humans the left main divides into two separate arteries at the bifurcation: a left descending artery (ramus interventricularis anterior) and a circumflex artery (ramus circumflexus). In one third of humans there is a division into three branches, called trifurcation. These arteries are named the left anterior descending (LAD), the ramus circumflexus (RCX) and the intermediate artery (ramus intermedius). The side branches of the LAD are called diagonals; they are important blood suppliers of the intraventricular septum. The side branches of the RCX are called posterolaterals. The right coronary artery is a single vessel; the side branches are the important sinus node artery and sometimes one or two large right ventricle branches. One of these, the atrio ventricular node artery, supplies the atrio ventricular node.

Many anomalies are known of the right as well as of the left coronary artery. In the human heart both arteries communicate distally by very small vessels (anastomoses) [6] with a diameter of 50-200 μm. Normally these anastomoses are not in use. However, when there are obstructions (stenoses) in the right or left coronary artery, these anastomoses open, giving rise to retrograde filling of the obstructed artery. These intravascular obstructions and other cardiac problems are nearly always caused by changes of the inner lining of the coronary arteries (which are epicardial vessels); the obstruction occurs progressively over time. This mostly eccentric narrowing due to intravascular plaque forming [7] causes flow obstruction in the affected artery. However, the obstruction becomes critical only in clinical terms, when more than 75% [13] lumen narrowing is reached. Only the epicardial (great) vessels are affected by this degenerative process, but not the small vessels (arteriolae).

This progressive process of narrowing over time was first made visible after introduction of coronary arteriography by means of catheterization of the coronary system, first in post mortem studies, 1907 by Jamin and Merkel [9]. Later it was also demonstrated in living persons. The first report about the possibility to catheterize the heart goes back to the year 1844, when the French physiologist Claude Bernard performed this in a living horse. Following this first successful procedure, many animal studies were done by a number of researchers. These experiments formed the basis of a new era in medicine in which much research was started to investigate the working of the circulation system by means of such catheterizations. In 1929

Forssmann [10] performed the first documented venous catheterization in a human person by using an urine catheter, introduced via his own vena brachialis, to enter the right side of the heart. This event was registered by an X-ray image. Arterial catheterization was introduced by Ichikara (1938) [11] and Fariñas (1941) [12] using a cut down of the arteria femoralis. The first report on a selective left-sided heart catheterization was by Zimmerman (1950) [13]. This report served as evidence of the possibility to catheterize the left heart side in living humans. Introduction of the percutaneous needle technique (femoral artery) by Seldinger (1953) [14], in combination with the rapid development of imaging techniques, new types of catheters and improvements of less toxic contrast agents, has resulted in better image quality and lower incidence of side effects. These developments caused enormous advances in the progression of knowledge concerning coronary heart disease and diagnostic possibilities. The first in vivo images of coronary arteries were published by Rousthöi [15] in 1933 in an animal study, the first images of coronary arteries in living humans were published by Radner [16] in 1944. Radner made images of the coronary vessels by injecting a bolus of contrast just above the aortic valve. He could thus visualize the aortic root, the ostia of the right and left coronary arteries and the first parts of the coronary arteries. This procedure was done by direct punction of the aortic arch. The images were vague and difficult to analyze, partly because of the inadequate X-ray technology and partly because of the feeble contrast agents available at that time. For that reason several other methods were developed to improve the image quality:

- Injection of a big bolus with a high flow rate of 50-100 cc contrast in 3-5 sec.
- ECG-triggered injection of contrast in diastole giving less movement of the heart and better visualization of the coronaries, Richards (1958) [17].
- Pharmacological interventions: intravenous acetylcholine injection by Arnulf (1958) [18] resulting in a short asystole at the time contrast was injected. This technique and procedure required general anaesthesia, making the procedure extra complicated.
- In 1961 Gensini [19] made some modifications to the Arnulf technique.
- Dotter and Frische [20] introduced the double lumen catheter technique (1961). This made it possible to block the aorta just above the valve with a big balloon and to inject the contrast via the other lumen of the catheter, filling the space between the aortic valve and the balloon. This technique resulted in reasonable visualization of both ostia and the first part of the left and right coronary arteries.

- Boerema and Bliekman [21] introduced the method of intrabronchial pressure elevation (1955) by the Vasalva maneuver, normally under general anesthesia, resulting in a slowdown of the blood flow. This enabled better filling of the coronary arteries when the contrast bolus was given just above the aortic valves.

- Bellman (1961) [22] introduced a semi-selective method by using modified catheters, in which the lumen of the catheter was directed towards the right or left coronary ostium, resulting a much better image of that coronary artery.

- Sones (1959/1960) [23] was the first to publish images of direct injections in the ostium of the coronaries of the human person with catheters that he had personally developed and made.

The introduction of the Sones technique and catheters, see Figure 3.3, resulted in an enormous increase of heart catheterisation procedures worldwide. It was the starting point of a new era of diagnostics in coronary heart disease, followed by new therapeutic options such as coronary bypass grafting and percutaneous interventions.

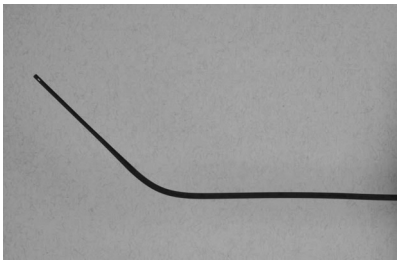

Figure 3.3: Example of a Sones catheter.

The Sones procedure of introducing the catheter into the arterial system was done via a cut down off the arteria brachialis in the right or left arm. This arteria brachialis is a relatively small vessel that causes many complications based on vascular and or neural damage during the procedure or shortly afterwards. In 1967 Judkins [24] introduced a new technique, the direct puncture of the arteria femoralis, a much bigger vessel compared with the arteria brachialis, resulting in fewer complications. This Judkins method has become the catheter introducing technique that is used most worldwide; in experienced hands the complications are rare. Since the start of the Judkins technique, several types of introducing systems and catheters with a variety in diameter from 4 to 8 French (1Fr = 0.33 mm) with different curve shapes have been developed and are available on the market, see Figure 3.4. Also the

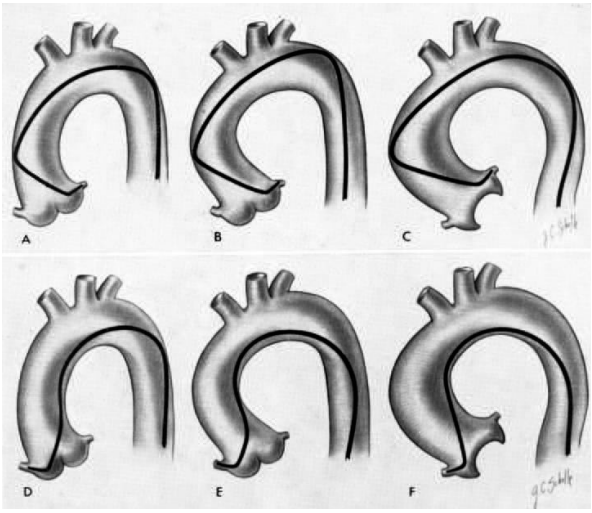

Figure 3.4: Various models of the right and left coronary catheters positioned in right and left coronary ostium.

catheter material itself has been improved, resulting in better torque and maneuvering. For the patient who is suspected to have coronary insufficiency, all these modifications have made the direct catheterization of the coronary vessels a routine procedure with an acceptably low risk compared with the cut-down method of the arteria brachialis. The risk of a catheterisation procedure can consist of bleeding around the puncture location, but there are also major problems: malignant rhythm disturbances and even death. However, the overall percentage is a very low 0.1% [25]. An exception to this number are patients with an important left main stenose: 3.6% [26]. This means that coronary angiography must be done by experienced hands, and only when there is a real indication for such a diagnostic procedure.

Claude Bernard, French physiologist, lived from 1813 (Saint Julien near Villefranche-sur-Saône) until 1878 (Paris). He received his early education in a Jesuit school. He started as a play writer but a critic advised him to study medicine for a living. During his medical studies he met the great French physiologist François Magendie, who asked him to work in his laboratory as "preparateur". In this laboratory Bernard discovered his real vocation: physiological experimentation. From Magendie, Bernard learned vivisection as principal means of medical research. His most important work was on the function of the pancreas gland and the glycogenic function of the liver, which threw light on diabetes mellitus. Another important work was the discovery of vaso-motor functions. Bernard is furthermore known for his work on homeostasis. In 1854 the French government created a chair for him at the Faculty of Sciences. In 1855, after the death of Magendie, Bernard succeeded him as a professor at the Collège de France. In 1861 he became a member of the Académie de Medicine. From: `www.whonamedit.com`

Werner Theodor Otto Forssmann, born in 1904 in Berlin and died in 1979 in Schopfheim, graduated from the medical faculty of Friedrich-Wilhelm University in Berlin in 1929. That same year he went to the Auguste-Victoria clinic in Eberswalde for clinical instruction in surgery. Here he did the first self-catheterization via an arm vein. His publication in 1929 and his oral presentation in 1931 received hardly any recognition, however. Afterwards he worked in several hospitals in training for urologist. In 1956 he was awarded, together with André Cournand and Dickinson W. Richards, the Nobel prize for Physiology and Medicine. The same year he was appointed Honorary Professor of Surgery and Urology at the Johannes Gutenberg University, Mainz. From: `www.nobelprize.org/nobel_prizes/medicine/laureates/1956`

Sven-Ivar Seldinger (1921-1998) graduated in 1948 from the Karolinska Institute in Stockholm. After a short period of deputyships at a surgical department, he started training in radiology in 1950. Two years later he developed the Seldinger method: needle in, wire in, needle off, catheter on wire, catheter advance, wire off. In 1966 he compiled his results in a supplement of Acta Radiologica as his thesis. Subsequently he was appointed associate professor. In 1967 he withdrew from academic life to return to his native city to become chief of the radiology department at a local hospital. From: `www.whonamedit.com`

F. Mason Sones, Jr. (1918-1985) graduated in 1943 from the University of Maryland. In 1950 he joined the Cleveland Clinic Ohio where he served as director of the Cardiac Laboratory. On October 29, 1958 Sones filmed in the basement of the laboratory the first coronary angiogram and demonstrated that the dye could be safely directly into the coronaries without ventricular fibrillation, the great fear at the time. However, ventricular fibrillation frequently occurred with the dyes in use at that time. This problem could be overcome after the introduction of the external defibrillator. This event was the real start of coronary angiography in the medical world. From: `www.pubmedcentral.nih.gov`

References

[1] L.H.S. van Mierop, "Embryology of the Heart," in *The CIBA Collection of Medical Illustrations*, F.H. Netter, vol. 5, pt I, p. 112, CIBA Pharmaceutical Co., Summit, N.J., 1969.

[2] R. Walmsley and H. Watson, *Clinical Anatomy of the Heart*, Churchill Livingstone, New York, 1978.

[3] E. Aikawa and J. Kawano, "Formation of coronary arteries sprouting from the primitive aortic sinus wall of the chick embryo," *Experientia* 38, pp. 816-818, 1982.

[4] S.B. King III and J.S. Douglas, *Coronary arteriography and angioplasty*, McGraw-Hill, New York, 1985.

[5] M.J. Schlesinger, "Relation of anatomic pattern to pathologic conditions of the coronary arteries," *Arch. Path.* 30, pp. 403-415, 1940.

[6] W.J. Pepler and B.J. Meyer, "Intra-arterial Coronary Anastomoses and Coronary Arterial Pattern," *Circulation* 22, pp. 14-24, 1960.

[7] R. Ross and J.A. Blomset, "The Pathogenesis of Atherosclerosis," *N. Eng. J. Med.* 295, p. 369, 1976.

[13] C.W. White, C.B. Wright, D.B. Doty et al., "Does Visual Interpretation of the Coronary Arteriogram Predict the Physiologic Importance of Coronary Stenosis?," *N.Eng. J.Med.* 310, p. 819, 1984.

[9] F. Jamin and H. Merkel, *Die Koronararterien des menschlichen Herzens unter normalen und pathologischen Verhältnissen*, Gustave Fischer, Jena, 1907.

[10] W. Forssmann, "Die Sondierung des rechten Herzens," *Klin. Wschr.*, 2, p. 2085, 1929.

[11] T. Ichikara, "Schatten der Nierarterie (I). Meine Methode zur röntgenologischen Darstellung der Nierenarterie," *Zschr. Urol.* 3, p. 563, 1938.

[12] P.L. Fariñas, "A new technique for arteriographic examination of the abdominal aorta and its branches," *Am. J. Roentgennol.* 46, pp. 641-645, 1941.

[13] H.A. Zimmerman, H.W. Scott and N.D. Becker, "Catherization of the left side of the heart in man," *Circulation* 1, p. 357, 1950.

[14] S.I. Seldinger, "Catheter replacement of the needle in percutaneous arteriography: a new technique," *Acta Radiologica* 39, p. 368, 1953.

[15] P. Rousthöi, "Über Angiokardiographie. Vorläufige Mitteillung," *Acta Radiologica* 14, pp. 419-423, 1933.

[16] S. Radner, "Attempt at roentgenologic visualisation of coronary vessels in man," *Acta Radiologica* 26, pp. 497-502, 1945.

[17] L.S. Richards and A.P. Thal, "Phasic dye injection control system for coronary arteriography in the human," *Surg. Gynecol. Obstet.* 107, pp. 79-743, 1958.

[18] G. Arnulf, "L'artériographie méthodique des artères coronaries grace à l'utilisation de l'achétylcholine. Données expérimentales et cliniques," *Bull. Acad. Natl. Med. (Paris)* 142, pp. 661-673, 1958.

[19] G.G. Gensini, S. Di Giorgi and A. Black, "New approaches to coronary arteriography," *Angiology* 12, pp. 223-38, 1961.

[20] C.T. Dotter and L.H. Frische, "An approach to coronary arteriography", in *Angiography*, H.L. Abrams, ed., pp. 259-273, Little, Brown, and Co, Boston, 1961.

[21] I. Boerema and J.R. Bliekman, "Reduced intrathoracic circulation as an aid in angiocardiography; an experimental study," *J. Thorac. Surg.* 30, pp. 129-142, 1955.

[22] S. Bellman, H.A. Franf, P.B. Lambert, D. Littman and J.A. Williams, "Coronary arteriography. I. Differential opacification of the aortic stream by catheters of special design - experimental development," *New Engl. J. Med.* 262, pp. 325-328, 1960.

[23] F.M. Sones, E.K. Shirey, W.L. Proudfit and R.N. Westcott, "Cine-coronary arteriography," *Circulation* 20, pp. 773-774, 1959.

[24] M.P. Judkins, "Selective coronary arteriography. A percutaneous transfemoral technic," *Radiology* 89, pp. 815-824, 1967.

[25] T.J. Noto, L.W. Johnson, R. Krone et al., "Cardiac catheterization 1990: a report of the Registry of the Society For Cardiac Angiography and Interventions (SCA&I)," *Cathet. Cardiovasc. Diagn.* 24, pp. 75-83, 1991.

[26] D.W. Miller, F.M. Tobis, T.D. Ivey and S.A. Rubenstein, "Risks of coronary arteriography and bypass surgery in patients with left main coronary artery stenosis," *Chest* 79, pp. 387-392, 1981.

Chapter 4

Coronary angiography: from analogue to digital imaging

The state - of - the - art diagnostic imaging system for coronary angiography, at the start of my career as cardiologist, is depicted in Figure 4.1. The X-ray source generates X-ray pulses at a frame rate of typically 50 / s synchronous to the cine camera that records the light output from the image intensifier. The image intensifier is a device that detects and converts the incoming high energy X-ray photons into many light photons. These visible output photons are further detected by cine - and TV camera's. The image intensifier is a vacuum tube, see Figure 4.2, at the input screen, the so-called "phosphor", the detected X-ray photons are converted into many light photons that generate electrons at the photocathode. The electrons are accelerated in the potential difference inside the tube, and are focussed by the electron lens on the output screen and generate ample light photons per detected X-ray. Vision is the most impressive confrontation between physics and biology. In the beginning of the evolution it was only possible to detect light as bits of energy "photons" or "quanta" by special cells. In the course of millions of years these cells are grouped together resulting in a vision organ being the eye, *i.e.* a conglomerate of special cells (rods and cones) able to count photons by absorption of the incoming light energy. See Figure 4.3. The absorption of the light energy (photons) gives rise to a complex cascade of chemical processes in rhodopsin, a light sensitive receptor, with variable gain resulting in the arousing of electrical potential differences (signals). See Figure 4.4. These signals travel along nerve fibres, the optic nerve, to the visual cortex in the brain, *i.e.* the central computer to perceive images. These electrical and chemical processes take some time, for the human eye this time is approximately a tenth of a second and is called exposure time.

Detection of an image needs a minimum number of photons, distributed in time and space as well, as guarding of false alarms *i.e.* spurious visual pat-

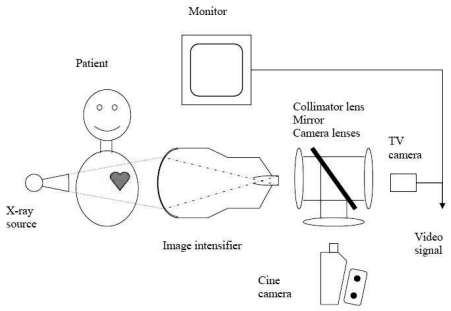

Figure 4.1: Block diagram of the cine - film based diagnostic imaging system for coronary angiography.

terns arising from the random character of the photon distribution but not from the original scene. All these aspects result in the need of a relative high number of photons necessary to transmit reliable information and to form a "real" image, see [4]. The signal - to - noise ratio (abbreviated SN, definition: ratio of the signal power to the noise power corrupting the signal) to form a genuine image should be 3 (normally 5) as absolute minimum to avoid false alarms. A signal is by definition the average number of photons falling on a subject, noise is the root mean square deviation of this number. See Figure 4.6 for an X-ray image of a test object, a so-called phantom, that is used for image quality assessment of diagnostic X-ray imaging system. The test object consists of circular objects of various radii and thicknesses. For a certain exposure level one should be able to see a certain number of disks in the image. In general one is able to discern larger disks with smaller contrast and smaller disks with higher contrast. In angiography both the noise and the contrast depends on the photon fluency, this is depicted in Figure 4.8. In this Figure we show a simulated bloodvessel of the size of an coronary artery (e.g. 3 mm) that is filled with a standard contrast material with 380 mg I / ml and that is imaged at 75 kVp with additional 20 cm water in the beam. The bloodvessel gradually decreases in diameter till 20% in the middle of the image and then restores the original diameter. The simulation mimics a (realistic) diagnostic X-ray image intensifier - television system [5], see Figure 4.7. The images show the relation between contrast, photon fluency and resolution, at the highest photon level, the image is still not ideal due to the electrical noise

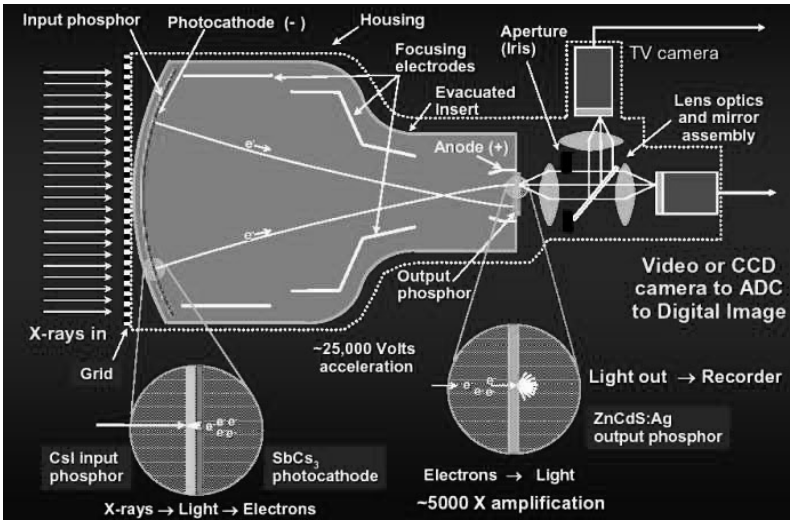

Figure 4.2: Schematic representation of an image intensifier with "invisible" X-ray photons as input and visible photons as output.

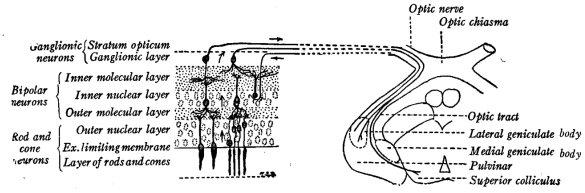

Figure 4.3: Anatomy of the visual system. From [1].

of the detector as reflected in the Detective Quantum Efficiency (DQE).

An other aspect of an image is the term "picture element" which means the smallest area of a spot of a given contrast that can be resolved. The shape of the spot is not important although bars [6] are better visible as compared to dots because the signal-to-noise ratio estimation tends to be based on the total area of the bars rather than on a single element area, leading to over estimation in image resolution. The resolution of a system, given as number of image elements per distance called dpi (dots per inch) or lpi (lines per inch), is based on the minimum discrimination of white and black bars having different values in a single frame or moving frames because of the time - lag of the eye. The geometry of an object is another aspect in image acquisition, although not very important in low contrast, and is furthermore determined by diffraction of the radiation, lens aberrations and the finite size of the picture elements. All these aspects apply to the visible light but are also valid for the total electromagnetic spectrum, including X - rays. X - rays, invisible

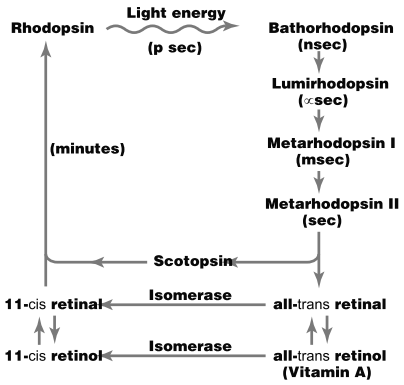

Figure 4.4: Photochemistry of the rhodopsin-retinal-vitamin A visual cycle. From [2].

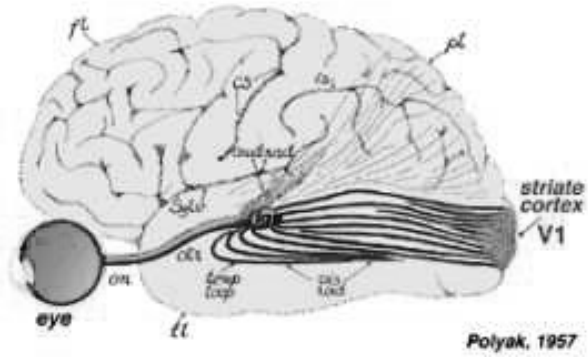

Figure 4.5: Visual input to the brain from eye to lateral geniculate nucleus (LGN) and then to the primary visual cortex, or area V1, the Brodmann area, which is located in the posterior of the occipital lobe. Adapted from [3].

for the human eye, are made visible by a conversion screen, a process called scintillation. The principle of this process is absorption of high energy photons (short wave electromagnetic radiation) and emission of photons in the range of visible light. This usually fast process, depending on the radiated materials, results in an analogue image of often poor quality, especially in the pioneering period because of low radiation intensity of the X-ray generator and poor quality of the "phosphor" screens (few photons emitted).

Crucial in this process of digitizing has been the development of video cameras [7], which has started with the Nipkow disc (Figure 4.9), based on the principle of light (photons) being transformed in an electrical current. Via all kinds of technical innovations, these kind of video cameras are replaced by solid state image sensors and applied in all modern cameras. The performance of these new sensors exceeds the human eye in efficiency and the

ability to operate at low light levels.

However, there is an important difference between the human eye and the video camera: the human eye can see an image as a total image in contrary to a camera, the camera scans only lines. The difference between analogue and digital images, also in radiology, is the transformation of the original analogue image generated by X-ray radiation on the phosphor screen (fluoroscopic image) into finite discrete numbers.

Images set in digital format enable to do all kind of computations, an operation called processing. The first efforts on digitizing images in cardiology, using A / D convertors, were done in the seventies of the last century by using the images on videotapes (analogue images) after a catheterisation procedure by Brennecke [8] in 1976. The next step in the development towards faster systems was the introduction of a system with a build in video camera directly collecting these analogue images. These images were instantaneously converted in data (numbers) and transmitted directly into the memory of the computer system. Initially only possible during continuous - mode fluoroscopy, but later on also during pulsed-mode imaging. Many different systems have been developed since the beginning, however, the basics are not changed. All the modern systems nowadays in use contain: video acquisition, analogue - to - digital conversion, image memory and display, arithmetic and video processing, archival storage, system and exposure control.

In the past, the vidicon camera was one of the most used video cameras, see Figure 4.10. The camera has a favorable signal - to - noise ratio giving rise to a broad scale of applications, however, because of a long persistence of the image on the phosphor screen, this camera is not ideal for moving images. Adding lead to the phosphor resulted in the plumbicon tube with shorter lag times but at the expense of a slightly reduced dynamic range and a small reduction of the signal - to - noise ratio. The camera combining the positive aspects of the vidicon and plumbicon is called saticon. The newest development in image formation is directed to a quite different solid-state technology: first the charged - coupled - device (CCD) (Figure 4.11) using a physical array of light sensors for direct measuring of the light (energy) levels and the CMOS (Complementary Metal Oxide Semiconductor) sensor later.

After the introduction of the CCD sensor system, there were many problems to be solved, especially in signal - to - noise ratio and matrix configuration, but these problems are nowadays nearly all solved and CCD systems are frequently used in X-ray image formation. Analogue - to - digital conversion in CCD systems is done by conversion of the light (energy) intensity as seen by the camera in voltage changes of the separate pixels. The electrical signal is sampled at regular times (conversion frequency) and quantized in numbers, corresponding with the magnitude of the signal at that moment. This means a fixed relation between brightness and voltage at fixed place

and time. The computer stores the values in groups in series of 8 bits (Byte) representing 256 values in grey scales although the human eye can only discriminate 5 bits [9], however, more bits are necessary for adequate flexibility of manipulations and proper handling of noise, see Figure 4.12.

In cardiology a standard image format consist of 512×512 or sometimes 1024×1024 pixels which can be considered adequate, see Figure 4.13.

The image memory size is expressed in MegaBytes. Arithmetic and video processing make use of mathematical manipulations of values per pixel, however, to perform these calculations, there is a need for a fast computer system and moreover for real time vision as these computations have to be as fast as the acquisition time, resulting in display rates equal to the incoming images. Special hardware and software is developed for image manipulations on groups of pixels at one time such as image enhancements, special filters and grey level manipulations. Image acquisition results in an enormous quantity of data, so the accessibility of the data in storage and the transfer rates need also be fast and undisturbed for manipulations and review. Development of these storage media (fast memories) in time has lead to the possibility to manipulate incoming data nearly always in real time, resulting in much faster and better procedures.

In digital angiography the quality of the acquired image is very important so noise, being a major cause of bad quality images, need to be reduced. However, noise reduction is not possible by using low dose continuous radiation because of quantum mottle. The solution is pulsed radiation, short bursts of radiation at higher exposure level, resulting in a much lower quantum mottle, less noise and less motion artifacts ("freezing") due to the moving heart. To avoid flickering, the image on the monitor is build up in an interlaced manner using progressive scan cameras and longer persistence phosphors to minimize fading. The newer X-ray systems are able to use ECG gated data acquisition resulting in a still lower radiation burden and quantum mottle. In these systems this gating, initiated and triggered by the R wave of the surfaced ECG, synchronizes the camera resulting in a variety of acquisition modes. The resolution of the digital image depends on the number of scanning lines (512 or 1024) and moreover on the bandwidth of the system [10].

An additional important aspect in image acquisition is the relative magnification of small vessels because of the limited resolving power of the image intensifier (pin cushion effect) next to the optical magnification decreasing the field - of - view. This problem is nearly fully resolved in the newest flat screen detectors, see Figure 4.14 and Figure 4.15. However, all these complex interactions of factors make it difficult to derive a single figure of merit regarding the system resolution but it is possible after acquiring the total image in a digital format, to display the image in a fast, accepted, format of 512×512 or

sometimes 1024×1024.

Image processing has become a very important tool in image reconstruction and has lead to an enormous increase in its use in research as well in clinical application in cardiology [11]. The digital format of the image makes it possible to apply grey level transformations by reassigning values on a pixel by pixel basis, image filtering based on transformations on values of the neighbouring pixels and operations between images. Grey level transformation is based on reassigning the value of each pixel by a predetermined mathematical relationship: a lookup table (LUT) resulting in fast transformation and low computational overhead. The power of grey level transformation is the possibility to compute in several ways the actual LUT. Image filtering means changing spatial distribution and frequency of pixel values. Frequency in this field means the rapidity of pixel value change as a function of the location. Deriving new values is based on the mathematical function of the neighbouring pixel; the size of the neighbourhood (the kernel size) is chosen to be equivalent with the size of the region of interest in the image. This filtering is used also for noise reduction by a low pass filter or a median filter, these methods require considerable computational capacity. Introduction of a statistical modification of this filtering, using for example Gaussian distribution of neighbouring pixels, resulted in a furthermore noise reduction. A derivative of the low pass filter is the convolution filter, in use as edge enhancement filter; many variations are in use, a complicated mathematical principle to use as a weighting factor in calculating new values for the neighbouring pixels.

All these techniques are to use in a single pixel but it is also possible to combine several techniques in processing. In digital subtraction procedures (DSA), a combination of these techniques is applied, however, in cardiology this technique is difficult to use because of the motion of the heart and the respiration but newer software has eliminated many of these difficulties. To use the subtraction technique, a mask is necessary, in cardiology difficult because of the moving heart and respiration partly solved by ECG gated image formation and breath holding, however, there is always some residual misregistration. The reason for this misregistration is the fact that this silhouette technique gives a two dimensional projection of a three dimensional moving object.

Although not all technical problems are solved, digital cardiac imaging has resulted in an enormous progression of knowledge of coronary anatomy and pathology. Reliable recognition of the anatomy and pathology of the coronaries was a first important step forwards to set the right diagnosis of a cardiac problem, later on also followed by therapeutic handling of these pathologic states. However, next to the possibility to image the anatomy and pathology of the coronary vessels, there are nowadays also, but not of-

ten used, possibilities to apply specially developed software to be informed about the metabolic state of the heart, extracted from routinely made images after digitizing. In combining the anatomical images with the extra "functional" images it is possible to make a more realistic and secure diagnosis concerning the clinical importance of the abnormality as seen in the imaged vessel and to make the right conclusion to solve the problem in that situation.

Paul Julius Gottlieb Nipkow, born in Lauenburg (Leçork Poland) August 22, 1860 died in Berlin August 24, 1940, graduated in physics at the University Berlin. Nipkow proposed and patented the world first electromechanical television system in 1884. Nipkow devised the notion of dissecting the image and transmitting it sequentially. To do this he designed the first scanning device. Nipkow used the photoconductive properties of the element selenium discovered in 1873. The electric conductance of selenium varies with the amount of illumination. The Nipkow disk was a rotating disk with holes arranged in spiral around its edge. Light passing through the holes produced a rectangular scanning pattern or raster which could be used to generate an electrical signal for transmitting or to produce in image from the signal at the receiver. After the development of the amplification tube in 1907 the Nipkow disc became practical. The electromechanical systems were outdated in 1934 with the start of the electronic systems.
From: `www.inventors.about.com/library/inventors/blnipkov`

A charge-coupled device (CCD) is an image sensor, consisting of an integrated circuit containing an array of linked or coupled, light sensitive capacitors, also known as a Charge Coupled Device. The CCD was invented in 1969 by Willard Boyle and George E. Smith at the AT&T Bell Labs. The essence of the design was the ability to transfer charge along the surface of a semiconductor. The CCD started as a memory device, one could only "inject" charge into the device, however, it was immediately clear that the CCD also could receive charge via the photo electric effect, so an electronic image could be created. The CCD image sensors can be implemented in several different architectures: full frame, frame - transfer and interline. The type used depends on the application, the most used form is the interline type (digital cameras). The containing grid of pixels responds to 70% of the incident light making them more efficient than photographic film, which only captures 2% of the incident light, so they are useful in less bright surroundings as in astronomy and X - rays. Boyle and Smith were awarded both $\frac{1}{4}$ of the Nobel Prize in Physics 2009. From: `www.nobelprize.org/nobel_prizes/physics/laureates/2009`

Arthur Holly Compton born at Wooster, Ohio, on September 10, 1892 died in Berkeley March 15, 1962. Compton was graduated at Princeton University in 1914 and received his PhD in 1916. In 1920 he was appointed Wayman Crow Professor of Physics and head of the Department of Physics at the Washington University. After some years as professor at the Chicago University he returned to Washington in 1945. In 1918 he started studying X-ray scattering, this led in 1922 to his discovery of the increase of wave length of X-rays due to scattering of the incident radiation by free electrons, which implies that the scattered quanta have less energy than the quanta of the original beam. This effect is known as the Compton effect which clearly illustrates the particle concept of electromagnetic radiation. In 1927 Compton was awarded the Nobel Prize in Physics. From: `www.nobelprize.org/nobel_prizes/physics/laureates/1927/compton-bio.html`

References

[1] S.W. Ranson, and S.L. Clark, *Anatomy of the nervous system*, 10th ed., Saunders, Philadelphia and London, 1964.

[2] A.C. Guyton, and J.E. Hall, *Textbook of medical physiology*, 11th ed., Elsevier, Philadelphia, 2006.

[3] S. Polyak, *The vertebral visual system*, Univ. of Chicago Press Chicago,IL, 1957.

[4] A. Rose, *Vision, human and electronic*, Plenum Press, New York, 1974.

[5] F.J. de Bruijn, and C.H. Slump, "Lossy cardiac X-ray image copression based on acquisition noise," in Medical Imaging: Image Display, Y. Kim, ed., *Proc. SPIE* 3031, pp.302 -311, 1997.

[6] J.W. Coltman, "Scintillation limitations to resolving power in imaging systems," *J. Opt. Soc. Am.* 44, p. 234, 1954.

[7] L.N. Biberman and S. Nudelman, *Photo electronic Imaging Devices*, Vols 1 and 2, Plenum Press, New York, 1971.

[8] R. Brennecke, T.K. Brown, J. Bursch et al., "Digital processing of video angiographic image series using a mini-computer," in *IEEE Comput. Cardiol.* p. 255, 1976.

[9] O.J. Grüsser, U. Grüsser-Cornehls, "Physiology of vision," in *Fundamentals of Sensory Physiology*, Springer-Verlag, New York, 1978.

[10] R.R. Price, A.E. James and J.J. Erickson et al. "Digital radiograph instrumentation and principles of operation: Research of the future," in *Digital Image Processing in Radiology*, Williams and Wilkins, pp. 28-42, Baltimore, 1985.

[11] S.M. Collins and D.J. Skorton, "Fundamentals of image processing," in *Cardiac Imaging and Image Processing*, McGraw-Hill, pp. 133-168, New York, 1986.

[1] A. Ersahin, S. Molloi, and Y.-J. Qian, "Scatter and veiling glare corrections for quantitative digital subtraction angiography," in *Medical Imaging: Physics of Medical Imaging*, R. Shaw, ed., *Proc. SPIE* 2163, pp. 172-183, 1994.

[2] L.A.J. Verhoeven, *Digital subtraction angiography: the technique and analysis of the physical factors influencing the image quality*, PhD thesis, University of Delft, The Netherlands, 1985.

[3] F.J. De Bruijn, and C.H. Slump, "Lossy cardiac compression based on acquisition noise," in *Medical Imaging*, Y. Kim, ed., *Proc. SPIE* 3031, pp. 302-311, 1997.

[4] J.H. Dernalowicz, H. Goszczynska, and P. Mazur, "Evaluation of indicator dilution process in X-ray angiographic images deteriorated by factors of technical origin," *Polisch J. Med. Phys. Eng.* 2(5), pp. 163-175, 1996.

[3] E.J. Topol, and S.E. Nissen, "Our preoccupation with coronary luminolgy," *Circulation* 92(8), pp. 2333-2342, 1995.

[5] J. Lesperérance, L. Bilodeau, J.H.C. Reiber, G. Koning, G. Hudon, and M.G. Bourassa, "Issues in the performance of quantitative coronary angiography in clinical trials," in J.H.C. Reiber and E.E. van der Wall, editors, *What is new in cardiovascular imaging*, volume 204, pp. 31-46. Kluwer Academic Publishers, Dordrecht, 1998.

[2] L.M. Zir, S.W. Miller, R.E. Dinsmore, J.P. Gilbert, and J.W. Harthorne, "Interobserver variability in coronary angiography," *Circulation* 53(4), pp. 627-632, 1976.

[8] Z. Vlodaver, R. Frech, R.A. van Tassel, and J.E. Edwards, "Correlation of the ante-mortem coronary angiogram and the post-mortem specimen," *Circulation* 47, pp. 162-169, 1973.

[32] B.G. Brown, E.Bolson, M.Frimer, and H.T.Dodge, "Quantitative coronary arteriography," *Circulation* 55(2), pp. 329-337, 1977.

[10] B.G. Ziedses des Plantes, "De toepassing van subtractie bij het röntgenonderzoek van het hart en de grote bloedvaten," *Ned. T. Geneesk.* 103, II.50, 1959.

[11] E.C. Pickering, "Seventy-six new variable stars," *Circulars* 79, p. 1, 1904.

[12] B.G. Ziedses des Plantes, "Een methode om bepaalde onderdelen van het röntgenologisch te onderzoeken voorwerp afzonderlijk in beeld te brengen," *Ned. T. Geneesk.* 78, p. 762, 1934.

[18] M. Schrijver, and C.H. Slump, "Estimation of missing data in tracking coronary artery motion," in *Proc. 3rd IEEE Benelux Signal Processing Symposium*, IEEE Benelux Signal Processing Chapter, Leuven, Belgium, 2002.

[14] M. Haude, G. Caspari, D. Baumgart, T. Ehring, R. Schulz, T. Roth, L. Koch, R. Erbel, P. Spiller, and H. Heusch, "X-ray densitometry for measurement of regional myocardial perfusion," *Basic. Res. Card.* 95, pp. 261-267, 2000.

[15] K. Amplatz, "The history of coronary angiography," in *Quantitative Coronary Arteriography*, J.H.C. Reiber and P.W. Serruys, editors, volume 117, pp. 367-383. Kluwer Academic Publicers, Dordrecht, 1991.

[16] R.M. Vogel, R. M. LeFree, E. Bates, W.O'Neill, R. Foster, P. Kirklin, D. Smith, and B. Pitt, "Application of digital techniques to selective coronary arteriography: use of myocardial contrast appearance time to measure coronary flow reserve," *Am. Heart J.* 107(1), pp. 153-164, 1984.

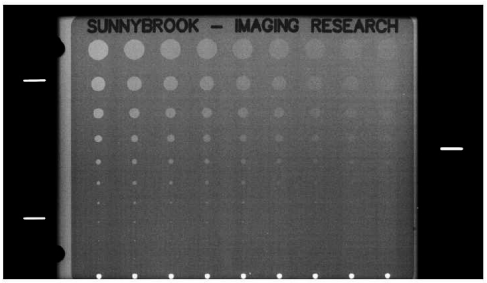

(a)

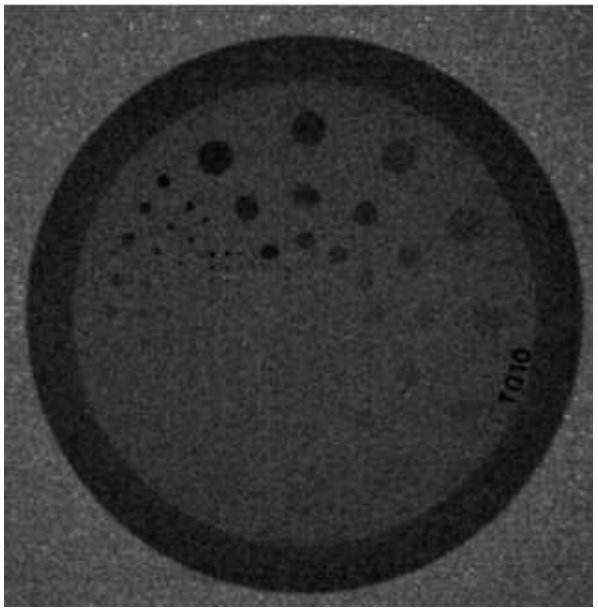

(b)

Figure 4.6: Contrast detail phantom, showing the visibility of larger objects with lower contrast and smaller objects with higher contrast in background noise (a), and the application to the Image Quality performance check of a diagnostic imaging system (b).

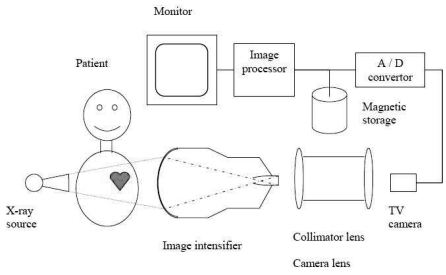

Figure 4.7: Block diagram digital cardiac imaging.

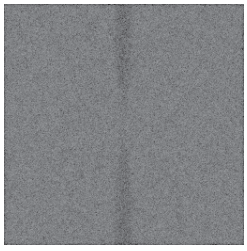

(a) 50 photons per pixel

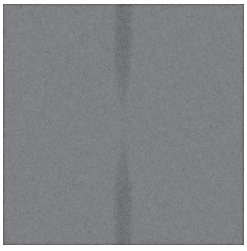

(b) 100 photons per pixel

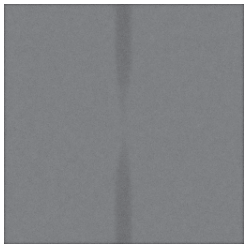

(c) 200 photons per pixel

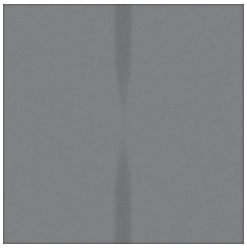

(d) 400 photons per pixel

Figure 4.8: Simulated angiographic image representing an 80% stenose, at different number of photons per pixel.

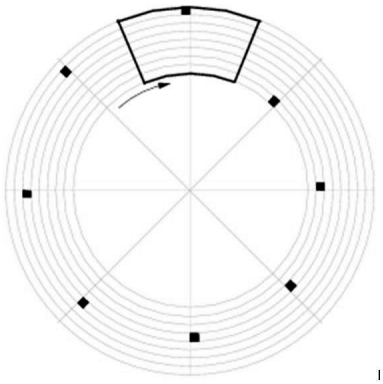

Figure 4.9: Principle of a Nipkow: a rotating spiral perforated disk dividing a picture in a mosaic of points and lines.

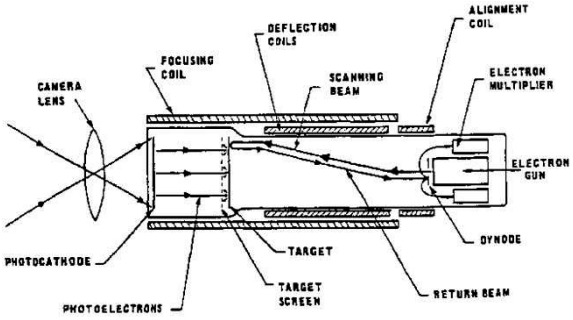

Figure 4.10: Example of an "old" type of video camera.

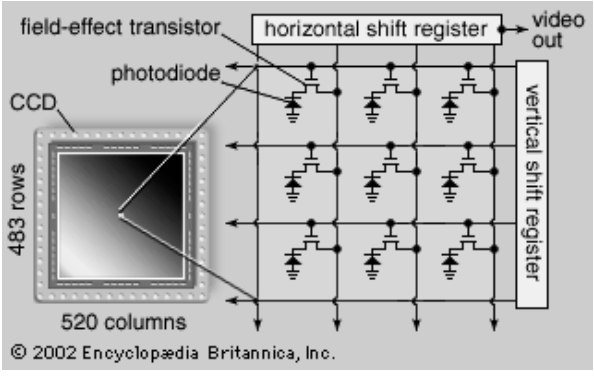

Figure 4.11: Scheme of a CCD.

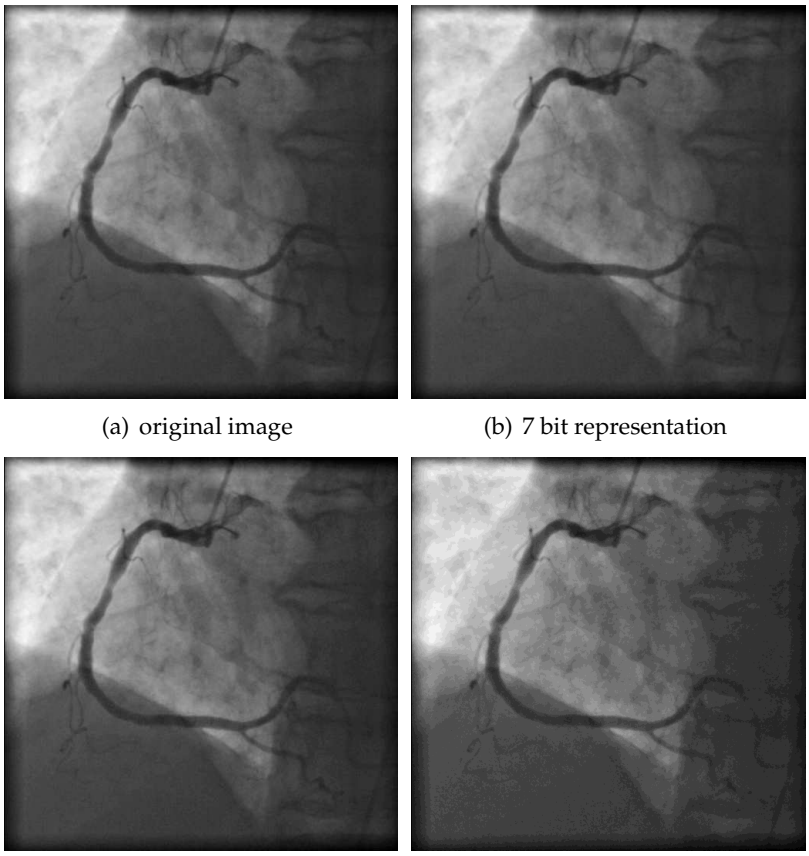

(a) original image (b) 7 bit representation

(c) 6 bit representation (d) 5 bit representation

Figure 4.12: Intensity representations of angiographic image with different number of bits, false contouring start to show up at the lower number of bits.

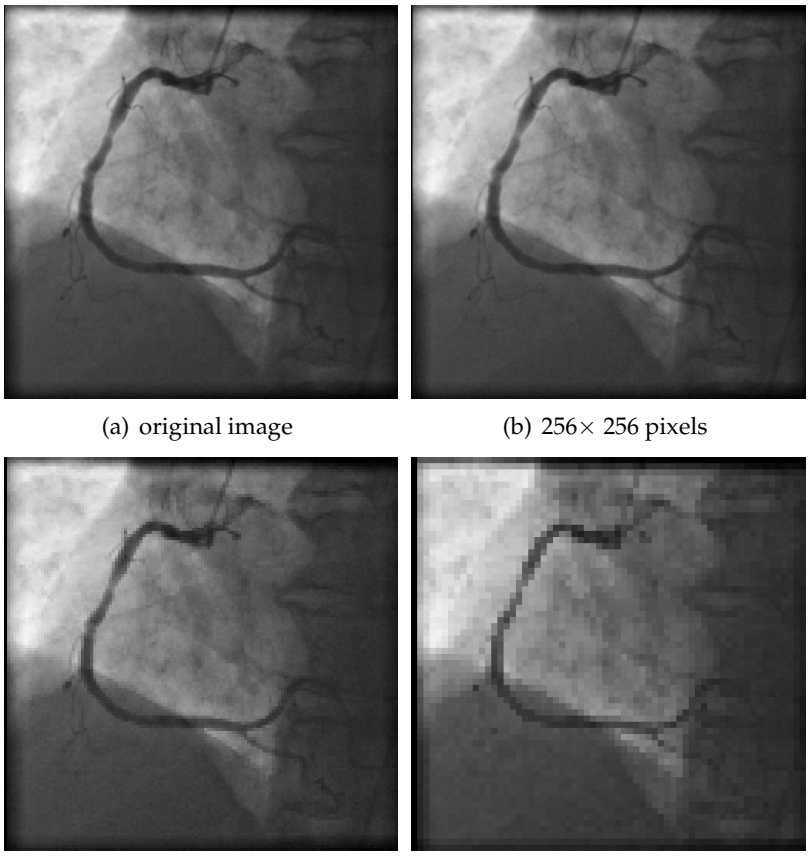

(a) original image (b) 256× 256 pixels

(c) 128 ×128 pixels (d) 64 × 64 pixels

Figure 4.13: Representations of angiographic image with different number of pixels.

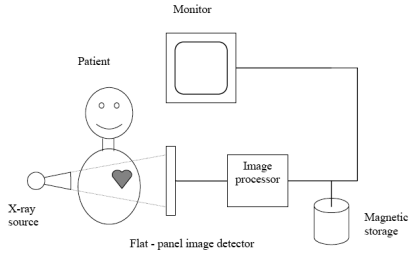

Figure 4.14: Block diagram flat - panel imaging.

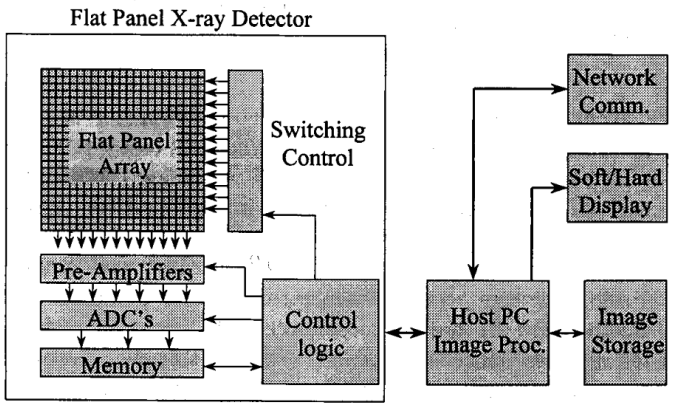

Figure 4.15: Diagram illustrating the configuration of a complete flat panel X-ray imaging system

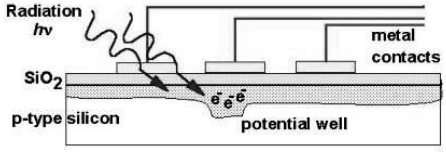

Figure 4.16: Magnified part CCD surface

Chapter 5

X - ray imaging in angiography, problems and solutions

The quality of X-ray images in (coronary) angiography is mainly determined by physical factors such as geometric distortions, focal spot blurring, the resolution of the detector, scatter and veiling glare, beam hardening, non uniform opacification and noise. These factors in the imaging process are not easy to modify, but some of these factors can be influenced in a positive way. Geometric distortions are in the newer imaging systems not so important, less than 2%, because of the nowadays mostly used flat panel X-ray detector, in contrast with the older image intensifiers having a spherical entrance screen. This spherical screen is the cause of some pincushion distortion, pinching at the center, however, this kind of distortion is relatively simple to correct by using image processing algorithms.

Another form of distortion independent of the X-ray system in use, is caused by the geometry of the X-ray beam itself. The beam is not parallel and has the shape of a fan, resulting in a disproportional magnification dependent of the location of an object placed in the beam between source and detector. This means that computer calculations are only reliable when an object of known dimensions, situated in the same position as the object (heart or vessel) under investigation, is present as reference. Normally in a 2-D projection of the heart, these distortions are not very important except when used for calculating a 3-D reconstruction. Focal spot blurring is the result of a finite focal spot of the X-ray tube, giving rise to blurred edges and hazy contrast transitions, limiting the resolution of the system on top of the negative influence of the image intensifier and the resolution of the camera. The influence of the detector in the camera is described by a block-shaped spread function, equivalent to the size of one detector element.

In clinical cardiology the usual image matrix consists of 512×512 pixels, resulting in an image of reasonable quality. The spatial resolution of a

system is assessed by the use of a special phantom, consisting of lines and circles of different dimensions, and expressed as the visible number of line pairs per mm. Increasing the resolution of a system can be reached by using more pixels per square unit in the detector, better filters resulting in less noise, improvement in camera systems and upgrading the amount of pixels in the image screen.

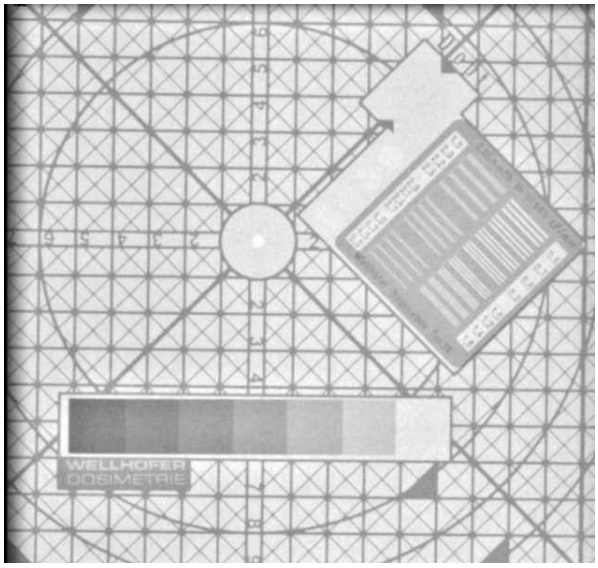

Figure 5.1: Example of the resulting image of a resolution phantom.

Scatter and veiling glare are two phenomena having nearly the same effect on image quality and are corrected using a simple correction scheme [1]. Scatter is caused by colliding of the X-ray beam (photons) with particles in the traversed tissue (Compton scattering) resulting in some energy loss and alteration in the direction of the beam. Some correction can be made by placing a collimation grid right above the detector catching photons with too wide angles in the beam but also some primary photons.

Veiling glare is an identical phenomenon in the optical chain (image intensifier - camera), although less important as scatter, it can sometimes be seen as bright spots, i.e. an area in which the X-rays reach the input screen unimpaired. Scattering and veiling result in energy leakage from one pixel to surrounding pixels resulting in decrease of contrast in the images and the reduction of the signal - to - noise ratio. These two phenomena vary with the thickness of the traversed object and diminish from centrum to the periphery. This effect is seen especially in combination with a curved input screen and is called vignetting. In the newer flat panel detectors this vignetting is absent. Beam hardening is caused by the fact that X-rays, when generated, are not monochromatic but polychromatic: the minimum wave length is de-

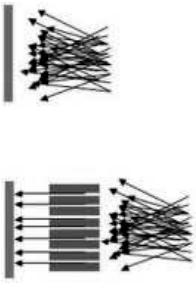

Figure 5.2: Example of scatter and an anti scatter grid.

termined by the peak voltage between anode and cathode of the X-ray tube. Attenuation of the beam depends on the wave length: preferential absorption of waves with longer wave lengths $\approx$ softer X - rays when traversing an object, results in the remaining of harder $\approx$ shorter wave length X - rays (Lambert and Beer law). The attenuation coefficient of polychromatic "light" (X-rays) increases with decreasing photon energy resulting in the fact that low energetic photons do not contribute to image intensity. These photons are absorbed in the filters before reaching the tissue. Filters of aluminum and copper are used to reduce the total X -ray dose. The total effect (filters and tissue) is that the beam after traversing an object has a shorter average wave length, and is therefore harder. In practice this means the more filtering between X-ray generator and image intensifier the harder the beam (shorter wavelength) strikes the image detector [31].

Noise, also in medical images, is an important disturbance factor caused by often a summation of quantum noise, electrical noise and digitization noise. Quantum noise is caused by the X-ray equipment due to the statistical fluctuations of the finite number of photons in each pixel having a Poisson distribution. This measure of combined effect of noise and contrast performance of an imaging system is called Detective Quantum Efficiency (DQE) and this value reflects the relation between signal-to-noise and photon statistics and allows the comparison of different image detector systems. Digitization noise is caused by the discrete increment between gray levels in digital images. The resulting final signal is low-pass filtered with the point spread function of the image acquisition chain. The electrical system adds Gaussian noise to the image [3]. The ultimate image quality is the result of the combined function of all the hard- and software in the image chain, much improved in the course of time, which has lead to a more reliable image of the real world and in medical use to better diagnosing and therapeutic handling. Developments in physics concerning the image acquisition will continue over time but the object of imaging (the patient), thin or obese, is not to correct or to influence. Especially the obese patient generates poor images because of the

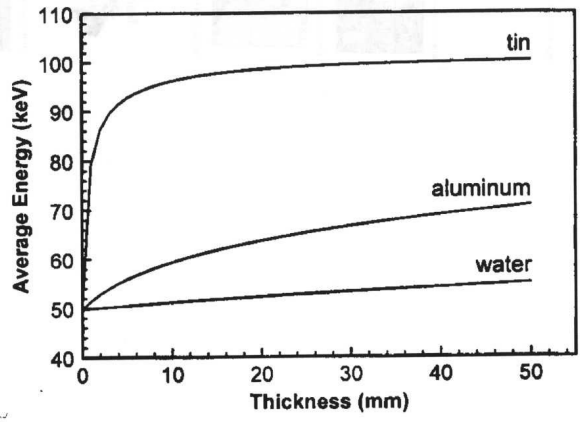

Figure 5.3: The average X -ray energy in a 100 kVp spectrum as function of thickness for three different attenuators. 50 mm of water produces only a slight increase in average X - ray energy, whereas 50 mm of aluminium causes a more noticable increase in average energy; because of the high atomic number, tin has a pronounced beam hardening.

effective increase of the attenuation coefficient of the X-rays resulting in extra hardening of the beam and an increase of quantum noise with as consequence hazy images hampering a reliable diagnose or therapeutic intervention. A solution could be to increase the cathode current or expending exposure time, however, this results in, especially in the early days, an overloading of the X - ray tube and an unacceptable X - ray dose for the patient. Image brightness is controlled by a built in exposure control loop, this loop scans the pixel values in the central part of the image adjusting the cathode amperage and the anode-cathode voltage to regulate the measured pixel value in a way it equals the preset values. Increasing the kVp hardens the beam resulting in a better penetration, increasing the amperage gives more photons. Input on the intensifier is not constant but varies with contrast fluctuations and motion (respiration, motion of the heart) and causes less accuracy in quantitative measurements. Correction is very difficult, however, Dernalowicz [4] in 1996 has developed some methods for retrograde corrections but these methods are not suitable for input intensity fluctuations caused by the control loop. Angiographic images do not have a linear relationship between X-ray settings and pixel value and the image has a high inherent dynamic range. A technique, white compression, can be used to reduce the dynamic pixel intensity range. In quantitative measurements this effect has to be corrected using an inverse white compression next to the need to know the gray scale transformation (the difference in degree between white and black in gray val-

ues) ratio in the image chain. The grayscale has to be calibrated by phantom measurements to know the relation between X-ray intensity and pixel values. However, in the practical settings (patients are difficult because of variable density and absorption) all these measurements and adjustments are to some extent unreliable because of the unknown variation in beam hardening, scatter and noise. Interpretation of a coronary angiogram depends first of all on the anatomical knowledge of the physician but an important part of this interpretation depends on the image quality. Next to the setting of the total imaging chain, hard- and software, the physician plays a very important role in the image acquisition. Images have to be made under appropriate angles to avoid overlap of separate vessels, an essential part of the investigation, but there are numerous other factors influencing the final image, even the most optimal images will sometimes lead to misinterpretations [3] such as missing of branches or total occlusions. The geometry of the coronary system can cause also important problems because the differences in magnification and foreshortening [5], place dependent, resulting in unreliable quantifications, only partly to be alleviated by optimizing the angles and laborious calibrations. Besides technical problems the inter- and intraobserver variability in visual inspection and analysis is even a more complex problem [2]. This problem can partly be diminished by Quantitative Coronary Angiography (QCA), however, many other uncertainties still remain. Some of these uncertainties are caused by the variation in injection techniques of the used contrast agent resulting in a not completely replacing the blood by the contrast agent making the edges of the vessel even more hazier especially the smaller vessels. This is an important imperfection, because the lining of a vessel is an important indication of the existence of atherosclerosis (plaques), next to this problem it is very difficult to assess the cross section and the length of an abnormality of a vessel lumen [8]. These facts are some of the possible problems in interpretation of a coronary angiogram resulting in under-or overestimation of an abnormality, mostly a stenosis, so the clinician should be aware of the pitfalls and being careful in the interpretation of the images. Introduction of digital techniques in the X-ray systems has resulted in the development of fast, almost online, image processing techniques; in the coronary angiography this introduction has lead to the development and application of a number of analyzing software programs. The most important introduction was QCA [32] and Digital Subtraction Angiography (DSA) [2] based on the principle of the analog subtraction technique introduced in medicine by Ziedses des Plantes [10] and the extension to DSA densitometry. The possibility to reconstruct, from orthogonal images, a 3D vessel tree of the coronary system became available using special software but this technique is seldom used because it is a time consuming procedure. QCA is a collective name for quantification in coronary angiography, based on intra-and extra vascular contrast

differences, mostly used for calculations of dimensions and length of an abnormality, percent of stenosis and or the length of the stenosis in coronary vessel. Another aspect in this quantification possibility is, by using the densitometric properties, to calculate flows but this technique is not often used. Dimensions, percentage of stenosis, based on the QCA technique, are calculated by using automatic enhancement techniques and edge detectors with a known catheter diameter as reference. Although a useful and practical tool many uncertainties are still present and these calculations and results are to use with prudence. Especially the assessment of physiological impairment of a stenosis is uncertain and unreliable in these calculations but densitometric subtraction calculations, mimicking flow in the vessel, could be more useful and informative. Subtraction of two images was introduced in the beginning of the last century to enhance the visibility of faint celestial objects in the astrometry by Pickering [11], introduced in the radiology around 1934 by Ziedses des Plantes [12] using darkroom photography, a time consuming process, a reason for being seldom used. After the introducing of digital image techniques in the seventieth of the last century this method became easier to use and popular in angiology although in theory ideal, in practice the application is complex because one has to correct for scatter, veiling, hardening and brightness control systems. Especially the subtraction technique of coronary vessel images give in contrast to, for instance, cerebral or peripheral vessel angiography extra difficulties because of the motion of the heart and respiration resulting in a not perfect aligning of the mask and contrast images. A solution to correct for the moving heart is ECG gated image collecting but that is nearly impossible when there are rhythm disturbances such as atrial fibrillation or extrasystoly. Next to ECG gating breath holding is necessary to exclude moving by ventilation. In non cardiac DSA corrections are nearly always possible after the investigation, however, in cardiac DSA these correction methods are not suitable [14], due to the motion of the heart. Densitometry is a special application of digital subtraction angiography by attaching a quantitative property to a pixel in the DSA image making it possible to calculate an average indicator (contrast) concentration in a before determined region. By knowing the relationship between pixel values and the amount of contrast it is possible to calculate volumes, but one has to correct for scatter and glare in order to obtain in a linear relationship. Applying this technique in coronary vessels is also possible but motion of the heart remains a great problem, even when all possible corrections are applied the accuracy of this method must be improved. Corrections can be divided in easy to correct or to neglect such as noise, geometric distortions, influence of beam hardening, automatic brightness control system and the limited spatial resolution. More difficult to correct is scatter: it can be done by placing a piece of lead in the viewing field blocking the primary radiation so the contribution of scatter

and glare can be assessed [18]. Motion corrections are necessary to obtain identical regions in mask and contrast images, in vivo a difficult problem due to motion of the heart (rhythm) and respiration. Over time several possible solutions are introduced: transient cardiac pharmacological cardiac arrest using acetylcholine [15], a more ethical solution is breath holding and ECG triggering although in a clinical setting it is more difficult than expected. A solution for variations in rhythm could be atrial pacing resulting in stable heart rhythm but the drawback of this method is the need to introduce an extra pacing catheter in the right atrium. Next to the mask method there is another type of DSA called Gated Interval Differencing [12] in which two images both with contrast are subtracted from each other to measure the differences in contrast densities. This method has some advantage especially in small changes in contrast density, however, the problems as described in "normal" DSA are the same. Although many problems are solved especially in time/density methods, based on great improvement in hardware and software, much of the obtained results remain unreliable because of the unknown variability in the same patient in time and position as well as the nearly unsolvable problems in the physics of the X-ray machines and the limitations of imaging systems and storage of the data.

Arthur Holly Compton born at Wooster, Ohio, on September 10, 1892 died in Berkeley March 15, 1962. Compton was graduated at Princeton University in 1914 and received his PhD in 1916. In 1920 he was appointed Wayman Crow Professor of Physics and head of the Department of Physics at the Washington University. After some years as professor at the Chicago University he returned to Washington in 1945. In 1918 he started studying X-ray scattering, this led in 1922 to his discovery of the increase of wave length of X-rays due to scattering of the incident radiation by free electrons, which implies that the scattered quanta have less energy than the quanta of the original beam. This effect is known as the Compton effect which clearly illustrates the particle concept of electromagnetic radiation. In 1927 Compton was awarded the Nobel Prize in Physics. From: `www.nobelprize.org/nobel_prizes/physics/laureates/1927/compton-bio.html`

References

[1] A. Ersahin, S. Molloi, and Y.-J. Qian, "Scatter and veiling glare corrections for quantitative digital subtraction angiography," in *Medical Imaging: Physics of Medical Imaging*, R. Shaw, ed., *Proc. SPIE* 2163, pp. 172-183, 1994.

[2] L.A.J. Verhoeven, *Digital subtraction angiography: the technique and analysis of the physical factors influencing the image quality*, PhD thesis, University of Delft, The Netherlands, 1985.

[3] F.J. De Bruijn, and C.H. Slump, "Lossy cardiac compression based on acquisition noise," in *Medical Imaging*, Y. Kim, ed., *Proc. SPIE* 3031, pp. 302-311, 1997.

[4] J.H. Dernalowicz, H. Goszczynska, and P. Mazur, "Evaluation of indicator dilution process in X-ray angiographic images deteriorated by factors of technical origin," *Polisch J. Med. Phys. Eng.* 2(5), pp. 163-175, 1996.

[3] E.J. Topol, and S.E. Nissen, "Our preoccupation with coronary luminolgy," *Circulation* 92(8), pp. 2333-2342, 1995.

[5] J. Lesperérance, L. Bilodeau, J.H.C. Reiber, G. Koning, G. Hudon, and M.G. Bourassa, "Issues in the performance of quantitative coronary angiography in clinical trials," in J.H.C. Reiber and E.E. van der Wall, editors, *What is new in cardiovascular imaging*, volume 204, pp. 31-46. Kluwer Academic Publishers, Dordrecht, 1998.

[2] L.M. Zir, S.W. Miller, R.E. Dinsmore, J.P. Gilbert, and J.W. Harthorne, "Interobserver variability in coronary angiography," *Circulation* 53(4), pp. 627-632, 1976.

[8] Z. Vlodaver, R. Frech, R.A. van Tassel, and J.E. Edwards, "Correlation of the ante-mortem coronary angiogram and the post-mortem specimen," *Circulation* 47, pp. 162-169, 1973.

[32] B.G. Brown, E.Bolson, M.Frimer, and H.T.Dodge, "Quantitative coronary arteriography," *Circulation* 55(2), pp. 329-337, 1977.

[10] B.G. Ziedses des Plantes, "De toepassing van subtractie bij het röntgenonderzoek van het hart en de grote bloedvaten," *Ned. T. Geneesk.* 103, II.50, 1959.

[11] E.C. Pickering, "Seventy-six new variable stars," *Circulars* 79, p. 1, 1904.

[12] B.G. Ziedses des Plantes, "Een methode om bepaalde onderdelen van het röntgenologisch te onderzoeken voorwerp afzonderlijk in beeld te brengen," *Ned. T. Geneesk.* 78, p. 762, 1934.

[18] M. Schrijver, and C.H. Slump, "Estimation of missing data in tracking coronary artery motion," in *Proc. 3rd IEEE Benelux Signal Processing Symposium*, IEEE Benelux Signal Processing Chapter, Leuven, Belgium, 2002.

[14] M. Haude, G. Caspari, D. Baumgart, T. Ehring, R. Schulz, T. Roth, L. Koch, R. Erbel, P. Spiller, and H. Heusch, "X-ray densitometry for measurement of regional myocardial perfusion," *Basic. Res. Card.* 95, pp. 261-267, 2000.

[15] K. Amplatz, "The history of coronary angiography," in *Quantitative Coronary Arteriography*, J.H.C. Reiber and P.W. Serruys, editors, volume 117, pp. 367-383. Kluwer Academic Publicers, Dordrecht, 1991.

[16] R.M. Vogel, R. M. LeFree, E. Bates, W.O'Neill, R. Foster, P. Kirklin, D. Smith, and B. Pitt, "Application of digital techniques to selective coronary arteriography: use of myocardial contrast appearance time to measure coronary flow reserve," *Am. Heart J.* 107(1), pp. 153-164, 1984.

Chapter 6

The radiation burden of coronary angiography

Absorption of X-rays or γ radiation in biological material may lead to ionisation of molecules or excitation of electrons - particles with a negative charge - in the radiated tissues. This absorption, a cumulative phenomenon, is the cause of what is called radiation burden. Excitation means bringing an electron from the ground state into a higher energy level. Ionisation means applying so much energy that an electron is liberated from an atom or molecule, or that an electron is added to an atom or molecule, thus giving rise to an ion with negative or positive charge. These high energy level electrons ($\geq$ 13.6 eV) are able to break chemical bonds in molecules, which can result in a change of the function of these molecules. The biological effects of X- and γ-rays are the same; the only difference is the way these rays are generated. Extra nuclear X-rays are produced by an electrical device (X-ray tube) using a high voltage to emit fast and high energy electrons from the cathode. Collision of these high energy electrons at the anode of the X-ray tube results in liberation of energy, mostly in the form of heat, but a small part of this kinetic energy is transformed in X-rays. γ-rays, on the contrary, are generated as a natural process, by the decay of instable nuclei of isotopes. X and γ- rays both belong to the area of the short waves part in the electromagnetic spectrum. See Figure 6.1, the only difference is in frequency; X-rays ($3 \times 10^{16} - 3 \times 10^{19}$ Hz) and γ-rays ($> 10^{19}$ Hz).

X- and γ-rays, which are both high frequency electromagnetic waves, can also be seen as energy packets containing an amount of energy equal to hv (h being the Planck constant 6.63×10^{-34} Js, v the frequency). High frequency refers to a short wavelength resulting in high energy capacity per photon (energy packet), where the energy of a photon is measured in keV (kilo electron volt, 1 eV corresponding to 1.6×10^{-19} J, while the wavelength is measured in Å (Anders Jonas Ångström, Swedish physicist, 1814 - 1874) , equivalent to

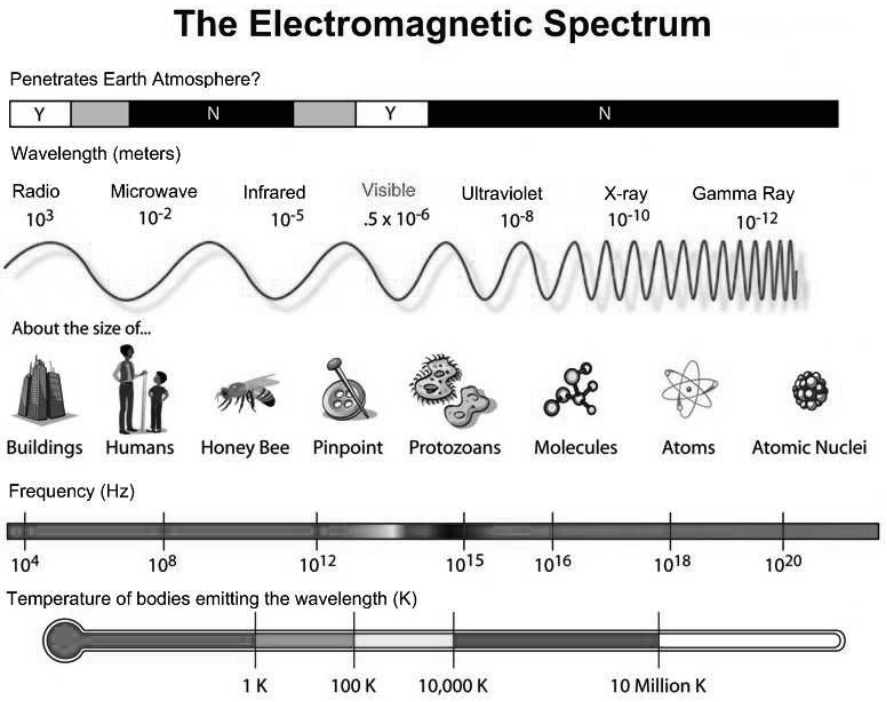

Figure 6.1: Scheme of electromagnetic wave length, adapted from: mynasadata.larc.nasa.gov.

10^{-10} m. Electromagnetic radiation can also lead to indirect ionization, meaning that the rays do not act directly on the tissues they have traversed but that some energy is absorbed in the tissue. This absorbed energy gives rise to fast moving particles, which have the potential of breaking down chemical bonds in molecules, initiating a series of events expressed as biological damage [1].

The absorption of the electromagnetic radiation depends on the atomic number of the separate atoms: the higher the atomic number the more absorption. The biological effects of radiation are primarily caused by damaging molecules in the nucleotides of the DNA strands, partly by a direct or indirect action. Direct means an immediate reaction of the radiation on chemical bonds. Indirect damage is caused by the formation of free radicals, mostly out of water molecules that interact with the nucleotides of the DNA strands. The effects of this possible damage in the DNA strand can sometimes be observed immediately after radiation, but it is also possible that the genetic damage will not emerge until much later, sometimes after several generations (not known in humans). The damage induced to the DNA strands can lead to cell killing, mutation and carcinogenesis. Damage is mostly caused by fractures [2] in the strand of the DNA helix. Although such damage is often repaired by the cell in the case of a single strand fracture, double strand

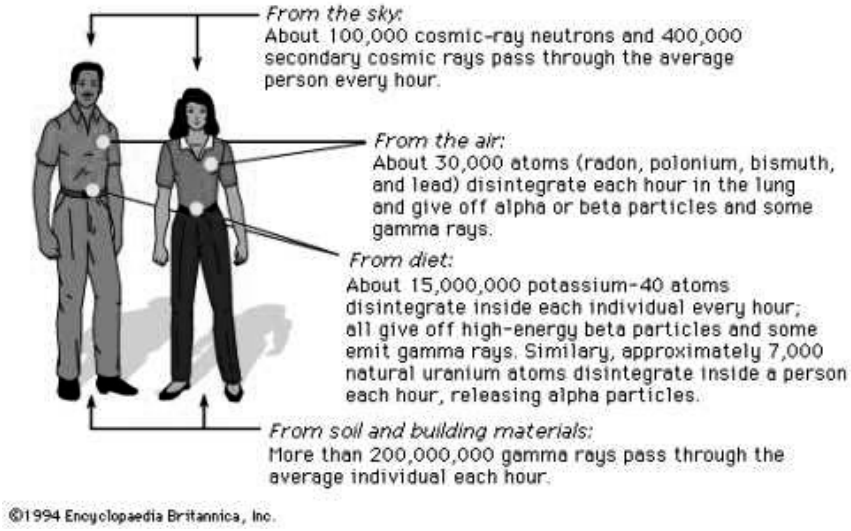

Figure 6.2: Sources of natural radiation

fractures often lead to cell death.

Incorrect rejoining of the strands by the cell leads to aberrations in the chromosome [3], with at times destructive effects on organs and organ systems. The first known clinical destructive effect of radiation was skin ulceration on the arm of Pierre Curie during his work on radioactivity, especially radium. DNA damage can be divided into three groups: lethal, sublethal and potential damage; the dose rate of the X- and γ - rays is the most important factor in terms of the biological effects of the radiation [4]. These injurious radiation effects can come to light because of the integration over time of all received radiation [5]. This integration burden comes from all kinds of mostly slightly radioactive materials manufactured in household equipment, from houses (especially concrete), and from cosmic radiation, by which radiation from by diagnostic procedures and therapeutic interventions is superimposed, see Figure 6.2.

As shown in Table 6.1, an important part of the radiation burden, equivalent for absorbed dose calculated in millisievert (mSv), comes from the radiation occurring in nature, being approximately 2.4 mSv/year [6] (1 - 10 mSv/year, especially location dependent).

The diagnostic and therapeutic radiation burden is difficult to compute because of the differences in equipment and techniques in the various institutes. However, this burden is seldom sufficiently powerful to give deterministic effects. The consequences of diagnostic and interventional radiology are thus limited to stochastic effects, meaning carcinogenesis [7] and hereditary

Table 6.1: Exposure to natural radiation, from [6].

Source	*Worldwide average annual effective dose (mSv)*	*Typical range (mSv)*
External exposure		
Cosmic rays	0.4	0.3 - 1.0[a]
Terrestrial gamma rays	0.5	0.3 - 0.6[b]
Internal exposure		
Inhalation (mainly radon)	1.2	0.2 - 1.0[c]
Ingestion	0.3	0.2 - 0.8[d]
Total	2.4	1 - 10

[a] Range from sea level to high ground elevation.
[b] Depending on radionuclide composition of soil and building materials.
[c] Depending on indoor accumulation of radon gas.
[d] Depending on radionuclide composition of foods and drinking water.

effects. See Table 6.2.

An important consideration is that there is no minimum dose below which there are no effects. This means that all medical radiation comes on top of the already received (natural) radiation, although there are differences in susceptibility between different organ systems. For this reason we speak of effective dose: *i.e.* the product of the kilogram weight (weighting factor W_R) integral of tissues and organs radiated, depending on organ system, and the absorbed dose in gray (Gy). In the SI system used nowadays, this calculated effective dose unit is called sievert (Sv), 1 Sv = 1 J / kg, substituting the term formerly used, the rem (Roentgen Equivalent Man, 1 rem = 0.01 sievert). This computing method makes it possible to calculate or estimate the overall risk for a single person. However, when speaking of a population, reference is made to the collective effective dose, meaning the product of effective dose and the numbers of persons.

During diagnostic or intervention procedures, the highest radiation burden is measured at the entrance place, normally the skin. This absorbed dose is nowadays measured in milligray per minute (mGy/min), rad in old terminology (radiation absorbed dose): units in the SI system 1 gray = 100 rad in J / kg being absorbed energy per tissue quantity. The highest values in clinical radiology are measured in the cardiac catheterisation laboratory, especially during filming. The radiation burden at the entrance place of an average invasive cardiac diagnostic procedure utilizing fluoroscopic imaging is approximately 30 mGy. However, to get approximately the same information with CT scans, the burden is much higher. Depending on the equipment it can be as high as 140 mGy.

Table 6.2: Effects of radiation on humans (ICRP 60 [8]).

Type of genetic abnormality	Incidence per million offspring		
	number attributable to all causes	number attributable to natural background irradiation*	
		first generation	equilibrium generations
Dominant traits + diseases	10,000	3 - 15	100 - 300
Chromosomal + recessive traits + diseases	10,000	< 30	120
Recognized abortions			
Aneuploidy + polyploidy	35,000	33	33
XO	9,000	9	9
Unbalanced rearrangements	11,000	216	276
Congenital anomalies	20,000		
Anomalies expressed after birth	10,000	150	30 - 300
Constitutional + degenerative diseases	15,000		
Total (rounded)	120,000	< 300 - 500	< 600 - 900

*Equivalent to 1 mSv per year, the average dose from background radiation, or 30 mSv per generation.

Apart from the patient, the maximum collective dose for the radiological worker is set by ICRP 60 [8] at 20 mSv per year (average over a period of 5 years with a maximum of 50 mSv in 1 year). This is an important limit because the group of radiological workers consists mostly of younger people in their reproductive age, in contrast to the majority of patients. The maximum for the collective or public dose is set on 1 mSv per year. Diagnostic and interventional procedures done after the reproductive phase of life are of less importance because they are less likely to induce cancer or hereditary effects. In the modern radiology department [9], 40% of the radiological burden comes for from CT scans, although in numbers only 4% of the diagnostics. This is a sobering thought, considering the rapid increase in the number of CT scans performed: a 20-fold increase in the US and a 12-fold increase in the UK. Even more important, however, is the increased use in young children, because of the greatly increased chance of cancer in time [10]. In cardiology the use of radiation is partly diagnostic - normally of short duration - and partly therapeutic (PCI, ablation and pacemaker implantation) - often of long(er) duration, even up to hours. That is why cardiac patients receive much more radiation compared to patients with other diagnostic or therapeutic radiological procedures. These extended procedures can sometimes result in skin damage, erythema or even ulceration at the entrance place. However, the chance of cancer or hereditary problems is very low. At the entrance place the dose using fluoroscopy is limited to 100 mGy/min. However, there are no stringent limits for fluoroscopy or digital acquisition, so the dose can reach up to 500 mGy/min. This skin burden can lead to erythema, dry desquamation, moist desquamation, epilation, and retarded effects such as dermal atrophy leading to necrosis (seen as ulcers, mostly because of damage to the blood vessels). These effects are sometimes observed months [11] after the exposure. The total radiation burden of a patient in a diagnostic or therapeutic process, apart from the procedure, depends also to a variable extent on the skill of the operator and the use of protective measures.

Although radiation is hazardous for the patient, it must be seen in relation to the illness and the possible therapeutic options. The risk-benefit equation is thus weighted by the substantial benefit of the procedure versus the known risk of radiation damage. The risk of radiation for operating physicians (intervention cardiologists [12] receive the most radiation of all radiological workers) and technicians in catheterisation laboratories [13] is the highest compared to other radiological workers. The most important cause for this high burden is the need to use angulations in coronary angiography resulting in much scatter, especially in the LAO direction. It is therefore very important to use as much as possible protection measures and to keep distance, see Figure 6.3.

Since the time that X-rays were introduced for diagnostic purposes, the

adverse reactions of radiation were only slowly recognized. It took a long time before the users became conscious of the risks. Cardiologists in general know deplorably little about radiation [15]. See Table 6.3.

Nowadays, due to the often compulsory courses, radiological workers are more aware of the risks of radiation and thus more willing to change their way of working to reduce the amount of radiation. Reducing the risks can be done in several ways: shorter radiation times, better shielding of the patient and the radiological worker, and introducing different types of radiation (fluoroscopic) techniques such as continuous fluoroscopy, pulsed fluoroscopy or high-output pulsed fluoroscopy which has recently been developed. Especially the high-output pulsed fluoroscopy technique can only be used when the newest generation of X-ray equipment is installed. So there is an absolute need, because of the necessity of reducing the radiation burden, for healthcare managers to invest in newer X-ray equipment. That is the only way to reduce the chance of deleterious radiation effects in the future, also because of the enormous increase in the use of diagnostic and therapeutic (intervention) procedures that work with X-rays [16]. Pulsed fluoroscopy[17] gives a reduction of about 60% compared to continuous fluoroscopy because of reduced scatter and as more than 70% when using the high-output technique with filters. The absolute need to use angulations to prevent vessel overprojection, an important source of errors, in diagnostic and therapeutic cardiac imaging is the cause of extra radiation burden, especially to the investigator. Reason for this extra burden is the augmentation of primary and secondary scatter, so it is very important to use adjusted shielding with a lead glass shield. This results in a radiation burden reduction of 70% for thorax and head, see Figure 6.4.

Aside from the measures to reduce the dose of X-rays, much effort has been put into the realization of better image quality, such as improvement of monitors, cameras and digital imaging techniques. In conclusion, much has been achieved in terms of technical development to reduce radiation burden without reduction of image quality. However, the radiation user (the physician) remains an important factor in the reduction of radiation and its consequences. So the physician, as user of radiation, has a significant moral duty to apply all possible measures to protect the patient and all support personnel in the immediate surroundings during radiological procedures. That is why adequate compulsory education for all the radiological workers is absolutely necessary in the effort to reduce the radiation load of human beings and thus prevent detrimental effects such as carcinogenesis or future genetic defects. However, much work still needs to be done before all radiological workers are aware of their key role in applying as low as reasonably achievable[18] radiation in obtaining the right images to establish an accurate diagnosis, or in eliminating the cause of ill-making or dangerous vascular abnormalities in

Table 6.3: Physicians' knowledge of radiation dose and risk for medical ionisation testing, adapted from [15].

Author, year	**Physicians**	**Radiological Awareness Evaluation**	**Results**
Shiralkar et al. 2003 [20]	British physicians	Radiation doses for common radiological investigations	97% of doctors underestimate dose. 5% believes that US uses ionising radiation. 8% believes that MRI uses ionising radiation
Finestone, A. et al. 2003 [21]	Israeli orthopaedists	Mortality risk of radiation-induced carcinoma from bone scan scintigraphy	Mortality risk was identified correctly by less than 5% of respondents
Lee, C. et al., 2004 [22]	Emergency department, physicians and radiologists	Radiation dose and possible risks associated with CT scan	Almost all doctors were unable to accurately estimate the dose. 9% emergency department physicians believed there was increased risk
Correia, M.J. et al., 2005 [15]	Adult and paediatric cardiologists	Environmental impact, individual bio-risks, dose exposure and medico-legal regulation of medical ionisation testing	Only 11%, 5%, 29% and 42% of physicians correctly identified environmental impact, individual bio-risks, dose exposure and legal regulation, respectively

CT = computed tomography; MRI = magnetic resonance imaging; US = ultrasound

therapeutic (cardiac) intervention procedures.

Max Karl Ernst Ludwig Planck was born in Kiel in 1858 and died in Göttingen in 1947. Planck studied at the universities of Munich and Berlin and received his doctorate of philosophy in Munich in 1879. In 1889 he was appointed professor of Theoretical Physics at Berlin University. His first work was on the topic of thermodynamics. At the same time he became interested in the problems of radiation. He demonstrated that these were to be considered as electromagnetic in nature. From these studies he was led to the problem of the distribution of energy in the spectrum of full radiation. Planck was able to deduce the relationship between energy and the frequency of radiation. His derivation was published in 1900 and was a turning point in physics: the start of the quantum theory, with far-reaching effect on classical physics. From: `ww.nobelprize.org/nobel_prizes/physics/laureates/1918`.

Pierre Curie was born in Paris in 1859 and was killed in a street accident in Paris on April 19, 1906. In 1895 he obtained his Doctor of Science degree and was appointed professor of Physics. His early work was on crystallography, later on the discovery of piezoelectric effects and magnetic properties. His work on radioactive substances was done together with his wife Marie Sklodowska. In 1895 they published the discovery of radium and polonium and elucidated the properties of radium and its transformation products. Their work formed the basis for subsequent research in nuclear physics and chemistry. They were awarded half the Nobel Prize, together with Becquerel, in 1903. From `www.nobelprize.org/nobel_prizes/physics/laureates/1903`.

Rolf Maximillian Sievert was born in Stockholm in 1896, where he died in 1966. He studied medicine and electrotechnique at the University in Stockholm. This was followed by studies of astronomy, meteorology and mathematics at the University of Uppsala. There his interest in radiation started. In 1932 he was appointed associate professor in medical physics at Stockholm University. In 1925 Sievert started an organization which was made responsible for continuous control of dosage levels at all clinics in Sweden that applied radiation treatment. In 1924 Sievert was nominated head of the physics laboratorium of Radiumhemmet, which he made into a renowned centre of radiation physics. In 1938 these activities were moved to Karolinska Hospital and were named Department of Radiation Physics. He developed a method to measure the intensity of the radiation: the Sievert chamber. Sievert was one of initiators of ICRP (International Commission on Radiological Protection) and ICRU (International Commission on Radiation Units and Measurement). To honour Sievert, the CGPM conference of 1979 accepted the sievert, Sv, as the unit for dose equivalent for ionizing radiation. This unit is a part of the SI system for units and measurement: 1 Sv = 1 J/kg. From" `www.radfys.ki.se/Sievert.html`.

Louis Harold Gray was born in London in 1905 and died in Northwood in 1965. Gray obtained his PhD at the Cavendish Laboratory (Cambridge) under Rutherford at a time when this laboratory was a world centre for fundamental research in nuclear physics. The practical applications of nuclear physics at that time were limited. Thus, deciding to devote his life to the public good, Gray turned his attention to medical physics and radiobiology. Gray was strongly interested in the efforts of medical research to develop methods of treating cancerous growths with ionising radiation. He took a position as physicist at Mount Vernon Hospital, a leading place in this field, continuing his research in measuring radium radiation and X-rays and investigating their effects on living tissue. Gray's contributions in this field gave radiobiology, a new science, a firm basis. His work with a 400 kV neutron generator resulted in an enormous mass of data that proved of incalculable value in the development of radiotherapy of cancer. After the war, Gray took on a position at the Radio-therapeutic Research Institute of London's Hammersmith Hospital, where he had the opportunity to build a powerful cyclotron. After several years at the Hammersmith, he returned to Mount Vernon in 1954. Located here is the worldŠs first radiobiological institute, built according to his plans and still named after Professor Gray: the Gray Laboratory of the Cancer Campaign. Gray (Gy) is the derived SI unit for absorbed dose, specific energy and kerma (kinetic energy in matter). 1 Gray is the dose of energy absorbed by homogeneously distributed material with a mass of 1 kilogram when exposed to ionising radiation bearing 1 joule of energy. 1 Gy = 1 J/kg. From: `www.graylab.ac.uk/usr/lhgraytrust/lhgraybiography.html`

References

[1] D.E.A. Lea, *Actions of Radiations on Living Cells*, Cambridge University Press, Cambridge, UK, 1956 (second edition).

[2] M.N. Cornforth, J.S. Bedford, "X-ray-induced breakage and rejoining of human interphase chromosomes," *Science* 222, pp. 1141-1143, 1996.

[3] H.J. Evans, "Chromosome aberrations induced by ionizing radiation," *International Review of Cytology* 13, pp. 556-593, 1960.

[4] E.J. Hall, "Radiation dose rate: A factor of importance in radiobiology and radiotherapy," *British Journal of Radiology* 45, pp. 81-97, 1972.

[5] National Council on Radiation Protection and Measurements: Exposures of the Population in the United States To Ionizing Radiation, Report No 100, NCRP, Bethesda, MD, 1987.

[6] Report of the United Nations Scientific Committee on the Effects of Atomic Radiation to the General Assembly. 2006

[7] S. Yoshinaga, K. Mabuchi, A.J. Sigurdson, M.M. Doody, E. Ron, "Cancer risk among radiologists and radiologic technologists: review of epidemiologic studies," *Radiology* 233, pp. 313-321, 2004.

[8] 1990 Recommendations of the international commission on radiological protection, ICRP publication 60, *Annals of the ICRP*, Volume 21/1-3, Elsevier, New York, 1991.

[9] P.W. Wiest, J.A. Locken, P.H. Heintz, F.A. Mettler, "CT scanning: a major source of radiation exposure, *Semin. Ultrasound CT MR* 23, pp. 402-410, 2002.

[10] E.J. Hall, D.J. Brenner, "Cancer risks from diagnostic radiology," *British Journal of Radiology* 81, pp. 362-78, 2008.

[11] A. den Boer, *Radiation safety during interventional procedures*, Thesis Erasmus Universiteit, Rotterdam, 2004.

[12] M. Delichas, K. Psarrakos, E. Molyvda - Athanassapoulou, G. Giannoglou, A. Sioundas, K. Hatziioannou, E. Papanastassiou, "Radiation exposure to cardiologists performing interventional cardiology procedures," *Eur. J. Radiol.* 48, pp. 268-273, 2003.

[13] F.G. Rueter, "Physician and patient exposure during cardiac catheterisation," *Circulation* 58, pp. 134-9, 1978.

[14] G. Barquet, S. Mallon, "Radiation principles and safety," in: *Interventional cardiology secrets*, Hanley & Belfus, 2003.

[15] M.J. Correia, A. Hellies, M.G. Andreassi, B. Ghelarducci, E. Picano, "Lack of radiologic awareness tertiairy care cardiological centre," International Journal of Cardiology 103, pp. 307-311, 2005.

[16] H. Dash, D.M. Leaman, "Operator radiation exposure during PTCA," *J. Am. Coll. Cardiol.* 4, pp. 725-8, 1984.

[17] D.R. Holmes, M.A. Wondrow, J.E. Gray, R.J. Vetter, J.L. Fellows, P.R. Julsrud, "Effect of pulsed progressive fluoroscopy on reduction of radiation dose in the cardiac catheterisation laboratory," *J. Am. Coll. Cardiol.* 15, pp. 159-62, 1990.

[18] National Council on Radiation Protection and Measurements: Implementation of the Principle of As Low As Reasonably Achievable (ALARA) for Medical and Dental Personnel. Report No. 107, NCRP, Bethesda, MD, NCRP, 1987.

[19] S. Balter, F.M. Sones, R. Brancato, "Radiation exposure to the operator performing cardiac angiography with U-arm systems," *Circulation* 58, pp. 925-932, 1978.

[20] S. Shiralkar, A. Rennie, M. Snow, R.B. Golland, M.H. Lewis, K. Gowers - Thomas, "DoctorsŠ knowledge of radiation exposure. A questionnaire study," *BMJ* 327, pp. 371-2, 2003.

[21] A. Finestone, T. Schlesinger, H. Amir, E. Richter, C. Milgrom, "Do physicians correctly estimate radiation risks from medical imaging?," *Arch. Environ. Health* 58, pp. 59-61, 2003.

[22] C.I. Lee, A.H. Haim, E.P. Monico, J.A. Brink, H.P. Forman, "Diagnostic CT scans: assessment of patient, physician, and radiologist awareness of radiation dose and possible risks," *Radiology* 231, pp. 393-8, 2004.

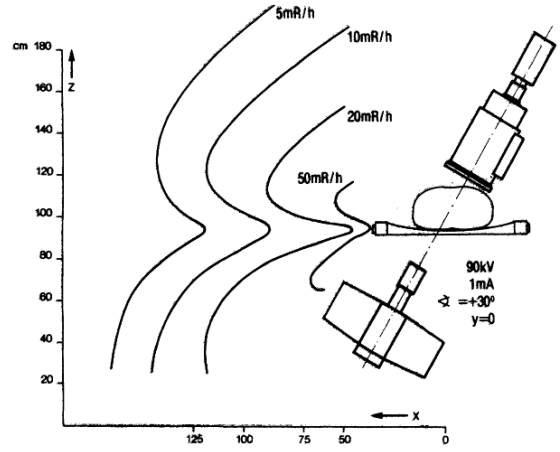

(a)

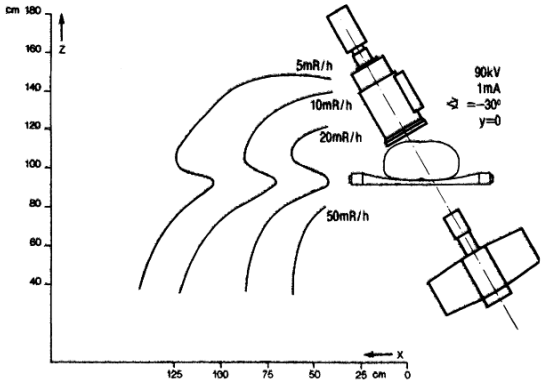

(b)

Figure 6.3: Scheme of transmission of X-rays through a patient and the generated scatter in 30^o LAO and 30^o RAO direction. From [19].

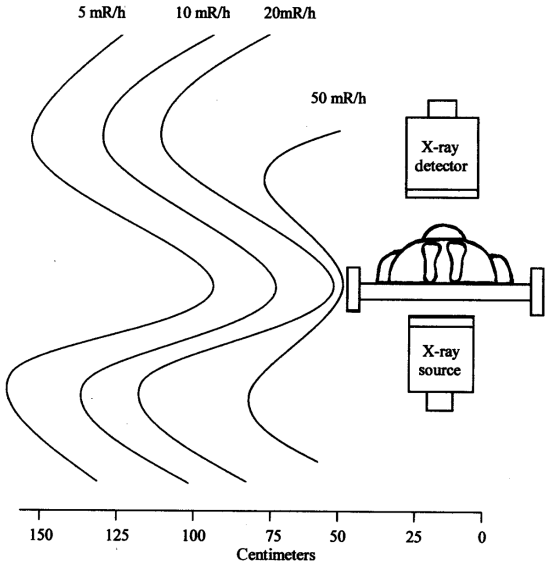

Figure 6.4: Example of radiation burden because of scatter dependent on distance [14], in modern SI terminology 1 Sv = 100 rem (Röntgen equivalent man) and an exposure of 1R corresponds for X-rays to an absorbed dose of 1 rem.

Chapter 7

X - ray contrast agents in coronary angiography

Contrast agents are fluids that are injected into a vascular system to make the inner part of the vessels visible, based on the difference in X-ray absorption between the contrast agent in the vessel and the surrounding tissues. In doing so, it is possible to copy the inner lumen of the vessel. Two techniques are available to get the contrast agent in the area of interest. The first technique involves direct injection of the contrast agent into the target vessel; the second technique involves injecting the contrast agent into a peripheral vessel, usually a vein, and waiting for the contrast to arrive via the blood flow into the intended vessel. Coronary angiography is nowadays always done by the direct way: contrast injection directly into the coronary artery using specially developed catheters, with the tip being placed in the ostium of the coronary artery. This direct method of making coronaries visible is quite different from the early days, when bolus injections were applied above the aortic valves with the intent to fill both coronary arteries, blood mixed with contrast, taking advantage of the physiological diastolic coronary blood flow, or by overpressure. In 1896, shortly after the discovery of X-rays, the first vascular image was made and published by Haschech and Lindenthal [2] the arterial system in a preparation of a human hand, see Figure 7.1. In this preparation the arterial system was made perfectly visible by injection of a Teichmanian mixture, a solution of bismuth and iron in oil, a very toxic solution not usable in living human beings. Because of the rapid development of diagnostics and the growing impact of cardiology in the early 1900s, the need to develop contrast agents with better contrast, less toxicity and usable in human beings increased. Requirements for such contrast agents usable in clinical medicine were: injectable with low viscosity, non-toxic and non-allergic, powerful contrast (a mixture of elements with a high atomic number because of the physical properties, *i.e.* absorption of X-rays), osmolality (os-

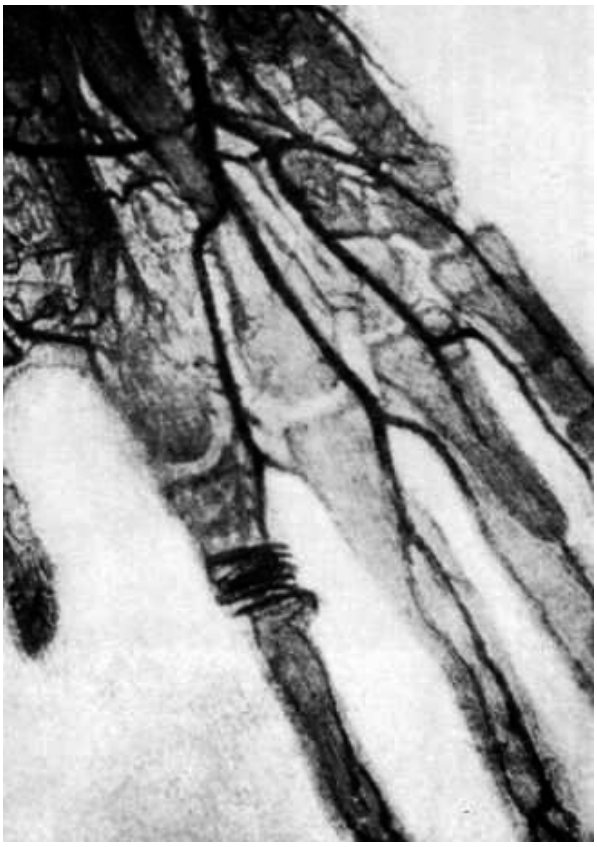

Figure 7.1: Arterial system of a hand, made by Haschech and Lindenthal [2] in 1896.

motic pressure) as blood, and fast elimination of the contrast fluid from the body.

Berberisch and Hirsch [3], in 1923, were the first to inject a solution of strontium bromide (SBr) as contrast agent in a living person. Also other compounds of bromide were used, such as lithium, potassium and sodium bromide (LiBr, KBr, NaBr). However, because of the toxicity of all these compounds the search for less toxic contrast agents continued. In 1924 Brooks [4] injected, as a better and less toxic alternative to these bromides, a sodium iodine solution with a high (25%) iodine concentration. This solution, however, produced only very hazy images whilst the burden of iodine for the body was very high, resulting in the possibility of developing thyroid disease.

The search for agents with a higher iodine concentration but lower side effects went on and was directed to the group of benzene derivatives. Based on this benzene ring, many new agents were developed and clinically tested, but many of them were too toxic and not usable in humans. Then in 1929

uroselectan, a less toxic benzene derivative, was introduced for clinical use by Swick [5]. The uroselectan molecule contains only one iodine atom and was not very toxic, but the low concentration of this heavy metal gave only a feeble distinction between the contrast agent and the surroundings, resulting in blurry images. The search for this type of molecular structure but with a higher iodine concentration continued. In 1930, a new type of contrast agent was introduced, containing two iodine atoms per molecule and also not very toxic, marketed as uroselectan B. This contrast agent was initially used in urology but later on also in angiography. Forssmann [6], who performed the first venous catheterisation in a human person (his own body via an arm vein) in 1929, used this contrast agent. All these contrast agents still only produced hazy images, thus the search for better contrast agents, resulting in sharper image quality, continued. The research focused on higher iodine concentration agents. For that reason the term iodine ratio was introduced, meaning the ratio between the number of iodine atoms to the number of active particles in a solution. The highest ratio at the moment of introduction was one. It took about twenty years (1953) before a higher ratio was developed, *i.e.* 1.5 by Wallingford [7], after changing from diiodinated pyridine derivatives to benzene derivatives with three substituted iodine atoms. From that compound as a base, a variety of side chains were introduced resulting in other often used contrast agents, such as Angiovist, Hypaque and Renografine and the well-known and very popular Conray and Vascoray, which were marketed in 1954.

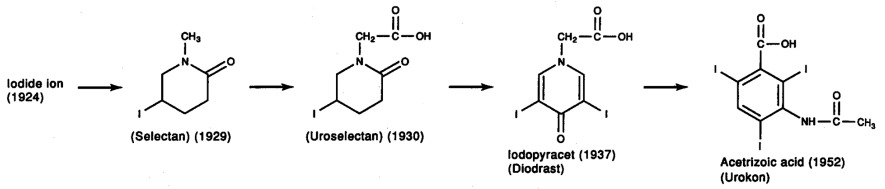

Figure 7.2: Development over time of iodine contrast agents from 1 iodine atom to 3 atoms per molecule. From [1].

All these newer agents are ionic, often as Na-salt. These solutions provided images that were satisfactory suitable for the examination of large vessels, but they were not ideal for imaging small coronary vessels, however, as they did not produce sharp images. A significant adventitious problem was the high ionic concentration of sodium (Na^+) or N-methyl glucamine$^+$ since, because of the high osmotic activity, this gives rise to malignant rhythm disturbances such as ventricle fibrillation, specially when injected into the coronary artery. Because of this serious problem, sodium(Na^+) was replaced by a non-active methyl group. However, though less problematic in the case of rhythm disturbances, the osmolality of that solution was six times higher

than blood plasma osmolality. This made it difficult to inject, plus there were still some side effects, though less problematic and mostly benign.

Since these ionic contrast agents often had unwanted and sometimes delirious side effects, the search for new non-ionic contrast agents continued. In 1974 iohexol (omnipaque), the first non-ionic contrast agent, with a low toxicity and low osmolality was introduced on the market. However, this contrast agent was thermolabile and very expensive, so its clinical use was limited. However, this was the starting point of a new direction of research into a better non-ionic contrast agent which would have the following properties: sharp image (high iodine concentration), normal osmolarity, stability, low cost, few side effects, and easy to use. Many slightly different new non-ionic agents were developed and introduced in the clinic. These contrast agents largely replaced the ionic contrast agents because of extensive promotion by the pharmaceutical industry and less adverse reactions; they thus became first choice for use in coronary angiography. Today this non-ionic group of contrast agents with high iodine concentration (320 - 350 mg iodine per ml) is used most in coronary angiography.

Much of today's knowledge about the newer, mostly used, contrast agents is based on an extensive study published by Katayama [8] in 1990. In this review Katayama showed six times more side effects, especially allergic (anaphylactoid) reactions, when using ionic contrast agents compared to the use of non-ionic agents. In his review, however, he did not examine nephrotoxicity, which leads to (mostly transient) renal insufficiency, one of the most important side effects of all contrast agents, even the most modern ones. The definition of acute renal insufficiency varies in the literature ($\geq$ 30 definitions are known) but a usable definition [9] is: *"increase of serum creatinine concentration of more than 44µmol/l or 25% of the reference value (value before the procedure) and a calculated creatinine clearance reduction of $\geq$50% within 48 hours after administration of radiological contrast media."* The cause of this renal problem is not clear. Some factors are mentioned: medullar hypoxia caused by vasoconstriction caused by the contrast agent, increase in oxygen consumption and direct tubular toxicity, as well as evidence of reperfusion damage after vasoconstriction by oxygen radicals, as discussed by Zager [10]. Important for the clinician before using contrast agents is to know whether a patient is known to have risk factors as described by Waybill [11]: pre-existing renal dysfunction, diabetes mellitus, heart failure, paraproteinaemia, anaemia, hypotension, advanced age and use of nephrotoxic medicine. These parameters are included in a risk score for prediction of contrast-induced nephropathy by Mehran [12], see Table 7.1.

No real therapy is possible for CIN (Contrast Induced Nephropathy), so prevention is very important: extra hydration with intravenous NaCl 0.9%, 1 to 1.5 ml kg hour, 3 to 12 hours before the procedure and 6 to 24 hours after

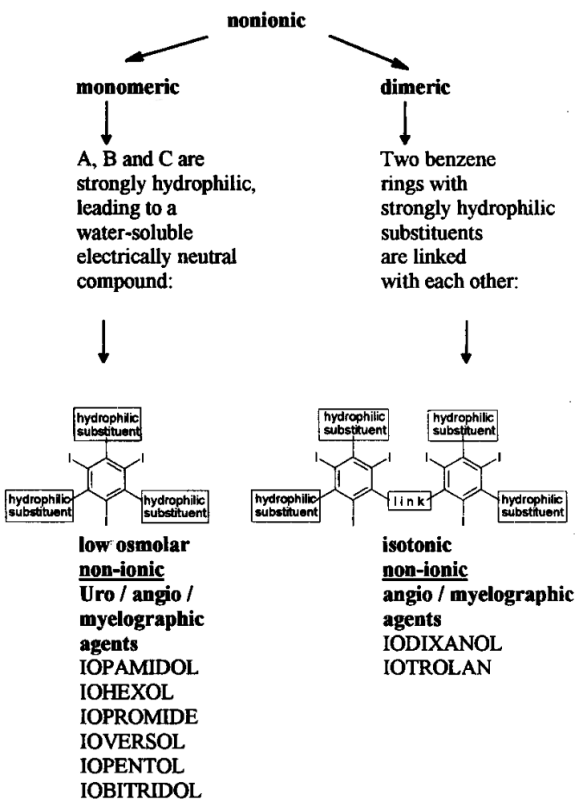

Figure 7.3: Chemical structure and names of frequently used non-ionic contrast agents. From [1].

the exposure to the contrast medium, or perhaps better sodium bicarbonate in the same concentration as NaCl as suggested by Merten [13]. Acetylcysteine before administration of contrast is controvertible, but the most important fact remains: to use as little as possible of the contrast agents. With the right preventive measures, including discontinuation of nephrotoxic medication such as loop diuretics, aminoglycosides, some antibiotics and NSAIDs (Non-Steroidal Anti-Inflammatory Drugs), it is nearly always possible to do a coronary angiography without permanent damage to the kidneys. However, even less than 50 ml of contrast agent can induce a serious nephropathy in patients with chronic kidney disease [14]. Concerning anaphylactoid reactions caused by contrast agents, corticosteroids should be administered in advance to a patient known to be allergic to iodine compounds or as a therapeutic afterwards. Remarkably, according the meta-analysis by Barrett [15] in 1993, there is a difference in arterial and venous injection of contrast fluid:

Table 7.1: Prediction of contrast-induced nephropathy, low risk 0 - 4, moderate 5 - 8, high 9 - 12, very high > 12. From [12].

Predictor Variables	*Score*
Basal creatinine $\geq 115 \mu mol/l$	7
Shock	3
Gender (female)	2
Multiple vessel stenting	2
Diabetes mellitus	2

intravenous injection of contrast seldom leads to problems, but when using the intra-arterial injection route there are many more problems. The explanation for this could be the release of endotheline-1 found in the arterioles, in reaction to hyper-osmolarity of the contrast agents and resulting in malignant vasoconstriction. The extensive report by Katayama [16](1991) on the difference between ionic and non-ionic contrast agents showed convincing evidence of the superiority of non-ionic contrast agents over ionic contrast agents.

The most important message from all the single contrast studies and a great meta-analysis concerning all types of intravascular angiographic studies, including coronary angiography, is to use as little contrast medium as possible to prevent or reduce the possibility of side effects. Side effects - sometimes permanent complications or even death - are closely correlated to the amount of contrast agents injected. While this is a very important message, there should also be a proper balance between image quality to set a diagnosis and the amount of contrast agent used. However, the incidence of important side effects, especially CIN, is low [17] in people without advanced risk (0.6 - 2.3%), in contrast with people with advanced complication risk, for instance diabetes patients [18] (8.7%). An overview of recent literature by Aspelin [19] (2003) gives a number of conclusions and suggestions concerning intracoronary angiography and contrast agents in general: always use dimeres (two iodine groups per molecule) instead of monomers (one group of iodine) especially in ionic contrast agents, although non-ionic agents are strongly preferred because of the low incidence of side effects by reason of isotonicity, viscosity and low nephrotoxicity and fewer late reactions.

Concluding, when the clinician takes the risks of a given patient into account and takes appropriate precautionary measures, it is nearly always possible to use this form of diagnostic investigation, whether a coronary angiogram or a therapeutic procedure such as PCI, without permanent damage to the patient. A properly conducted and thoroughly analyzed coronary angiogram enables the clinician to set the right diagnosis and to advise on

how to handle the clinical problem: whether by medicines, coronary bypass surgery or percutaneous coronary intervention, with a view to decreasing or eliminating the complaints and to improve the quality of life.

References

[1] P.H. Dawson, *Contrast media in practise*, Springer Verlag, 1993.

[2] E. Haschech and O.T. Lindenthal, "Ein Beitrag zur praktischen Verwertung der Photographie nach Röntgen," *Wiener Klin. Wschr.* 9, p. 63, 1896.

[3] J. Berberisch and S. Hirsch, "Die röntgenographische Darstellung der Arterien und Venen am Lebenden Menschen," *Klin. Wschr.* 2, p. 22-26, 1923.

[4] B. Brooks, "Intra arterial injection of sodiumiodide. Preliminary report," *J. Am. Med. Ass.* 82, pp. 1016-1019, 1924.

[5] M. Swick, "Darstellung der Niere und Harnwege im Röntgenbild durch intravenöse Einbringung eines neues Kontraststoffes, des Uroselectan," *Klin. Wochenschr.* 8, pp. 2087-2089, 1929.

[6] W. Forssmann, "Die Sonderung des rechten Herzens," *Klin. Wschr.* 8, p. 2085, 1929.

[7] V. H. Wallingford, "The development of organic iodine compounds as X-ray contrast media," *J. Am. Pharmaceut Ass. Sci. Ed.* 42, pp. 721-728, 1953.

[8] H. Katayama, K. Yamaguchi, T. Kozuka, T. Takashima, P. Seez and K. Matsuura, "Adverse reactions to ionic and nonionic contrast media. A report from the Japanese Committee on the Safety of Contrast Media," *Radiology* 175, pp. 621-628, 1990.

[9] P.L. Marino, *The ICU book*, Lippincott, Williams & Wilkins, Philadelphia, 1998 (third edition).

[10] R.A. Zager, A.C. Johnson and S.Y. Hansen, "Radiographic contrast media induced tubular injury: evaluation of oxidant stress and plasma membrane integrity," *Kidney Int.* 64, pp. 128-139, 2003.

[11] M.M. Waybill, P.N. Waybill, "Contrast media induced nephrotoxcity: identification of patients at risk and algorithms for prevention," *J. Vasc. Interv. Radiol.* 12, pp. 3-9, 2001.

[12] R. Mehran, E.D. Aymong, E. Nikolsky, Z. Lasic, I. Iakovou, M. Fahy, G.S. Mintz, A.J. Lansky, J.W. Moses, G.W. Stone, M.B. Leon and G. Dangas, "A simple risk score for prediction of contrast induced nephropathy after percutaneous coronary intervention," *J. Am. Coll. Cardiol.* 44, pp. 1393-1399, 2004.

[13] G.J. Merten, P. Burgess, V. Lee, L.V. Gray, J.H. Holleman, T.S. Roush, G.J. Kowalchuk, R.M. Bersin, A. Van Moore, C.A. Simonton, A. Robert, R.A. Rittase, H.J. Norton and T.P. Kennedy, "Prevention of Contrast-Induced Nephropathy With Sodium Bicarbonate. A Randomized Controlled Trial," *JAMA* 291, pp. 2328-2334, 2004.

[14] G.C. Kane, B.J. Doyle, A. Lerman, G.W. Barsness, P.J. Best and C.H. Rihal, *J. Am. Coll. Cardiol.* 51, pp. 89-90, 2008.

[15] B.J. Barrett and E.J. Carlisle, "Meta analysis of the relative nephrotoxicity of high-osmolality iodinated contrast media," *Radiology* 188, pp. 171- 178, 1993.

[16] H. Katayama, K. Yamaguchi, T. Kozuka, T. Takashima, K. Matsuura, H. Nakata, M. Tanabe and C. Brunger, "Full scale investigation into adverse reaction in Japan. Risk factor analysis. The Japanese Committee on the safety of Contrast Media," *Invest. Radiol.* 26 Suppl. 1, pp. S33-6, discussion S40-1, 1991.

[17] M. Vercellino, G.P. Bezante and M. Balbi, "Contrast media induced nephropathy: new insights into prevention and risk management," *Cardiovasc. Hematol. Agents Med. Chem.* 7, pp. 166-180, 2009.

[18] O. Toprak, M. Cirit, S. Bayata, M. Tansirev, U. Varol, R. Ersoy, E. Esi, "Impact of diabetic and pre-diabetic state on development of contrast-induced nephropathy in patients with chronic kidney disease," *Nephrol. Dial. Transplant.* 22, pp. 819-826, 2007.

[19] P. Aspelin, P. Aubry, S.G. Fransson, R. Strasser, R. Willenbrock and K.J. Berg, "Nephrotoxic effects in high-risk patients undergoing angiography. Nephrotoxicity in High-Risk Patients Study of Iso-Osmolar and Low-Osmolar Non-Ionic Contrast Media Study Investigators," *N. Eng. J. Med.* 348, pp. 491-499, 2003.

Chapter 8

In vitro and in vivo experimental work

Along with the introduction of new hardware and software for catherisation purposes, new imaging possibilities have also become available since the 1980s. Firstly, this involved indirect imaging, after the procedure the analogue cine - film images were digitized [1]; later possibilities grew, involving direct availability of digital images during the procedure. In view of these new possibilities, we decided to evaluate the algorithms [2] in use at that time for calculating percentage and length of stenoses in coronary arteries. Several projects were started using phantoms under normal circumstances. This involved imitating a situation such as with a real patient, light or heavy, by varying the absorption of X-rays using different quantities of metal plate materials (aluminum and/or copper) placed on top of a water tank. The tank, filled with 20 cm of water, mimics the X-ray absorption of an average patient. The first project was to evaluate the reliability of Quantitative Coronary Arteriogram (QCA) calculations using a commercial built-in software program. We used two types of phantoms: a soft X-ray phantom and a hard X-ray phantom. The soft phantom consisted of radio opaque catheters with different but known diameters filled with a normal (350 mg/ml iodine) contrast agent to imitate a normal coronary artery; the hard phantom consisted of a metal (copper) bar. Both types of phantoms contain stenoses of variable grade and length. See Figure 8.1. Examples of soft phantoms are presented in Figure 8.2.

The results of these experiments, carried out in many types of light or heavy "patients", revealed variable and inconstant findings [3], especially in the soft group. An important factor was the thickness (diameter) of the phantom, which was less than 2 mm. In both soft and hard phantoms this always resulted in an unreliable outcome because of the hazy borders of the phantom in the X-ray image. The reason for this phenomenon is the low resolution

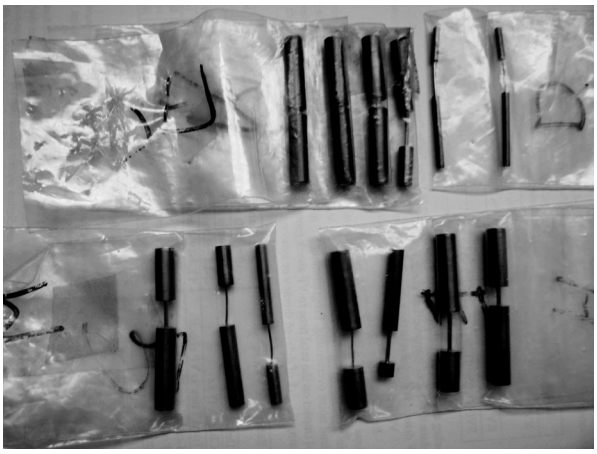

Figure 8.1: Phantoms of copper, different diameters and different length of the “stenoses”.

power of the total image chain of the X-ray system. Nonetheless, the resolution has strongly improved over time. The reliability of the measurements in a heavy patient, with much absorption, causing hardening of the X-rays, is lower than in a light patient because of problems that the software encounters in edge detection. The reason for this phenomenon is both scatter and beam hardening because of the need for a higher kVp to get an image of such a patient, resulting in change of the contours of the vessel wall. The inaccuracy of the "soft" vessel wall is caused by the vague change of contrast in the transition from vessel to tissue. Calculating the length of a stenose is sometimes also a problem because of the mostly hazy transition between vessel and tissue, resulting in an underscore of the real stenose especially in a short, sharp stenose. In conclusion, several researchers [4], plus our own detailed measurements, as shown in the Figures 8.3 - 8.6, have demonstrated that the reliability of QCA is more or less variable, even depending on the system in use, mostly because of hazy transitions between vessel wall and tissue. The QCA should thus only be used as an indication of the length and diameter of a stenose in a coronary vessel and not as absolute values. These findings have consequences for follow-up studies in the "same" patient because of the possibility that the body composition of a patient changes over time, becoming heavier or lighter. This change results in mostly automatic adjustment of the kVp of the X-ray tube, leading to more or less beam hardening, causing a change in vessel contour (edge detecting problem), not only in a change in diameter of the vessel but also in the percentage of narrowing and length of the stenose. In addition, problems in obtaining a reliable QCA can also be expected because of blurred images due to change of position of the patient in the X-ray beam and because of motion artifacts. Although QCA methods

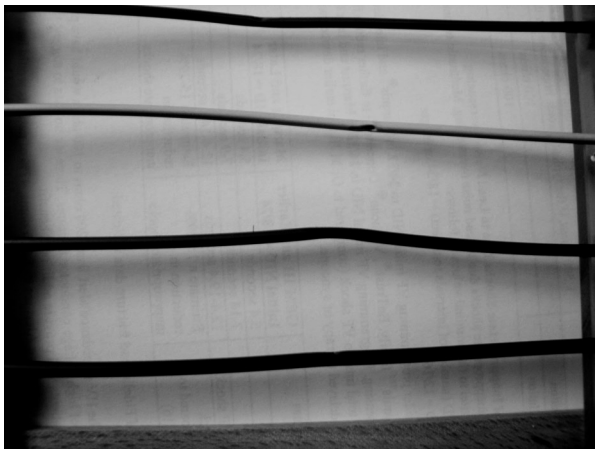

Figure 8.2: Examples of soft phantoms

are known to be imperfect, they are still superior to human observation or to the caliper method when it comes to measuring a stenose or the length of it.

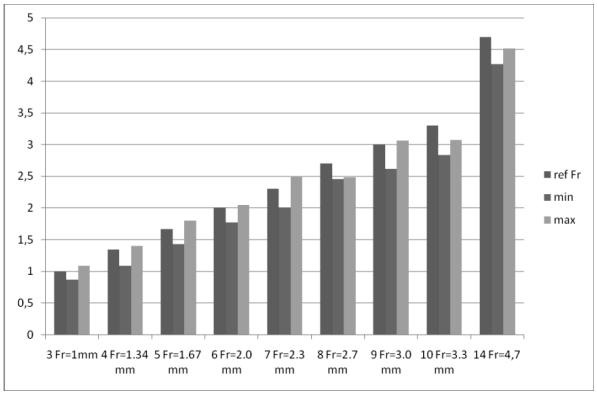

Figure 8.3: Repeated QCA measurement of catheter size versus real size at 60 kVp.

In addition to this static work, experimental research has been done in a standard catheterization laboratory with dynamic flow patterns, using densitometric calculations in a tubular glass model in which a variable resistance system was implemented. Figure 8.9 shows an overview of the experimental set-up: the diagnostic X-ray system, together with the pump and the glass tubular system. This tubular system was meant to be an imitation of a left coronary artery and the bifurcation in the left descending artery and circumflex artery. In one of these branches a variable resistance valve was placed. This system was positioned in the X-ray beam, also with variable shielding, to imitate a real patient, light or heavy, with an alterable stenose in one of the

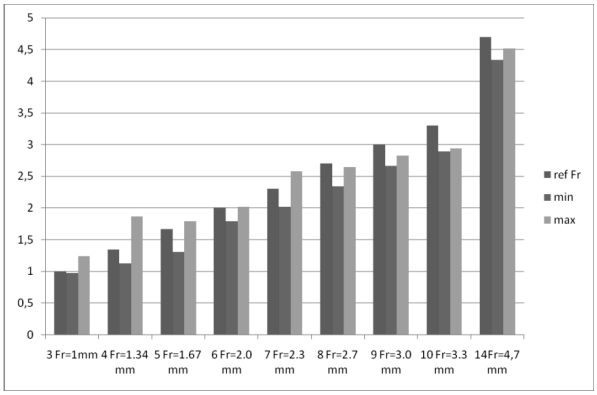

Figure 8.4: Repeated QCA measurement of catheter size versus real size at 70 kVp.

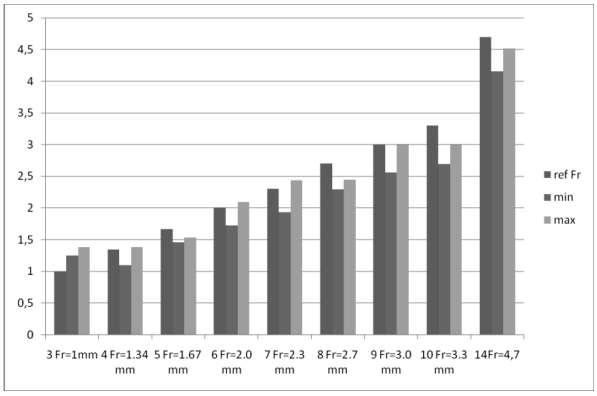

Figure 8.5: Repeated QCA measurement of catheter size versus real size at 80 kVp.

arteries, see Figure 8.7.

At the start of these experiments, laminar flow was used. Later on, this laminar flow model was changed to a variable pulsatile flow model to imitate the normal physiological coronary flow, using a specially built rotating pump system. Figure 8.8 shows the rotation pump and glass model in detail.

Based on the results of these in vitro experiments, new algorithms programs were developed, or existing software adapted, to investigate the possibility of using this software in a clinical setting to calculate the physiological impact [11] of a stenose in a coronary vessel. Next to this software, which calculates the physiological impact of a stenose, new software programs have been developed. These automatically track the course of an artery in the moving image to eliminate motion artifacts, for summation of ECG-triggered images, to get better discrimination between vessel wall and tissue, a sharper

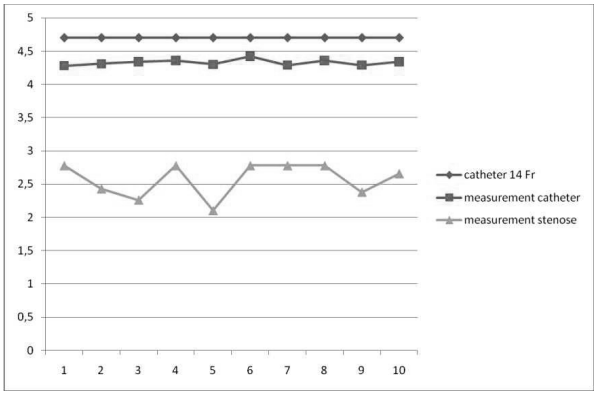

Figure 8.6: Repeated QCA measurement of 14 Fr catheter and measurement of the width of a stenose at several locations.

edge to get more reliable QCA results, while at the same time reducing the amount of data requiring storage.

These new or adapted algorithms and software have been extensively tested at first and, when necessary, modified in an experimental setting in a standard catherisation laboratory, see Figure 8.9.

Later on these adapted algorithms have been subsequently clinically tested in patients with complaints of angina pectoris and stenoses in the coronaries. In addition to making the ”normal” QCA calculations, this newly developed software looked especially for the hemodynamic, physiological consequences of these stenoses, based on densitometric calculations in the nurture area of the affected artery. The findings of these hemodynamic calculations have been compared with other accepted methods of assessing the impact of a stenose, such as nuclear medicine or Doppler flow measurements [6]. The results of this experimental and clinical work are described in the following chapters.

References

[1] P.A. Doriot, F. Chappuis and W. Rutishauser, "Digitalized angiography in coronary disease," *Ann. Cardiol. Angiol.* 37, pp. 575-578, 1988.

[2] J.B. Hermiller, J.T. Cusma, L.A. Spero, D.F. Fortin, M.B. Harding and T.M. Bashore, "Quantitative and qualitative coronary angiographic analysis: review of methods, utility, and limitations," *Cathet. Cardiovasc. Diagn.* 25, pp. 110-131, 1992.

[3] D.M. Herrington, M. Siebes and G.D. Walford, "Sources of error in quan-

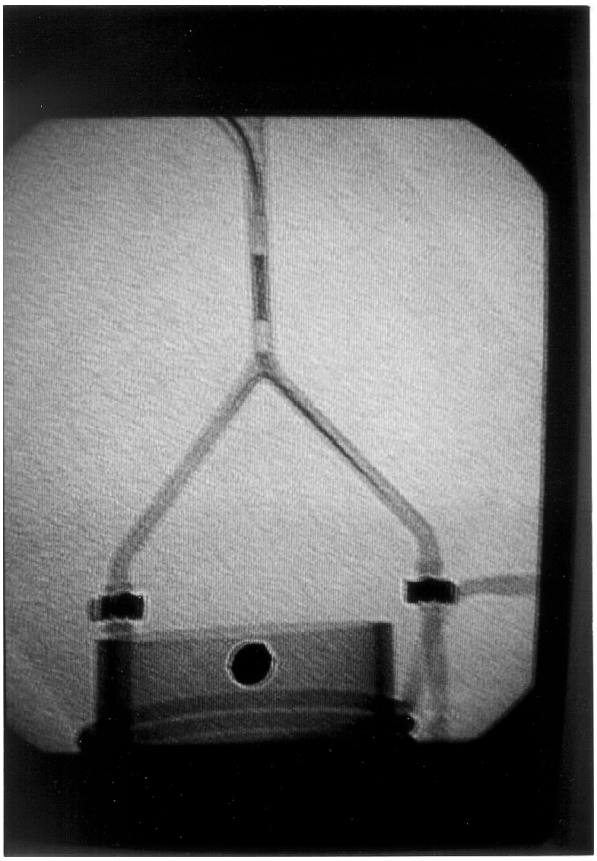

Figure 8.7: Glass model of the left main and bifurcation in RCX and LAD.

titative coronary angiography," *Cathet. Cardiovasc. Diagn.* 29, pp. 314-321, 1993.

[4] G.J. Beauman, J.H. Reiber, G. Koning and R.A. Vogel, "Comparisons of angiographic core laboratory analyses of phantom and clinical images: interlaboratory variability," *Cathet. Cardiovasc. Diagn.* 37, pp. 24-31, 1996.

[11] J.T. Cusma, E.J. Toggart, J.D. Folts, W.W. Peppler, N.J. Hangiandreou, C.S. Lee and C.A. Mistretta, "Digital subtraction angiographic imaging of coronary flow reserve," *Circulation* 75, pp. 461-472, 1987.

[6] C.J. Storm, B. Buis, J. Marinus, A. van Benthem, A. van Dijk and A. Bruschke, "X-ray video densitometry vs. intracoronary Doppler flow. Two methods evaluating myocardial perfusion by calculating coronary reserve," X^{th} Congress of the European Society of Cardiology, Vienna, 1988.

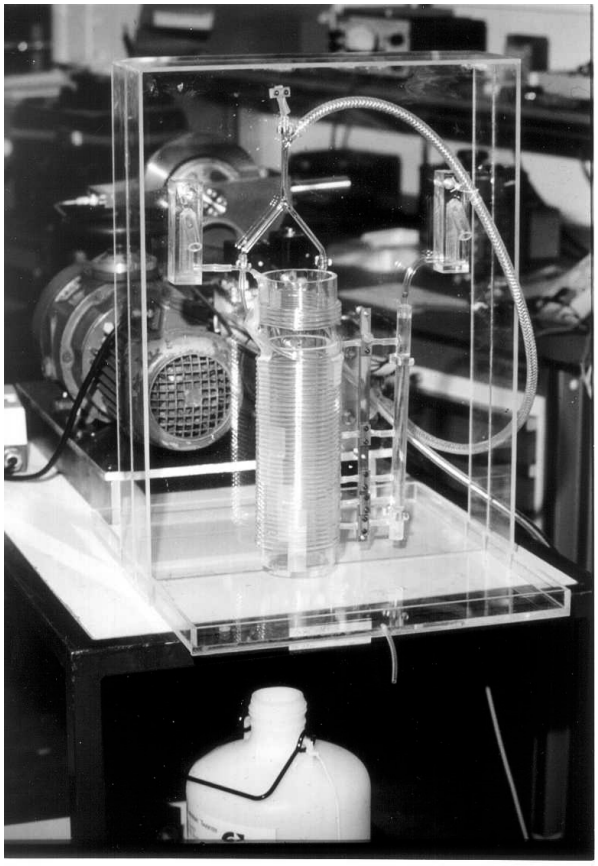

Figure 8.8: The developed pump system imitating a pulsatile flow pattern, including the Y tube to measure flow.

Figure 8.9: Overview of the experimental set-up to measure coronary flow, consisting of the pump system and X-ray equipment.

Chapter 9

3D reconstruction and visualization of coronary artery segments[1]

In this paper we report results from an ongoing study about the diagnostic benefits of 3D visualization and quantification of stenosed coronary artery segments. Biplane angiographic images do not provide enough information for the exact reconstruction of the coronary arteries. Therefore, *a priori* information about the 3D shape to be reconstructed must be incorporated into the reconstruction algorithm. One approach is to assume a circular cross-section of the coronary artery. Hence, the diameter is estimated from the contours of the vessel in both projections. Another approach is based on densitometry and searches for a solution of the reconstruction problem close to the previously reconstructed adjacent slice. In this paper we apply contour information as well as the densitometrical profiles of the two orthogonal vessel projections. We present a new probabilistic densitometric reconstruction algorithm, which extends the correct handling of the stochastic properties of the density profiles into the network flow based reconstruction algorithm. The reconstructed coronary segment is visualized in three dimensions. In order to assess the accuracy of the reconstruction, the method is applied to tubes with artificial obstruction of known geometry, modeling coronary artery stenoses. These catheter tubes are filled with normal iodine contrast material. The results of the reconstruction and visualization are discussed with respect to clinical usefulness. Keywords: 3D reconstruction, 3D display, densitometry, coronary arteriography, biplane acquisition.

[1]presented in part at the 4^{th} International Symposium on Coronary Arteriography, Rotterdam, The Netherlands, June 23-25, 1991, and published as: J.G.M. van den Broek, C.H. Slump, C.J. Storm, A.C. van Benthem, and B. Buis, "Three-dimensional densitometric reconstruction and visualization of stenosed coronary artery segments," *Comput. Med. Imag. Graph.* 19, pp. 207 - 217, 1995.

9.1 Introduction

With coronary arteriography the assessment of the clinical relevance of a stenosis in a coronary artery is complicated and prone to error. Even in the case of biplane imaging where two orthogonal views of the stenosed vessel segment are acquired, the interpretation requires much skill. A good overview about the quantitative assessment of stenosed coronary arteries can be found in Reiber *et al.* [4].
This paper reports about a part of a larger study devoted to the question of whether quantification and 3D visualization of a stenosed artery will benefit the cardiologist in the diagnostic task mentioned above. A previous paper [2] in this study was based upon the assumption that the cross-sections of the vessels are circular. In [2] the reconstruction and visualization of the vessel and the assessment of the flow impedance based on the reconstructed geometry is presented by applying the developed algorithms to clinical coronary biplane exposures. An alternative approach to 3D reconstruction and visualization is the calculation of a functional measure of the clinical relevance of the pertinent stenosis, *i.e.* the so-called Coronary Flow Reserve (CFR), *e.g.* [12, 11]. In [22] we report a less complicated and demanding procedure than CFR, in which we determine densitometrically the relative flow distribution between the two main branches *i.e.* the Left Arterial Decending (LAD) and the Circumflex Artery (RCX) of the left coronary artery. The comparison between basal and pharmacologically induced hyperemic flow provides useful functional information about the relevance of stenoses situated in the vascular tree.
When the 3D geometry of a stenosis is known, the resulting flow can be calculated in principle by means of a fluid dynamical computation. However, the computational complexity of this inverse problem is prohibitive. The vascular geometry together with the boundary conditions are not known, since only recordings of flow patterns of injected contrast material are available. Therefore, in [2] our approach has been modest and we have assessed the flow impedance on the basis of a cylindric geometrical model of the shape of the stenosed artery segment.
In this paper we abandon the assumption of symmetric coronary vessels and allow asymmetric or even irregular cross sections, likely to occur in normal clinical practise. The main topic of this paper is the densitometric reconstruction of the stenosed artery segments from biplane projections. In [6] many of the older pertinent contributions to the literature are referenced, recent work on the 3D reconstruction of coronary arteries from biplane angiograms is *e.g.* [7, 8, 9]. The approach in this paper is in line with previous work [6, 5, 11] with digitized cine-film images. The ill-posed problem of binary 3D reconstruction from biplane exposures is regularized by incorporating into the reconstruction algorithm *a priori* information, such as the shape of the adjacent

(previously reconstructed) slice.
In order to test the validity of the method, we reconstruct static phantom vessels with occlusions of known geometry. The artificial stenotic arteries consist of radiophaque catheter tubes filled with contrast material. Examples of the performance of the developed algorithms on the phantom data are shown with a clinical coronary artery as a final result. In Section 2 the image acquisition and data handling procedures are described. The reconstruction, display and phantom experiment are described in the subsequent sections.

9.2 Image acquisition and data handling

The images processed in the research reported in this paper, are acquired with a Philips Digital Cardiac Imaging (DCI) system which is the all digital cath. lab. The system is schematically depicted in Fig. 1 (only the frontal image acquisition is indicated). X-ray pulses are generated (typ. 5 - 8 ms) at a rate of 15 - 30 frames/s in order to freeze the motion of the coronary arteries which are injected with a contrast agent by means of a stable positioned coronary catheter. The X-ray photons which have traversed the patient are converted into a video image by the image intensifier - TV system. The resulting video signal is digitized in 8 bits after analog processing. The images are stored on a real time digital disk in $512 \times 512 \times 8$ bit up to 60 frames/s or in case of biplane up to 2×30 frames/s. Parallel to the storage on disk, the images are processed (*i.e.* the Modulation Transfer Function (MTF) is corrected by unsharp masking, see *e.g.* [12] for the lowpass filtering by the imaging components) and displayed on a monitor. A versatile user-interface is provided for viewing and post-processing.
For our purpose selected clinical and phantom biplane runs from Leiden University Hospital were transferred from the disk and archived on a digital streamer tape in an off-line process. The tapes were transferred to the HP - Apollo network of workstations at the University of Twente for further off-line processing.
Specially prepared segments of catheters in the range of 4 - 12 french are filled with contrast material and positioned with respect to the frontal and lateral image intensifier. The catheter tubes have been prepared with a variety of artificial stenosis, *i.e.* symmetrical and asymmetrical, (relative) short and long narrowings, entrance resp. exit angle variations, etc.. Obtaining a homogeneous catheter filling without air bubbles appeared to be not so simple and a special filling technique had to be developed. We have used a needle positioned close to the artificial obstruction as a reference point in both projections. The tubes have been imaged at normal magnification and X-ray parameter settings, additional perspex plates were placed at the X-ray collimator.

In general, the densitometric analysis of angiograms requires corrections to be applied to the images. A not exhaustive list includes correction of the nonlinear analog preprocessing (white compression), removal of background structures by log-subtraction of an empty mask image acquired prior to iodine injection (a cumbersome procedure in cardiac imaging due to object movements, however, very convenient in our case of imaging static phantom tubes), correction for pincushion distortion due to the curved detector screen of the image intensifier, restoration of the effects of X-ray scatter and veiling glare. Also the differences between the frontal and lateral imaging chain should be taken into account. In our case we have positioned the phantom tubes such that the stenosed part is projected near the resp. center of the image intensifier and with the frontal and lateral geometrical magnifications approximately equal. Therefore, we discard corrections for pincushion distortion and magnification differences.

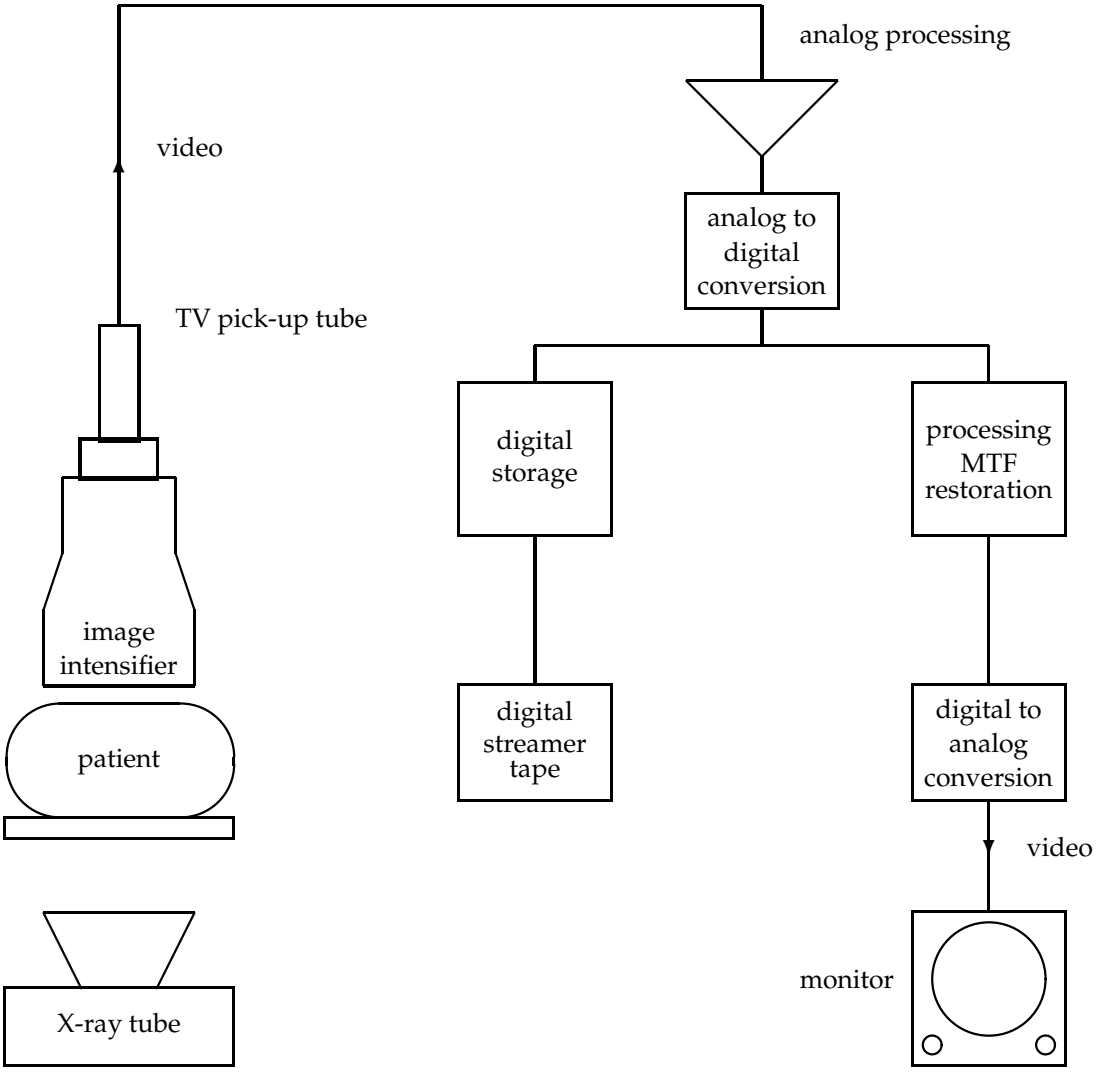

Figure 9.1: Block diagram of Digital Cardiac Imaging (DCI), frontal acquisition.

In general the data handling and reconstruction procedure contains the following steps:

1. Selection of the pair of orthogonal images showing the stenosed vessel part.

2. Selection of the region of interest, identification of reference points such as *e.g.* the catheter tip

3. Preprocessing, lateral shift for aligning the projections [2], (optional) subtraction of a prerecorded empty mask [13]. As the X-ray control unit sets the X-ray parameters kVp and mA such that a fixed average video level is attained, this subtraction is a first order (linear) correction for the effects of scatter, glare, vignetting and white compression.

4. In the selected image regions the contours of the stenosed vessel segments are traced manually under cursor control [2], the selected contour points are stored in a file together with the extracted density profiles.

5. Reconstruction slice by slice using the probabilistic minimum cost algorithm. The next section describes this procedure in greater detail.

6. Entering viewing angles and 3D surface rendering with shading followed by 3D display of the stack of slices

9.3 Densitometric 3D reconstruction

In this section we describe the probabilistic densitometric reconstruction algorithm for coronary artery segments from biplane projections. Orthogonal biplane images which are (almost) simultaneously acquired, are required for the reconstruction. In both projections the contours of the vessel are traced, as described in the previous section. The axis of the vessel segment should not be parallel to one of the X-ray beams. In practice, the angle must be more than 10 degrees with the xz-plane (see the projection geometry as indicated in Fig. 2). Note the left orientation of the coordinate frame, which is often used in 3D computer graphics.

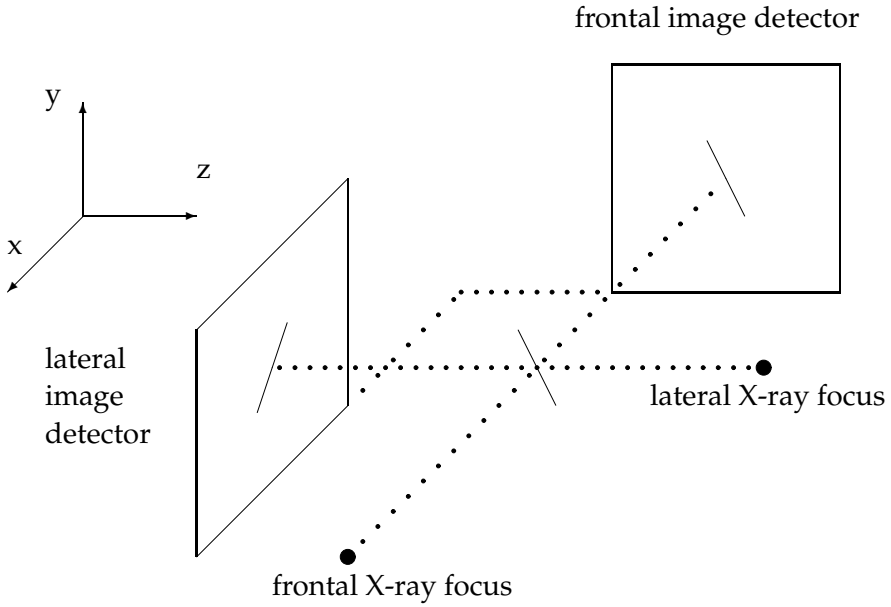

Figure 9.2: The projection geometry and the coordinate frame.

We assume that the vessel segment of interest is homogeneously filled with contrast agent, and that the X-ray absorption is mainly due to the contrast agent. The latter condition is certainly fulfilled for the case of our prepared tubes. At this stage we neglect X-ray quantum noise, scattered radiation and beam hardening. The reconstruction problem can be described as a binary detection task in which we have to detect the presence absence of in-

jected X-ray contrast agent in each volume cell in 3D. Further simplifications of the acquisition model, such as assuming that the X-ray beams can be considered to be parallel over a length of the order of the size of the cross section of the vessel and dividing the vessel segment into a stack of parallel slices, reduce the complexity of the reconstruction problem [6]. Each 2D slice has to be reconstructed from its two one-dimensional absorption profiles which correspond with the row resp. column sums of a binary matrix. This image matrix represents the cross section of the vessel. The entries equal to one denote the presence of contrast agent in the cross section, a zero indicates the absence of contrast.

Let X be a m $\times$ n matrix with entries $x_{i,j} \in \{0, 1\}$, where α_i represents the row sums of X and β_j represents the column sums.
The reconstruction problem is to determine the $x_{i,j}$ subject to:

$$\sum_{j=1}^{n} x_{i,j} = \alpha_i, \quad i = 1, \cdots, m \tag{9.1}$$

$$\sum_{i=1}^{m} x_{i,j} = \beta_j, \quad j = 1, \cdots, n \tag{9.2}$$

with the condition that total mass density S of the pertinent slice is equal to the total row sum and is equal to the total column sum:

$$S = \sum_{i=1}^{m} \alpha_i = \sum_{j=1}^{n} \beta_j. \tag{9.3}$$

In general this problem is underdetermined and has many solutions. To regularize this ill-posed problem, additional, *e.g. a priori* information is necessary to obtain a unique solution. We base our approach [6] on the shape similarity between consecutive slices. The vessel segment is reconstructed slice-by-slice and we recursively use information from the adjacent, previously reconstructed slice. We therefore define an m $\times$ n matrix C of cost coefficients with entries $c_{i,j}$ which denote the cost of assigning $x_{i,j}$ equal to one. The $c_{i,j}$ coefficients are proportional to the distance to the contour of the adjacent slice.

We now have the following optimization problem:

$$Minimize \sum_{i} \sum_{j} c_{i,j} x_{i,j}, \tag{9.4}$$

subject to the constraints (1) - (3). It is convenient to consider this integer optimization problem as a directed capacitated network flow. A capacitated directed network consists of nodes and directed arcs connecting the nodes. We have two special nodes, the source and the sink, and two sets of intermediate nodes. The source is connected with the m nodes of the first set of

intermediate nodes. Likewise, the sink node is connected to the n nodes of the second set. Directed arcs connect each node of the first set with each node of the second set. A directed arc is able to transport in its direction a discrete number of flow units less than or equal to its capacity. The capacity of the intermediate arcs is equal to one. If we set the capacity of the source and sink arcs equal to the measured row and column sums, $\alpha_i, i = 1, \cdots, m$ and $\beta_j, j = 1, \cdots, n$, respectively, we obtain a maximal flow of S units of flow through the network [6]. As indicated in Fig. 3 the flow through the intermediate arcs corresponds with the binary matrix X satisfying (1) - (3). By assigning the cost coefficients $c_{i,j}$ to the pertinent intermediate arcs, the cost minimization problem (4) is stated as the network flow problem of sending S units of flow from source to sink at the lowest costs given the capacities of the source and sink arcs. The advantage of this approach [6] is that efficient algorithms from the field of operations research can be applied, *e.g.* the maximal flow algorithm [14] and the minimum cost algorithm [15].

So far we have neglected the X-ray quantum noise. Because of the high frame rate (typ. 30 - 60/s) at which the images are acquired in cardiac catheterization, the number of X-ray quanta per frame is limited. X-ray quantum noise is present in the acquired images and the measured density profiles have become realizations of a stochastic process. In [11] we have analyzed the effects of quantum noise on the measured density profile, neglecting scatter and assuming an ideal X-ray detector *i.e.* with MTF equal to unity for all pertinent spatial frequencies. Due to the noise it is highly unlikely that there exists a solution to Eq. (1) - (3). We transform the reconstruction problem in a probabilistic minimum cost flow in a capacitated directed network. The first step is to estimate the number of flow units $\hat{S}$ to be transported from source to sink in the network (we use the "^" symbol to denote stochastic variables). $\hat{S}$ is proportional to the projected total mass density in the pertinent slice, it is estimated by the average of the total stochastic row sum and the total stochastic column sum:

$$\hat{S} = \frac{1}{2}\left(\sum_{i=1}^{m} \hat{\alpha}_i \; + \; \sum_{j=1}^{n} \hat{\beta}_j \right). \tag{9.5}$$

To the source and sink arcs a cost function is assigned proportional to the probability distribution of the pertinent row and column sums. The solution to the reconstruction problem is now obtained by sending the $\hat{S}$ flow units from source to sink at the lowest cost. In [11] results of this approach are shown. In [16] the X-ray quantum noise is characterized in a more realistic way, incorporating the spatial filtering by the non-ideal image intensifier - television system. The modeling of noise has been the subject of many papers, see the references cited in [16]. We base our characterization of the noise in the density profiles on [16], neglecting the electrical noise of the imaging

system components. If there is no object in the X-ray beam, the random number $\hat{n}$ of photons impinging on the image intensifier input screen per mm^2 is Poisson distributed:

$$P(\hat{n} = k) = e^{-\lambda} \frac{\lambda^k}{k!}, \quad k = 0, 1, 2, \cdots \tag{9.6}$$

with λ the average number of photons per mm^2. At the output screen of the image intensifier the incoming photons are imaged with the two-dimensional shot noise process $i_o(x_o, y_o)$,

$$i_o(x_o, y_o) = \eta c \sum_i h(x_o - x_i, y_o - y_i) \tag{9.7}$$

with (x_i, y_i) the random positions of the detected incoming photons, $h(\ ,\ )$ the two-dimensional spatial impulse response characterizing the imaging system, η the Detection Quantum Efficiency (DQE) of the detection process and the total detection gain is denoted by c. According to Campbell's theorem [17, p. 561] the expectation value of the output stochastic process is given by:

$$E(i_o(x_o, y_o)) = \lambda \eta c \int_{-\infty}^{\infty} \int_{-\infty}^{\infty} h(x, y)\ dx\, dy, \tag{9.8}$$

and the variance is given by:

$$\sigma^2(i_o(x_o, y_o)) = \lambda \eta c^2 \int_{-\infty}^{\infty} \int_{-\infty}^{\infty} h^2(x, y)\ dx\, dy \tag{9.9}$$

We can now characterize the stochastic image process by the signal - to - noise ratio:

$$\frac{S}{N} = \sqrt{\frac{\lambda \eta}{\int_{-\infty}^{\infty} \int_{-\infty}^{\infty} h^2(x_o, y_o)\ dx_o\, dy_o}} \tag{9.10}$$

or [18, 19] expressed in the system's MTF:

$$\frac{S}{N} = \sqrt{\frac{\lambda \eta}{2\pi \int_0^{\infty} \nu\, MTF^2\,(\nu)\, d\nu}}. \tag{9.11}$$

The influence of the low pass spatial filtering as expressed in the systems MTF is an improvement in the signal-to-noise ratio. With an ideal detector characterized by $MTF = 1$ we obtain the SNR:

$$\frac{S}{N} = \sqrt{\lambda \eta A_e} \tag{9.12}$$

with A_e the area of a pixel. For non-ideal MTF's A_e represents the effective noise sampling aperture [18, 19]:

$$A_e = \left(2\pi \int_0^{\infty} \nu\, MTF^2\,(\nu)\, d\nu \right)^{-1} \tag{9.13}$$

For a typical image intensifier - television chain in the 9 " mode with 8 μR / frame, the theoretical signal - to - noise ratio is $\approx$ 16. In close agreement with the MTF of the system, we have measured with acquired digital images a $\frac{S}{N} \approx 50$ [16].

In order to obtain the row and column sums from the pertinent frontal, respectively lateral projection image we proceed according to standard practice in Digital Subtraction Angiography (DSA). For reasons of noise reduction, we generate a so-called empty mask image by averaging a large number of exposures before the iodine signal is present in the image. The logarithm of the exposure containing the iodine signal is subtracted from the logarithm of the empty mask image. In good approximation for narrow X-ray beams and with neglect of scattered radiation the empty mask image is proportional to:

$$\lambda_m = \lambda_o \, e^{-\mu_m d_m} \, , \tag{9.14}$$

with λ_m the average number of (detected) X-ray quanta behind the imaged object, λ_o the average number of quanta in the exposure, μ_m the total attenuation coefficient (cm^{-1}) of the imaged object and d_m the pertinent effective thickness (cm). In order to simplify the notation, the dependence of all quantities on the spatial coordinates has been dropped. The image containing the iodine signal is a realization of a stochastic process, with expectation:

$$E(i_{o,iodine}) = \lambda_{iodine} = \lambda_o \, e^{-\mu_m d_m - \mu_{iodine} d_{iodine}} \, . \tag{9.15}$$

The effective iodine thickness d_{iodine} equals the row α_i respectively column β_j sum value to be determined times the pixel size d_{pixel}:

$$\left.\begin{matrix} \alpha_i \\ \beta_j \end{matrix}\right\} = \frac{d_{iodine}}{\mu_{iodine} \times d_{pixel}}. \tag{9.16}$$

The DSA subtraction results in:

$$\left.\begin{matrix} \hat{\alpha_i} \\ \hat{\beta_j} \end{matrix}\right\} = \frac{log(i_{o,mask}) \; - \; log(\hat{i}_{o,iodine})}{\mu_{iodine} \times d_{pixel}}. \tag{9.17}$$

Because the log function is a smooth function and the pertinent probability distribution of the projection data is peaked around the expectation value we obtain in good approximation that the expectation value of the row respectively column sum is equal to the true value, *i.e.* the estimates are unbiased. For the variance we obtain in the same way [17, p. 151-152]:

$$\sigma^2_{\alpha_i,\beta_j} = \left((\mu_{iodine} d_{pixel})^2 e^{-\mu_{iodine} d_{iodine}} \right)^{-1} \sigma^2, \tag{9.18}$$

with σ^2 given in Eq. (9). From this result we see that higher row and column sums do have a larger variance, which is intuitive pleasing because in this case less quanta are detected.

We now assign a parabolic cost function to the source and sink arcs in the network flow description [11]. The width of the cost function is chosen proportional to $\sigma^2_{\hat{\alpha}_i,\hat{\beta}_j}$ because it reflects the uncertainty in the measurement of the projection values. A small variance corresponds with less uncertainty and thus a steep (parabolic) cost function centered around the obtained values for $\hat{\alpha}_i, \hat{\beta}_j$. A large variance reveals more uncertainty which is reflected in a larger width of the cost function The total procedure is clarified by the following example. Suppose we image a 10 french catheter on the 16 cm II format (6.5") at a geometrical magnification of 1.6, we have for the d_{pixel} of 0.31 mm an iodine shadow projection of 5.3 mm in diameter, corresponding to about 17 pixels. At 75 kV_p the effective mass attenuation coefficient of iodine $(\mu/\rho)_{iodine}$ equals [31, p.87] 13 cm^2/g. With an iodine mass density ρ of 270 mg/cm^3 the iodine filled catheter reduces at its center the photon fluence by 69 %. The product of $\mu_{iodine} \times d_{pixel}$ equals 0.11. For the case of the image intensifier - TV subsystem [16] in the 6.5" mode, the effective noise sampling aperture A_e equals 1.12 mm^2. Imaging with $75kV_p$ and 1.5 mm Cu prefilter at the X-ray collimator we have 60 keV effective, corresponding with $3.2 \times 10^{14} quanta/m^2$ per R. With an exposure of $16\mu R/frame$ exposure at the input of the II and a DQE η of 60 %, we have according to Eq. (9) and Eq. (12) a σ^2 equal to:

$$\sigma^2 = \frac{S_{ignal}}{\lambda \eta A_e} = 4.76 \tag{9.19}$$

for a signal level S_{ignal} at half the AD converter range of 8 bits. With the above numbers, the $\sigma^2_{\hat{\alpha}_i,\hat{\beta}_j}$ of the estimated projections values $\hat{\alpha}_i, \hat{\beta}_j$ and thus the width of the cost function in the probabilistic network flow reconstruction algorithm is fully specified.

0	1	1	0	0	2
0	1	1	1	0	3
1	1	1	1	1	5
0	1	0	1	0	2
1	4	3	3	1	

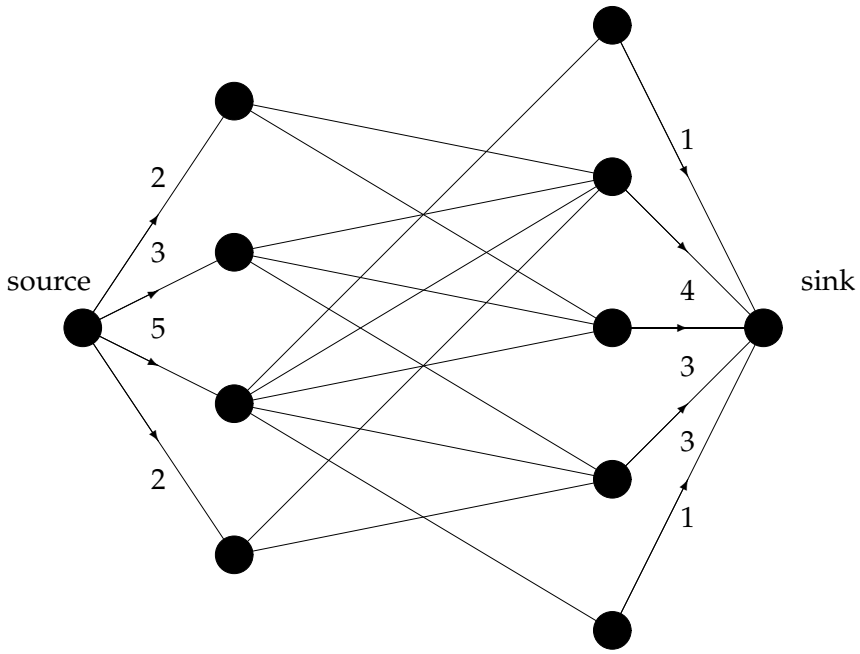

Figure 9.3: An example showing the equivalence of the binary reconstruction problem from row and column sums with the flow in a capacitated directed network. The capacities of the source and sink arcs are equal to the row and column sums, respectively. The drawn intermediate arcs do transport a unit of flow equivalent with a corresponding entry in the matrix equal to unity.

9.4 Results

In this section the probabilistic densitometric reconstruction algorithm described in the previous section, is applied to two phantom tube segments with known occlusion. In addition we present one clinical case. Of each stenosed segment, the acquired frontal and lateral X-ray projections are presented, followed by 3D visualization of the pertinent segment for two different viewing angles. For the display of the stack of reconstructed slices the coordinates of the surface points are required. Similar to [2] for circular cross sections we represent the contour of the reconstructed slice by a polygon. The surface of the reconstructed segment is build by triangles between adjacent polygon - shaped slices. For circular cross sections the tiling of the surface is quite simple if each polygon has the same number of vertices.

The densitometric reconstructions are more irregular and therefore it is not possible to define the shape of the cross sections with a fixed number of vertices at known angles. The adjacent slices represented by polygons have to be connected by triangles. For this purpose a special tiling procedure was developed. The search procedure starts generating triangles for a pair of corresponding vertices on the two pertinent polygons. The algorithm stops when the starting vertices are reached again. We apply the software package 3D GMR [20] for the display of the stack of reconstructed slices. In order to apply this package we need to specify the position of a light source and a viewing angle in the xyz - frame as well. The reflected light intensities from the triangular surfaces are calculated using interpolation according to the Phong shading algorithm [22] and displayed as an image.

The frontal and lateral projection of the first example, a 12 french catheter tube are presented in Figures 4 and 5, respectively. Note the presence of a needle which is visible in both projections and is used as a reference marker to relate the two projections with respect to each other. The reconstructed results for different viewing angles are shown in Figures 6 and 7. The next phantom example is a 12 french catheter with an asymmetric narrowing, Figures 8 and 9 do contain the projections and Figures 10 and 11 the reconstructed results. In the final example we present a clinical case. Fig. 12 and 13 do contain the frontal and lateral projection of a stenosed right-coronary artery. The result of the reconstruction of the stenosed segment is shown for several viewing angles in Fig. 14 - 16.

9.5 Discussion of the results

In comparison with previous results [2] based on circular cross sections, the vessel segments reconstructed by the probabilistic densitometric reconstruction algorithm do appear to have rather rough walls. Our first impression

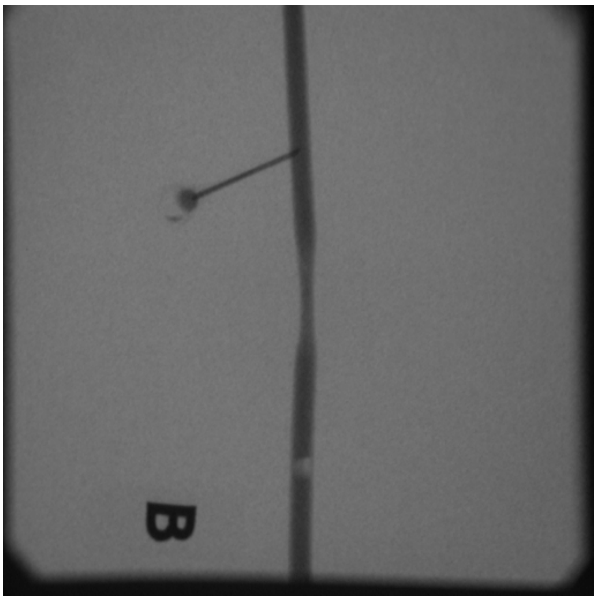

Figure 9.4: Frontal angiogram occluded 12 french catheter.

was a little bit of a disappointment. On the other hand the asymmetric occlusion does show up in the reconstruction result, not visible for the circular cross section method. Second thoughts about the roughness leads us to the following analysis. Due to noise variations the stack of slices even of a cylindrical tube does show up irregular. At no occasion in the set of phantom tubes, the reconstructed result diverged from the true shape. The tiling procedure which is a crucial non-trivial step for finding a good match for the triangles, tends to enhance the roughness. Finally, the Phong shading algorithm [22] we apply is based upon second order interpolation and requires the calculation of spatial derivatives. Existing small discontinuities are greatly enhanced by this procedure. Also the position of the light source is important. Viewing a surface with light coming in with a large angle with respect to the normal on that surface, enhances the conspicuity of small surface variations. The reconstruction algorithm is based upon a slice-by-slice approach. In order to increase the local continuity of the reconstructed vessel we will continue our research for reconstruction algorithms treating the stenosed vessel segments as a whole. One of our goals is the calculation of the flow impedance based on the reconstructed geometry. The present results are not suitable for this purpose. However, we expect that 3D visualization and quantification of the flow impedance of the stenosis are useful diagnostic tools, provided the computations can be carried out on-line between cardiac exposure runs. The realization of this goal is still far away and will require much effort.

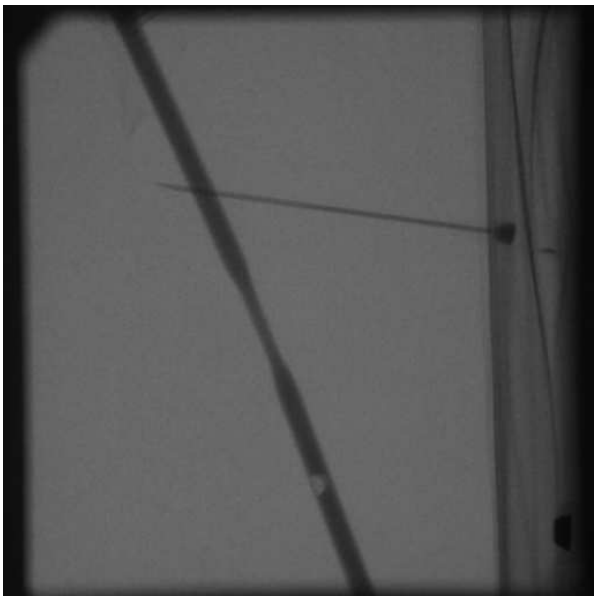

Figure 9.5: Lateral angiogram occluded 12 french catheter.

Acknowledgements

The help of Mr. H. Stegehuis M.Sc. from Philips Medical Systems, Best, the Netherlands, in making the hardcopies of the images presented in this paper is gratefully acknowledged.

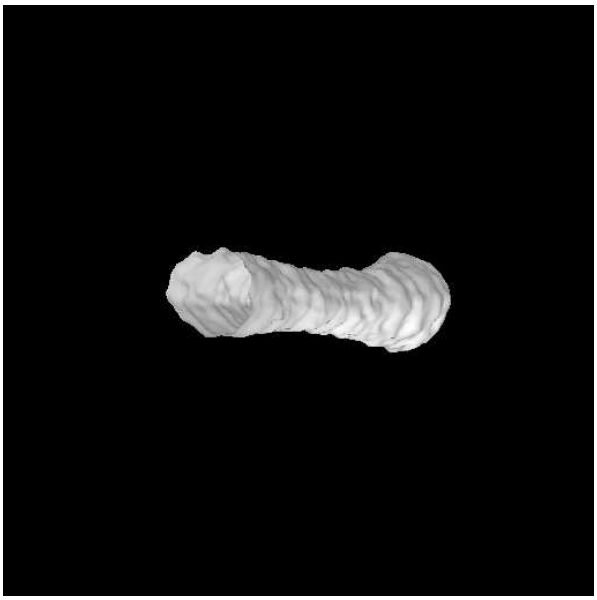

Figure 9.6: Reconstructed view of the stenosed arterial segment of Figures 4 and 5.

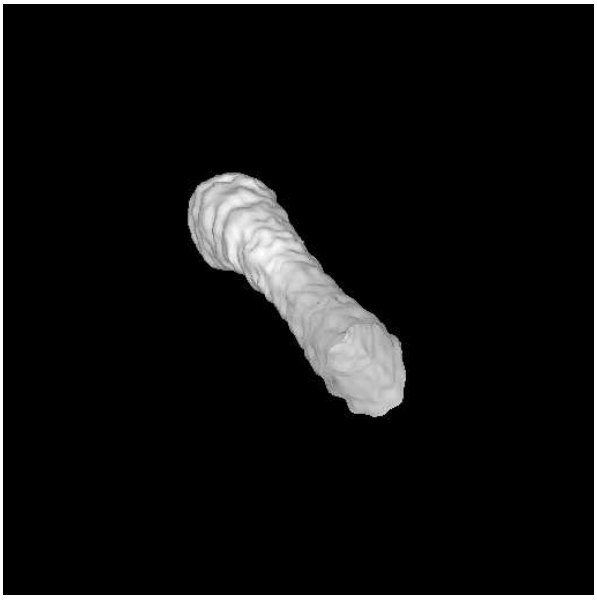

Figure 9.7: Reconstructed view of the stenosed arterial segment of Figures 4 and 5.

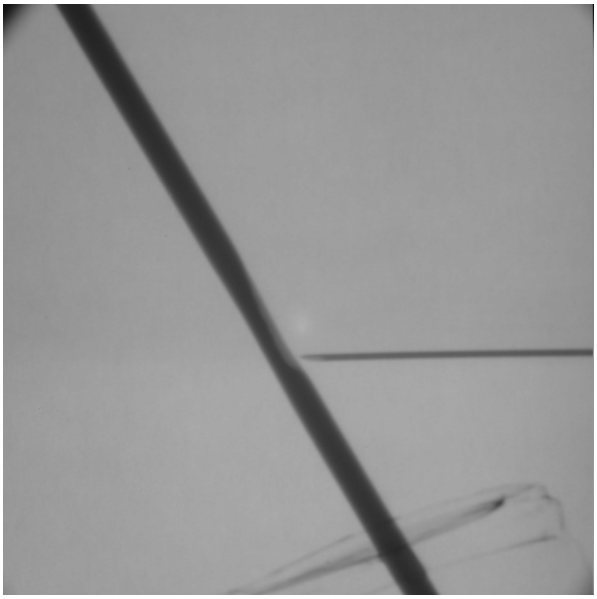

Figure 9.8: Frontal angiogram occluded catheter.

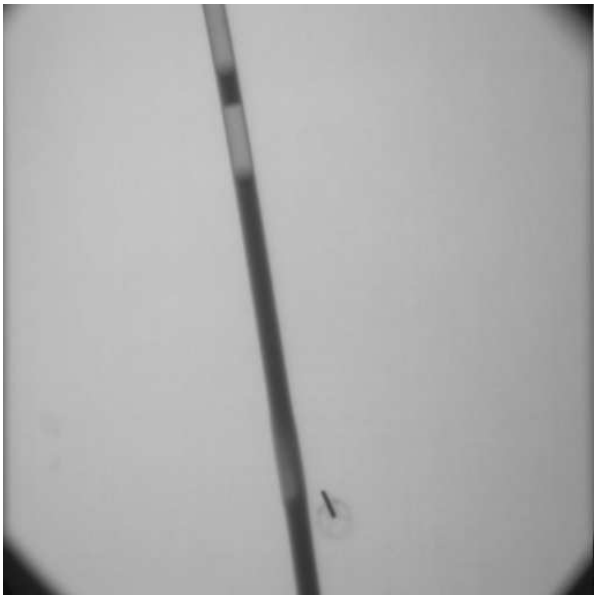

Figure 9.9: Lateral angiogram occluded catheter.

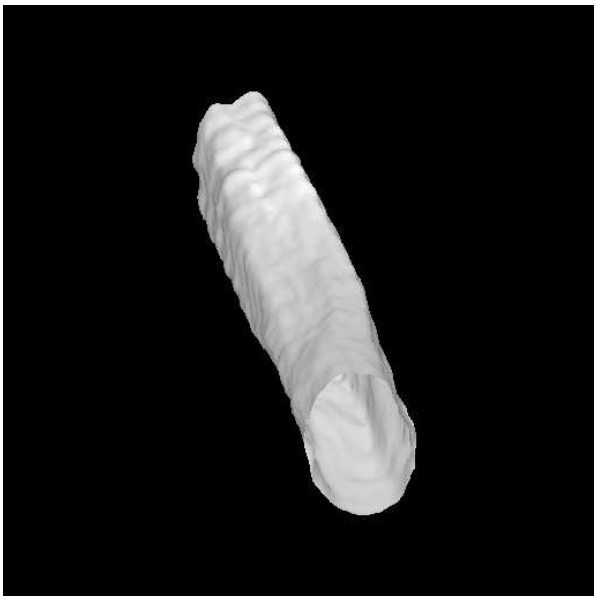

Figure 9.10: Reconstructed view of the stenosed catheter segment of Figures 8 and 9.

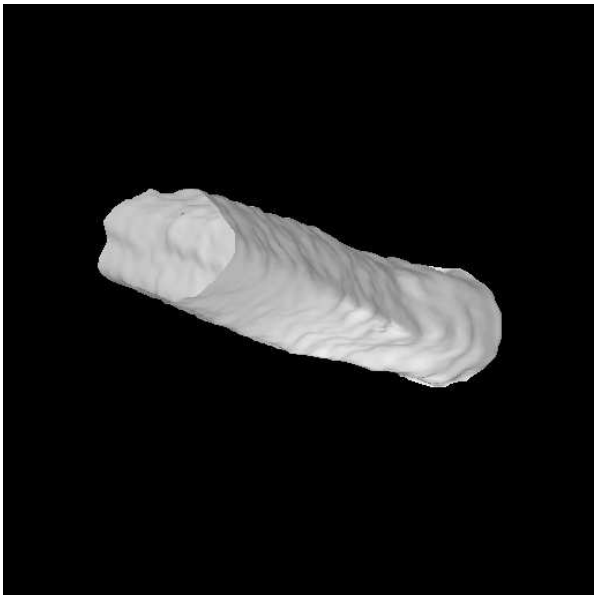

Figure 9.11: Reconstructed view of the stenosed catheter segment of Figures 8 and 9.

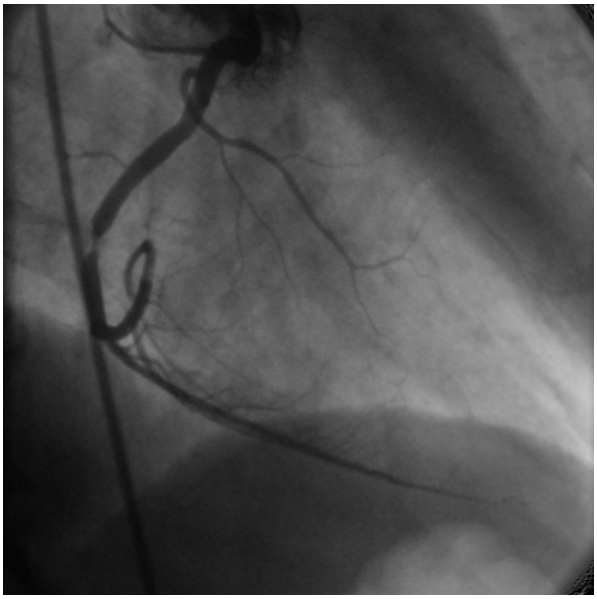

Figure 9.12: Frontal angiogram clinical example.

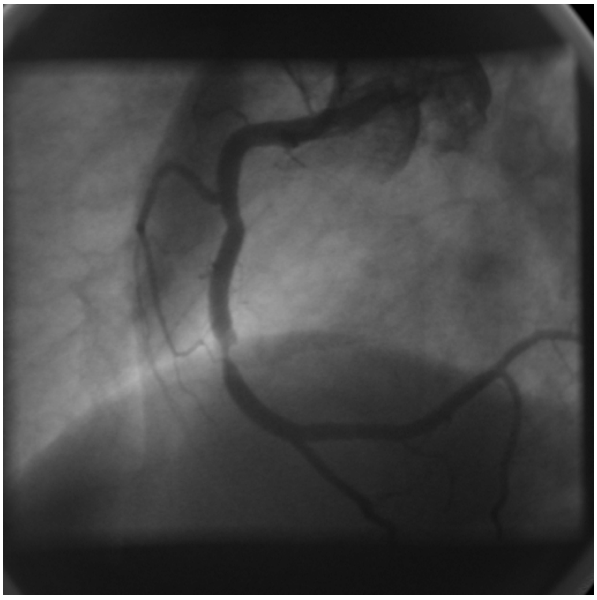

Figure 9.13: Lateral angiogram clinical example.

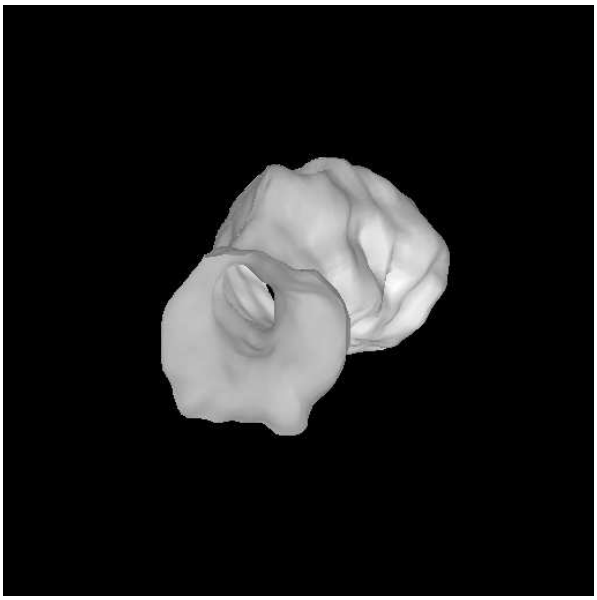

Figure 9.14: Reconstructed view of the stenosed catheter segment of Figures 12 and 13.

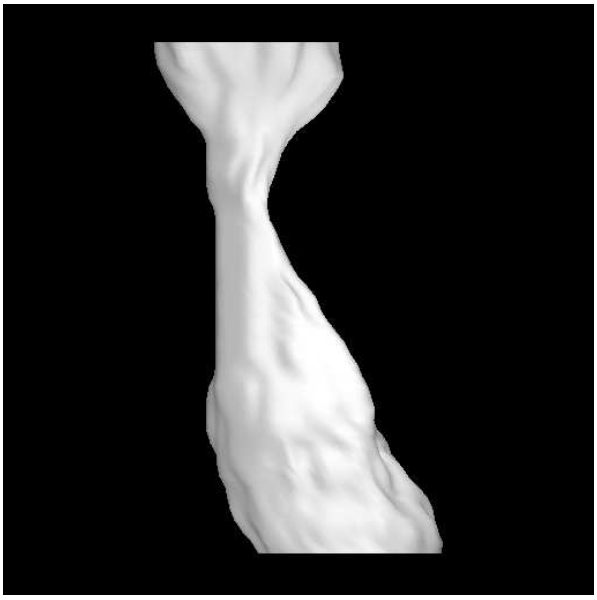

Figure 9.15: Reconstructed view of the stenosed catheter segment of Figures 12 and 13.

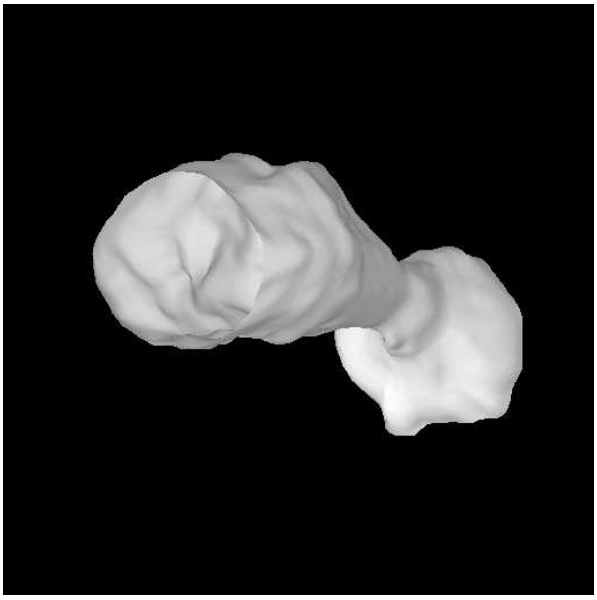

Figure 9.16: Reconstructed view of the stenosed arterial segment of Figures 12 and 13.

Summary

This paper is a part of an ongoing study about the diagnostic benefits of 3D visualization and quantification of stenosed coronary artery segments. Biplane angiographic images do not provide enough information for the reconstruction of the coronary arteries. Therefore, *a priori* information about the 3D shape to be reconstructed must be incorporated into the reconstruction algorithm. One approach is to assume a circular cross-section of the coronary artery. Hence, the diameter is estimated from the contours of the vessels in both projections.

In this paper we base the reconstruction on densitometric information slice-by-slice. We search for a solution of the reconstruction problem close to the previously reconstructed adjacent slice. We apply contour information as well as the densitometrical profiles of the two orthogonal vessel projections which are transformed to the row and column sums, respectively, of a binary matrix.

We present a new probabilistic densitometric reconstruction algorithm, which extends the correct handling of the stochastic properties of the density profiles into the network flow based reconstruction algorithm. The equivalence of the binary reconstruction problem from row and column sums with flow though a capacitated network has been shown by us before. The cost function associated with a flow realization through the network is used to model *a priori* information about the solution to be obtained.

New to this approach is the assigning of a cost function to the source and sink arcs of the network, such that the width of the convex costfunction is inverse proportional to the variance of the probability distribution of the noisy densitometric projection data, *i.e.* the row and column sums respectively.

The reconstructed coronary segment is visualized in three dimensions. In order to assess the accuracy, the method is applied to tubes with artificial obstruction of known geometry, modeling coronary stenoses. These catheter tubes are filled with contrast material. Two typical cases are shown together with one clinical example. The results of the reconstruction and visualization are discussed with respect to clinical usefulness. The results do appear to have rather rough walls which turns these results not suitable for flow impedance calculations. On the other hand, asymmetric occlusions not visible with circular based reconstruction methods, do show up clearly. We will continue this research with the development of densitometrical reconstruction algorithms not based on a slice-by-slice approach in order to preserve the local continuity.

References

[4] Reiber, J.H.C.; Serruys, P.W.; Slager, C.J. Quantitative coronary and left ventricular cineangiography. Dordrecht, The Netherlands: Martinus Nijhoff Publishers, 1986.

[2] Hulzebosch, A.A.; Slump, C.H.; Viergever, M.A. Three-dimensional reconstruction of stenosed coronary artery segments with assessment of the flow impedance. International Journal of Cardiac Imaging 5:135-143, 1990.

[12] Vogel, R.; LeFree, M.; Bares, E.; O'Neill, W.; Forster, R.; Kirlin, P.; Smith, D.; Pitt, B. Application of digital techniques to selective coronary arteriography: use, myocardial contrast appearance time to measure coronary flow reserve. Am. Heart J. 107:153-164, 1884.

[11] Cusma, J.T.; Toggart, E.J.; Folts, J.D.; Peppler, W.W.; Hangiandreou, N.J.; Lee, C-S; Mistretta, C.A. Digital subtraction angiographic imaging of coronary flow reserve. Circulation. 75:461-472; 1987.

[22] Lubbers, A.P.G.; Slump, C.H.; Storm, C.J. Digital densitometric determination of relative coronary flow distributions. In: Acharya, R.S., Goldgof, D.B., eds. Biomedical image processing and biomedical visualization. SPIE 1905, to appear, IS&T/SPIE 1993 International Symposium on Electronic Imaging: Science & Technology, San Jose, CA, 1993

[6] Slump, C.H.; Gerbrands, J.J. A network flow approach to reconstruction of the left ventricle from two projections. Comput. Graph. Image Process. 18:18-36; 1982.

[7] Garreau, M.; Coatrieux J.L.; Collorec R.; Chardenon C. A knowledge-based approach for 3-D reconstruction and labeling of vascular networks from biplane angiographic projections. IEEE Trans. Med. Imag. 10:122-131, 1991.

[8] Van Tran, L.; Bahn, R.C.; Sklansky, J. Reconstructing the cross sections of coronary arteries from biplane angiograms. IEEE Trans. Med. Imag. 11:517-529; 1992.

[9] Pellot, C.; *et al.* A 3D reconstruction of vascular structures from two X-ray angiograms using an adapted simulated annealing algorithm. IEEE Trans. Med. Imag. 13:48-60; 1994.

[5] Reiber, J.H.C.; *et al.* 3D reconstruction of coronary arterial segments from two projections. In: Heintzen, P.H.; Brennecke, R., eds. Digital Imaging in Cardiovascular Radiology. Stuttgart: Thieme; 1983:151-163.

[11] Gerbrands, J.J.; Slump, C.H. 3D reconstruction of homogeneous objects from two Poisson-distributed projections. Pattern Recognition Letters 3:137-145; 1985.

[12] Gonzalez, R.C.; Woods, R.E. Digital image processing. Reading, MA: Addison-Wesley, 1992.

[13] Cowen, A.R.; Haywood, J.M.; Clarke, O.F.; Rause, S. Digital grey-scale fluography: a new approach to radiographic imaging. British Journal of Radiology. 57:533-538; 1984.

[14] Ford, L.R.; Fulkerson, D.R. A simple algorithm for finding maximal network flows and an application to the Hitchcock problem. Canad. J. Math. 9:210-218, 1957.

[15] Klein, M. A primal method for minimal cost flows with application to the assignment and transportation problems. Manag. Sci. 14:205-220; 1967.

[16] Brok, M.; Slump, C.H. Automatic determination of image quality parameters in digital radiographic imaging systems. In: Schneider, R.H.; Dwyer III, S.J.; Jost, R.G.,eds. SPIE vol. 1090, Medical Imaging III: Image Formation; 1989:246-256.

[17] Papoulis, A. Probability, random variables and stochastic processes. NY:McGraw Hill; 1965.

[18] Wagner, R.F. Toward a unified view of radiological imaging systems, part II: noisy images. Med. Phys. 4:279-298; 1977.

[19] Barnes, G.T. Radiographic mottle: a comprehensive theory. Med. Phys. 9:656-667; 1982.

[20] Domain 3D Graphics Metafile Resource Call Reference. HP / Apollo, Palo Alto; 1989.

[31] Verhoeven, L.A.J. Digital Subtraction Angiography. Ph.D Thesis. Technical University Delft, the Netherlands, 1985.

[22] Phong, B.T. Illumination for computer generated pictures. Comm. ACM 18:311-317; 1975.

Chapter 10

Coronary artery diameter variations due to pulse flow propagation[1]

Information about local diameter variations as a response to the pulse flow in the human coronary arteries may indicate the development of artherosclerosis before this can be seen as a stenosis on coronary angiograms. This paper describes the design of an image processing tool to measure this diameter variation from a sequence of digital coronary angiograms. If a blood vessel responds less elastically to the pulse flow, this may be an indication of artherosclerosis in an early stage. We have developed an image analysis and processing algorithm which is able after vessel segment selection by the user, to calculate automatically the vessel diameter variations from a standard sequence of digital angiograms. Several problems are treated. The periodic motion of the vessel segment in the consecutive frames is taken into account by tracking the vessel segment using a 2-dimensional logarithmic search to find the minimum in the mean absolute distance. A robust artery tracing algorithm has been implemented using graph searching techniques. The local diameter is determined by first resampling the image perpendicular to the found trace and afterwards performing edge detection using the Laplacian operator. This is repeated for all frames to show the local diameter variation of the artery segment as a function of time.

[1]presented in part at the 4^{th} International Symposium on Coronary Arteriography, Rotterdam, The Netherlands, June 23-25, 1997, and published as: C.H. Slump, M. Winkelman, H.R. Rutgers, C.J. Storm, and A.C. van Benthem, "Coronary Artery Diameter Variations due to Pulse Flow Propagations," in *Medical Imaging: Physiology and Function from Multidimensional Images*, E.A. Hoffman, ed., *Proc. SPIE* 3033, pp. 187 - 198, 1997.

10.1 INTRODUCTION

10.1.1 Motivation

Coronary angiography plays a critical role in the diagnosis and treatment of patients with heart disease. The severity of circulatory inefficiencies associated with stenoses is commonly indicated by the relative diameter reduction in the stenotic region measured in the angiograms. In general, the influence of stenoses on the blood flow is much more complex.

Besides information about the pressure distribution along an artery, also diameter dynamics may give an estimate of the clinical significance of atherosclerosis. Due to the elasticity of the vessel wall the vessel diameter will vary with pressure. [1] This induces a pulsatile conduction enlarging the blood flow capacity. The diameter variation depends on the elasticity of the wall. An artery with a flexible, healthy wall is therefore likely to show more diameter variations than a non-flexible, diseased part with artherosclerosis.

Since the endothelium of the coronary arteries is already affected before this can be shown as a stenosis on an angiogram, atherosclerosis may be diagnosed in an early stage by measurement of diameter variation as a function of time. Early diagnosis of the disease may simplify treatment considerably. It is anticipated that the quantities to be determined will be such small that it is extremely difficult for a human observer to determine the required quantities with high enough accuracy. This paper is directed to automatic measurement of the local diameter of an artery segment as a function of time.

10.1.2 Problem structuring

As put forward in the previous section, information about the diameter variation of an artery segment as a function of time may yield information about the clinical relevance of atherosclerosis in that segment. To obtain this information we thus need to measure the vessel diameter in the same arterial segment in several consecutive frames over at least one period of the cardiac cycle. In this section we analyze the requirements to solve the problem.

A cardiologist would be able to indicate the segment of interest to be analyzed in all frames manually, but this is a very time-consuming approach. Furthermore one of the main reasons for the development of quantitative coronary arteriography (QCA) was the reduction of inter- and intra-observer variability. We thus choose for an automated approach of the selection of the regions of interest (ROIs) in a series of frames. In the clinical application it is still the cardiologist who is responsible for the selection of a ROI in the first frame.

The difficulty in finding the same artery segment back in subsequent frames is that the ROI will not be located at the same place in all the frames

due to the cardiac motion. In [2] a useful method of finding the indicated ROI back in subsequent frames is described. The main features of this method are discussed in Section 10.2. In the ROI as selected by the cardiologist, starting point and end point of the segment to be analyzed must be indicated. To enable measurement of vessel diameter we must first trace the artery segment between starting point and end point. The tracing algorithm is described in Section 10.3.2. After tracing the segment we can detect the edges in the segment and determine the diameter. Edge detection is discussed in Section 10.4.

This procedure must be repeated for every found ROI. We can, however, not assume that the locations of starting point and end point remain the same in all ROIs. These locations will vary (slightly) due to changes in the size and shape of the arteries to be seen in the ROIs. The localization of starting point and end point of the artery in consecutive ROIs is discussed in Section 10.3.1.

The result demands user input at two stages. First the user must indicate the ROI, and second the user must indicate starting point and end point of the artery segment in the first ROI.

10.2 MOTION COMPENSATION

During a cardiac cycle the wall of the heart and therefore also the coronary arteries are in periodic motion. The location of the segment of interest will thus vary from frame to frame. To obtain reliable diameter measurements it is necessary to analyze the same arterial segment throughout the whole cardiac cycle. Apart from noise, wash-out of contrast agent and other disturbing phenomena caused by the acquisition system, also geometrical factors may complicate the motion compensation algorithm. The algorithm should be able to keep track of the pertinent artery in the case other vessels of similar shape and orientation are in the vicinity or even occasionally overlap the artery. The artery may also change shape and orientation through the cardiac cycle caused by the constriction and dilation of the heart wall.

10.2.1 Mean absolute distance

The new position of the artery segment can be found using correlation techniques. These techniques use a ROI including the artery segment we are interested in. This ROI, selected manually in the first frame, is 'fitted' in the next frame by shifting the ROI over the frame and determining for every position the degree of similarity between the ROI and the underlying picture. The position for which the similarity is maximal is chosen as the new position of the arterial segment. So we need a measure for the similarity. The mean absolute distance (MAD) is such a measure. The mean absolute distance $d_{n,m}$

between the ROI $h_{x,y}$ and the underlying image $f_{x,y}$ at a position (n, m) in the image is found in the following way:

$$d_{n,m} = \frac{1}{(2K+1)(2L+1)} \sum_{k=-K}^{K} \sum_{l=-L}^{L} |f_{n+k,m+l} - h_{k,l}| \tag{10.1}$$

The constants K and L give the sizes of the ROI. This means that the template always has odd values for the width $(2K+1)$ and height $(2L+1)$. The n and m values where the difference function is minimal is the new position of the ROI.

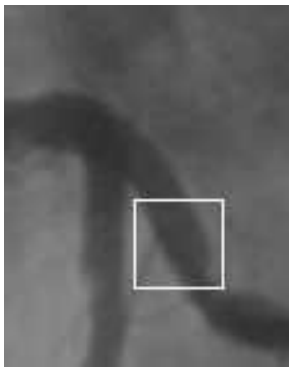

(a) Original image, with ROI

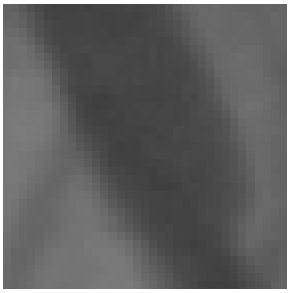

(b) ROI, enlarged

(c) Inverted difference image

Figure 10.1: Computation of summed absolute difference.

10.2.2 Minimization of the difference function using direct search

Equation 10.1 describes a criterion function indicating the similarity between our ROI and the underlying image. To find the position of the artery segment in the next frame, we need to minimize this function. Minimization of the criterion function is for two reasons not as trivial as it may seem. First, the number of points for which the difference function must be calculated is very large. Second, several local minima may be present. Searching the entire difference image for the global minimum is simple, but very time-consuming. It is more efficient to search for a local minimum starting from an initial position. In that case it is not necessary to compute the difference function for all possible positions. This simple, but efficient approach is described below [2].

The position of the ROI is vector $\mathbf{c}_k$. In a 4-neighborhood (horizontally and vertically adjacent points) or a 8-neighborhood (horizontally, vertically or diagonally adjacent points) of $\mathbf{c}_k$ we determine the position with the lowest difference function (Equation 10.1). This gives us the direction $\mathbf{d}_k$ of the gradient in the point $\mathbf{c}_k$.

$$\mathbf{d}_k = \mathbf{c}_{k+1} - \mathbf{c}_k \tag{10.2}$$

The position thus found is the new starting position $\mathbf{c}_{k+1}$. Now we continue to look in the direction $\mathbf{d}_k$ and localize the new minimal neighbor. When we arrive at a local minimum there is no point in a 4- or 8-neighborhood with a lower difference function than the current position, thus $\mathbf{d}_k = \mathbf{0}$. If we do not find a position in a 4- or 8-neighborhood with a lower difference function, but we do find a point with an equal value for the difference function, we still proceed in that direction. The complete procedure is illustrated in Figure 10.2a and 10.2b.

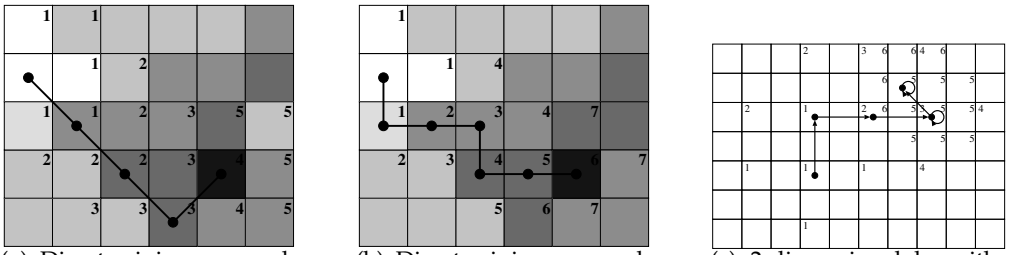

(a) Direct minimum search in a 8-neighborhood

(b) Direct minimum search in a 4-neighborhood

(c) 2-dimensional logarithmic minimum search, initial step size 2^1

Figure 10.2: Minimum search, the numbers i in the squares indicate the search steps in which the differences were calculated for the first time.

The procedure described in the previous section will always result in a local minimum. However, it is not guaranteed that we end up in the minimum we are actually looking for. In fact since we only use local information, it is very likely that the search results in a false local minimum if the distance between the position in the previous frame and the correct position in the current frame is very large. This distance can be reduced by using a suitable motion prediction algorithm[2] or a high frame rate.

10.2.3 Minimization of the difference function using 2-dimensional logarithmic search

The two-dimensional logarithmic search tries to overcome the problems mentioned in the last paragraph by evaluating points at a larger distance from the starting point of search. The algorithm is also described in [3, p. 99–100]. At each step, the search is done only at the five positions that include a middle point and four points in the two main directions, horizontal and vertical. In the first step, the five points evaluated are the starting point of search and the four points at a horizontal or vertical distance 2^n of the starting point. This is repeated with the minimal point from the previous step as the new center point. If the optimum is at the middle point, among the five points, then the search area is decreased by half. Thus the new step size then becomes 2^{n-1}.

This procedure continues until a 3 x 3 search area is obtained (step size is 2^0). In this last step, all nine positions are tested in order to determine the position of the minimum. Figure 10.2c illustrates the search method with an initial step size of 2.

10.3 ARTERY LOCALIZATION AND ARTERY TRACING

After having compensated the motion of our ROI, we need to do the same for the artery segment within the ROI. Even though we have localized the arterial segment globally by applying motion compensation to our ROI, changes in shape, orientation and size of the artery segment we are interested in may cause local variations in the position of the starting point and the end point of the arterial segment to be measured. Figure 10.3a and 10.3b illustrate this localization problem, note the movement of the starting point and end point. Having obtained a starting point and an end point inside the artery segment, we need to trace a path line within the artery. This path line is necessary to determine scan lines (approximately) perpendicular to the local artery direction.

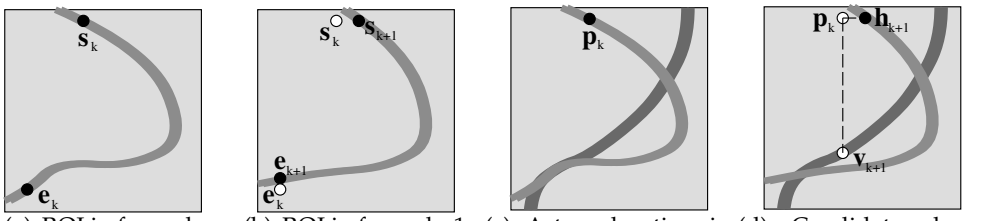

(a) ROI in frame k (b) ROI in frame k+1 (c) Artery location in frame k (d) Candidate locations in frame k+1, using the nearest local minima along axes

Figure 10.3: Artery localization

10.3.1 Artery localization

From Figure 10.3b arises a possible solution to the localization problem. As the darkest points are likely to correspond with the centre of the artery, we should search for a local minimum starting at the position found in the previous ROI. To avoid local minima due to noise, we apply uniform low-pass filtering first. Starting from the initial point, we look for the nearest local minima in two directions: along a horizontal and along a vertical line. We thus find the nearest local minima $\mathbf{h}_{k+1}$ (on a horizontal line through $\mathbf{p}_k$) and $\mathbf{v}_{k+1}$

(on a vertical line through $\mathbf{p}_k$) as candidate points for the new position $\mathbf{p}_{k+1}$. Figure 10.3c and 10.3d illustrate the method.

This approach is not disturbed by structures like overlapping arteries and background noise, but there is an other important source of errors. Consider the case where a part of the artery is in horizontal or vertical direction. If the initial search point is already located inside the artery, the new position we find may have drifted along the artery to the thickest and thus darkest point of the artery.

To circumvent this problem we try to search in a direction perpendicular to the local orientation of the artery itself. However, since we have not localized the artery segment at this point yet, we do not have any data about the local orientation of the artery. Still, we can find a reasonable estimate of the direction. We use the direction of the artery segment in the previous frame as an estimate for the local orientation in the current frame.

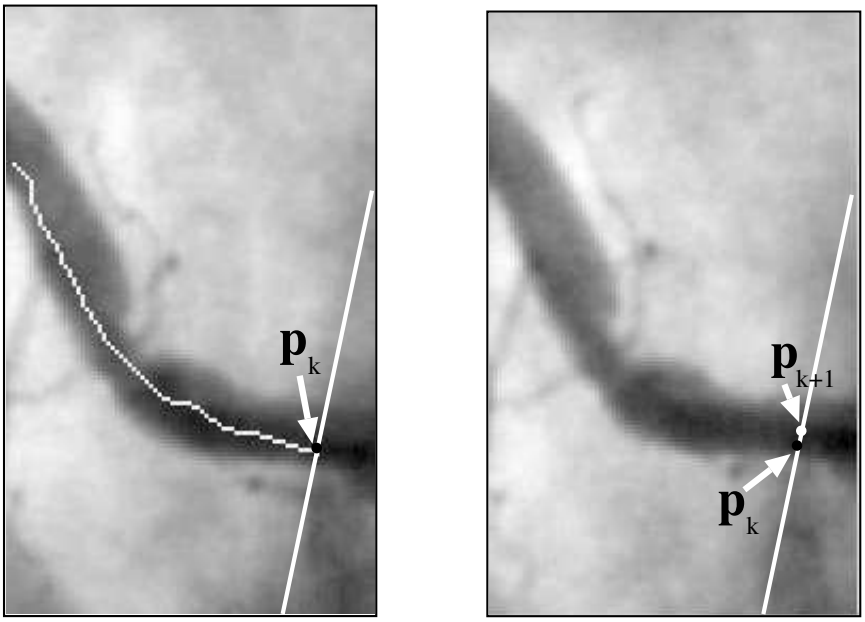

(a) Artery location in frame k (b) Artery location in frame k+1

Figure 10.4: Artery localization using perpendicular search line

Figure 10.4a shows ROI k and a traced path line in the artery segment. The straight line is perpendicular to the artery orientation in the point $\mathbf{p}_k$. Figure 10.4b shows ROI $k+1$. The point $\mathbf{p}_k$ and the straight line have been copied from ROI k. The point $\mathbf{p}_{k+1}$ is the nearest local minimum along the line starting from $\mathbf{p}_k$.

Even though the local direction may have changed from one frame to the other, this change is not likely to be such that the point we are looking for is

drifting along an artery. This method overcomes the problems described in the previous sections. Note, however, that we are implicitly assuming that the movement of the artery within the ROI is approximately perpendicular to the local artery direction. Movements parallel to the local artery direction still cause an incorrect localization.

10.3.2 Artery tracing

This section deals with a tracing method based on graph searching techniques. The advantage of this approach is the use of global information to reduce the sensitivity for local disturbing effects as side branches, overlaying arteries and dark background structures. Since arteries are shown as dark structures on a light background, we are looking for a path line connecting the starting point and end point with the lowest average pixel value. This searching is simplified considerably if we know in advance the number of points in the path. We can fix the number of points in the path using resampling and directed graph searching. After having obtained the path, it has to be positioned back in the original image space.

Image resampling

Figure 10.5a illustrates the resampling proces. The white circles in Figure 10.5a show the pixel positions in the original image space. Let $\mathbf{s} = (x_s, y_s)$ be the starting point and $\mathbf{e} = (x_e, y_e)$ the end point. In Figure 10.5a these are the black circles. Draw a line $\mathbf{l}$ between $\mathbf{s}$ and $\mathbf{e}$. Calculate the coordinates of all points on the line $\mathbf{l}$ and at a distance d from $\mathbf{s}$ that is an integer multiple of the pixel distance. These points are given by the black squares in Figure 10.5a. Now resample the original image along lines perpendicular to $\mathbf{l}$ and through the black squares. The pixel positions in the resampled image are given by the squares. In general the grid points in the resampled space will not correspond to grid points in the original image space. We therefore need to apply an interpolation to obtain the grey values at the grid points in the resampled image space.

We use bilinear interpolation. The choice for this interpolation technique is the result of a tradeoff between the algorithmic complexity on one hand and the accuracy of the frequency response on the other hand [4, p. 18–22]. The points $\mathbf{p}_1 (= (x_1, y_1))$ to $\mathbf{p}_4$ in Figure 10.5b are grid points in the original image space, $\mathbf{p}_5$ is a grid point in the resampled image space. Define $g(x, y)$ as the grey value at the point (x, y). Then Equation 10.3 describes the bilinear interpolation mathematically.

$$\begin{aligned} g(x_5, y_5) \;=\; & (1-b)(1-a)\, g(x_1, y_1) + a(1-b)\, g(x_2, y_2) \\ & + (1-a)b\, g(x_3, y_3) + ab\, g(x_4, y_4) \end{aligned} \tag{10.3}$$

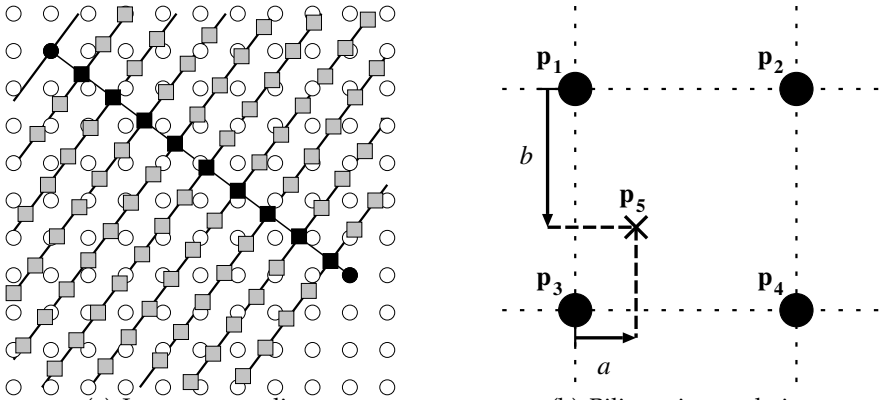

(a) Image resampling (b) Bilinear interpolation

Figure 10.5: Image resampling, in the left figure, the black dots are the user indicated starting and end points, white dots are pixel positions in the original image space, squares are pixel positions in the resampled image space.

Directed graph searching

After the resampling has been performed, we need to search for a path from top to bottom in the resampled image connecting the middle element of the top row to the middle element of the bottom row.

The graph searching without the restriction of starting and ending in the middle of the top and bottom row is described below. We only want to find a path, connecting top and bottom row, with one element of each row in the path. Each pixel in row number k can only be connected to the three nearest points in row number $k+1$. We thus guarantee 8-connectedness of the found path in the resampled image space. Figure 10.6 illustrates this.

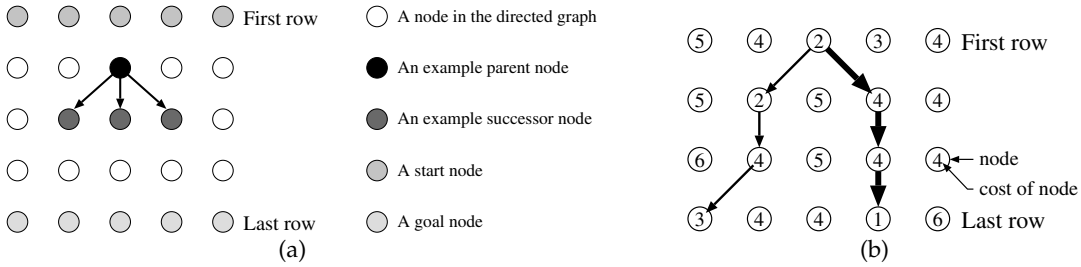

Figure 10.6: Directed graph searching, (a) directed graph in which each node corresponds to a pixel in the resampled image, (b) two example paths through the directed graph, the cost associated with each node (number in circle) is equal to the pixel value in the resampled image, the path marked with the bold arrows is the lowest cost path.

The nodes of the graph correspond to the pixels in the resampled image.

Now associate a cost with each node. The costs should be inversely related to the likelihood that the node belongs to the path line through the artery. Let us define the cost of a certain node in the directed graph as the grey value of the corresponding pixel in the resampled image. This corresponds to our idea of dark points (lower pixel values) having a large likelihood of belonging to the artery segment. The search algorithm can be described as follows (according to [5] [6]).

Heuristic search

The algorithm starts with a sorted list containing the candidate start nodes in the first row. This list is referred to as the OPEN list. The lowest cost node (the current node) is removed from the OPEN list and if it is not a goal node its successors are generated. In this step also a link from the successors back to the parent is made. The cost of the path to a successor is calculated as the sum of the cost of the successor and the cost of the path to the parent. A node can only be expanded as a successor node if it is not already on the OPEN list or has been removed from that list. If a node is removed from the OPEN list, it is marked as CLOSED, thus avoiding duplicate expansion of that node. The process of removing nodes from the OPEN list and expanding them stops when the node to be removed is a goal node in the last row. If the final node is reached, a path is traced back from the goal node to the start node.

The algorithm described before guarantees that we find the minimal cost path from top to bottom. However, we have an additional restriction, the path should connect the middle of the top row to the middle of the bottom row. We can implement this restriction very simply in the graph searching technique. Figure 10.7 shows this.

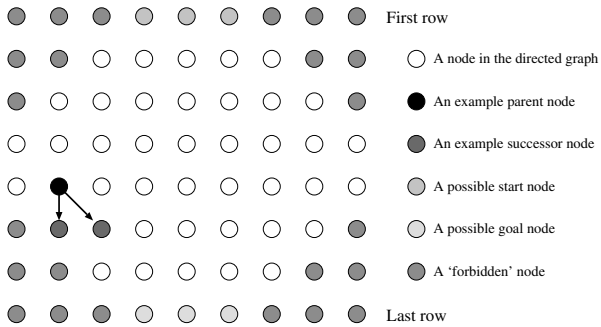

Figure 10.7: Restricted graph searching, the resulting trace must start and end 'near' the center column.

We demand that the path starts and ends 'near' the middle of the top and bottom row respectively. The specification of 'near' is given by the number of pixels that the start or end of the path is allowed to deviate from the center pixel. In Figure 10.7 this number is 1. This value is an input parameter for

the restricted graph searching algorithm. Since we demand 8-connectivity of the complete path, we can tell beforehand what nodes can never be included in the resulting path. We mark these nodes as 'forbidden'. 'Forbidden' nodes can never be added as successor nodes in a path.

The center column in Figure 10.7 is the resampling line. The path that is obtained through the graph searching algorithm consists of 8-connected nodes, exactly one at each row. We define the local path orientation as the direction of the line connecting two adjacent points in the path. From Figure 10.7 it is clear that the maximal angle between the resampling line and the resulting path is 45 degrees.

Back projection to original image space

After the step described in the previous section a path line through the artery in the resampled image space has been found. Now this path line has to be projected back to a path in the original image space. We know the width of the scan lines used in the resampling, we know the original position of the center pixel of each scan line in the resampled image and we know the angle between horizontal lines in the original and the resampled image.

All ingredients for conversion of a position in the resampled image to a position in the original image are thus available. The coordinates in which the back projection results will in general not be integers. We convert the resulting coordinates to pixel positions in the original image space by rounding to the nearest integers.

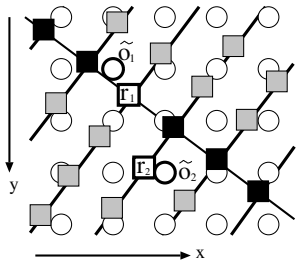

Figure 10.8: Back projection to original image space, $r_1 = (x_{r,1}, y_{r,1})$ and $r_2 = (x_{r,2}, y_{r,2})$ are points in the resampled image space, $\tilde{o}_1 = (\tilde{x}_{o,1}, \tilde{y}_{o,1})$ and $\tilde{o}_2 = (\tilde{x}_{o,2}, \tilde{y}_{o,2})$ are the respective nearest neighbors in the original image space.

We demanded 8-connectivity of the path line in the resampled image space. Due to the back projection into the original image space, this 8-connectivity is no longer guaranteed. In [7] is found that the size of the holes in the back projected path line can never be larger than 1 by 2. A simple dilation operation [6] will close these gaps. The dilation operation results in a line that will be more than one pixel wide. In order to obtain a path line

of single pixel width we need to extract the skeleton of this line, meanwhile keeping 8-connectivity. The skeletonization procedure is described in more detail in [8].

The result of the procedure described here is a smooth path connecting start and end point through the artery. Two error sources may disturb the results of this method. First, there is the possibility of a second artery branch crossing the artery we wish to detect at least twice between the start and end point. Second, the resulting path deviates maximally 45 degrees from the vertical axis of the resampled image due to the demanded 8-connectivity, (refer to the text at the end of Section 10.3.2) Thus if the real artery deviates more than this amount from the vertical axis in the resampled image, the trace will leave the artery. Both problems are not likely to cause erroneous results if the segment to be traced is relatively short. For longer segments, the two problems mentioned above may cause errors. However, both problems can be solved very simply. Because one can visibly identify both error sources in advance, one can circumvent the errors by selecting a third or even fourth point and tracing the artery between consecutive points.

10.4 DIAMETER DETERMINATION

In the previous step we find a path line through the artery. We therefore know that the vessel edges must lie on both sides of this detected path line. We search for the edges by examining the changes in grey level in a direction perpendicular to the local artery direction. Edge detection is simplified considerably if we resample the image along lines perpendicular to the centerline, as in Section 10.3.2 , to obtain a stretched artery segment in vertical direction. Our approach is an edge enhancement of the stretched image followed by the Laplacian edge detector.

10.4.1 Edge enhancement

Smoothing an image by applying some kind of weighted averaging in a subwindow of the original image, tends to blur changes in the image. In fact we would like to filter the image in order to reduce noise and small disturbing features without blurring the real edges in the image. This procedure is known as edge preserving smoothing. In uniform (low-pass) filtering, every pixel in the image is replaced by the averaged pixel value of its $N \times N$ neighbors. In edge preserving smoothing, this procedure is slightly adapted. The image is scanned with a moving window with dimensions $N \times N$. This moving window is subdivided into four sub-windows. In each sub-window the variance of the pixel values is calculated. The window with the lowest variance is taken as the averaging window. The resulting average value is stored

in the center pixel of the current location of the moving $N \times N$ window. This approach tends to avoid blurring of the sub-windows with large variations in pixel values, e.g. due to the presence of an edge.

10.4.2 The Laplace operator

The Laplacian of an image function $f(\mathbf{x})$ is defined to be the sum of the second spatial derivatives. We use three different 3x3 window operators as a discrete approximation for the Laplacian:

$$l_1 = \begin{bmatrix} 0 & -1 & 0 \\ -1 & 4 & -1 \\ 0 & -1 & 0 \end{bmatrix} \qquad l_2 = \begin{bmatrix} -1 & -1 & -1 \\ -1 & 8 & -1 \\ -1 & -1 & -1 \end{bmatrix} \qquad l_3 = \begin{bmatrix} 1 & -2 & 1 \\ -2 & 4 & -2 \\ 1 & -2 & 1 \end{bmatrix} \tag{10.4}$$

Convolution of an image in the spatial domain with the windows given above, is equal to multiplication of the Fourier transforms in the frequency domain. Let the Fourier transforms of the windows l_1, l_2 and l_3 be given by $L_1(u,v) = \mathcal{F}\{l_1(\mathbf{x})\}$, $L_2(u,v) = \mathcal{F}\{l_2(\mathbf{x})\}$ and $L_3(u,v) = \mathcal{F}\{l_3(\mathbf{x})\}$. Figure 10.9a shows the Fourier spectrum of the Laplacian. Figures 10.9b–d show the Fourier spectra of the discrete approximations to the Laplacian.

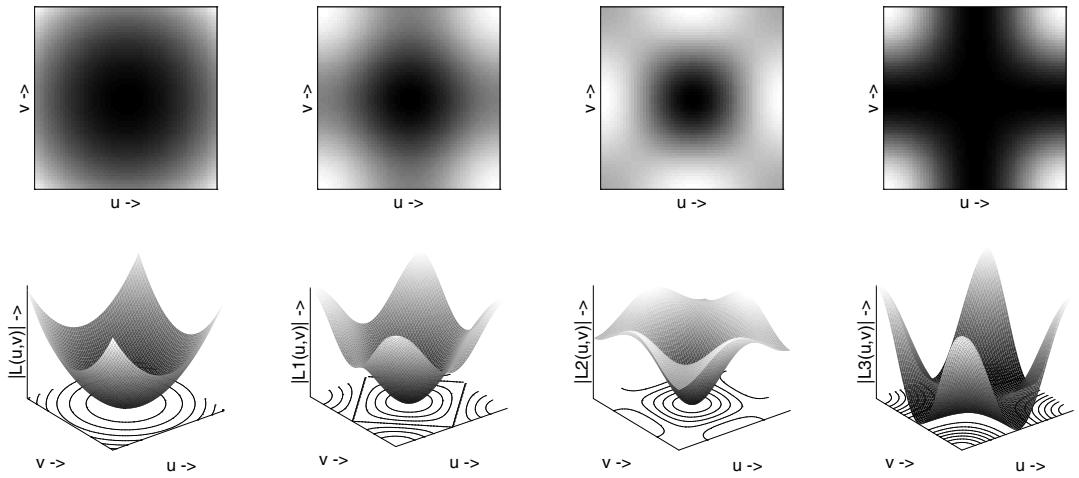

(a) Laplacian (b) 3x3 window l_1 (c) 3x3 window l_2 (d) 3x3 window l_3

Figure 10.9: Fourier spectra of the Laplacian and three discrete approximations.

From Figure 10.9a it is clear that the Laplacian is an isotropic or directionally invariant operator. The window operators l_1 and l_2 show approximately the same behavior for low spatial frequencies. For higher frequencies, however, l_1 emphasizes diagonal changes more than horizontal or vertical

changes and l_2 emphasizes horizontal and vertical changes more than diagonal changes. The window operator l_3 approximates the Laplacian only in diagonal directions, in horizontal and vertical directions it does not emphasize changes at all. Based on the emphasis on vertical and horizontal edges of operator l_2 (from Figure 10.9) and the fact that we want to detect edges in vertically oriented arteries, we choose to use the window l_2.

10.5 RESULTS

In this section we will discuss the results of the subproblems one by one. We will use images from several test runs to illustrate the complete implementation.

10.5.1 Motion compensation

Both search methods (direct search and 2-dimensional logarithmic search) were performed and compared. In our case, the direct searching is considerably faster than the 2-dimensional logarithmic (2DL) search. However, we can see from Table 10.1 that the 2DL search method is more robust. In sequences with larger motions of the ROI between frames, the 2DL search method performs better than the direct search method.

10.5.2 Artery localization and artery tracing

The artery localization algorithm seems robust. In all test runs the found location was inside the correct artery. However, the exactness of the algorithm is very hard to judge. One can never be sure that the found point is exactly the same as the point in the previous frame. In some runs it was observed that the found position shifted along the artery due to movement of the artery within the ROI along its own orientation. Figures 10.10a and 10.10b give an illustration of the artery localization results.

The graph searching method used for artery tracing is very robust. Starting and end point are always connected and in the case of short segments the errors as mentioned in Section 10.3.2 never occurred. Also in the case of side branches the path still follows the center line of the artery and does not deviate in the direction of the side branch. Figures 10.10c and 10.10d give an illustration of the artery tracing results.

10.5.3 Diameter determination

Figures 10.11a-c show a comparison of measured phantom vessels of known size. We see a slightly better performance of the largest window, Figure 10.11c. The least squares fit crosses the vertical axis closest to the origin.

Table 10.1: Results of motion correction algorithm, n is the number of frames to be corrected, $\overline{e}$ is the average number of MAD evaluations per frame, $\overline{|dx|}$ and $\overline{|dy|}$ are the average distances (in x- and y-directions) between starting point of search and correct location, f is the number of the frame where the algorithm first failed to find the true location of the ROI.

		direct search				2-d logarithmic search			
run nr	n	$\overline{e}$ [1]	$\overline{\|dx\|}$ [1]	$\overline{\|dy\|}$ [1]	f	$\overline{e}$ [1]	$\overline{\|dx\|}$ [1]	$\overline{\|dy\|}$ [1]	f
1	19	29.95	2.89	5.42	-	42.00	3.42	5.68	-
2	19	44.50	4.83	8.33	7	45.83	4.83	8.33	7
3	19	26.95	3.21	4.00	-	41.47	3.32	3.84	-
4	18	11.67	0.78	1.44	-	34.56	0.78	1.56	-
5	24	95.00	7.00	21.00	2	51.50	8.67	10.17	7
6	24	35.82	2.54	7.21	-	40.13	2.46	7.21	-
7	20	22.45	4.00	1.82	12	41.32	4.16	2.05	-
8	39	10.92	0.67	1.18	-	33.10	0.69	1.31	-
9	27	31.07	2.89	5.30	-	38.85	2.81	5.59	-

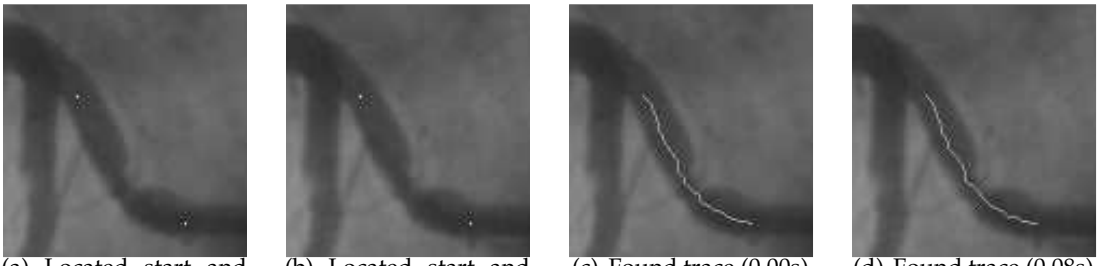

(a) Located start and end point (0.00s)

(b) Located start and end point (0.08s)

(c) Found trace (0.00s)

(d) Found trace (0.08s)

Figure 10.10: Artery location and tracing in 2 consecutive frames (12.5 frames per second).

For small diameters the results are better if the size of the edge enhancement window is smaller.

After evaluation of the edge detector on phantom images, the edges were determined on the stretched artery segments. The edge enhancement window size used in the edge detection is 5×5. The discrete Laplacian approximation is given by mask number 2 (window l_2 and spectrum $|L_2|$ in Figure 10.9c).

Since we do not know the true location of the edges, it is very hard to specify the quality of the edge detection. One situation where the algorithm does not place the edges at the expected correct place is in the case of side branches or crossing vessels. In these cases the algorithm tends to follow the side

[1] Data from frames where the algorithm had already 'lost' the ROI have not been included.

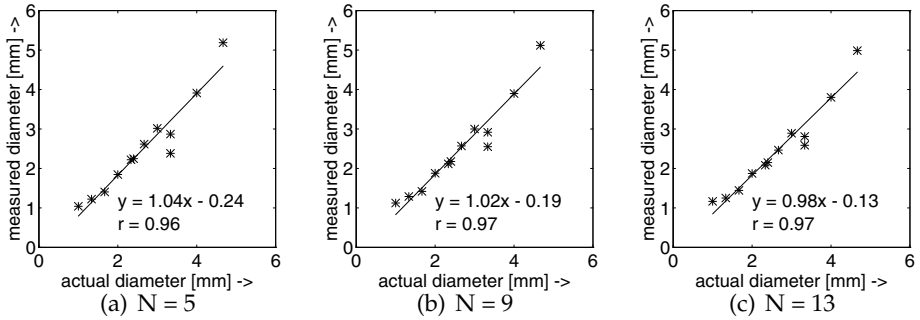

Figure 10.11: Comparison of phantom diameters using edge enhancement followed by the Laplace edge detector type l_2, the size of the edge enhancement window is $N \times N$.

branch or crossing vessel to return to the intended artery later. Figure 10.12c illustrates this. Though this problem may in many cases be avoided by careful selection of the ROI in the first frame it can never be ruled out completely. Since the relative position of vessels is not fixed, it may happen that a secondary vessel does not appear in the ROI in the first frame, but does cross the artery of interest in one of the later frames.

10.5.4 Complete results

The algorithm performs the diameter determination for all frames and finally generates a curve that shows the average diameter and standard deviation of the selected artery segment as a function of time, see Figure 10.13a. The image sequence was obtained with an acquisition rate of 50 frames per second and a cardiac cycle period of 0.60 seconds. Unfortunately no ECG-triggering information was available. The artery segment was taken from a proximal site of the left anterior descending coronary artery. The curve shows pulsatile diameter changes of $\pm 4\%$, with an artery diameter of 3.5 mm corresponding to diameter deviations of approximately 150 μm. The standard deviation originates for a large part from the roughness of the arterial wall and thus cannot be used as a measure for the accuracy of the edge detection.

The algorithm also generates a map of the local artery diameter as a function of time (horizontal) and position at the artery segment, see Figure 10.13b. This artery segment of about 20 mm length was taken from the same branch as Figure 10.13a and contained a stenosis. The user is able to move a crosshair over the map to examine simultaneously the diameter as a function of time at a certain position (horizontal black curve) and the diameter as a function of position at a certain time (vertical black curve). The map shows that before the stenosis, at the position of the crosshair, the diameter changes are larger

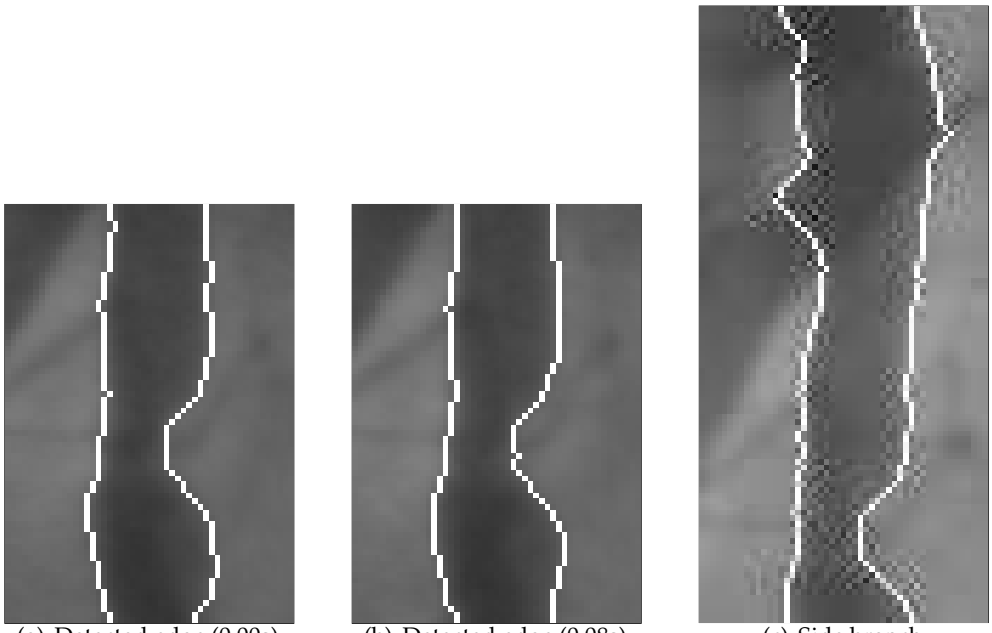

(a) Detected edge (0.00s) (b) Detected edge (0.08s) (c) Side branch

Figure 10.12: Detected edges in 2 consecutive frames, (c) detected edge in the case of a side branch.

than at and after the stenosis, at positions near the time axis.

10.6 CONCLUSIONS

Concluding we can say that the preliminary results are promising, but that still a lot remains to be done. The motion compensation algorithm should be more robust. Currently, we are trying to reach greater robustness by using a hierarchical search algorithm. The user should be able to intervene if the algorithm fails to find a satisfactory ROI.

The artery localization still suffers from inaccuracies (drifting of begin and end point in the artery direction). One way to solve this problem may be to apply the motion compensation algorithm once more *inside* the ROI, restricting the area of interest to a rectangular region containing the trace in the previous frame. The artery tracing algorithm is very robust. The main problem is that the found trace usually deviates from or winds around the real centerline. This causes errors in the diameters derived from edge detection. This deviation can be minimized using an iterative algorithm. Taking the current trace as an estimate for the real centerline, determine the edges, and re-estimate the centerline choosing a trace midway between the found edges.

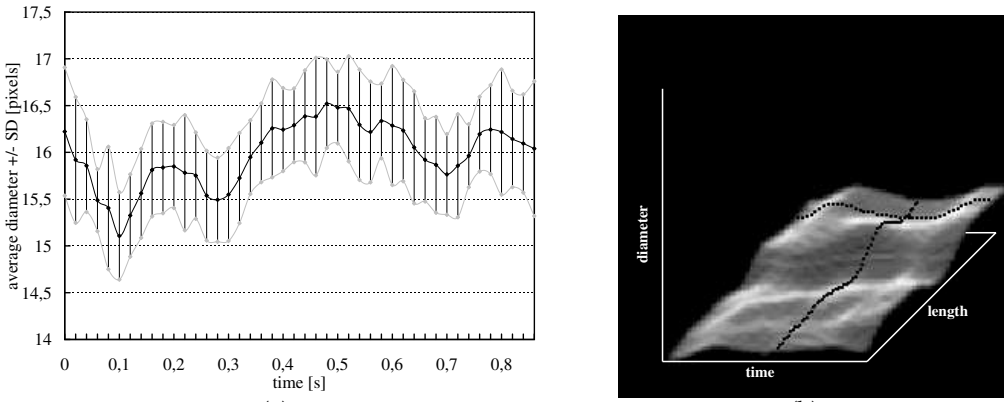

Figure 10.13: (a) Artery diameter in pixels versus time, (b) Local artery diameter map.

The edge detection algorithm never fails to find two candidate edges from top to bottom of the stretched image, but is still too sensitive to side branches (as can be seen in Figure 10.12c). The representation of the diameter in a map as a function of time and length of the artery segment gives a clear overview of the diameter dynamics of the selected artery segment.

A general recommendation can be made. Extra information could be included in the judgement of the result if we would have available the ECG corresponding to the image sequence. We would then also have phase information available.

REFERENCES

References

[1] W. Nichols and M.O'Rourke, *McDonald's Blood Flow in Arteries, theoretical, experimental and clinical principles*, Edward Arnold, London, 1990 (third edition).

[2] M. Winkelman, *Coronair Angio Dynamica*, 250-hours assignment report EL-BSC-043N95, University of Twente, Enschede, the Netherlands, 1995 (in Dutch).

[3] G. Tziritas and C. Labit, *Motion Analysis for Image Sequence Coding*, vol. 4 of *Advances in Image Communication*, Elsevier, Boston, 1994.

[4] M. Bosma and J. Terwisscha van Scheltinga, *Efficient Super Resolution Volume Rendering*, Master's thesis EL-BSC-079N95, University of Twente, Enschede, the Netherlands, 1995.

[5] S. Fleagle, M. Johnson, C. Wilbricht, D. Skorton, R. Wilson, C. White, M. Marcus, and S. Collins, "Automated Analysis of Coronary Arterial Morphology in Cineangiograms: Geometric and Physiologic Validation in Humans," *IEEE Transactions on Medical Imaging* 8, pp. 387 - 400, 1989.

[6] F. van der Heijden, *Image Based Measurement Systems, Object Recognition and Parameter Estimation*, John Wiley, New York, 1994.

[7] H.R. Rutgers, *Determination of Coronary Artery Diameter Variation from Digital X-ray Images*, Master's thesis EL-BSC-012N96, University of Twente, Enschede, the Netherlands, 1996.

[8] C. Hilditch, "Linear Skeletons from Square Cupboards," *Machine Intelligence IV*, pp. 403 - 420, 1969 (reprinted in [9]).

[9] J. Sklansky, ed. *Pattern Recognition: Introduction and Foundations*, vol. 4 of *Benchmark Papers in Electrical Engineering and Computer Science*, Dowden, Hutchingson & Ross, Stroudsburg, PA, 1973.

Chapter 11

Densitometric determination of the flow distribution[1]

The long term goal of this research is to determine the clinical relevance of stenosis. Where most QCA algorithms calculate the decrease in lumen from one angiocardiogram, we seek to determine directly the influence of the stenosis on the blood flow. The method uses only a slightly different clinical approach as compared to 'traditional' noninterventional catheterizations. Instead of injecting a steady flow of contrast agent, we propose to inject a string of small droplets. The resulting string of droplets will enable us to estimate the relative blood flow by measuring their time of arrival in some designated regions. Repeating the same procedure after administering a vasodilative drug, we obtain a relative decrease (or less increase) in blood flow in one of the two distal branches of the bifurcation due to the presence of stenosis. From the resulting X-ray image sequence multiple frames are selected, and the information is combined to find the relative blood velocity. The conclusion is that it is possible to use sequences of images instead of just one image to calculate quantitative results. Major problems to overcome are the respiratory and heart-motions, and differences in acquisition parameters between runs. The usefulness of the new method in real clinical applications and the coherence with other measures are currently under trial.

11.1 INTRODUCTION

Currently, there are several systems available that enable cardiologists to view and analyze coronary angiograms. The more recent ones provide fa-

[1]presented at Medical Imaging 1999: Physiology and Function from Multidimensional Images, and published in part as: M. Schrijver, S. de Bont, C.H. Slump, C.J. Storm, "Densitometric determination of the flow distribution in the bifurcation of the left coronary artery," in *Medical Imaging: Physiology and Function from Multidimensional Images*, Chin-Tu Chen, Anne V. Clough, ed., *Proc. SPIE* vol.3660, pp. 395 - 406, 1999.

cilities for Quantitative Coronary Angiography (QCA). An overview of such systems, together with their advantages and disadvantages can be found for example in articles by Reiber et al. [4, 5, 3]. In modern practice, most stenoses are still being judged by the cardiologist, based on only a few coronary angiograms. Estimation of the (relative) decrease in lumen seems to be the only QCA method generally accepted [11]. Many articles discuss the problems associated with such two-dimensional analyzes of complex three - dimensional phenomena. These problems include proper frame selection,[5] single versus biplane (orthogonal) views, [5] 'eye balling', [6] inter- and intra-observer variability, [7, 1, 2, 10] coherence with post-mortem findings [11] etc. Also the value of lumen estimation in assessing the functional severity of stenoses is subject of many discussions [12, 13]. The current usage of these well-known techniques from the cineflim era is in contrast to availability of more elaborate methods exercising modern digital technology (digital X-ray equipment, fast digital signal processing etc.). The digital technology provides much more opportunities than just viewing the images and measuring (minimal) distances. Especially the fact that the acquired sequences of X-ray images contain much more (digital) information than used in the present-day decision making attracts researchers. Our research mainly focuses on methods to extract that extra information by combining the data from multiple images. The usage of multiple images may cause a slightly cumbersome procedure in comparison with methods only estimating the decrease in arterial diameter. But the combination of information from multiple images and sequences may reveal very useful information about the condition of the heart, its arteries and its veins.

11.2 JUSTIFICATION

As can be concluded from the discussion on the question whether or not lumen estimates can predict the functional severity of a stenosis, [11, 12, 13] it would be beneficial to be able to measure that severity directly. In our research, the functional severity of a stenosis is defined as the extend in which the stenosis influences the blood flow. The method compares blood flow distributions in a large coronary artery, in basal and hyperemic states. The resulting measure, called the Relative Coronary Flow Reserve (RCFR) relates the properties of the two distal branches of the bifurcation to each other. That is, it is a measure of the flow restricting properties of one of the branches as compared to the other branch. The correspondence between the RCFR and the actual severity of the stenosis will be one the topics of our continuing research in this field.

11.2.1 Coronary Artery Bifurcation

In the remaining of this section, we assume that we are able to measure the average blood velocities in reasonably large coronary arteries. The way to do that is described in more detail in the next section (11.3). The velocities to be measured are given by the arrows in Fig. 11.1a. The stenosis in the Left Anterior Descending (LAD) is depicted as a narrowing of the artery (labeled 'Lesion') . The narrowing at the bottom of the picture is a schematic representation of the myocardial bed. This section of the circulation system has normally the largest resistance to the blood flow, and thus dictates the total flow (together with the heart rate and heart stroke volume, of course). In such normal situations, the main arteries and veins do not restrict the blood flow considerably. However, if there is a stenosis as depicted in the LAD, this stenosis may introduce an extra restriction to the blood flow. We are interested in the extend of this restriction. For the development of a more

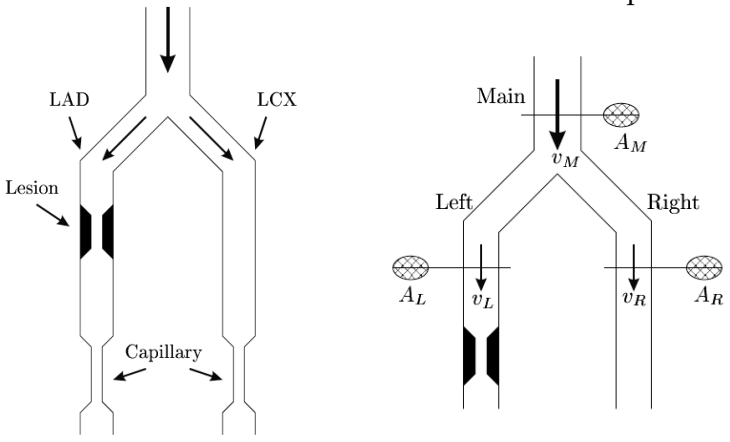

(a) Basic flow model (b) Simplified model

Figure 11.1: Modeling the flow.

general description, we will simplify this model even further, as depicted in Fig. 11.1b. The blood velocities in the three branches of the bifurcation are designated by the symbols v_M for the velocity in the main trunk, and v_L and v_R for the left and right distal branches, respectively. The cross-sectional areas of the arteries at the locations where the velocities are measured are indicated by symbols A, with similar indices. As easily can be seen, we have:

$$\phi_M = \phi_L + \phi_R \quad \text{with} \quad \phi = Av \tag{11.1}$$

since the total volume of blood entering the main trunk must leave the two distal branches. In deriving this equation, we have assumed that there is no storage of blood inside the (arteries of the) bifurcation: the arteries are

modeled by rigid tubes. Now, suppose we have determined that the (baseline) blood flow in the left distal branch has a $\lambda^{(0)}$ times higher velocity than the blood velocity in the right distal branch (the superscript '0' indicates the basal conditions):

$$\phi_L^{(0)} = \lambda^{(0)} v_R^{(0)} \tag{11.2}$$

After administering a vasodilative drug (such as papaverin), we can repeat the procedure to arrive at a second relative blood flow λ in the left distal branch, as compared to the right branch (the superscript 'h' indicates the hyperemic conditions):

$$\phi_L^{(h)} = \lambda^{(h)} v_R^{(h)} \tag{11.3}$$

11.2.2 (Relative) Coronary Flow Reserve (CFR)

A common measures of the severity of a stenosis is the so-called Coronary Flow Reserve (CFR), [14, 7, 16] which is defined as the ratio of maximal coronary blood flow (during maximal vasodilation) to baseline flow. This can be written as (for the left and right distal branches respectively):

$$CFR_L = \frac{\phi_L^{(h)}}{\phi_L^{(0)}} = \frac{A_L^{(h)} v_L^{(h)}}{A_L^{(0)} v_L^{(0)}} \quad \text{and} \quad CFR_R = \frac{\phi_R^{(h)}}{\phi_R^{(0)}} = \frac{A_R^{(h)} v_R^{(h)}}{A_R^{(0)} v_R^{(0)}} \tag{11.4}$$

However, what value to expect? Nissen [17] reports values ranging from 4 to 8 for humans. Also, in an article by Klocke [9] several other factors affecting the CFR, other than the severity of the stenosis are mentioned. Obviously, there will be great variability in the threshold that will (or can) be used as a criterion for a 'severe' stenosis. Also, some methods underestimate the coronary flow reserve due to mixing between contrast and blood [11].

So, our proposal is not to look solely at the CFR of one of the arteries, but to compare it with the CFR of another (known-good) artery and capillary bed. One possibility to do so is to divide them onto each other. The resulting number will be called the Relative Coronary Flow Reserve (RCFR):

$$RCFR_{L,R} = \frac{CFR_L}{CFR_R} \tag{11.5}$$

where the index L, R indicates that this RCFR compares the CFR's of the arteries labeled L and R respectively. After substitution of Eqs. (11.2), (11.3) and (11.4), we get:

$$RCFR_{L,R} = \frac{A_L^{(h)} A_L^{(0)}}{A_R^{(h)} A_R^{(0)}} \frac{v_L^{(}h)}{v_R^{(h)}} \frac{v_R^{(}0)}{v_L^{(0)}} = \beta_{L,R} \frac{\lambda^{(h)}}{\lambda^{(0)}} \quad \text{with} \quad \beta_{L,R} = \frac{A_L^{(h)} A_L^{(0)}}{A_R^{(h)} A_R^{(0)}} \tag{11.6}$$

The factor $\beta_{L,R}$ introduced in this equation represents the (relative) dilation of the left distal branch as compared to the right one. As the coronary arteries will only react slightly to the administration of a vasodilating drug, it is to be expected that the dilation is approximately equal to unity ($A^{(h)}A^{(0)} \cong 1$). From this observation, together with the fact that the left and right distal branches of the bifurcation will react similarly, we can conclude that $\beta_{L,R}$ approximates unity. Using this result, the equation for the RCFR (equation 11.6 reduces even further, to:

$$RCFR_{L,R} = \frac{\lambda^{(h)}}{\lambda^{(0)}} \tag{11.7}$$

We see that there is no need to assess the arterial lumen, which is normally liable to errors without the use of elaborate techniques like IntraVascular UltraSound (IVUS). Comparing equation (11.5) with equation (11.7) reveals that the ratio of the flow distributions measured for hyperemic and basal states, approximates the previously introduced fraction of the CFR's of two distinct arteries. It is to be expected that two healthy arteries (or artery segments) of one single patient have similar values. Of course, in practice some variation will exist, but these are expected to be much smaller than the variability of the CFR's of healthy arteries of different patients. So, any deviation of the RCFR from unity indicates the presence of a flow restriction in one of the two distal branches. In the case the $RCFR_{A,B}$ (defined as the ratio of the CFR of artery A to the CFR of artery B, see equation (11.5) is greater than unity, the flow restriction (stenosis) resides in artery B and vice versa. This is summarized in 11.1. The boundaries between the various categories will have to be determined experimentally, although a preliminary comparison with other measures reveals that values of 0.75 and 1.33 are realistic thresholds between possible and severe stenoses.

Table 11.1: Interpretation of RCFR values.

$RCFR_{A,B}$	Interpretation
$\ll 1$	severe stenosis in artery A
< 1	Possible stenosis in artery A
$\cong 1$	No stenosis, or in both arteries?
> 1	Possible stenosis in artery B
$\gg 1$	Severe stenosis in artery B

11.2.3 Limitations

The method presented here has some limitations. One of the most important limitations is the fact that not each outcome leads to a sensible conclusion.

If the calculated RCFR deviates much from unity, the conclusion is that one or more severe stenoses are present in one of the arteries considered. But we can not conclude that there exists no flow-restricting stenosis in the case the RCFR turns out to be equal to unity. In that case, it is equally well possible that both arteries exhibit flow restricting behavior. This indecisive conclusion is indicated in table 1 by the question mark. So, care must be taken when attaching conclusions in terms of clinical relevance to the actual outcome of the RCFR. Another restriction upon the feasibility of the method is the presence of a bifurcation that meets all requirements. First of all, one (and only one) of its two distal branches should contain the stenosis that is to be analyzed. The second distal branch should contain no (visible) stenosis or other obstruction(s), and should preferably be healthy. Furthermore, the bifurcation should be accessible by the catheter for selective contrast administration. The bifurcation should be projected free from other (crossing) arteries. It is also required that the physician is able to place the ROI's on the three branches of the bifurcation in such a way that each ROI contains only one artery, and such that the ROI's are on appropriate distance from the bifurcation (as close as possible for the ROI covering the main trunk, and as far as possible for the two distal ROI's, see section 11.3.3, without having any side-branches between the ROI and the bifurcation. Depending on the position of the stenosis being analyzed, the main bifurcation of the left coronary artery is a good candidate. However, abnormalities like a very short Left Main Coronary Artery (LMCA), or no LMCA at all, forces us to use other (smaller) bifurcations, or even to resort to other methods.

11.3 METHOD

In order to apply the method described above to assess the functional severity of stenoses, it is necessary to measure the blood flow distribution in one of the main bifurcations of the coronary arteries. The method to actually measure that distribution is based on the arrival time of contrast agent in some designated regions of the coronary arteries, using densitometric techniques [11, 20, 21]. We will show that the measurement will take advantage of the fact that the results will be used in the calculation of a *relative* measure, the RCFR (see section 11.2.2).

11.3.1 Time-density curves

The first step in assessing the blood flow distribution is the calculation of *time-density curves* [22]. Other authors call these curves 'transfer functions' [20], 'contrast pass curves' [11],'contrast concentration curves' or other similar names. What these curves represent is the amount of contrast in a selected

region (the Region-of-Interest ,or ROI), plotted against time. The amount of contrast agent that resides inside the ROI is determined using densitometry, which is based on the law of Lambert-Beer. This law relates the intensity of the light (or X-ray) beam passing through an object (I_{out}), to the incoming intensity (I_{in}), the length of the path through the object (d), and the object properties (represented by the attenuation constant μ):

$$I_{out} = I_{in}e^{-\mu d} \tag{11.8}$$

From this equation, it can be derived that by logarithmic subtraction of a so-called 'mask' image, we only retain those objects that are *not* present in the mask image. If we choose as a mask image a so-called pre-contrast image, all we will see in the resulting (logarithmic) image is the contrast agent. In that case, the grey level of each pixel in the resulting (logarithmic) image is proportional to the length of the path through the contrast agent. If we then sum all pixel values over a small region of interest (ROI) , the result will be a measure of the amount of contrast agent in the section of the artery that is enclosed by the ROI. Plotting these values for multiple successive frames results in a time-density curve.

11.3.2 Delay Measurements using Time-density Curves

In order to determine the (relative) flow velocity, we will measure the time required for the contrast bolus to travel a certain path through the arteries. With two ROI's positioned at the start and end of this path respectively, the velocity can be calculated by measuring the delay between the arrivals of the bolus in the two ROI's, and by measuring the length of the path traveled (that is, the real length of the three-dimensional path). The latter is hard to determine, but as will be shown, that does not hamper the measurement of the flow distribution. The delay between the arrivals of the contrast bolus in the two ROI's is measured using the time-density curves calculated for each of the two ROI's.

To investigate some techniques to determine the delay between two ROI's (or between two time-density curves), we have developed a simple but adequate model of the dispersion of the contrast agent. An example of a similar but less accurate model is presented by Lubbers[22]. Using this model it is possible to calculate a theoretical time-density curve, depicted in Figure 11.2a. If we compare this with the time-density curve obtained during an in-vitro experiment (Figure 11.2b), we see that the model is quite accurate in predicting the global shape of the curve. Note that these curves were acquired using a *small* amount of contrast agent, which is in concurrence with the proposals described in section 11.3.4.

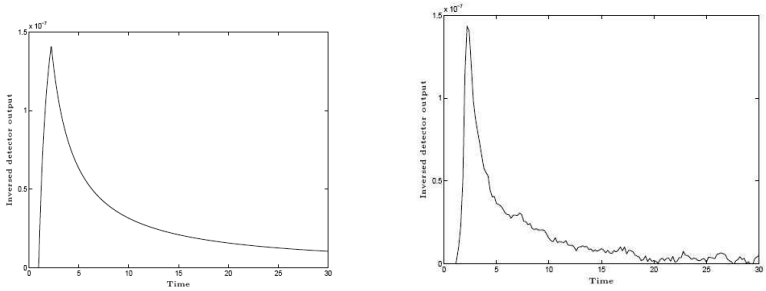

(a) Theoretical time-density curve based on dispersion model

(b) Real time-density curve of an in-vitro experiment

Figure 11.2: Time-density curves, from Csizmadia et al. [23].

In measuring the delay between two such curves, we can adopt several methods. Most straight forward is to use the Time of Arrival (ToA), which is defined as the point of time in which the front of the contrast bolus reached the ROI. From Figure 11.2 this seems quite easy to determine, but in real (in-vivo) applications, the curves do not have such a steep edge as the ones measured in-vitro, and are degraded by noise. This makes a simple measurement of the time of arrival liable to errors.

Another method is to use the peak of the curve: the point of time in which the total amount of contrast inside the ROI is maximal. But this method is also sensible to noise. If the peak of the curve is blunt (which occurs with a large contrast bolus and large ROI's), the noise can easily result in a maximum at a location where the noise-free curve does not have its maximum at all. Therefore, if we simply try to find the location of the maximum value of the time-density curve, the result will not be reliable.

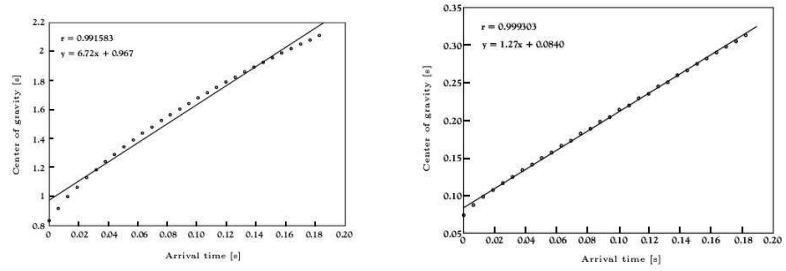

(a) Straightforward center of gravity

(b) Center of gravity after thresholding at 55%

Figure 11.3: Correspondence between the arrival time and the center of gravity (modified from Csizmadia[23]).

The third possible method uses the so-called Center of Gravity (CoG),

defined as the point of time t_{cog} according to:

$$\int_{-\infty}^{t_{cog}} D(t)\,dt = \int_{t_{cog}}^{\infty} D(t)\,dt \tag{11.9}$$

with $D(t)$ the time density curve. The main benefit of this method is the integrating action involved, which levels most of the effects of noise on the measurement of the curves. Unfortunately, the tails of the curves (see figure 11.2) make it necessary to cut off the curves after a certain (finite) amount of time (see also section 11.3.4). This cut off time influences the outcome of the calculation of the center of gravity considerably (see Figure 11.3). To prevent this influence, we first threshold the curves to a certain fraction α of the maximal value.

$$\hat{D}(t) = \begin{cases} D(t) - \Delta & \text{if } D(t) > \Delta \text{ with } \Delta = \alpha \cdot \max_t D(t) \\ 0 & \text{otherwise} \end{cases} \tag{11.10}$$

If the fraction α is high enough (*e.g.* 60%), we end up with a curve in which only the peak is still present. Applying the center of gravity method to the thresholded curve results in a number very close to the location of the peak value of the original curve (with or without noise). In-vitro experiments show that the CoG determined this way has a linear relation with the actual time of arrival ($\alpha = 55\%$)[23], see figure 11.3. As the exact relation depends on the length of the ROI (defined as the dimension parallel to the artery axis), it is good practice to use fixed-sized ROI's.

11.3.3 Application to RCFR Measurements

If we place three distinct ROI's as in figure 11.4(a), and determine time-density curves for each of them, we can assess the relative flow distribution (the parameter λ in equation 11.2) by measuring the delays between the three curves:

$$\lambda = \frac{v_L}{v_R} = \frac{\ell_L}{\Delta t_L}\frac{\Delta t_R}{\ell_R} = \frac{\ell_L}{\ell_R}\frac{\Delta t_R}{\Delta t_L} \tag{11.11}$$

with Δt_L and Δt_R the traveling times of the contrast agent over the left and right branches of the bifurcation. Each path has a length of ℓ_L and ℓ_R respectively.

However, the quantities Δt_L and Δt_R are hard to measure in this setup: the delay between the three time-density curves give us Δt_{M+L} and Δt_{M+R}, which are greater than Δt_L and Δt_R due to the delay in the main trunk. The solution is to relocate the ROI on the main trunk, such that the delay Δt_M is small compared to the delay in one of the distal branches Δt_L and Δt_R. This optimal situation is depicted schematically in figure 11.4(b) and applied to an

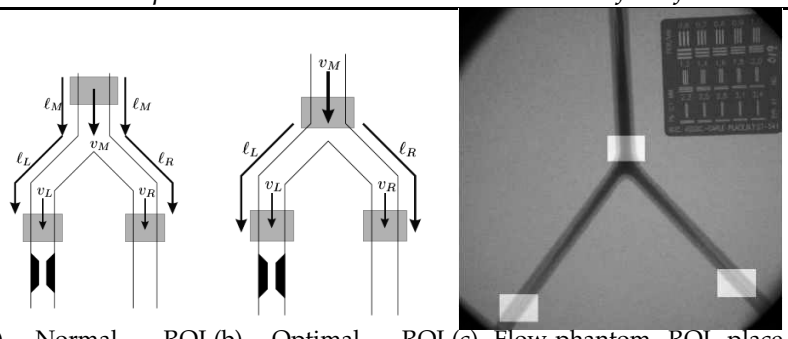

(a) Normal ROI placement (b) Optimal ROI placement (c) Flow-phantom ROI placement

Figure 11.4: Placement of the Regions of Interest (ROI).

image of a flow phantom in figure 11.4(c)). The influence of the exact positioning of the ROI's on the sensibility, reproducibility and ease of placement in clinical application is still under trial.

Since there is a linear relationship between the arrival time t_a and the center of gravity (CoG) t_{cog} (see Figure 11.3(b)), we can rewrite equation 11.11 to:

$$t_a = a \cdot t_{cog} + b \Rightarrow \tag{11.12}$$

$$\begin{aligned} \lambda &= \frac{\ell_L}{\ell_R} \cdot \frac{\Delta t_R}{\Delta t_L} = \frac{\ell_L}{\ell_R} \cdot \frac{t_{aR} - t_{aM}}{t_{aL} - t_{aM}} = \frac{\ell_L}{\ell_R} \cdot \frac{a \cdot t_{cogR} + b - a \cdot t_{cogM} - b}{a \cdot t_{cogL} + b - a \cdot t_{cogM} - b} \\ &= \frac{\ell_L}{\ell_R} \cdot \frac{t_{cogR} - t_{cogM}}{t_{cogL} - t_{cogM}} \end{aligned} \tag{11.13}$$

Substitution of this result in equation 11.7 yields:

$$\begin{aligned} RCFR_{L,R} &= \frac{\lambda^{(h)}}{\lambda^{(0)}} = \frac{\ell_L^{(h)}}{\ell_L^{(0)}} \cdot \frac{\ell_R^{(0)}}{\ell_R^{(h)}} \cdot \frac{t_{cogR}^{(h)} - t_{cogM}^{(h)}}{t_{cogL}^{(h)} - t_{cogM}^{(h)}} \cdot \frac{t_{cogL}^{(0)} - t_{cogM}^{(0)}}{t_{cogR}^{(0)} - t_{cogM}^{(0)}} \\ &\cong \frac{t_{cogR}^{(h)} - t_{cogM}^{(h)}}{t_{cogL}^{(h)} - t_{cogM}^{(h)}} \cdot \frac{t_{cogL}^{(0)} - t_{cogM}^{(0)}}{t_{cogR}^{(0)} - t_{cogM}^{(0)}} \quad \text{if } \ell_L^{(h)} \cong \ell_L^{(0)} \text{ and } \ell_R^{(h)} \cong \ell_R^{(0)} \end{aligned} \tag{11.14}$$

It might be argued that the exact relation between the time of arrival and the center of gravity (see equation 11.12) depends on much more factors. As already mentioned, it depends on the (actual) length of the artery enclosed by the ROI, and it turns out that the constant term b in equation 11.12 also depends on the amount of contrast injected (actually, the length of the injection period). In calculating the RCFR using the center of gravity instead of the arrival time (equation 11.12), most differences in regression coefficients a will disappear as long as the b-coefficients are all the same. Therefore it is recommended to perform the measurement of the baseline and hyperemic

flow distributions during similar conditions, preferably using an automatic injection of contrast.

From equation 11.14 we see another benefit of the RCFR: if we are able to place the ROI's in the same spots during basal and hyperemic states, there is no need to measure any dimensions of the coronary arteries. This reduces errors caused by foreshortening, pincushion distortion etc. And by using the same acquisition angles for the baseline and hyperemic images, the foreshortening as encountered inside the ROI's is the same, and the only additional requirement is that the ROI sizes (measured in pixels) should be the same in basal and hyperemic states. This is easy to accomplish.

On one hand, it is beneficial to place the two distal ROI's as far from the bifurcation as possible to increase the accuracy of the time measurement. On the other hand, increasing that distance will decrease the total accuracy due to the possibility of (more) collaterals being present between the bifurcation and a far distal ROI. In that case, the collaterals will handle the extra blood flow caused by hyperemia, instead of the artery that is being monitored by the ROI, leading to a seemingly smaller Coronary Flow Reserve. Similarly, there should not be any side-branches between the bifurcation being considered and the distal ROI's.

11.3.4 Improving the Accuracy

There are several issues that can be employed to improve the method. These issues include amongst others the fine-tuning of the ROI sizes, and the use of a string of small droplets of contrast agent, instead of just one bolus.

ROI size

The size of the region of interest has a great impact on the shape of the time-density curves. Of course, the ROI's should be wide enough to enclose the whole width of the artery, but the length can be adjusted to need. If the ROI is very short, the time-density curve will be a very sharp spike, facilitating the measurement of the delay between the ROI's However, the number of pixels involved in calculating the curve is only small, making it more sensitive to noise etcetera. On the other hand, making the ROI very long leads to a smooth and wide peak, making the determination of the arrival time very inaccurate. In our in-vitro experiments, we use lengths of 20 to 30 pixels for images of size 256 times 256 with good results.

Contrast bolus size

It is well known that the administration of contrast agent influences the blood flow [19]. Not only is the blood flow increased during injection due to the

replacement of blood with contrast agent, but there is also a decrease in flow immediately following the injection during a few seconds, and a peak after approximately 10 seconds. Similar responses have been reported for nonionic contrast media.

Cusma et al. [19] state that as small a contrast volume as possible should be used to minimize the effects of the contrast agent on the blood flow (which still results in good image quality). As our approach does not depend on the absolute blood flow, but only on the flow restricting properties of the stenosis and the arterial bed, there seems not to be much advantage in decreasing the contrast volume. However, by doing so, we can increase the accuracy. The injection of a string of small contrast droplets, or 'dots', will result in time-density curves with a number of very harp peaks. Applying the center of gravity method to each of these peaks will most of the time result in just the location of the maximum, due to its peakedness. Also, the results (*e.g.* the measured delays) obtained from each of the separate droplets, can be averaged, giving a more accurate result.

11.3.5 Small contrast droplets in pulsatile flow

So far, we have considered the blood flow to be continuous. However, in the case of a small droplet of contrast agent, it is beneficial to also take the pulsatile character of the blood flow into account. This special nature of the flow gives the usage of a series of small contrast droplets even more potential. In steady (non - pulsatile) flow, each droplet is 'torn apart', while in pulsatile flow, the contrast agent remains a small droplet with limited length.

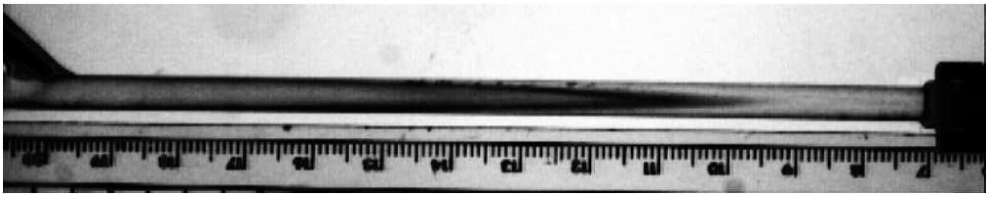

Figure 11.5: Contrast bolus in laminar flow, 0.5 s after injection.

Steady (non-pulsatile) flow through a straight rigid tube, can be described by Poiseuille's equation [24].This equation implicates that the flow is laminar (consisting of fluid layers parallel to the wall with no mixing of particles between layers), and that the velocity profile is parabloc (see Figure 11.5):

$$v(r) = \frac{(p_1 - p_2}{4\mu L}(r_i^2 - r^2) \tag{11.15}$$

with r_i the inner diameter of the tube, r the distance to the center of the tube, μ the viscosity of the fluid, L the length of the tube, and p_1 and p_2 the

pressures at both sides of the tube, respectively. This is also the equation that is used to model the time-density curves in section 11.3.2. From this equation, the long tail in Figure 11.2 can be explained: at the walls ($r = r_i$) the velocity is zero, and thus theoretically, the contrast agent will never disappear (see Figure 11.5. However, there is also diffusion, slowly interchanging particles between the layers of fluid that move with the same velocity (laminar flow). So, eventually, the contrast agent positioned at the walls will move to layers that have a velocity unequal to zero, and then pass the ROI. The absence of diffusion in the model of Figure 11.2(a) accounts for the different slope of the tail as compared to the measured time-density curve in Figure 11.2(b).

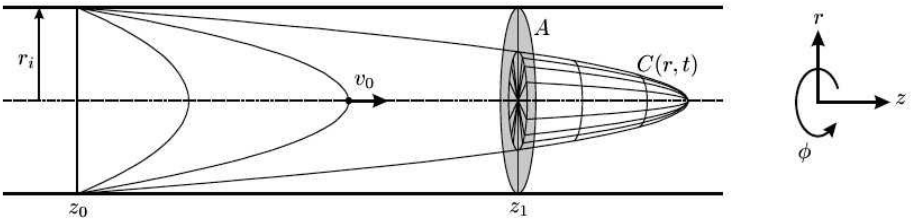

Figure 11.6: Axial cross-section of a rigid cylindrical tube with a laminar flow (modified from Csizmadia [23]).

Poiseuille's equation does not give any time (transient) information. So, in order to describe time-dependent behavior (pulsatile flow) , we need another mathematical description. A common description of non-steady flow in rigid tubes is given by the Navier-Stokes equations [24, 25], of which Poiseuille's equation is only a special case. This is a set of differential equations, describing the general behavior of a fluid interacting with its environment. Due to its generality, its is also possible to solve the set of equations for flexible tubes etcetera. However, as the problem becomes more complex so does the solutions, and in most such cases only a numerical solution can be calculated [26, 27]. The problem of describing the blood (a non-homogeneous non-linear fluid), in coronary arteries (curved, non-linear elastic and collapsible tubes having a non-uniform cross-sectional area) under non-steady flow conditions, is far too complex to solve using the Navier-Stokes equations. Therefore, Womersley [28, 29, 30] made some assumptions, enabling an analytical and linear solution to the set of differential equations, expressed in Bessel functions. But also this approximation of blood flow does not fully predict the effects of pulsatile flow on the shape of a contrast droplet that we measured.

A more qualitative discussion on the fluid dynamics of pulsatile flow will give more insight into the effects on the shape of a contrast droplet. Let us simplify the situation and assume that the particular pulsatile behavior of the

blood flow in the coronary arteries can be described by two states: (1) no flow and (2) continuous flow. These states are alternating at the heart rate. On a transition of no flow to a continuous flow, we can *not* apply Poiseuille's equation, because it assumes that the flow has fully developed, both in time and in space. This means that start conditions are not properly described by that equation. The same applies for the flow at a location too close to the ends of the tube (commonly denoted as the inlet- and outlet-regions). The velocity profile in the inlet of a tube is known to be blunter that the profile of fully developed flow. In fact, the velocity profile transforms from a completely flat profile (at the inlet side) to a parabolic profile (at the outlet side). This also determines the minimum length of the inlet-region to ensure a fully developed flow in the center section of the tube. It is to be expected that (sections of) coronary arteries are too short to allow the flow to fully develop, resulting in a blunter velocity profile than predicted by Poiseuille's equation.

The other (already mentioned) reason why Poiseuille's equation is not applicable to the transition from no flow to steady flow, is the 'steady-state' nature of that equation. It assumes the flow to be in that state for such a long time, that its properties (such as velocity profile) are not changing anymore. It is evident that this condition can not be satisfied. The solutions of the Navier-Stokes equations describing the development of the flow to a Poiseuille flow, is a common one and can be found in McDonald et al. [24], for example. This development in time also has a quite blunt velocity profile, only in the end leading to a parabolic (Poiseuille) flow profile. Now, since the two states (no flow and continuous flow) switch in rapid succession, the flow has no time to develop to a real parabolic velocity profile. Combined with the previous observation concerning the length of the artery segments, it can be concluded that the velocity profile in coronary arteries during normal (clinical) conditions is blunter than a parabolic curve. This is in agreement with the results found by Verhoeven [31]. The result is that the tail of the measured time-density curves will become shorter, making time delay measurements more accurate. Also, as the droplets more or less keep their shape, individual droplets are easier identified and separated from each other if a string of droplets is injected.

11.4 GOING IN-VIVO

Of course, the method presented so far here is not so straightforward in practice as might be concluded from the preceding alone. There are several issues that have to be taken care of before reliable results are obtained. Some of these problems are common to Quantitative Coronary Angiography or Digital Subtraction Angiography in general [32, 14]. Even more issues are to be considered when using videodensitometry [34]. As there are many articles

on these common problems, they are not described in this section. Only the specific problems encountered when applying our method in real clinical applications are mentioned here.

11.4.1 Clinical Setup

Although the method acts upon data acquired during a standard procedure, there are (unfortunately) some requirements on that data. The performing physician should take care in supplying relevant images at a high frame rate (at least 30 fps) , acquired during specific conditions. These specific conditions are common practice during standard procedures, but normally there is no acute need to restrict the procedure to predefined angles, positions etc. It is evident that the performing physician should at least acquire two image sequences with exactly the same camera positions and magnifications, one during basal and another during hyperemic flow conditions. Preferably, the patient should not move too much between the acquisitions of these two sequences, as that causes problems in putting the ROI's at exactly the same positions on the coronary arteries. Also, the requirements as discussed in Section 11.2.3 should be considered. However, in most cases the physician would already try to find a position in which the main coronary arteries are easily visible, and not masked by other (crossing) arteries. According to our proposal to use a string of contrast droplets, we tried to accomplish that using standard catheterization equipment. Preferably, the contrast injection should be synchronized to the cardiac cycle, and be of a (fixed) pre-determined volume and rate. Our experiments reveal that the standard 'power injector' that is used to automatically inject contrast in order to visualize the cardiac chambers, is not able to meet our demands. Although it can be synchronized to the cardiac cycle, it is not able to deliver a small amount of contrast during a short period of time, let alone to repeat that within only a fraction of a second. We therefore employ manual injection of a small amount of contrast (< 1 ml) with a reasonable high injection rate for the in-vitro experiments, yielding only one droplet per image sequence. New techniques and devices enabling us to administer a real string of droplets are currently being considered.

11.4.2 Major Problems

There are some problems to be solved before the method can be applied with success to clinical data. Although some problems common to almost all similar QCA methods have been solved by introducing the RCFR (such as the measurement of path lengths, foreshortening, effects of the contrast agent on the blood flow, dilution etcetera.), there are also some new problems that are more or less specific to this method.

One of the major problems is the need to exactly position the ROI's in two different image sequences, and to maintain that position while the heart beats, and moves due to patient movements and breathing. This not only implies that both sequences should be acquired using the same camera positions and magnifications, but also that we will have to be able to follow the arteries as they move. At present time, the algorithm requires much user-interaction, but before it can be introduced into the catheterization laboratories, those interactions should be minimized to choosing the bifurcation to be analyzed, possibly with the need to select only a few other specific points. The tracking of the artery motion is also very important for the logarithmic subtraction performed in determining the time-density curves (see Section 11.3.1. Mancini [14] even states that, in general, coronary arteriography using standard forms of temporal subtractions are not recommended. In our case, however, we can restrict ourselves to digital subtraction of the small ROI's, which can be corrected for artery motions quite well. Proper background selection can be accomplished by extrapolating measured artery motions to the precontrast images. Image acquisition that is synchronized to the cardiac cycle eases that process.

No experiments were performed using a series of contrast droplets. The biggest problem we expect to encounter is that there will not be a single image anymore, in which the complete coronary artery tree is visible. Instead, we will have to combine the information of multiple (synchronized) images to trace the arteries.

11.5 CONCLUSIONS

We have found that the RCFR can be determined by measuring the flow distribution of a coronary bifurcation. This flow distribution is determined by analyzing two sequences of angiographic images, acquired during baseline and hyperemic coronary blood flow. This approach has the advantage that there is no need to determine geometrical parameters of the coronary arteries, and that the outcome can be compared with a fixed threshold for all patients. A drawback is that the RCFR is not decisive in case the outcome is (approximately) equal to unity. In measuring the flow distributions under different conditions of the patients body, there are a few issues to be considered. First of all there has to be a bifurcation meeting all the demands, and secondly the performing physician will have to make sure to acquire all the data needed, although that is normally no more than what is obtained during a classical procedure. Thirdly, in analyzing the acquired sequences of images, the motion of the arteries requires us to apply (3D) motion correction techniques in order to arrive at reliable results.

The method has not yet been tested with a series of contrast droplets in-

stead of one contrast bolus. Major problems to expect are the equipment necessary to make such a string in clinical applications, and the difficulties in tracing the arteries using only the images with small droplets of contrast, instead of a large bolus.

ACKNOWLEDGMENTS

We like to thank Eelco van Akker, who has helped us to understand the fluid dynamics by doing some numerical simulations. We would also like to express our gratitude to the staff of the Zuiderziekenhuis in Rotterdam, for placing the X-ray equipment at our disposal.

References

[4] J.H.C. Reiber, "An overview of coronary quantitation tecniques as of 1989," in *Quantitative coronary arteriography*, J.H.C. Reiber and P.W. Serruys, eds., vol. 117, pp. 55-132, Kluwer Academic Publishers, 1996.

[5] J.H.C. Reiber, L. Schiemanck, et al., "State of the art in quantitative coronary arteriography as of 1996," in *Cardiovascular imaging*, J.H.C. Reiber and E. van der Wall, eds., vol. 186, pp. 39-56, Kluwer Academic Publishers, 1996.

[3] J.H.C. Reiber, J. Dijkstra, et al., "Current and future developments in qca and image fusion with IVUS," in *What's new in cardiovascular imaging*, J.H.C. Reiber and E. van der Wall, eds., vol. 204, pp. 17-30, Kluwer Academic Publishers, 1998.

[11] J. Cusma, K. Morris, and T. Bashore, "Angiographic measurement of coronary blood flow," in *Advances in Quantitative Coronary Arteriography*, J.H.C. Reiber and P.W. Serruys, eds., vol. 137, pp. 235-52, Kluwer Academic Publishers, 1993.

[5] J. Lesperérance, L. Bilodeau, et al., "Issues in the performance of quantitative coronary angiography in clinical trials," in *What's new in cardiovascular imaging*, J.H.C. Reiber and E. van der Wall, eds., vol. 204, pp. 31-46, Kluwer Academic Publishers, 1998.

[6] C. Nienaber, K. Schaps, and G. Stiel, "The cost-effectiveness of QCA in interventional cardiology," in *What's new in cardiovascular imaging*, J.H.C. Reiber and E. van der Wall, eds., vol. 204, pp. 47-60, Kluwer Academic Publishers, 1998.

[7] T. DeRouen, J. Murray, and W. Owen, "Variability in the analysis of coronary arteriograms," *Circulation* 55, pp. 324-328, 1977.

[1] K. Detre, E. Wright, M. Murphy, and T. Takaro, "Observer agreement in evaluating coronary angiograms," *Circulation* 52, pp. 979-86, 1975.

[2] L. Zir, S. Miller, et al., "Interobserver variability in coronary angiography," *Circulation* 53, pp. 627-32, 1976.

[10] J. Gaibraith, M. Murphy, and N. de Soyza, "Coronary angiogram interpretation: Inter-observer variability," *JAMA* 240, pp. 2053-56, 1978.

[11] C. Grondin, I. Dyrda, et al., "Discrepancies between cineangiographic and postmortem findings in patients with coronary artery disease and recent myocardial revascularization," *Circulation* 49, pp. 703-8, 1974.

[12] D. Harrison, C. White, et al., "The value of lesion cross-sectional area determined by quantitative coronary angiography in assessing the physiologic significance of proximal left anterior descending coronary arterial stenosis," *Circulation* 69, pp. 1111-9, 1984.

[13] C. White, C. Wright, et al., "Does visual interpretation of the coronary arteriogram predict the physiologic importance of a coronary stenosis?," *N Eng J Med* 310, pp. 819-24, 1984.

[14] R. Bach, "Current status and future expectations of the flow velocity guidewire," in *Cardiovascular imaging*, J.H.C. Reiber and E. van der Wall, eds., vol. 186, pp. 389-402, Kluwer Academic Publishers, 1996.

[7] K. Gould and K. Lipscomb, "Effects of coronary stenoses on coronary flow reserve and resistance," *Am J Cardiol* 34, pp. 48-55, 1974.

[16] K. Gould, R. Kirkeeide, and M. Buchi, "Coronary flow reserve as a physiologic measure of stenosis severity," *J Am Coll Cardiol* 15, pp. 459-74, 1990.

[17] S. Nissen and J. Gurley, "Application of indicator dilution principles to regional assessment of coronary flow reserve from digital angiography," in *Quantitative Coronary Arteriography*, J.H.C. Reiber and P.W. Serruys, eds., vol. 117, pp. 245-63, Kluwer Academic Publishers, 1991.

[9] F. Klocke, "Measurement of coronary flow reserve: defining pathophysiology versus making decisions about patient care," *Circulation* 76, pp. 1183-9, 1987.

[19] J. Cusma, E. Toggart, et al., "Digital subtraction angiography imaging of coronary flow reserve," *Circulation* 75(2), pp. 461-72, 1987.

[20] N. Eigler, J. Pfaff, et al., "Digital angiographic transfer function analysis of regional myocardial perfusion: measurement system and coronary contrast transit linearity," in *Progress in digital angiocardiography*, P. Heintzen and J. Bursch, eds., pp. 265-74, Kluwer Academic Publishers, 1988.

[21] S. Nissen, J. Elion, and A. DeMaria, "Methods for calculation of coronary flow reserve by computer processing of digital angiograms," in *Progress in digital angiocardiography*, P. Heintzen and J. Bursch, eds., pp. 237-51, Kluwer Academic Publishers, 1988.

[22] A.P.G. Lubbers, C.H. Slump, and C.J. Storm, "Digital densitometric determination of relative coronary flow distributions," in *Biomedical Image Processing and Biomedical Visualization*, R. Acharya and D. Goldgof, eds., vol. 1905, pp. 43-54, SPIE, 1993. Part one.

[23] N. Csizmadia, C.H. Slump, et al., "On the digital densitometric determination of relative coronary flow distributions." Submitted to Medical & Biological Engineering and Computing.

[24] D. McDonald, W. Nichols, and M. O'Rourke, *McDonald's Blood Flow in Arteries: theoretical, experimental and clinical principles*, Edward Arnold, London, third ed., 1990.

[25] J. Wendt, *Computational fluid dynamics*, Springer-Verlag, New York, 1992.

[26] W. Philips, "Modeling of flows in the circulatory system," *Advances in Cardiovascular Physics* 5, pp. 26-48, 1983. Part 1.

[27] M. Rutten, *Fluid-solid interaction in large arteries*. PhD thesis, University of Eindhoven, Eindhoven, The Netherlands, 1998.

[28] J. Womersley, "Method for the calculation of velocity, rate of flow and viscous drag in arteries when the pressure gradient is known," *J. of Physiology* 127, pp. 533Ů63, 1955.

[29] J. Womersley, "Oscillatory motion of a viscous liquid in a thin-walled elastic tube; the linear approximation for long waves," *Phil. Mag.* 46 199, 1955.

[30] J. Womersley, "An elastic tube theory of pulse transmission and oscillatory flow in mammalian arteries," Tech. Rep. TR 56-614, Wright Air Development Center, US Air Force Base, Ohio, 1957.

[31] L.A.J. Verhoeven, *Digital Subtraction Angiography: The Technique and an Analysis of the Physical Factors Influencing the Image Quality*. PhD thesis, University of Delft, Delft, The Netherlands, 1985.

[32] B. Brown, P. Simpson, et al., "Quantitative and qualitative coronary arteriography," in *Quantitative Coronary Arteriography*, J.H.C. Reiber and P.W. Serruys, eds., vol. 117, pp. 3-21, Kluwer Academic Publishers, 1991.

[14] G. Mancini, "Digital coronary angiography: advantages and limitations," in *Quantitative Coronary Arteriography*, J.H.C. Reiber and P.W. Serruys, eds., vol. 117, pp. 23-42, Kluwer Academic Publishers, 1991.

[34] J. Whiting, J. Pfaff, and N. Eigler, "Advantages and limitations of videodensitometry in quantitative coronary angiography," in *Quantitative Coronary Arteriography*, J.H.C. Reiber and P.W. Serruys, eds., vol. 117, pp. 43-54, Kluwer Academic Publishers, 1991.

Chapter 12

On the assessment of the pulse flow propagation[1]

Our purpose is to assess the pulse flow propagation from series of digital coronary angiograms. The local dilation - contraction pattern along the vessel is a measure for the elasticity and endothelian function. A small distensability could be a indication for the presence of atherosclerosis also in cases where the angiogram is not abnormal. We have developed an analytical model of the pulse flow propagation in coronary arteries. In the model the artery is a straight elastic tube and is not moving due to the motion of the heart. The pulsatile flow of contrast agent is modeled for clinically relevant parameters and predictions of coronary angiograms are obtained for various characteristics of elasticity such as modulus, compliance and ratio. In the clinical angiograms, we compute the local vessel diameter from frame to frame. Because of the heart motion it is not so easy to track the vessel diameter on the same spot. Motion estimation and compensation are required. Algorithms for these processing steps are implemented. We have obtained satisfactory model simulations and predictions of angiograms. The simulated - dilation - contraction patterns help to understand the more complicated clinical angiograms. We have obtained various pulse flow patterns from coronary angiograms of a small patient population.

12.1 INTRODUCTION

The mammalian heart is composed of four chambers of hollow muscle, which are organized in two pairs. The thin-walled atrium on each side is connected through a valve with a thick-walled muscular ventricle. The output of the

[1]presented at Medical Imaging 2000: Physiology and Function from Multidimensional Images, and published in part as: C.H. Slump, M. Schrijver, H. Kuipers, C.J. Storm, "On the assessment of the pulse flow propagation based upon digital coronary angiograms," in *Medical Imaging: Physiology and Function from Multidimensional Images*, Chin-Tu Chen, Anne V. Clough, eds., *Proc. SPIE* vol.3978, pp. 426 - 435, 2000.

ventricle is through a valve to the main arteries. Most important is the left ventricle that pumps the blood into the aorta, see Figure 12.1. The coronary arteries branch of the aorta close to the aortic valve and receive in rest about 5% of the cardiac output of 5 l / minute. The flow through the coronaries de-

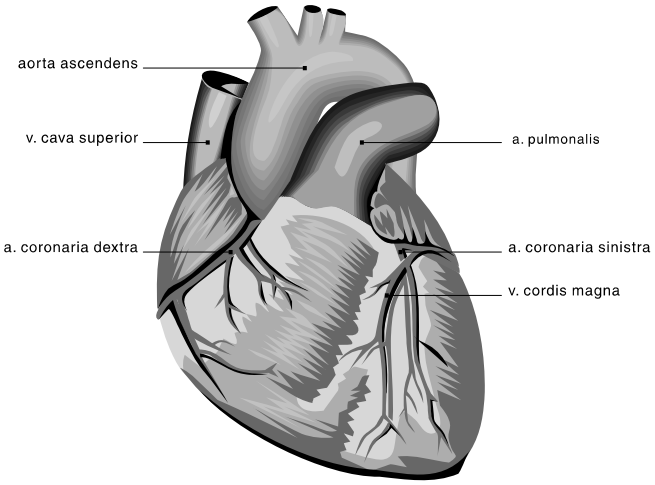

Figure 12.1: Overview of the human heart

pends on the pressure gradient and the resistance of the vessels. Every time the left ventricle contracts and injects blood into the aorta, a pulse wave is generated that travels along the vascular system [2, 6]. In the cardiovascular system the propagating pressure pulse influences the local pressure gradient which drives the motion of the blood. Measured experimental velocity profiles in coronary arteries differ from the velocity waveforms in other arteries. The coronary blood flow depends on the cardiac cycle. During systole the ventricle contracts and the myocardial vessels are compressed and may even collapse due to the high intraventricular pressure, the resistance to flow will be large. In this period the flow is minimal even though the pressure in the aorta and the flow in the aorta is maximal. In diastole, the ventricular muscle expands and the vessels will open and the blood will start to flow [7]. Ischemic heart disease is, together with stroke, a leading causes of death in the western society. Ischemic heart disease is caused by the imbalance between the oxygen demand of the myocardium and the supplying blood flow. Reduction in coronary blood flow is related to progressive atherosclerosis with increasing narrowing and stiffening of the coronaries. Atherosclerosis is a

common form of arterial disease in which fat deposits gather on the inner layer of the arterial wall. These fat deposits grow into regions of disease called plaque; as the plaque increases, the intimal layer thickens and the arterial wall loses its elasticity. This narrowed condition of the artery, called local stenosis, typically is not detected until blood flow is restricted or a clot has formed. A buildup of plaque in the coronary arteries, which supply blood to the heart muscle, may develop into coronary heart disease. An important characteristic of arteries is their capability to expand in order to accommodate a pulse of blood from the cyclically pumping heart and recoil to keep the blood flowing while the heart relaxes. Consequently, arteries perform like elastic reservoirs, converting the heart's pulsatile flow to steady flow in peripheral vessels. All arteries have a similar structure [8], see Figure 12.2. In Figure 12.2, the inside layer, or tunica interna, consists of endothelial cells. The outer layer, or tunica adventitia, is made up primarily of collagen. The middle layer, or tunica media, contains smooth muscle and elastin layers, and it provides most of the elasticity.

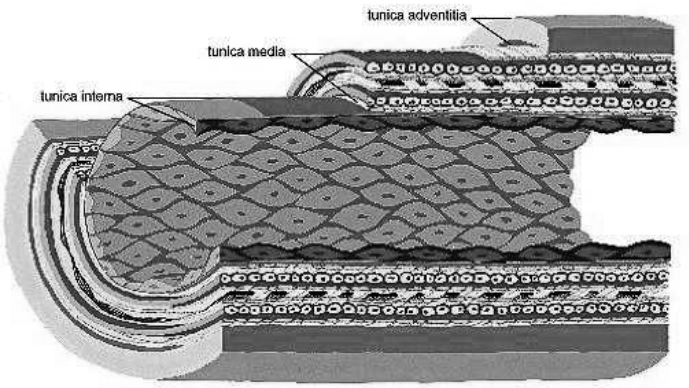

Figure 12.2: Characteristic of a typical artery with the three layers, from [8].

Stenosed coronary arteries are visualized by angiography, *i.e.* the injection of iodine X-ray contrast material by means of a positioned catheter. The images are detected by an image intensifier-television system. The video signal is A to D converted, processed and displayed on a monitor and in parallel stored on a disc. Both by atherosclerosos and aging, the blood vessel wall becomes stiffer, with effects on flow perfusion and the heart has to work harder as the elastic recoil does not function anymore with potential danger of heart failure. Objective of this study is whether we can assess the (loss of) elasticity from coronary angiograms acquired according the standard clinical cath. lab. procedures. This may prove important information for the early detec-

tion of atherosclerosis. This paper is organized as follows. In the next section we focus our attention to the pulsatile flow propagation. After that we describe some flow experiments with a pulsating pressure pump for the case of a straight flexible tube. We measure pressure and diameter variations. After that we present a clinical example, where the vessel is also in motion due to the heart contraction. This motion makes the measuring of the diameter variation not simple. To enable this, we have to resort to image processing techniques, which are briefly indicated.

12.2 THEORY

The study of blood flow in arteries is well treated in the literature, see [1, 2, 3, 4, 5, 6, 7] for only few of the major references. In this section we describe the pulsatile character of arterial blood flow as a one-dimensional wave propagation problem. If we neglect the elasticity of the arteries, we can describe the blood velocity response at positions inside the vessel as a function of the local pressure gradient pulsatile variations. As arterial diameter variations are in the order of 2% due to the successive heartbeats, this first approximation is not too bad. In this situation we can follow the analysis of Womersley [10, 11], see also [6]. The velocity distribution corresponding to a Fourier coefficient of the periodic heart pump pulse, with radian frequency ω, depends on the dimensionless parameter α which is defined as the ratio of the vessel radius a to the oscillating boundary - layer thickness $\sqrt{\nu/\omega}$, with ν the kinematic viscosity of blood. In large arteries ν equals 4 mm^2s^{-1}. For a heart -rate of 60 beats per minute, we have a fundamental frequency ω_0 equal to 2π s^{-1} and from:

$$\alpha = a\sqrt{\frac{(n+1)\omega_n}{\nu}}, \tag{12.1}$$

we obtain for the thickness of the oscillating boundary - layer a value of 0.8 mm. With a typical value of the diameter of the larger coronary arteries, which is our interest, we find for α a value of 2.5. For harmonic coefficient n in the Fourier expansion, the layer thickness decreases by a factor $(n+1)^{-1/2}$, and α increases. The response to the higher Fourier components of the pressure gradient is a uniform velocity distribution over the cross-section of the vessel, except in the oscillating boundary layer of $\alpha^{-1}\times$ 100 % of the vessel radius. The main effect of these pressure gradient components is therefore on the mass of the blood and not to overcome the viscous effects of the blood. In the linear case we add up the different Fourier responses to find the total response. However, our interest is in the pulse propagation and in the distensibility of more or less elastic blood vessels. The extra pressure pulse in the arteries caused by the ventricular contraction is in the order of 10 % of the

normal atmospheric pressure. This pressure pulse increases the vessel cross section with the same percentage, under normal physiological circumstances.

In order to make this paper somewhat self-contained, we describe in the appendix the derivation of the main formula's of the pulsatile flow through an elastic tube. We now continue with the simple linear theory, with viscous effects neglected, for an artery with uniform undisturbed area A with pressure pulses not too large so that we can approximate the distensibility D of the artery by a constant and neglect the convective component $u\nabla u$.

$$D = \frac{1}{A}\frac{dA}{dp}. \tag{12.2}$$

From Newton we have that the mass times acceleration along the axis of the tube in the z-direction with neglect of the viscous effects, $\rho\partial u/\partial t$ per unit volume of fluid with u the fluid velocity and ρ the density, equals the pressure gradient. This yields the equation:

$$\rho\frac{\partial u}{\partial t} = -\frac{\partial p}{\partial z}. \tag{12.3}$$

The equation of continuity is:

$$D\frac{\partial p}{\partial t} = -\frac{\partial u}{\partial z}. \tag{12.4}$$

Eliminating the velocity u from 12.3 and 12.4, we obtain a wave equation:

$$\frac{\partial^2 p}{\partial^2 t} = c^2\frac{\partial^2 p}{\partial^2 z^2}, \tag{12.5}$$

with c the wave speed given by:

$$c = \frac{1}{\sqrt{\rho D}}, \tag{12.6}$$

also known as the Moens-Korteweg equation, with E the Young modulus of the vessel wall, h the thickness and d the diameter. With 12.6 (6) we can predict values for the wave speed for distensibility values of normal blood vessels, *i.e.* $10^{-5}\mathrm{N}^{-1}\mathrm{mm}^2$. The problem of interest is then if we can also measure the distensibility from angiograms.

12.3 FLOW EXPERIMENTS

We have generated pressure pulses with an artificial heart pump, see Figure 12.3, the average pressure range was 150 mm Hg and the amount of flow was 250 ml minute. As blood substitute we used normal water. The pressure

pulses are generated in a transparent flexible polyurethane tube of inner diameter of 4 mm, outer diameter 6 mm and length 7 m. From static pressure - diameter measurements the distensibility is computed as 0.16 $10^{-5}N^{-1}mm^2$. The propagation of the pressure pulses is depicted in Figure 12.4, at the beginning of the tube, and the end of the tube in Figure 12.5. With a CCD camera we have observed the corresponding diameter variations. The imaging conditions have been such that we had about 400 pixels over the tube diameter.

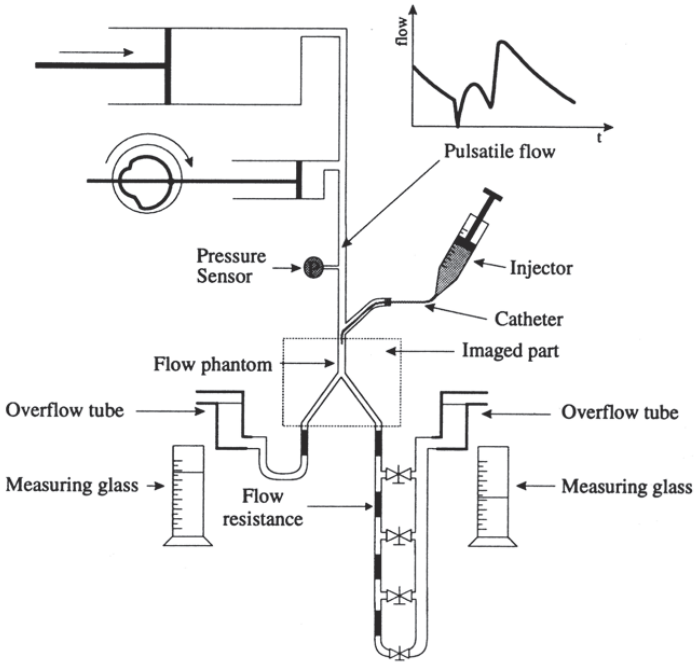

Figure 12.3: The setup of the flow experiments.

Comparison of Figures 12.4 and 12.5 reveals that the linear wave propagation predicted by the Moens-Korteweg equation 12.6 holds quite nicely. Of course there is attenuation of the pressure pulse. From the measured distensibility we predict a very small diameter variation of about 0.06 mm. This is confirmed by plotting the minimal and maximal edge of the acquired video images of the tube, see Figure 12.6 and 12.7, respectively.

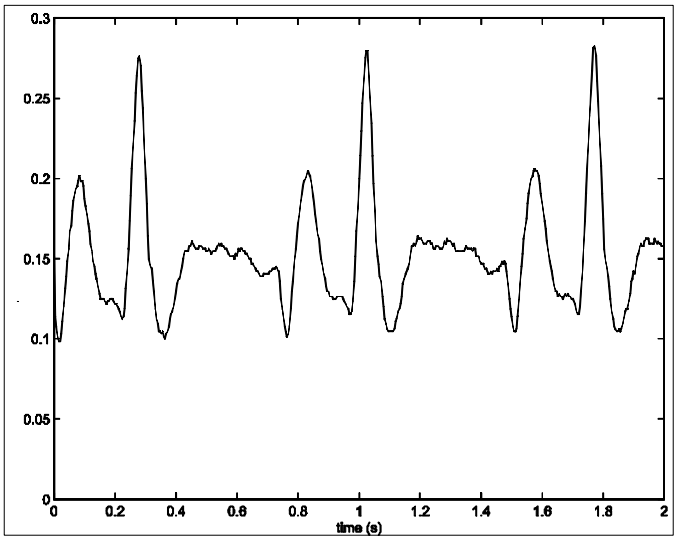

Figure 12.4: The measured pressure pulse near the entrance of the 7 m polyurethane tube.

12.4 CLINICAL STUDY

Information about local diameter variations as a response to the pulse flow in the human coronary arteries may indicate the development of atherosclerosis before this can be seen as a stenosis on coronary angiograms. In [9] we have described the design of an image processing tool to measure this diameter variation from a sequence of digital coronary angiograms. If a blood vessel responds less elastically to the pulse flow, this may be an indication of atherosclerosis in an early stage. We have developed an image analysis and processing algorithm, which is able after vessel segment selection in a Region of Interest (ROI) by the user, to calculate automatically the vessel diameter variations from a standard sequence of digital angiograms. Several problems occur and are taken care of. The periodic motion of the vessel segment in the consecutive frames is taken into account by tracking the vessel segment using a 2-dimensional logarithmic search to find the minimum in the mean absolute distance. A robust artery-tracing algorithm has been implemented using graph-searching techniques. The local diameter is determined by first resampling the image perpendicular to the found trace and afterwards performing edge detection using the Laplacian operator. This is repeated for all frames to show the local diameter variation of the artery segment as a function of time. In this section we briefly indicate the results of the sub-problems encountered in the approach one by one.

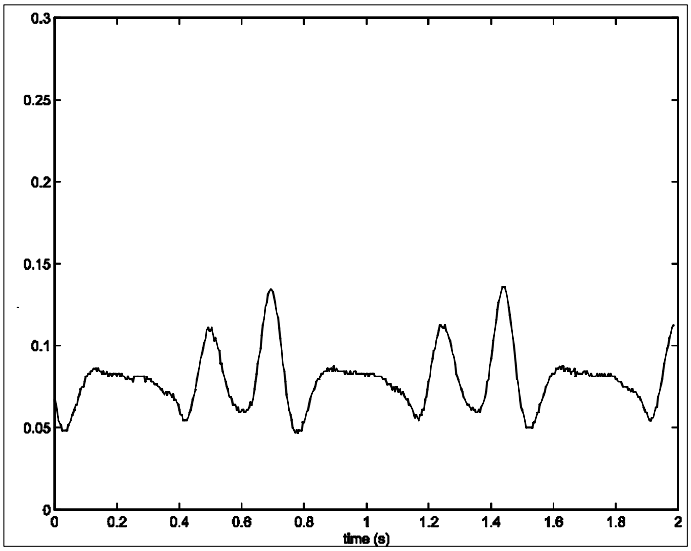

Figure 12.5: The measured pressure pulse at the end of the 7 m polyurethane tube.

12.4.1 Motion compensation

In [9] we have described two search methods, *i.e.* direct search and 2-dimensional logarithmic search, which have been implemented and compared. It appears that for our purpose, the direct searching is considerably faster than the 2-dimensional logarithmic (2DL) search. However, we also have observed that the 2DL search method is more robust. In image-sequences with larger motions of the ROI between frames, the 2DL search method performs better than the direct search method.

12.4.2 Artery localization and artery tracing

The artery localization algorithm seems robust. In the performed tests the found location was inside the correct artery. However, the accuracy of the algorithm is very hard to judge. One can never be sure that the found point exactly corresponds to the point in the previous frame. In some runs it was observed that the found position shifted along the artery, due to movement of the artery within the ROI along its own orientation. For our purpose this effect was not considered to be a problem. The graph searching method used for artery tracing is very robust. Start and endpoint are always connected and also in the case of side branches the path still follows the center line of the artery and does not deviate in the direction of the side branch.

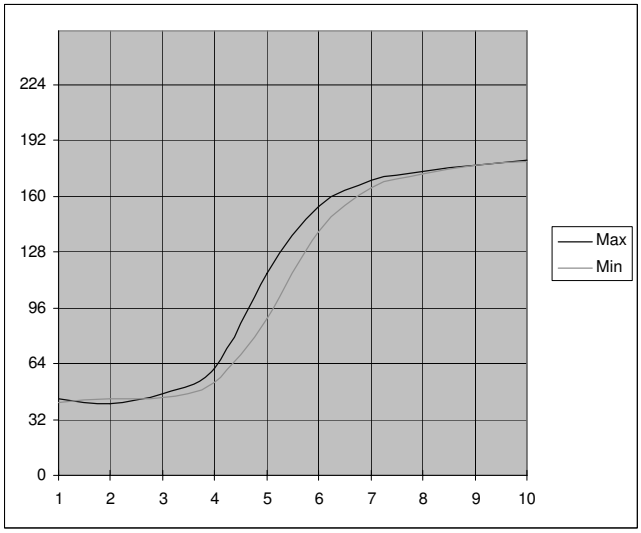

Figure 12.6: The measured edge variation near the entrance of the tube, grey level versus pixel.

12.4.3 Diameter determination

The edges are determined on the stretched artery segments. The edge enhancement window size used in the edge detection is 3×3. The discrete Laplacian approximation is applied according to:

$$\ell_2 = \begin{bmatrix} -1 & -1 & -1 \\ -1 & 8 & -1 \\ -1 & -1 & -1 \end{bmatrix} \tag{12.7}$$

Since we do not know the true location of the edges, it is very hard to specify the quality of the edge detection. One situation where the algorithm does not place the edges at the expected correct place is in the case of side branches or crossing vessels. In these cases the algorithm tends to follow the side branch or crossing vessel to return to the intended artery later. Though this problem may in many cases be avoided by careful selection of the ROI in the first frame it can never be ruled out completely. Since the relative position of vessels is not fixed, it may happen that a secondary vessel does not appear in the ROI in the first frame, but does cross the artery of interest in one of the later frames.

The set of algorithms performs the diameter determination for all frames

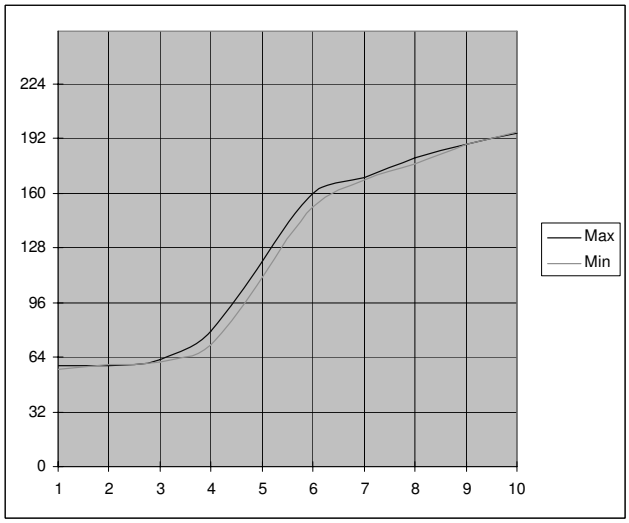

Figure 12.7: The measured edge variation at the end of the tube, grey level versus pixel.

and finally generate a curve that shows the average diameter and standard deviation of the selected artery segment as a function of time, see Figure 12.8.

The image sequence was obtained with an acquisition rate of 50 frames per second and a cardiac cycle period of 0.60 seconds. The artery segment was taken from a proximal site of the left anterior descending coronary artery. The graph shows pulsatile diameter changes of $\pm 4\%$. With an artery diameter of 3.5 mm this corresponds to diameter deviations of approximately 150 μm. The algorithm also generates a map of the local artery diameter as a function of time (horizontal) and position at the artery segment, see Figure 12.9. This artery segment of about 20 mm length was taken from the same branch as Figure 12.6 and contains a stenosis. The user is able to move a crosshair over the map to examine simultaneously the diameter as a function of time at a certain position (horizontal black curve) and the diameter as a function of position at a certain time (vertical black curve). The map shows that before the stenosis, at the position of the crosshair, the diameter changes are larger than at and after the stenosis, at positions near the time axis.

The image processing required for this estimation method is quite heavy. More measurement are needed, perhaps also with artificial blood vessels. For coronary angiography applications 1024^2 imaging seems to be necessary.

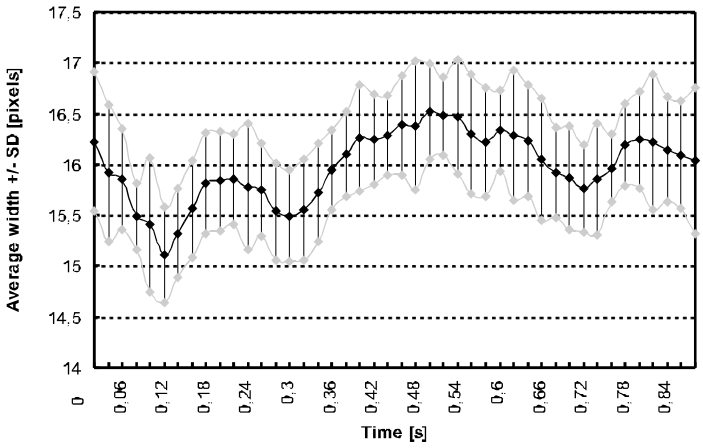

Figure 12.8: Artery diameter in pixels versus time.

References

[1] H.B. Atabek, "Wave propagation through a viscous liquid contained in a tethered, initially stressed, orthotropic elastic tube", *Biophys. J.* 8, pp. 626-649, 1968.

[2] C.G. Caro, T.J. Pedley, R.C. Schroter, and W.A. Seed, *The Mechanics of the Circulation*, Oxford University Press, Oxford, 1978.

[3] R.H. Cox, "Comparison of linearized wave propagation models for arterial blood flow analysis", /em J. Biomechanics, vol. 2, pp. 251-265, 1969.

[4] J.K.-J. Li, J. Melbin, R.A. Riffle, and A. Noordergraaf, "Pulse wave propagation", *Circ. Res.*, vol. 49, pp. 442-452, 1981.

[5] J. Lighthill, *Mathematical Biofluiddynamics*, Society for Industrial and Applied Mathematics, Philadelphia, 1975.

[6] D.A. McDonald, *Blood Flow in Arteries*, 2nd ed., Edward Arnold, London, 1974.

[7] T.J. Pedley, *The Fluid Mechanics of Large Blood Vessels*, Cambridge University Press, Cambridge, 1980.

[8] R.E. Shadwick, "Elasticity in arteries", *American Scientist*, vol. 86, pp. 535-541, 1998.

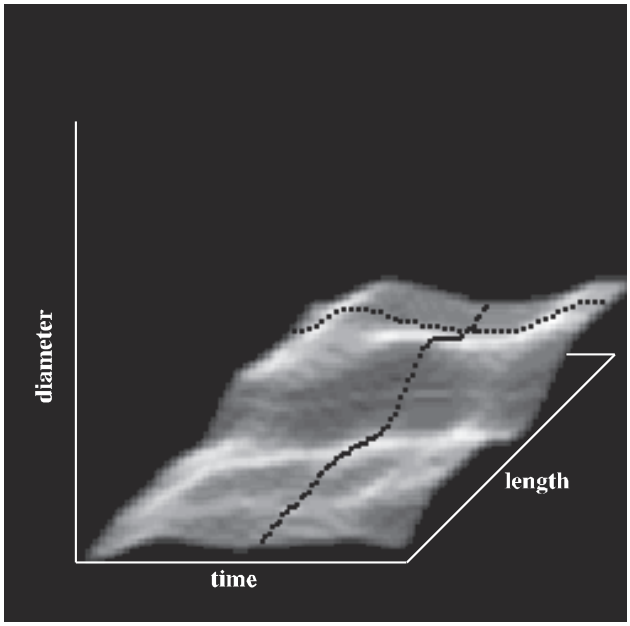

Figure 12.9: Local artery diameter map.

[9] C.H. Slump, M. Winkelman, R. Rutgers, C.J. Storm, and A.C. van Benthem, "Coronary artery diameter variations due to pulse flow propagation", SPIE Medical Imaging '97, vol. 3033, pp. 187-198, 1997.

[10] J.R. Womersley, "Oscillatory motion of viscous liquid in a thin-walled elastic tube. I. The linear approximation for long waves", *Phil. Mag.*, vol. 46, pp. 199-221, 1955.

[11] J.R. Womersley, "Oscillatory flow in arteries: the constrained elastic tube as a model of arterial flow and pulse transmission", *Phys. Med. Biol.*, vol. 2, pp. 178-187, 1957.

APPENDIX

We describe a simple one-dimensional model of an artery [5, 7] and consider the propagation of pressure pulse waves in a uniform, straight elastic tube of cross-sectional area A_0. The axis of the tube is along the z-coordinate. We assume the blood to be homogeneous and incompressible with density ρ. We now first assume that blood is inviscid because the velocity profiles in large arteries are rather flat which indicates that viscosity is only of importance in

thin boundary layers on the walls. We also assume that the wavelength of disturbances in our scope of interest, are long in comparison with the radius of the tube. The motion of the blood can, therefore, be described by the velocity component in the z-direction $u(z,t)$. The tube cross-sectional area is $A(z,t)$ and $p(z,t)$ denotes the (transmural) pressure, see Figure 12.10.

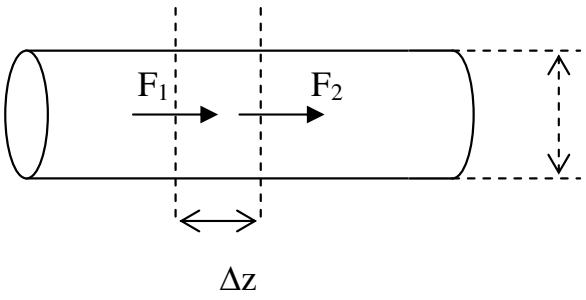

Figure 12.10: Tube segment of volume $A\Delta z$.

We consider the horizontal tube segment with volume $A\Delta z$ of Figure 12.10. Because of conservation of mass, the difference per second between the flow F_1 inwards the tube segment and flow F_2 out of the segment, equals the rate of increase in the amount of fluid in the tube segment:

$$\rho(F_1 - F_2) = \rho\frac{\partial(A\Delta z)}{\partial t}. \tag{12.8}$$

Using the identity $F = uA$, we obtain in the limit $\Delta z \to 0$:

$$\lim_{\Delta z\to 0}\frac{u_1A_1 - u_2A_2}{\Delta z} = -\frac{\partial}{\partial z}(u(z,t)A(z,t)) = \frac{\partial}{\partial t}A(z,t), \tag{12.9}$$

the equation of mass conservation:

$$\frac{\partial}{\partial t}A(z,t) + \frac{\partial}{\partial z}(u(z,t)A(z,t)) = 0 \tag{12.10}$$

If we apply the equation of motion on the fluid segment, neglecting the viscous force and, because of the horizontal orientation of the tube, the gravitation, we arrive at:

$$p_1A_1 - p_2A_2 = \rho a\Delta z\frac{d}{dt}u(z,t), \tag{12.11}$$

with: $\frac{du}{dt} = \frac{\partial u}{\partial z}\frac{dz}{dt} + \frac{\partial u}{\partial t}$, we obtain in the limit $\Delta z \to 0$:

$$\lim_{\Delta z\to 0}\frac{u_1A_1 - u_2A_2}{\Delta z} = \rho A\left(\frac{\partial u}{\partial t} + u\frac{\partial u}{\partial z}\right), \tag{12.12}$$

which results in:

$$\frac{\partial}{\partial t}u(z,t) + u(z,t)\frac{\partial}{\partial z}U(z,t) + \frac{1}{\rho}\frac{\partial}{\partial z}p = 0, \tag{12.13}$$

the momentum equation. Besides the two conservation equations, *i.e.* of mass (A.3) and momentum (A.6), we need a relation between p and A. For a thin-walled elastic tube the law of Laplace states that an extra pressure p inside a tube of internal radius a, causes a circumferential tensile stress, averaged across the wall thickness h, equal to:

$$\sigma = \frac{pa}{h}. \tag{12.14}$$

In thin-walled tubes such as arteries h/d_0 is small, with d_0 the undisturbed diameter of the tube, the mean circumferential tensile stress is larger than the radial stress. For the corresponding circumferential strain we have with $l = 2\pi a$ the perimeter of the vessel and with E the Young modulus of the wall:

$$E = l\frac{d\sigma}{dl}. \tag{12.15}$$

In our situation we have:

$$\frac{\Delta a}{a} \ll \frac{\Delta p}{p}, \tag{12.16}$$

so that we assume a to be constant in the Laplace equation. From this the desired relation between p and A follows:

$$\frac{dp}{da} = \frac{Eh}{a^2}. \tag{12.17}$$

Chapter 13

Digital densitometric determination of relative coronary flow[1]

In clinical cardiology, stenosis in a coronary artery is measured on the basis of visual assessment. The reading of coronary arteriograms leads, however, to large inter- and intra-observer variability. Image analysis and computer assistance result in a more consistent assessment, but this approach is mainly based upon static geometric parameters, such as diameter reduction of a segment of the stenosed artery. A more functional, physiological measurement is thus desirable. This can be realised by measuring the difference between the normal coronary blood flow and the increased flow under hyperaemic conditions, yielding the so-called coronary flow reserve (CFR). In clinical practice, however, this method is difficult and time-consuming. A less demanding approach is reported, in which relative flow distributions are determined densitometrically from digital angiograms acquired under basal and hyperaemic conditions. The proposition is that, if the relative flow distribution in hyperaemic state differs from that during rest, the functional severity of a stenosis downstream from the bifurcation can be indicated. The new approach is validated by comparing the results of a theoretical model for steady flow with a flow phantom experiment for steady and pulsatile flow. The obtained flow ratios correlate very well, both in steady and pulsatile flow, with correlation coefficients exceeding 0.95.

[1]N.P. Csizmadia, C.H. Slump, A.P.G. Lubbers, M. Schrijver, C.J. Storm, "Digital densitometric determination of relative coronary flow distributions", *Med. Biol. Eng. Comput.*, 39, pp. 301 - 309, 2001.

13.1 INTRODUCTION

In cardiology, the standard technique of cine-angiography is widely used to assess the clinical relevance of stenosed coronary arteries. This visual assessment is impaired by a large inter- and intra-observer variability (DeRouen, 1977) and does not provide information about the actual blood flow (Harrison, 1984). Digital image acquisition enables on-line image analysis and computer assistance, such as quantitative coronary angiography. The so-called Coronary Flow Reserve or CFR (Vogel, 1985 and Gould, 1990) is a functional measure that provides information about the perfusion of the heart muscle. In CFR calculations, the measured local maximum contrast density represents the vascular volume, and the measured local contrast arrival time is assumed to be inversely proportional to flow (Cusma et al., 1987). The contrast is measured in a Region of Interest (ROI) on the heart muscle (without an overlaying major blood vessel) as a function of time. This is the so-called time-density curve. The required hyperemic state of exercise can be induced artificially by the injection of a vasodilator drug, e.g. papaverine. In this hyperemic state, the capillary vessels are maximally open, thus increasing the blood flow to the physical limits set by the sizes of the coronary arteries, and especially the stenosed segments.

The CFR can be visualized in a functional image, in which the image gray values are directly proportional to the increase in blood flow in the applicable part of the heart muscle. Areas with less blood flow increase show up dark, thereby indicating the effects of impaired blood flow because of stenosed segments in the coronary arteries and possible (partial) infarction. Although good results have been reported with the CFR method, in clinical practice the procedure is demanding. In particular, the correction for background disturbances is difficult because of the contracting heart dynamics. The prerequisite is that the two registered image sequences are identical. However, patient movements cannot be eliminated completely. Therefore, pacing of the heart together with ECG-triggered image acquisition is recommended.

In this paper we report on an approach which is less time-consuming and less demanding in procedure. Our goal is restricted to the densitometric determination of the relative flow distribution in the two main branches of the left coronary artery, the Left Circumflex Artery (LCA) and Left Anterior Descending (LAD) artery. The intent is that the comparison between the distributions in hyperemic and basal states provides clinical information about the severity of stenosed artery segments in the relevant branch. To this end, we acquire a sequence of digital angiograms at a typical rate of 50 frames per second. All images for this research are generated at the Leiden University Hospital with a Philips Digital Cardiac Imaging cath. lab. A short contrast bolus (typically 1 to 2 ml) is injected via a positioned catheter. X-ray pulses are generated with a duration of typically 5 to 8 ms at a typical rate of 12.5 to

50 frames per second. The X-ray image is detected by the image intensifier and converted into a video image through an optically coupled videocamera. After analog preprocessing, the video image is converted into a matrix of 512 $\times$ 512 pixels with 8 bits/pixel.

Time-density curves are obtained from the acquired image sequences, by integrating the image density within properly positioned Regions of Interest (ROI's) on the main artery and on the branches behind the bifurcation. The relative flow distribution is obtained from the time differences between the Center of Gravity (COG) of the time-density curve in the main artery and the branches, respectively. In Lubbers et al. (1993), we have shown the usefulness of the COG parameter in an experimental flow study, with a glass model phantom of the left coronary artery for the case of steady flow. In this paper we describe a theoretical model for the generation of time-density curves for steady flow. The experimental validation is extended to include pulsatile flow effects. The paper concludes with a discussion of the clinical outlook of the proposed method.

13.2 METHOD

We will first describe the generation of the time-density curves. The logarithm of each pixel is calculated for all the images in the acquired sequence. Similar to digital subtraction angiography (Kruger and Riederer, 1984; Verhoeven, 1985), we subtracted a logarithmic so-called pre-contrast image, acquired prior to the injection of contrast fluid. In this way we obtained pixel gray values that are directly proportional to the projection of the local amount of contrast fluid in the artery. The total amount of contrast fluid in the ROI is directly proportional to the sum of the pixel values in the relevant ROI. As this is done for each image in the sequence, the calculated amount of contrast fluid in the ROI as a function of time is reflected in the time-density curves.

Assume a straight cylindrical tube as a model of an artery along which two ROI's are placed (see Figure 13.1). The volume flow rate ϕ_v (m^3s) in the tube is linearly proportional to the average velocity $v_{av}(ms)$ of the fluid in the tube:

$$\phi_v = v_{av} \cdot A = \frac{L}{\Delta t} \cdot A, \tag{13.1}$$

where $A(m^2)$ is the cross-sectional area of the tube, $L(m)$ is the distance between the ROI's and $t(s)$ is the transit time of the contrast bolus between the ROI's.

The Relative Flow Distribution (RFD) between the branches in a bifurcation is equal to the ratio of the transit times of the contrast bolus in the left and the right branch:

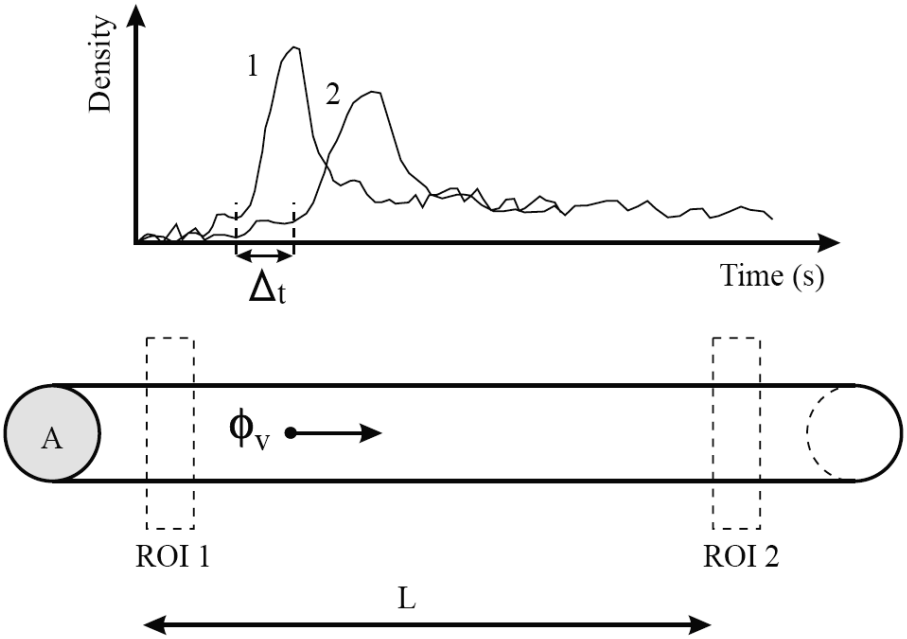

Figure 13.1: An artery modeled as a straight cylindrical tube. ROI's are placed to generate time-density curves.

$$RFD = \frac{\phi_{v_{lb}}}{\phi_{v_{rb}}} = \frac{\frac{L}{\Delta t_{lb}} \cdot A_{lb}}{\frac{L}{\Delta t_{rb}} \cdot A_{rb}} = \frac{\Delta t_{rb}}{\Delta t_{lb}}, \tag{13.2}$$

where the subscripts *rb* and *lb* denote right branch and left branch respectively (Schrijver, 1999). It should be noted in Equation 13.2 that it is assumed that the cross-sectional areas in the left and the right branch, A_{lb} and A_{rb} respectively, are the same. If the cross-sectional areas are not the same, the right-hand side of Equation 13.2 has to be multiplied by the ratio of the cross-sectional areas. This factor cancels, however, if the relative flow distributions in hyperemic and basal state are divided to obtain the indication proposed in this paper, see Equation 13.3. The same holds for the path lengths (indicated by the symbol $'L'$ in Eqn. 13.2).

$$Indication = \frac{RFD_h}{RFD_b} = \frac{\frac{A_{lb}}{A_{rb}}}{\frac{A_{lb}}{A_{rb}}} \cdot \frac{(\frac{\Delta t_{rb}}{\Delta t_{lb}})_h}{(\frac{\Delta t_{rb}}{\Delta t_{lb}})_b} = \frac{(\frac{\Delta t_{rb}}{\Delta t_{lb}})_h}{(\frac{\Delta t_{rb}}{\Delta t_{lb}})_b} \tag{13.3}$$

The transit times, or mean transit times in case of pulsatile flow, which are needed to obtain the indication proposed in Equation 13.3, can be de-

termined from generated time-density curves. The transit time of a contrast bolus between two ROI's, is equal to the difference in arrival time of the tip of the contrast bolus at the two ROI's (see Figure 13.2). Unfortunately, time-density curves are rather irregular, making it almost impossible to determine the arrival time of the contrast bolus.

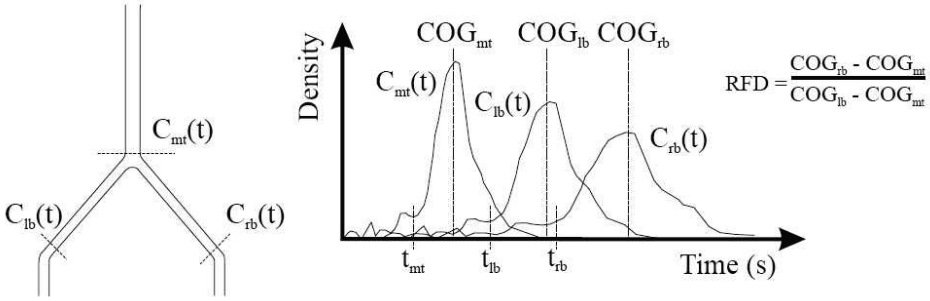

Figure 13.2: Example of applying the arrival time and the center of gravity to determine the transit time of a contrast bolus.

The point along the time axis, where the area under a time-density curve $D(t)$ to the left of that point equals the area under the time-density curve $D(t)$ to the right of that point, is the COG of $D(t)$:

$$\int_{-\inf}^{COG} D(t)dt = \int_{COG}^{\inf} D(t)dt. \tag{13.4}$$

Assuming a linear relationship between the arrival time and the COG, the relative flow distribution in a bifurcation can be calculated from:

$$RFD = \frac{\Delta t_{rb}}{\Delta t_{lb}} = \frac{t_{rb} - t_{mt}}{t_{lb} - t_{mt}} = \frac{a \cdot COG_{rb} + b - a \cdot COG_{mt} - b}{a \cdot COG_{lb} + b - a \cdot COG_{mt} - b} = \frac{COG_{rb} - COG_{mt}}{COG_{lb} - COG_{mt}}, \tag{13.5}$$

where t_{mt}, t_{lb} and $t_{rb}(s)$ are the arrival times of the contrast bolus in the main trunk, left branch and right branch respectively, and COG_{mt}, COG_{lb} and $COG_{rb}(s)$ are the COG's in the main trunk, left branch and right branch respectively (see Figure 13.2).

It is important to note that the COG is determined by integrating the time-density curves. This implies that a kind of averaging is incorporated. Therefore, the COG method is expected to be less liable to errors due to the rather noisy nature of the time-density curves obtained. A problem in this approach is that the contrast fluid disperses as it travels through the tube, since the flow velocity is not a constant but a parabolic function of the radius inside the tube. In the next section this phenomenon is examined in detail.

13.3 APPLICATION TO STEADY POISEUILLE FLOW

Consider a rigid, straight and cylindrical tube (Figure 13.3) in which a Newtonian fluid flows at an average flow velocity, such that the Reynolds number is below its critical value. In that case, flow is laminar and the flow velocity profile is a parabolic function:

$$v(r) = v_0(1 - \frac{r^2}{r_i^2}), \tag{13.6}$$

where v_0 is the flow velocity at the axis of the tube, and r_i is the inner radius of the tube. Assume that the flow begins to develop at $t = 0$ according to the flow velocity profile given in Equation 13.6. From this equation, it is clear that fluid particles which are arranged in cylindrical laminae along the axis of the tube all begin to move at the same velocity (Landau and Lifschitz, 1959) (see Figure 13.3).

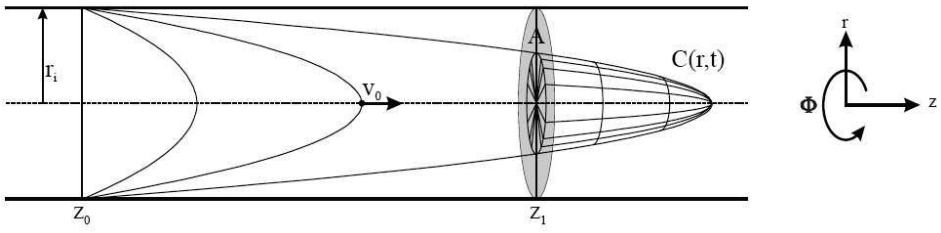

Figure 13.3: Axial cross-section of a rigid cylindrical tube in which Poiseuille flow starts to develop.

The volume $V(z_0, z_1, t)(m^3)$ enclosed by $C(r, t)$ and the cross-sectional area A at z_1 is equal to (integrate Eqn. 13.6 both over time and over the volume):

$$V(z_0, z_1, t) = \pi r_i^2(z_0 - z_1 + \frac{(z_0 - z1)^2}{2v_0t} + \frac{v_0t}{2}). \tag{13.7}$$

Equation 13.7 can be used to model the dispersion of contrast fluid in an infinite, rigid and cylindrical tube, as shown in the Appendix. Using the model developed there, we obtain the time-density curve of Figure 13.4.

For comparison with the theoretical time-density curve of Figure 13.4 (based on the model developed in the Appendix), a measured time-density curve from the experiments is presented in Figure 13.5.

Several time-density curves were generated computationally to investigate the relationship between the arrival time and the COG. The COGs of these time-density curves are plotted against the corresponding arrival times

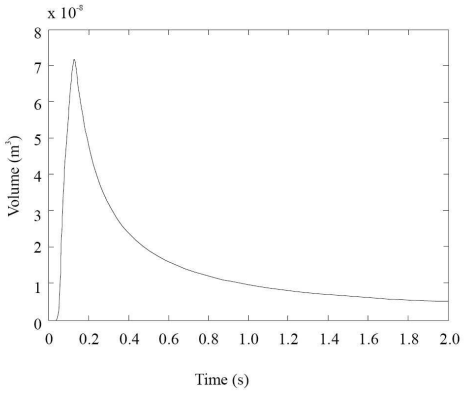

Figure 13.4: A time-density curve calculated using the model developed in the Appendix.

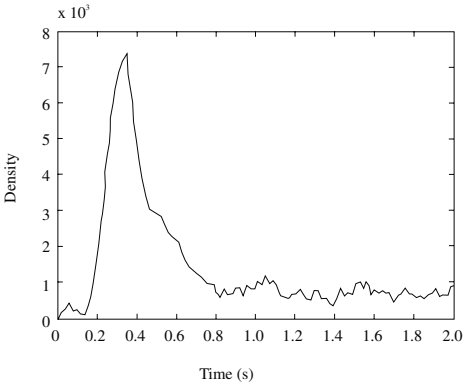

Figure 13.5: An example of a measured time-density curve.

in Figure 13.6. Several time-density curves were generated computationally to investigate the relationship between the arrival time and the COG. The COGs of these time-density curves are plotted against the corresponding arrival times in Figure 13.6.

From these curves, it is clear that the relationship between the COG and the arrival time can be approximated by a straight line. The correlation can be improved, however, if the time-density curves are thresholded at 55% of their peak value before determining of the COG (see Figure 13.7).

13.4 EXPERIMENTAL VALIDATION

this section, we discuss the design of the flow experiments at Leiden University Hospital. A flow phantom made of glass was developed, as a model of

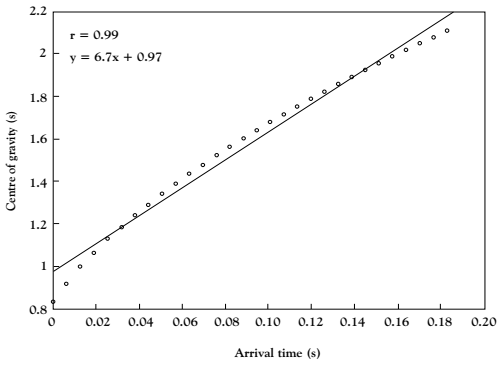

Figure 13.6: The relationship between the COG and the arrival time of time-density curves obtained from the contrast dispersion model. $r = 0.99, y = 6.7x + 0.97$

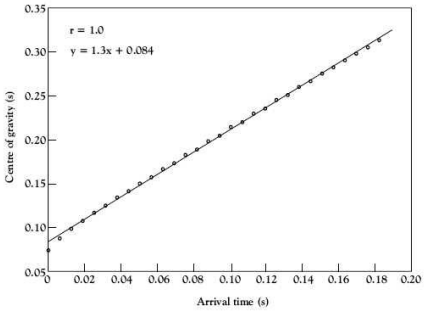

Figure 13.7: The relationship between the COG and the arrival time of time-density curves is more linear when the time-density curves are thresholded prior to determining the COG. $r = 1.0, y = 1.3x + 0.084$

the bifurcation in the proximal part of the left coronary artery (see boxed area of Figure 13.8).

The flow phantom consists of a main trunk with an inner diameter of 4 mm, bifurcating into branches with an inner diameter of 3 mm. The bifurcation is symmetrical with a bifurcation angle of 80 degrees (Reul, 1983), although Pedley (1980: p. 12) states 45 degrees. Upstream in the main trunk, an extra branch has been attached, to position the catheter by which the contrast fluid will be injected. Note that the bifurcation has a blunt flow divider.

In arteries having a relatively large internal radius when compared to the size of blood cells, blood behaves like a Newtonian fluid with a dynamic viscosity of 4×10^{-3} kg/ms at 37.7 ^{o}C (Nichols, 1990). In the experiments we use a solution of crystal sugar in demineralized water, in a ratio of one mass part of sugar to two mass parts of water. This solution was found to have

nearly the same dynamic viscosity as blood. Steady flow in the experimental setup is generated by squeezing the solution out of a large cylinder using a piston (see Fig. 8). Through a rigid supply tube, the solution is forced through the flow phantom. This steady flow is modulated by a smaller cylinder in order to simulate the pulsatile nature of blood flow in the left coronary artery. As a reference of left coronary blood flow, the blood flow as described by Schlant et al. (Schlant, 1990) is used.

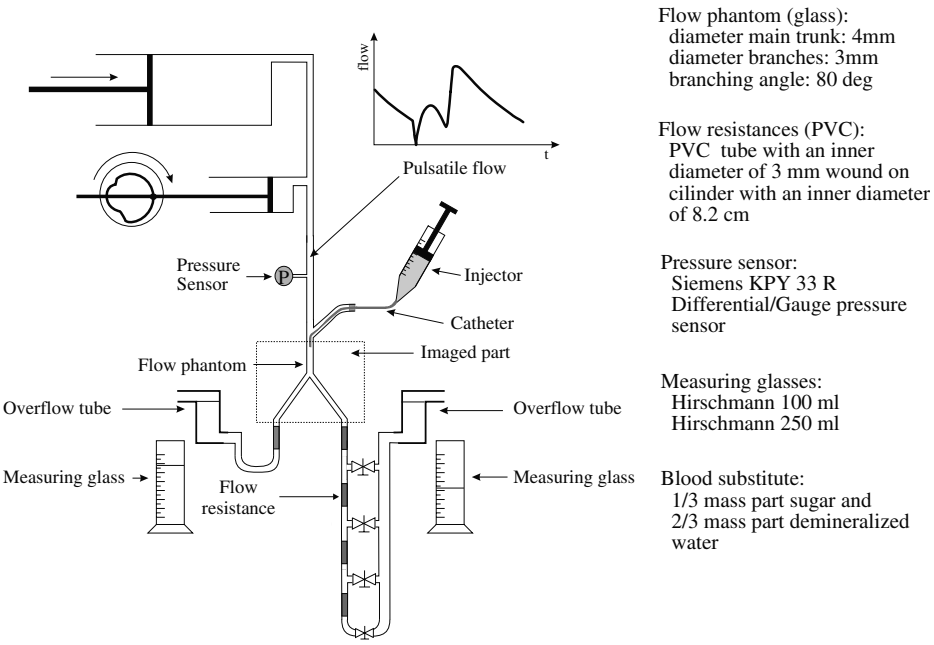

Figure 13.8: Overview of the experimental setup.

In the experimental setup depicted in Figure 13.8, the flow ratio in the bifurcation is adjusted by modifying the length of the tube between the outflow openings of the bifurcation and the overflow tubes. The modification of the tube length L is realized by cascading a number of tubes, all with a length of approximately 1 meter. To prevent evaporation, rigid PVC tubes have been used in the experimental setup.

13.5 RESULTS

Prior to the image acquisition, a catheter was positioned in the main trunk (see Figure 13.8). A timing device started the generation of flow and the

image acquisition. After three seconds, the timing device signaled the cardiologist to inject contrast fluid. This was injected by hand. After a specified period, after assuring that the measuring glasses were filled at least halfway, the flow was interrupted. The amount of fluid collected in each measuring glass was assessed and registered. Between runs, the flow rate and the flow ratio in the flow phantom were adjusted. The results for a steady flow are depicted in Figure 13.9, similarly for a pulsatile flow in Figure 13.10.

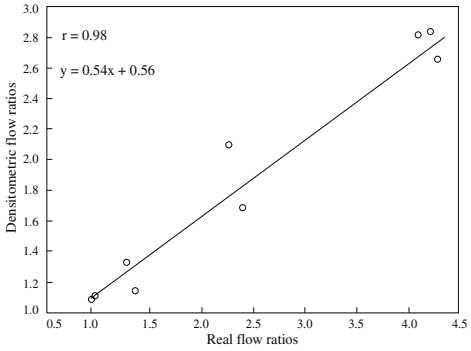

Figure 13.9: Correlation between the densitometric and real flow ratios in case of steady flow.

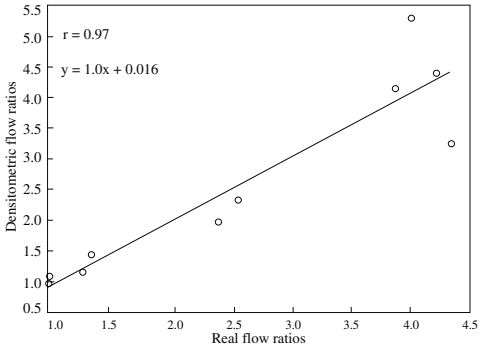

Figure 13.10: Correlation between the densitometric and real flow ratios in case of pulsatile flow.

It is worth noting that the slopes of the two graphs differ because of the specific definition of the RFD (Eqn. 13.2), where the path lengths are left out of the equation.

The method described above has also been applied to digital angiograms, to examine its applicability to clinical data. ROI's were positioned on the

main bifurcation of the left coronary artery (see Figure 13.11), and time-density curves were generated. The motion of the left coronary artery in the angiograms, resulting from respiratory, cardiac and random patient motion, hampers the generation of time-density curves. During each run, the ROI's had to be repositioned frequently in order to maintain their proper position. In the future we expect to automate this process through motion estimation.

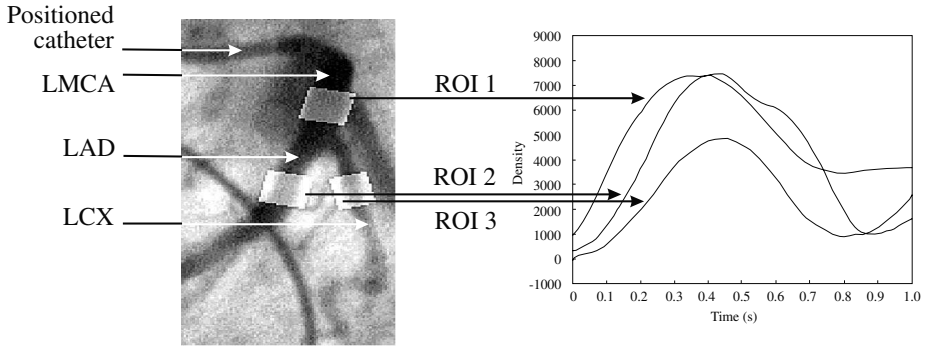

Figure 13.11: Positioning of ROI's on the bifurcation of the left main coronary artery in the left circumflex artery and left anterior descending artery.

The relative flow distributions in the bifurcations have been calculated from the generated time-density curves, yielding 1.18 for the bifurcation depicted in Figure 13.11. Since no other information was available about the relative flow distributions, it is not possible to evaluate the correctness of the determined relative flow distributions. From the investigations it is clear, however, that the method can be applied easily, is robust and has no extra technical demands.

13.6 DISCUSSION and CONCLUSION

The COG method gives adequate results in case of irregular time-density curves. The obtained flow ratios correlate very well both in steady and pulsatile flow, with correlation coefficients exceeding 0.95 (see Figures 13.9and 13.10). The best results are achieved if the densitometric flow ratio is determined from time-density curves situated as far as possible downstream from the bifurcation, since that results in the greatest difference in traveling times. The position of the ROI in the main trunk was found to be far less significant. Application of the technique with clinical coronary angiograms shows similar time-density curves. However, the correctness of the method has not been evaluated yet. It must also be noted that the method

may incorrectly yield a negative outcome when both arteries distal to the bifurcation exhibit stenoses (Schrijver, 1999).

ACKNOWLEDGMENTS

The technical support by H. Kuipers in the design and realization of the flow phantom, as well as during the experiments, is gratefully acknowledged. The mechanical workshop of the Department of Electrical Engineering of Twente University, headed by J.E. Westendorp, did an excellent job in realizing the pulsatile flow system. Furthermore we like to thank the late Prof. Dr. B. Buis and co-workers of the Cardiology Department of University Hospital Leiden for using the digital X-ray equipment, and A.C. van Benthem and Ms. M. van Osta of the Application Department of Philips Medical Systems in Best for their support in the experiments. We also wish to acknowledge the fruitful discussions that we had with Prof. Dr.-Ing. O.E. Herrmann.

APPENDIX

Time - density curve for steady Poiseuille flow

Consider the tube depicted in Figure 13.12. A1, which is filled with a Newtonian fluid. This fluid is completely replaced by a contrast fluid between z_{cl} and z_{cr}. Owing to the relative high viscosity of the contrast fluid, we assume no mixing with the blood stream. An ROI is placed between z_{rl} and z_{rr}. Assume that flow begins to develop at $t = 0$.

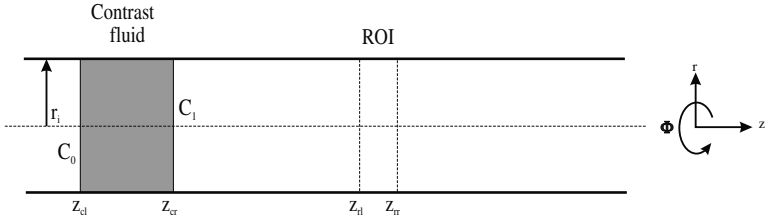

Figure 13.12: A rigid cylindrical tube filled with a Newtonian fluid. Between z_{cl} and z_{cr} the fluid is replaced by contrast fluid. An ROI is placed between z_{rl} and z_{rr}.

In the following sequential steps, we consider the relative positions of the ROI with respect to the contrast bolus separately:

$$\text{(i)} \qquad 0 \leq t < \frac{z_{rl} - z_{cr}}{v_0} \tag{13.8}$$

In this case, the contrast fluid has not yet appeared in the ROI. This implies that the time-density curve $D(t)$ is zero.

$$\text{(ii)} \qquad \frac{z_{rl} - z_{cr}}{v_0} \leq t < \frac{z_{rr} - z_{cr}}{v_0} \tag{13.9}$$

In this case, contrast fluid begins to appear in the ROI (see Figure 13.13). The amount of contrast fluid in the ROI at time t, can be obtained from Eqn. 13.7:

$$D(t) = V(z_{cr}, z_{rl}, t) \tag{13.10}$$

$$\text{(iii)} \qquad \frac{z_{rr} - z_{cr}}{v_0} \leq t < \frac{z_{rl} - z_{cl}}{v_0} \tag{13.11}$$

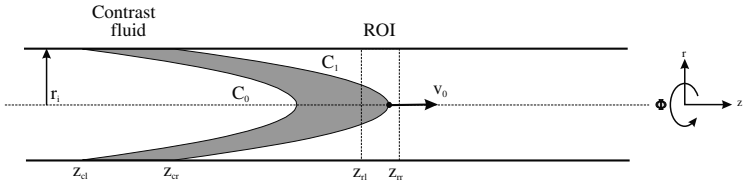

Figure 13.13: Contrast fluid appears in the ROI.

The amount of contrast fluid in the ROI is equal to the volume enclosed between C_1 and the cross-sectional area at z_{rl}, less the volume enclosed between C_1 and the cross-sectional area at z_{rr} (see Figure 13.14).

$$D(t) = V(z_{cr}, z_{rl}, t) - V(z_{cr}, z_{rr}, t) \tag{13.12}$$

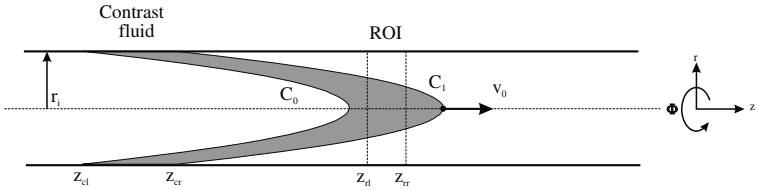

Figure 13.14: Cone C_1 has traversed the tube past z_{rr}. Cone C_0 has not yet reached z_{rl}.

$$\text{(iv)} \qquad \frac{z_{rl} - z_{cl}}{v_0} \leq t < \frac{z_{rr} - z_{cl}}{v_0} \tag{13.13}$$

In this case, the apex of cone C_0 has traversed the tube beyond the cross-section at z_{rl}. The amount of contrast fluid in the ROI at time t is equal to the amount in case (iii), less the volume enclosed between C_0 and the cross-sectional area at z_{rl}:

$$D(t) = V(z_{cr}, z_{rl}, t) - V(z_{cl}, z_{rr}, t) - V(z_{cl}, z_{rl}, t) \tag{13.14}$$

$$\text{(v)} \qquad t \geq \frac{z_{rr} - z_{cl}}{v_0} \tag{13.15}$$

Both C_1 and C_0 have traversed the tube beyond z_{rr} (see Figure 13.14). In this case the time-density curve is equal to:

(11)

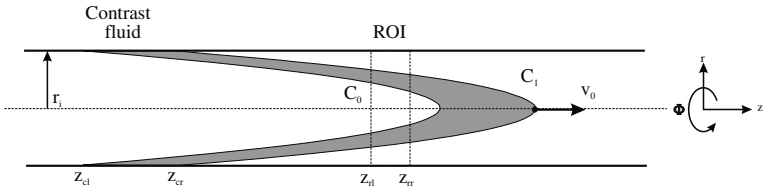

Figure 13.15: C_0 has traversed the tube past z_{rr}.

$$\text{(iii)} \qquad \frac{z_{rr} - z_{cr}}{v_0} \leq t < \frac{z_{rl} - z_{cl}}{v_0} \tag{13.16}$$

Chapter 14

Myocardial fractional flow reserve[1]

Pijls and De Bruyne (1993) developed a method employing intravascular blood pressure gradients to calculate the Myocardial Fractional Flow Reserve (FFR). This ow reserve is a better indication of the functional severity of a coronary stenosis than percentage diameter or luminal area reduction as provided by traditional Quantitative Coronary Angiography (QCA). However, to use this method, all of the relevant artery segments have to be selected intra-operatively. After the procedure, only the segments for which a pressure reading is available can be graded. We previously introduced another way to assess the functional severity of stenosis using angiographic projections: the Relative Coronary Flow Reserve (RCFR). It is based on standard densitometric blood velocity and ow reserve methods, but without the need to estimate the geometry of the artery. This paper demonstrates that this RCFR method yields - in theory - the same results as the FFR, and can be given an almost identical interpretation. This provides the opportunity to use the RCFR retrospectively, when pressure gradients are not available for the segment(s) of interest.

14.1 INTRODUCTION

In recent cardiology, there has been an increasing interest in the assessment of the severity of coronary stenoses. This renewed interest is partly due to the advent of new imaging techniques[1], but also to the recognition of the fact that an accurate diagnoses reduces overall costs[2]. Also, with the current variety of therapies and interventional procedures, it has become important

[1]presented at Medical Imaging 2001: Physiology and Function from Multidimensional Images, and published in part as: M. Schrijver, C.H. Slump, C.J. Storm, "Myocardial fractional flow reserve: a biplane angiocardiographic alternative to the pressure gradient method," in *Medical Imaging: Physiology and Function from Multidimensional Images*, Chin-Tu Chen, Anne V. Clough, eds., *Proc. SPIE* vol.4321, pp. 458 - 466, 2001.

to study the effectiveness of each of them. This means that the long-term effects should be taken into account, since measures of the short-term results of interventions are poor predictors for new cardiac events due to transient effects of the reperfusion[3]. In conclusion, there clearly is a need for a reliable, reproducible and cost-effective measure of the true physiologic severity of coronary stenoses, before and after treatment.

Despite the fact that many researchers have published methods to assess the severity of coronary stenoses[2, 4, 5, 6, 7], none of them seems to have been adopted on a worldwide scale. One can speculate upon the reasons for this failure to define one standard method, but one of the major reasons undoubtedly is the fact that most methods actually measure something different. Although each of them assesses some sort of 'severity', they all define this severity differently, making them less comparable than they appear to be. Consequently, it is generally impossible simply to replace one method with the other; depending on the clinical application one specific method is utilized[4, 6, 8]. In this light, the lack of a true worldwide standard is not surprising.

The purpose of this article is not to introduce yet another method to assess the severity of coronary stenosis. Instead, we want to show that, under specific conditions, two different measures yield comparable results. In this particular case, comparing the Fractional Flow Reserve (FFR)[7] and the Relative Coronary Flow Reserve (RCFR)[6, 9], this may become advantageous, because the former is quite accurate but can only be determined intra-operatively, while the latter can be applied retrospectively.

14.2 PHYSIOLOGIC SEVERITY OF CORONARY STENOSES

For many years, the severity of a stenosis has been defined by the geometrical dimensions of that stenosis, as determined using (quantitative) coronary angiography (QCA). Although the problems with such methods have been recognized for decades[3], only the last couple of years it seems to lose its "golden standard" position, except for describing the true mechanical severity of an artificial obstruction in animal studies. Apart from the technical problems associated with angiographic determination of stenosis dimensions (insufficient contrast injection, jet streaming, calibration problems, foreshortening, overlap, considerable inter- and intra-observer variations etc.)[3, 5] there is some controversy on the correlation of stenosis geometry with the functional severity of that stenosis. Only when all geometric properties (area, length, shape etc.) are taken into account, the results are quite favorable[6].

However, even when the mechanical severity of a stenosis can be derived from accurately determined stenosis dimensions and hydraulic theory,

it does not predict the *physiologic* influence on the actual regional myocardial perfusion. The physiologic influence of a stenosis on the perfusion is highly dependent on factors like collateral blood flow, myocardial hypertrophy, hypertension, and necrosis. Also, the mechanical severity is poorly correlated with the results to be expected after thrombolysis or intervention[1, 2, 3]. The advent of newer imaging modalities that enable more accurate assessment of stenosis dimensions like EBCT or three-dimensional intravascular ultrasound, will not improve these shortcomings. Therefore, the main improvement to be expected from those new developments is in perfusion imaging, not necessarily in determining mechanical stenosis severity.

In contrast to the geometry based methods, blood flow measures try to assess the influence of a stenosis on the overall myocardial circulation. The rationale is that in patients with an epicardial stenoses, the regional myocardial blood flow is not only determined by the arteriolar auto-regulation system of the perfused cardiovascular bed (as is the case in completely healthy subjects), but also by that epicardial stenosis[10]. These blood flow based methods range from very simple ones like maximum blood flow, to quite sophisticated measures taking collateral blood flow into account. The advantages and disadvantages of each of them consequently differ, depending on the exact approach chosen to measure the blood flow and to quantify the severity. In the research at hand, the flow reserve methods play an important part, and are subsequently described in more detail in the next sections.

14.2.1 Definition of Flow Reserve

By measuring the increase in blood flow in response to a flow increasing stimulus (such as exercise or pharmacological arteriolar vasodilation), an estimate is obtained of the capacity of the arteries to supply the amount of blood that matches the metabolic demand of the myocardium. So, if the increase in blood flow is not as high as expected, this can be attributed to the stenosis in the supplying artery. However, other influences on blood flow, such as impaired ventricular function or changes in heart rate, should be ruled out before this conclusion can be drawn[4, 10].

Although many different definitions exist to quantify the increase in blood flow during an arteriolar vasodilative stimulus[4], the *flow reserve* is the most common one. It is defined as the mean blood flow during maximal arteriolar vasodilation, divided into the mean normal baseline blood flow[11] as illustrated in Figure 14.1(a):

$$\text{Flow Reserve} = \frac{\text{maximum flow}}{\text{normal resting flow}} = \frac{Q^{(h)}}{Q^{(0)}} \tag{14.1}$$

The superscripts (h) and (0) denote mean hyperemic blood flow (during maximal arteriolar vasodilation) and mean resting blood flow, respectively.

Myocardial and coronary flow reserve

When the concept of flow reserve is applied to the myocardium itself, that is, the regional myocardial blood flow is considered, the resulting *myocardial flow reserve* may not reflect the true influence of the epicardial stenosis on the blood flow through that stenosis. This is due to the compensatory effect of collateral blood flow Q_c, which bypasses the stenosis to help perfuse the myocardial region as shown in Figure 14.1(b).

If, in contrast, the flow reserve is calculated by measuring the blood flow Q_S through the stenosis itself, the resulting *coronary flow reserve* does reflects the effect on the blood flow through that stenosis. However, it overestimates the negative influence of that stenosis on the regional myocardial perfusion, due to the compensating effect of collateral blood flow. Therefore, the myocardial flow reserve is in general higher than the coronary flow reserve, especially with well developed collateral vessels as a result of a long history of atherosclerosis.

This is one example where two seemingly equal measures are hard to compare in practice. And it probably is not even desirable to try to decide which one is the better measure of stenosis severity. If the objective of the measurement is to determine whether or not to defer an interventional procedure, the myocardial flow reserve is probably more indicative (the myocardial perfusion is the main concern, not the specific path the blood follows). In contrast, the coronary flow reserve is more useful in evaluating the extend of success of such a procedure. And by measuring *both* the coronary and the myocardial flow reserves, assessment of the contribution of collateral blood flow to the regional myocardial perfusion is possible[7]. In conclusion, the combination of the two measures is probably more useful then each of them separately.

Absolute and relative flow reserve

For healthy humans, the flow reserve is known to be about five, although considerable variations exist due to physiologic or pathologic factors other than the stenosis that influence the resting and maximum blood flows. Consequently, the absolute flow reserve is sometimes compared to the flow reserve in another region of the myocardium, resulting in a *relative* flow reserve[6, 9, 10]:

$$RCFR_{a,b} = \frac{CFR_a}{CFR_b} \tag{14.2}$$

Gould and coworkers report that this relative flow reserve is less sensitive to changing hemodynamic factors than the absolute flow reserve, but that absolute coronary flow reserve is essential in assessing diffuse coronary artery disease[1, 6]. This is another example where two different measures of

stenosis severity provide complementary information, just like myocardial and coronary flow reserve do.

14.2.2 Fractional Flow Reserve

The Fractional Flow Reserve (FFR) as popularized by Pijls et al.[7] uses a slightly different approach compared to the normal flow reserve. Instead of comparing maximum blood flow to resting blood flow, it uses the theoretical mean blood flow in the *absence* of the disease during maximal arteriolar vasodilation, $Q^{(*)}$, as the reference:

$$FFR_{myo} = \frac{\text{maximum flow}}{\text{theoretical maximum flow}} = \frac{Q^{(h)}}{Q^{(*)}} \tag{14.3}$$

Normally, the maximum blood flow $Q^{(h)}$ can be measured during maximal arteriolar vasodilation. The challenge is to obtain a good estimate of the theoretical maximum blood flow (during maximal arteriolar vasodilation and assuming the stenosis were not there) based on measurable physiological quantities. The accuracy of that estimate heavily influences the validity of the method.

Pressure gradient method for myocardial FFR

Pijls et al.[7] have developed a convenient method to determine the fractional flow reserve, using only intraarterial pressure measurements. This technique, based on initial work by Gould and Kirkeeide[6, 12], has only become applicable since the introduction of ultra thin pressure monitoring guide wires that have little or no influence on blood flow when measuring transstenotic pressures, even with very severe stenoses. It assumes that the pressure–flow relationship during maximal arteriolar vasodilation is linear, *i.e.* that the resistance of the vascular bed is constant. This is by approximation correct for a maximally vasodilated cardiovascular bed[10]. Under that assumption, the theoretical maximum blood flow can be derived (relative to the actual maximum blood flow) by measuring intraarterial pressures, thereby circumventing the need for more troublesome blood flow measurements such as Doppler flow techniques or videodensitometry.

Referring to Figure 14.2(a), the theoretical maximum blood flow $Q^{(*)}$ occurs if there were no stenosis at all, and hence the pressure distal to the stenosis, P_d, would be equal to the main arterial pressure P_a. It is assumed in the sequel that all intraarterial pressures are measured during maximal arteriolar vasodilation, and are averaged over one or more heart cycle(s). Assuming that the blood flow and pressure are indeed linearly related, $Q^{(*)}$ can be estimated as:

$$Q^{(h)} = \frac{P_a - P_v}{R^{(h)}} \tag{14.4}$$

The myocardial resistance $R^{(h)}$ during maximal arteriolar vasodilation can be determined by measuring the myocardial blood flow $Q^{(h)}$ and the driving pressure that causes it:

$$R^{(h)} = \frac{P_d - P_v}{Q^{(h)}} \tag{14.5}$$

And hence, the fractional flow reserve (FFR) of the myocardium can be calculated by combining Equations 14.3 through 14.5:

$$FFR_{myo} = \frac{Q^{(h)}}{Q^{(*)}} = \frac{P_d - P_v}{P_a - P_v} \tag{14.6}$$

Pressure gradient method for coronary FFR

The myocardial FFR depends on both the blood flow through the normal supplying epicardial arteries, as well as on the contribution of collateral blood flow from adjacent areas (if any) to the total myocardial perfusion (see Figure 14.2(a)). If the influence of the stenosis alone is to be assessed, the *coronary fractional flow reserve*, FFR_{cor}, should be used. It is defined as the measured mean blood flow through the stenosed coronary artery during maximal arteriolar vasodilation, divided by the theoretical mean blood flow though that artery without the stenosis, under the same conditions. Using a similar but more complex approach as above, the FFR_{cor} is calculated as[7]:

$$FFR_{cor} = \frac{Q_s^{(h)}}{Q_s^{(*)}} = \frac{P_d - P_w}{P_a - P_w} \tag{14.7}$$

where P_w is the so-called wedge pressure. This pressure is the pressure distal to the stenosis during a complete occlusion of that stenosis (see Figure 14.2(b)). This is also one of the drawbacks of the pressure gradient method: a balloon catheter is necessary to instrument the temporary occlusion. During normal catheterization procedures where such a balloon is not available, only the myocardial FFR can be determined, not the coronary FFR[7].

14.3 Comparing FFR and RCFR

When examining the concepts of fractional flow reserve and relative coronary flow reserve, they appear to be very different, but they also show some useful similarities. We will show this similarity by calculating an estimate of the theoretical maximum blood flow $Q^{(*)}$ in the absence of the epicardial stenosis, based on the flow reserve of another (healthy) epicardial artery.

Where the pressure gradient method as described in section 14.2.2 assumes a linear relationship between blood pressure and flow to get an estimate of the theoretical maximum blood flow $Q^{(*)}$, let's assume here that there is another - healthy - epicardial vessel with a corresponding cardiovascular perfusion bed. In that case, the maximum blood flow in that reference artery during maximal arteriolar vasodilation can be used as an estimate of the theoretical maximum blood flow $Q^{(*)}$ in the diseased artery. It must be corrected for the sizes of the corresponding perfusion beds, since the blood flow is proportional to these sizes[13]. Put in an equation:

$$Q^{(*)} = Q^{(*)}_{ref}\frac{V}{V_{ref}} = Q^{(h)}_{ref}\frac{V}{V_{ref}} \tag{14.8}$$

where V and V_{ref} are the volumes of the perfusion beds of the diseased and the reference artery, respectively (see Figure 14.3). In general, it is hard to determine the exact sizes of regional myocardial perfusion areas in vivo, but since the resting myocardial blood flow is normally also proportional to the size of the corresponding perfusion beds, the volume fraction in Equation 14.8 can be approximated by the ratio of the resting blood flows:

$$\frac{V}{V_{ref}} = \frac{Q^{(0)}}{Q^{(0)}_{ref}} \tag{14.9}$$

Substitution of this result into Equation 14.8 leads to:

$$Q^{(*)} = Q^{(h)}_{ref}\frac{Q^{(0)}}{Q^{(0)}_{ref}} = CFR_{ref} \cdot Q^{(0)} \tag{14.10}$$

Since the reference artery is assumed to be healthy, there is no collateral blood flow, and hence, the values of the myocardial and the coronary flow reserve of this artery are the same ($CFR_{ref} = CFR_{myo} = CFR_{cor}$). Using Equation 14.10 in Equation 14.3 yields:

$$FFR = \frac{Q^{(h)}}{Q^{(*)}} \approx \frac{Q^{(h)}}{CFR_{ref} \cdot Q^{(0)}} = \frac{Q^{(h)}}{Q^{(h)}} \cdot \frac{1}{CFR_{ref}} = \frac{CFR}{CFR_{ref}} = RCFR \tag{14.11}$$

From this we can conclude that the FFR and the RCFR yield the same result, provided that the selected reference artery is representative of the theoretical maximum blood flow in the stenosed artery.

14.4 ANGIOCARDIOGRAPHIC DETERMINATION OF THE RCFR

In this research, coronary stenoses will be assessed by two different measures of severity: the fractional flow reserve (FFR) and the relative coro-

nary flow reserve (RCFR). The FFR is determined using the pressure gradient method (section 14.2.2), and the RCFR using an angiocardiographic method explained in the following sections. Although there is great variation in the results reported with angiographic determination of flow reserves[14], it is our believe that the method is very valuable, provided it is used with caution[8].

14.4.1 Angiocardiographic Densitometry

For the measurement of (regional) myocardial blood flow by angiography, there are roughly two different methods. The first method uses small regions of interest on the myocardium to determine the coloring of that myocardial region by the contrast dye, as a function of time[15, 16]. The advantage of this approach is that the distribution of the myocardial perfusion can be shown (sometime referred to as parametric perfusion imaging) with reasonable spatial resolution. One of the big disadvantages, especially with the utility of angiographic projections, is the overlap of the myocardial region of interest with the cardiac chambers and the opposing cardiac wall[16]. If not properly corrected for, the coloring of these overlapping structures distorts the indicator-dilution curve, and hence the accuracy of the results.

The second method, which will also be employed here, uses angiographic regions of interest that are placed over main epicardial arteries to measure the transit time of the contrast bolus through a designated arterial segment[17]. Historically, the resulting curves are called 'indicator-dilution' curves[18] due to similarities with the indicator-dilution method described above. However, names like contrast-pass curves or time-density curves better reflect the underlying assumption that the indicator (contrast dye) will *not* dilute and will not diffuse into extravascular space. The main advantage of the arterial blood flow method over the indicator dilution method is that the contrast bolus passes very fast, which reduces the influence of the contrast material on the myocardial blood flow and reduces the interference of myocardial blush.

14.4.2 Determination of the RCFR

We previously published an angiocardiographic method to assess the relative coronary flow reserve (RCFR)[9]. The method does not require any arterial geometry to be measured, thereby eliminating one of the major problems with traditional densitometric approaches. It is calculated as a fraction of contrast transit times[9]:

$$RCFR_{a,b} = \frac{CFR_a}{CFR_b} \approx \frac{\Delta t_b^{(h)}}{\Delta\, t_a^{(h)}} \cdot \frac{\Delta t_a^{(0)}}{\Delta t_b^{(0)}} \tag{14.12}$$

These transit times Δt are calculated as the time differences between the *mean* contrast passages in each of the regions of interest (see Figure 14.4). Although various other timing parameters have been proposed[14], the mean transit time (sometimes referred to as the center of gravity) has been validated both in vivo and in vitro to be strongly correlated with the true average blood flow velocity[9, 14].

It can be concluded that the number of measurements is greatly reduced by using this particular method to assess the relative coronary flow reserve. Where most other methods require accurate measurements of distances, diameters or areas, equation 14.12 only contains time differences. These time differences can normally be determined quite accurately, although the time resolution is sometimes too low to obtain accurate results. This low time resolution is secondary to the necessity to use ECG-gated image acquisition, resulting in only one measurement per cardiac cycle, normally during late diastole because of minimal cardiac motion during that period[15, 14]. Combined with the fact that the contrast bolus resides only very shortly inside the arterial segment between the two regions of interest, this means that there are only a few measurements available to estimate the mean transit time.

To handle the problem with the reduced time resolution of the time-density curves, the initial work by Smith et. al.[18] used multiple time points within each cardiac cycle, combined with enlarged regions of interest to ensure the epicardial artery passed through the regions during the complete cycle. The disadvantage of this approach, which was also recognized by the original authors, is that large regions of interest increase the influence of overlapping structures on the shape of the time-density curve. Current developments in image processing might enable the use of small regions of interest that encompass the same artery segment during the complete heart cycle, by automatically tracking the motion of anatomic landmarks.

14.5 PROPOSED STUDY PROTOCOL

The objective of the study is to experimentally validate the theory that the FFR and the RCFR yield similar results. The proposed protocol requires the acquisition of two image runs, one at rest and one during maximal arteriolar vasodilation, with the same camera positions, source-to-detector distances etc.

The patients for this study are selected based on the following criteria: focal proximal stenosis in either the left anterior descending artery or the left circumflex artery, normal anatomy of the left main coronary artery, and no abnormalities like severe left ventricular dysfunction, hypertrophy or arrhythmia. Based on the immediate results of the FFR measurements, the stenoses are divided into two groups: $FFR \leq 0.75$ and a control group with

an $FFR > 0.75$. It is assumed that the stenoses in the control group are clinically not relevant[7].

The images are acquired at 30 frames per second, and contrast material is injected by hand into the ostium of the left coronary artery. The camera position is selected to visualize the proximal sections of the LAD and LCx with little overlap or foreshortening. Image acquisition starts before the start of contrast injection, and does not end until the contrast agent reaches the distal epicardial artery segments. During the acquisition, panning is disallowed.

Routine vasodilation is induced as prescribed by the FFR measurement protocol. Since the vasodilator is administered intracoronary (adenosine or papaverine), two injections are used, one for the FFR measurement and one for the imaging. The actual FFR measurement is completed before the image acquisition starts, to eliminate the influence of long term effects of contrast agent injection on myocardial blood flow.

Unfortunately, the actual implementation of this study did not yet provide enough information to present any results here.

14.6 DISCUSSION

The numerous limitations and disadvantages of each of the methods used in this research have been described in many excellent articles[3, 4, 6, 8, 10, 11], and are therefore not discussed here. However, some of them directly or indirectly influence the comparison of the FFR and the RCFR methods:

- Both methods rely on the induction of maximal arteriolar vasodilation, which preferably should be accomplished by intracoronary injection of an arteriolar vasodilator (papaverine or adenosine). Since the image acquisition required for the angiographic RCFR measurement takes more time than the pressure gradient method (FFR), it is important to ensure maximal arteriolar vasodilation during the complete hyperemic image acquisition.

- Since the FFR is independent of the resting blood flow but the (R)CFR is not, regional changes in resting blood flow (due to changes in *e.g.* aortic pressure, heart rate or cardiac work load[6]) invalidates the comparison between the two methods.

- The RCFR method assumes that, neglecting epicardial stenoses, the vasodilative flow reserves of all the main coronary arteries are the same[10]. However, that will not always be the same, especially not in pathological cases. This can make the selection of a suitable reference artery to be used in the RCFR measurement more difficult[9].

- The model that is used to show the similarity between the FFR and the RCFR methods is easily invalidated, for example by temporal changes in recruitable collateral blood flow, coronary steal (leading to flow reserves smaller than one) or diffuse coronary artery disease[7].

At this moment, it is unclear whether the RCFR correlates best with the myocardial, or with the coronary fractional flow reserve. If the collateral vessels simply bypass the stenosis and supply the distal part of the epicardial artery with blood, it is possible that the angiographic method actually takes collateral blood flow into account. In that case, the RCFR would correlate with the myocardial FFR. However, it is more likely that the collateral vessels directly connect to the intramural vessels or arterioles, since retrograde filling of the distal segments is observed during complete proximal occlusion.

We do not expect a very good correlation between the fractional flow reserve and the relative coronary flow reserve, simply because there are too many factors influencing the results. However, with our proposed study we hope to be able to show that the angiocardiographic determination of the RCFR is a reasonable alternative that can be used retrospectively. This not only means that the flow reserve can be determined for stenoses stored in a database (provided images were acquired during maximal arteriolar vasodilation), but also that arterial segments can be assessed that were not selected for intraarterial pressure measurements during the clinical procedure.

ACKNOWLEDGMENTS

We thank dr. Jack T. Cusma for his invaluable input. Furthermore, we are grateful to dr. Richard A. Robb of the Biomedical Imaging Resource (Mayo Foundation) for allowing parts of this research to be conducted in his laboratory.

References

[1] M. Kern, "Focus for the new millennium: diffuse coronary artery disease and physiologic measurements of severity," *ACC Cur. J. Rev.* **9**(2), pp. 13–19, 2000.

[2] R. Wilson, "Assessing the severity of coronary-artery stenoses," *N. Eng. J. Med.* **334**(26), pp. 1735–1737, 1996. Editorial.

[3] E. Topol and S. Nissen, "Our preoccupation with coronary luminology," *Circulation* **92**(8), pp. 2333–2342, 1995.

[4] A. Nitenberg and I. Antony, "Coronary vascular reserve in humans: a critical review of methods of evaluation and of interpretation of the results," *Eur. Heart J.* **16**(Suppl. I), pp. 7–21, 1995.

[5] B. Brown, E. Bolson, M. Frimer, and H. Dodge, "Quantitative coronary arteriography," *Circulation* **55**(2), pp. 329–337, 1977.

[6] K. Gould, R. Kirkeeide, and M. Buchi, "Coronary flow reserve as a physiologic measure of stenosis severity," *J. Am. Coll. Cardiol.* **15**(2), pp. 459–474, 1990.

[7] N. Pijls, J. van Son, R. Kirkeeide, B. de Bruyne, and K. Gould, "Experimental basis of determining maximum coronary, myocardial, and collateral blood flow by pressure measurements for assessing functional stenosis severity before and after percutaneous transluminal coronary angioplasty," *Circulation* **86**(4), pp. 1354–1367, 1993.

[8] E. Ritman, "Angiographic measurement of coronary blood flow reserve: does it work?," *Circulation* **82**(4), pp. 1533–1535, 1990. Editorial Comment.

[9] M. Schrijver, S. de Bont, C. Slump, and C. Storm, "Densitometric determination of the flow distribution in the bifurcation of the left coronary artery," in *Medical Imaging 1999: Physiology and Function from Multidimensional Images*, C. Chen and A. Clough, eds., vol. 3660, pp. 395–406, SPIE, 1999.

[10] J. Bourdarias, "Coronary reserve: concept and physiological variations," *Eur. Heart J.* **16**(Suppl. I), pp. 2–6, 1995.

[11] K. Gould, K. Lipscomb, and G. Hamilton, "Physiologic basis for assessing critical coronary stenosis," *Am. J. Cardiol.* **33**, pp. 87–94, 1974.

[12] R. Kirkeeide, K. Gould, and L. Parsel, "Assessment of coronary stenoses by myocardial perfusion imaging during pharmacologic coronary vasodilation. VII. validation of coronary flow reserve as a single integrated functional measure of stenosis severity reflecting all its geometric dimensions," *J. Am. Coll. Cardiol.* **7**(1), pp. 103–113, 1986.

[13] C. Seiler, R. Kirkeeide, and K. Gould, "Basic structure-function relations of the epicardial coronary vascular tree: basis of quantitative coronary arteriography for diffuse coronary artery disease," *Circulation* **85**(6), pp. 1987–2003, 1992.

[14] M. Haude, G. Caspari, D. Baumgart, T. Ehring, R. Schulz, T. Roth, L. Koch, R. Erbel, P. Spiller, and G. Heusch, "X-ray densitometry for

the measurement of regional myocardial perfusion," *Basic. Res. Card.* **95**, pp. 261–2000, 2000.

[15] J. Cusma, E. Toggart, J. Folts, W. Peppler, N. Hangiandreou, C. Lee, and C. Mistretta, "Digital subtraction angiography imaging of coronary flow reserve," *Circulation* **75**(2), pp. 461–472, 1987.

[16] R. Vogel, M. LeFree, E. Bates, W. O'Neill, R. Foster, P. Kirlin, D. Smith, and B. Pitt, "Application of digital techniques to selective coronary arteriography: use of myocardial contrast appearance time to measure coronary flow reserve," *Am. Heart J.* **107**(1), pp. 153–164, 1984.

[17] W. Rutishauser, W. Bussmann, G. Noseda, W. Meier, and J. Wellauer, "Blood flow measurement through single coronary arteries by roentgendensitometry. part I: a comparison of flow measured by a radiologic technique applicable in the intact organism and by electromagnetic flowmeter," *Am. J. Roentgenol. Radium. Ther. Nucl. Med.* **109**, pp. 12–20, 1970.

[18] H. Smith, R. Frye, D. Donald, G. Davis, J. Pluth, R. Sturm, and E. Wood, "Roentgen videodensitometric measure of coronary blood flow: determination from simultaneous indicator-dilution curves at selected sites in the coronary circulation and coronary artery-saphenous vein grafts," *Mayo Clin. Proc.* **46**, pp. 800–806, 1971.

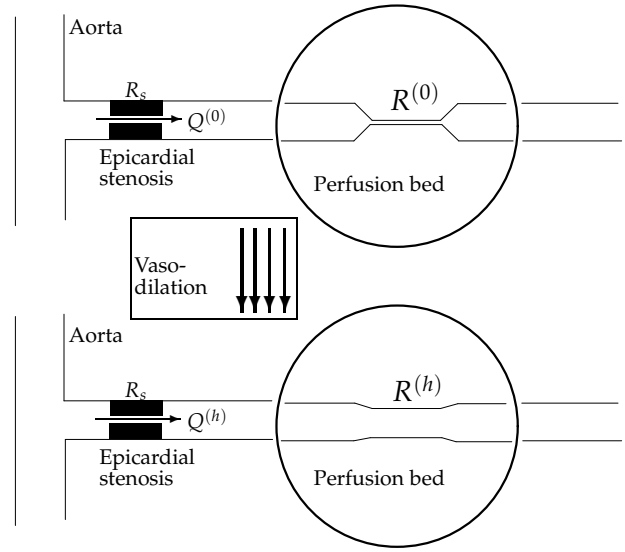

(a) Flow Reserve

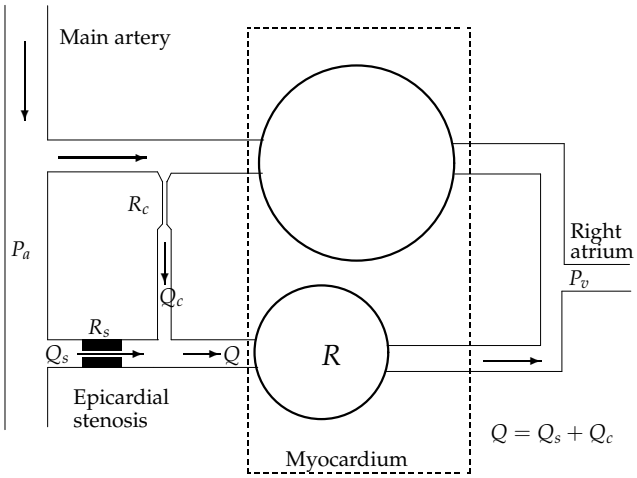

(b) Influence of collateral flow. Modified from Pijls et al.[7]

Figure 14.1: The concept of flow reserve. A model of an epicardial stenosis affecting myocardial and collateral blood flows.

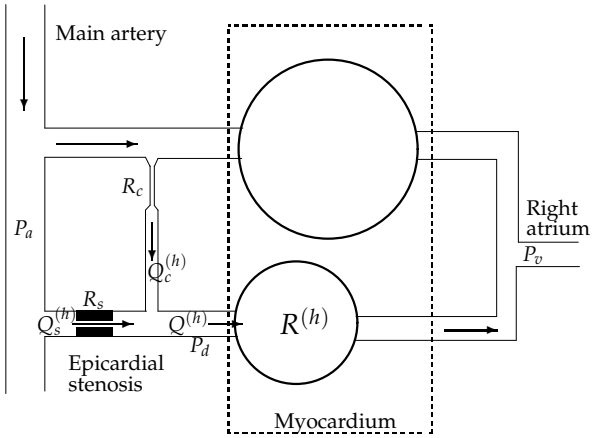

(a) Myocardial fractional flow reserve

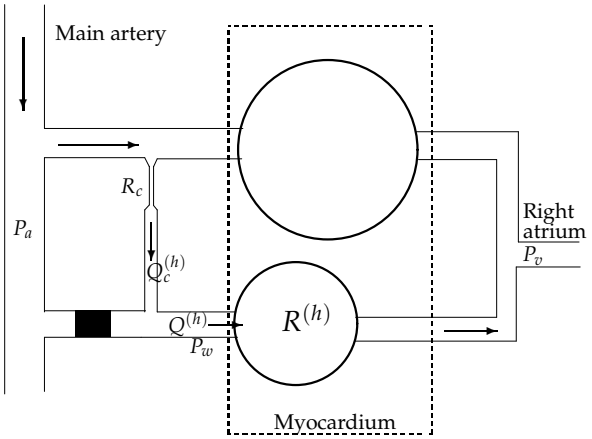

(b) Coronary fractional flow reserve

Figure 14.2: Concept of the pressure gradient method to determine the fractional flow reserve. Modified from Pijls et al.[7]

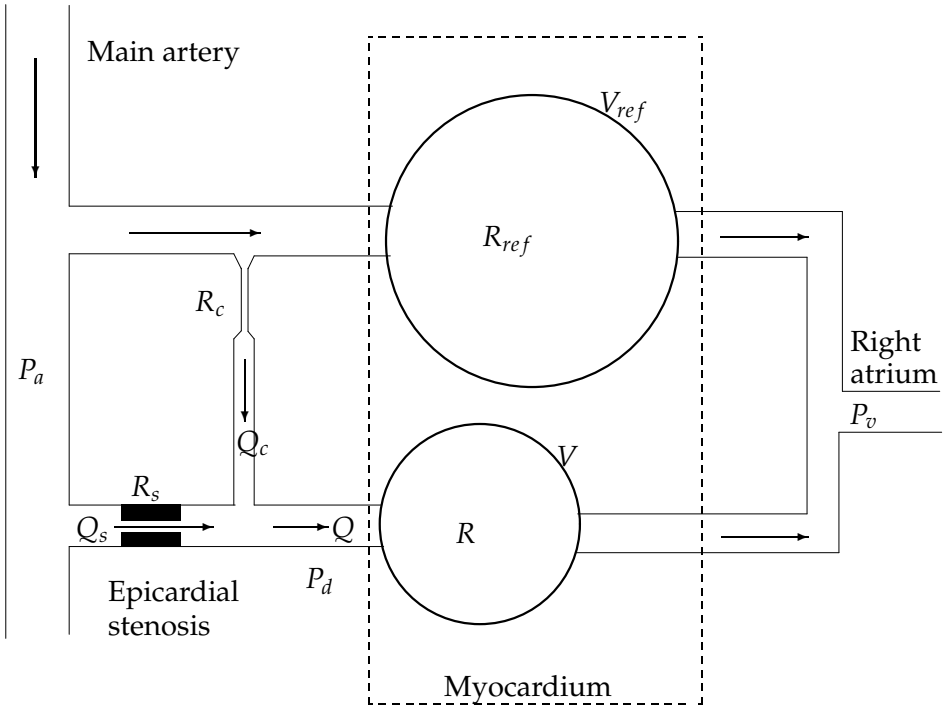

Figure 14.3: Relative coronary flow reserve

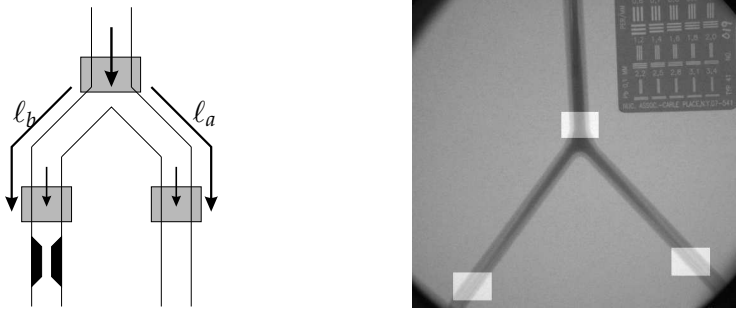

(a) Theoretical model

(b) Validation with a flow-phantom

Figure 14.4: Placement of the regions of interest[9]

Chapter 15

CAD of myocardial perfusion[1]

Our purpose is in the automated evaluation of the physiological relevance of lesions in coronary angiograms. We aim to extract as much as possible quantitative information about the physiological condition of the heart from standard angiographic image sequences. Coronary angiography is still the gold standard for evaluating and diagnosing coronary abnormalities as it is able to locate precisely the coronary artery lesions. The dimensions of the stenosis can be assessed nowadays successfully with image processing based Quantitative Coronary Angiography (QCA) techniques. Our purpose is to assess the clinical relevance of the pertinent stenosis. We therefore analyze the myocardial perfusion as revealed in standard angiographic image sequences. In a Region-of-Interest (ROI) on the angiogram (without an overlaying major blood vessel) the contrast is measured as a function of time (the so-called time-density curve). The required hyperemic state of exercise is induced artificially by the injection of a vasodilator drug e.g. papaverine. In order to minimize motion artifacts we select based on the recorded ECG signal end-diastolic images in both a basal and a hyperemic run in the same projection to position the ROI. We present the development of the algorithms together with results of a small study of 20 patients which have been catheterized following the standard protocol.

15.1 INTRODUCTION

Coronary angiography is up till now the most important modality to diagnose coronary abnormalities especially stenoses causing the clinical syndrome angina pectoris. In clinical cardiology the measure of stenosis in a coronary artery is in standard practice still based on visual assessment leading to large inter and intra observer variability in reading coronary arteriograms [1, 2, 3]. Image analysis and computer assistance do result in a more

[1] presented at Medical Imaging 2007: Computer - Aided Diagnosis, and published in part as: C.J. Storm, C.H. Slump, "CAD of myocardial perfusion," in *Medical Imaging: Computer - Aided Diagnosis*, M.L. Giger, N. Karssemeijer, eds., *Proc. SPIE*, vol. 6514, 65142D, 2007.

consistent judgment, however, this approach is mainly based upon static geometric parameters such as percentage of diameter and area reduction of a single segment of the stenosed artery [4, 5]. In 70-90% of the coronary angiograms there are abnormalities to justify the diagnosis angina pectoris, however, in the 10-30% of the coronary angiograms there are no abnormalities at all in the epicardial vessels although the patients do have real anginal complaints [6]. This group of patients may benefit from additional diagnostic procedures demonstrating disturbances in the micro circulation of the myocardium. These disturbances are often, but not always, secondary to specific heart diseases affecting the microcirculation such as hypertension and/or diabetes. In case the disturbances are not secondary, the syndrome is called syndrome X. The microcirculation of the myocardium is responsible for optimizing the functional capacity of the myocardial cells. The extent of myocardial perfusion to nourish the myocardial cells is regulated on demand and activated by local and general factors: exercise, stress and many others. The imbalance of demand and supply causes complaints such angina pectoris or heart failure. The anatomical basis of the microcirculation consists of a proximal and distal compartment in which the prearterioles in the proximal compartment play an important role in optimizing the perfusion pressure in the arterioles. These regulation is the combined action of neural (sympathetic), humoral and local vasoactive factors. In contrast the arterioles are sparsely innervated resulting in a regulation mostly depended on local factors in particular the oxygen concentration. That is why these arterioles play a very important role in the regulation of blood flow in the myocardium to ensure equilibrium in supply of nutrients and the washout of waste products.

Through this mechanism the coronary flow is regulated in proportion to the need of the myocardium for oxygen, which is closely related to the amount of cardiac work load. In the absence of disease in the epicardial vessels there is hardly any resistance to the flow in these vessels in contrast to the micro vascular component. So the microvascular vessels determine the amount of blood the myocardium will get in a factor three to six times the basal amount depending on the demand. This is called Coronary Flow Reserve (CFR) [7, 8]. Coronary flow reserve depends mostly on the dilation of the arterioles. Micro vascular dysfunction is mostly a combination of factors: vascular, vessel wall thickening, and myocardial, myocardial wall thickening in hypertension, components. In syndrome X there is no anatomical substrate in a coronary angiograms to explain a reduced CFR although in ultra sound studies in a high percentage there are vessel wall abnormalities possible causing a reduced release of vasoactive hormones leading to a decrease in vasodilatation of the arterioles. Diagnostic tests are necessary when multi angulated angiograms, to reduce the chance missing asymmetric lesions, give no lumen changes resulting in critical narrowing to explain complaints. Spasm of the

epicardial vessels should be excluded by provocative, ergonovine intracoronary, tests during angiography. When both procedures are negative micro vascular dysfunction has to be excluded by measuring coronary flow reserve. The CFR is measured by pharmacologic intervention to get maximal vasodilatation, in humans three compounds are used, *i.e.* some intravenous (dipyridamole, adenosine), others intracoronary (papaverine, adenosine). There are several methods to measure the CFR: invasively or non-invasively. The non-invasive methods are using radioactive materials (nuclear medicine), the invasive technique consist of mostly expensive catheters for measuring flow difference in the epicardial vessels in basal conditions and after pharmacologic interventions. Doppler flow measurement has an extra problem because of epicardial vessel dilatation. Quantitative angiography is to our opinion a useful method to evaluate the extent of possible dilatation of the arterioles after pharmacologic intervention in an easy way without extra catheters or procedures in connection of a normal coronary angiography using the standard. This paper is organized as follows. In the next section we describe our approach in detail. Thereafter we describe the data and present results. We finalize with a discussion and conclusions.

15.2 METHODS

15.2.1 Theory

The relation between coronary pressure and flow has been studied by many authors and has resulted in a variety of models [9] with varying complexity. A very crude and simple approach is to model the circulation of the myocard by a single current loop in an electric circuit. The heart is then the battery; the voltage V corresponds to the pressure in the aortic root and the current I represents the flow in the coronary artery. The artery is characterized by a resistance R_{artery}, the myocard by a variable resistance $R_{myocard}$. The approach is shown in Figure 15.1.

From Figure 15.1 one easily reads that I can be expressed as:

$$I = \frac{V}{R_{artery} + R_{myocard}} = \frac{V}{R_{artery}} \left(\frac{1}{1 + \frac{R_{myocard}}{R_{artery}}} \right) \tag{15.1}$$

The myocard resistance $R_{myocard}$ is much larger than the arterial resistance R_{artery}. The vasodilation of the arterioles regulates the flow through the myocard. From 15.1 (1) it follows that in case the artery contains a stenosis, this stenosis influences the flow only if its resistance is of the same order of magnitude as the resistance by the myocard, i.e. as the arterioles are totally

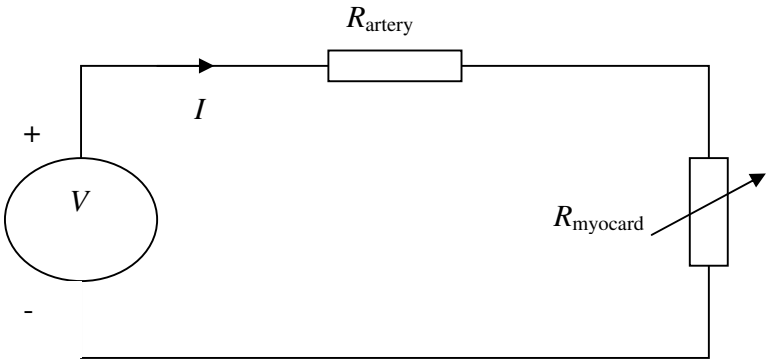

Figure 15.1: A simple single current loop model of the myocard circulation, I represents the flow, V the pressure in the aortic root, R_{artery} and $R_{myocard}$ represent the flow resistance of the artery and myocard, respectively.

dilated. This insight has stimulated the search for a physiologic measure of the severity of a stenosis [10].

15.2.2 CFR

In the previous section we have advocated that a more functional, physiological measure is to be preferred over geometric parameters characterizing a stenosis. The functional measurement of Coronary Flow Reserve (CFR) provides information about the perfusion of the heart muscle. With CFR the measured local maximum contrast density represents the vascular volume and the measured local contrast arrival time is taken to be inversely proportional to flow [11]. In a Region-of-Interest (ROI) on the angiogram (without an overlaying major blood vessel) the contrast is measured as a function of time (the so-called time-density curve). The required hyperemic state of exercise can be induced artificially by the intracoronary injection of a vasodilator drug *e.g.* papaverine. In this hyperemic state, in contrast to the "rest"state, the arterioles are maximally dilated, thus the normally increasing the blood flow to the physical limits is set by the sizes of the epicardial coronary arteries and especially the stenosed segments. The CFR can be visualized in a functional image in which the image grey values are proportional to the increase in blood flow in the pertinent part of the heart muscle. Areas with less blood flow increase do show up dark, no essential difference comparing the "rest"state, indicating effects of impaired blood flow because of stenosed segments in the coronary arteries and possible (partial) infarction. Although good results with the CFR method have been reported [12, 13, 14], in clinical practice the procedure is demanding, especially the correction of the back-

ground contributions is difficult because of the contracting heart dynamics. The requirement is that the two image sequences, "rest" state and hyperemic state, should be registered exactly the same. However, movements due to patient respiration cannot be eliminated completely. In order to avoid misregistration artifacts, pacing of the heart together with ECG triggered contrast injection and image acquisition appeared to be mandatory.

As the measurement of the absolute CFR is difficult[15], alternatives such as the Relative Coronary Flow Reserve (RCFR) [8] and the Fractional Flow Reserve (FFR) [16] have been developed. Dual energy subtraction [17] has been proposed to overcome the motion artifacts. The main advantage of the FFR method is that all measurements are made during maximum arteriolar vasodilatation. On the other hand the method is not that easy incorporated in daily clinical routine because this method is time consuming and expensive. In this paper we present in the next section a less demanding approach which is less time-consuming and less demanding in procedure.

15.2.3 Model

In this section we model the integration over a ROI positioned on the myocard in the angiogram. We assume that within the ROI there are no overlaying major bloodvessels. The integration *i.e.* the summation of the (log of the) pixel intensities inside the ROI together with the radiographic projection basis of the angiogram, provides for a 3D volume measurement of the amount of contrast agent contained in the myocard. We assume that the injected contrast completely replaces the blood. The myocard can be considered to be a reservoir which holds temporarily the contrast agent for a certain mean transit time $\tau_{transit}$. The result of the integration is proportional to the concentration contrast material under the ROI. A schematic diagram of the myocard model is shown in Figure 15.9, the inflow of contrast at the arterial side is $I(t)$, the outflow is at the venous side. The single pass output of the integration over the reservoir with mean transit time $\tau_{transit}$ is given by the contrast concentration $C(t)$:

$$C(t) = \begin{cases} 0, & t < \tau_{inject} \\ \int_{\tau_{inject}}^{t} I(\tau)d\tau, & \tau_{inject} < t < \tau_{peak} \\ C_{max}, & \tau_{peak} < t < \tau_{transit} \end{cases} \tag{15.2}$$

After a certain time τ_{peak} the contrast concentration saturates as the whole contrast bolus is contained in the myocard. The contrast concentration starts to diminish after the mean transit time $\tau_{transit}$. The contrast concentration is shown in Figure 15.3. The rising slope of the $C(t)$ curve of Figure 15.3 is proportional to flow. We will compare this slope in basal and hyperemic conditions. There is a small time - offset between the moment of injection and

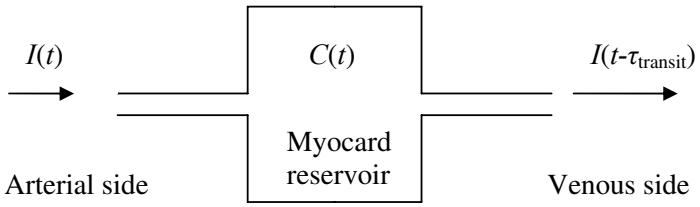

Figure 15.2: Schematic diagram of the ROI integration resulting in the contrast concentration $C(t)$ in the myocard reservoir.

the start of the image sequence. In the ECG guided selection we take our first image slightly before the second R - peak after the start of the run.

15.3 DATA

The images analyzed in this paper are acquired with an Axiom Artis dFC single plane C-arm system with a dynamic flat detector for cardiology from Siemens Medical. The frame rate is 15 frames / second. During the acquisition, the ECG is recorded simultaneously. The handling of the data is as follows: The basal and the hyperemic runs are typically acquired at the end of the patient study. In this paper we have chosen for the vascular bed of the right coronary artery because of less overlaying larger bloodvessels, see Figure 15.4. The hyperemic state is evoked by intracoronary injection of 8 mg papaverine and flushed with contrast agent. Overall 6Fr cathethers are used. The image data is archived on CD. With a computer script the Dicom files are converted to 8 bit 512×512 bitmap format for the ease of further processing by Matlab. The script, originally made by Schrijver [18] for his Ph.D research and adapted to include the Siemens format by ten Brinke [19] for his MSc research, relies heavily on the Dicom2 program by Barre [20].

The converted Dicom files are read into Matlab anonymized together with the ECG data. From the ECG data the R-peaks are detected and the end diastolic images are selected in each heartbeat. For this we select the image at *e.g.* 80% of the R-R interval after the previous R-peak. See Figure 15.5 for an example of an ECG signal with detected R-peaks and the selected diastolic images.

In this way we obtain a set of the order of 10 - 15 images. We then manually select a ROI in the middle of the sequence. This is done because the larger bloodvessels are visible and we can place the ROI such to avoid to

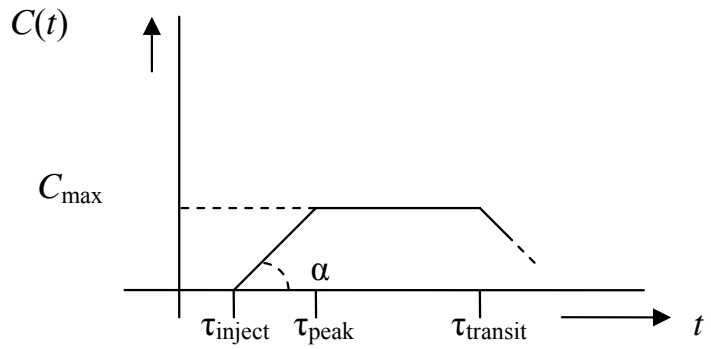

Figure 15.3: The contrast concentration $C(t)$ and the describing parameters. Of special interest is the slope α as it is related to the flow.

overlay these vessels. See Figure 15.6 for an example of selected images corresponding to Figure 15.5. Figure 15.7 shows the ECG signal of the consecutive hyperemic run, together with the detected R-peaks and the selected end-diastolic images. Figure 15.8 displays these hyperemic images.

The intensity is integrated over the ROI for each of the images at the same ECG phase. Also from the hyperemic run the selected images are measured with the same ROI. The contrast is computed as function over time from both runs, normalized and the comparison between normal and hyperemic run can be made. Together with the peak positions, we compute the slopes of the curves in order to estimate the increase in flow between the normal and the hyperemic run. The results are archived under a file number and reported to and examined by the cardiologist (CJS).

15.4 RESULTS

We have performed the analysis described in the previous section on a small group of 20 patients. A selection of the results is summarized in Table 15.1. The analysis is automated.

The program performs all computations after entering the pertinent patient number. The obtained responses are fitted with straight lines and the fitting parameters slope and peak position are used to compute the hyperemic-basal slope ratio and the hyperemic-basal time-to-peak ratio, respectively. Table 15.1 indicates that the differences between basal and hyperemic response can be described by the simple model parameters shown in Figure 15.3. For

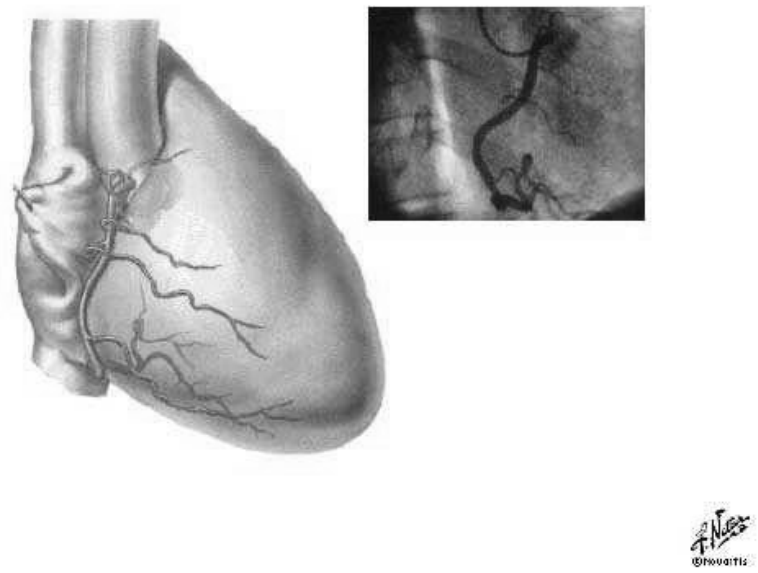

Figure 15.4: Right coronary artery in right anterior oblique view, Netter [21], plate 214 . The right coronary artery nourishes the lower part of the left ventricle.

example, patient numbers 6503 and 6541 show hardly any difference in response, indicating that there is hardly CFR. On the other hand, patient number 7014 has a good hyperemic-basal slope ratio and corresponding CFR.

15.5 DISCUSSION AND CONCLUSION

Our purpose is in the automated evaluation of the patho-physiological relevance of lesions, stenoses, in the coronary arteries as seen in an angiogram. We aim to extract as much as possible quantitative information about the physiological condition of the heart from standard angiographic image sequences. Coronary angiography is still the gold standard for evaluating and diagnosing Coronary Artery Disease (CAD) as it is able to precisely locate stenoses and the length of it in the coronary artery imaged.The dimensions of the stenosis can be assessed nowadays successfully with image processing based Quantitative Coronary Angiography (QCA) techniques. This technique reveals only the (projected) shape of the lesion, but there is no information about the clinical, pathophysiological consequences of the stenosis. In this paper our aim is to assess the clinical significance of the stenosis. We therefore analyze the myocardial perfusion as revealed in standard angio-

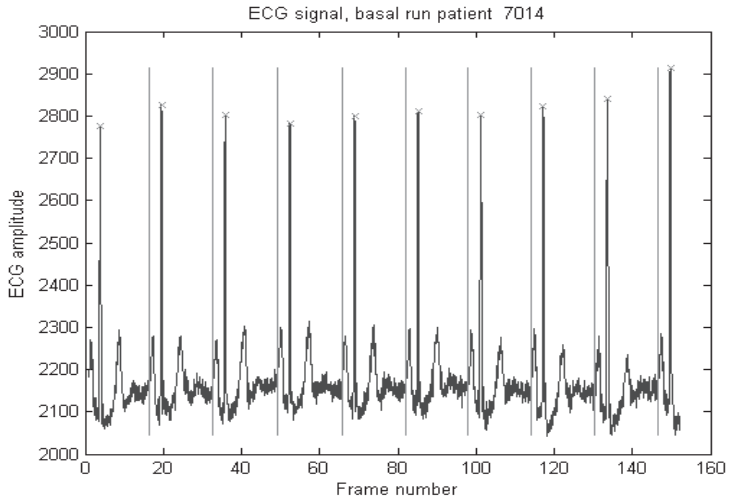

Figure 15.5: Example of a patient ECG signal, indicated are the detected R-peaks and the selected diastolic images.

graphic image sequences. We present the development of the algorithms together with results of a small study of 20 patients which have been catheterized following the standard protocol. The image sequences consist of 8 bit images with a resolution of 512 $\times$ 512 pixels at a frame rate of 15 images / s. The frame lengths are somewhat longer than usual in order to include the registration of the perfusion. In this paper we report a simple approach which is less time-consuming, less difficult and cheap as compared with other methods, above all there no extra hazards for the patient. Time density curves are obtained over the myocardium separated from the overlaying coronary vessels. Because of the motion of the coronary arteries and the local myocardium we use the ECG signal to select images at the same (diastolic) phase. The placement of an elliptical ROI appeared feasible for standard "L-shaped" RCA projections. Because of anatomical variations, manual correction was necessary in 4 of the 20 cases studied. The results depend to a major extend on the X-ray exposure control dynamics, i.e. we want to measure the response of the vascular bed in the myocardium and not the response of the X-ray exposure control. Preferably we acquire the images with a fixed kVp and mA during the acquisition of the image sequence. The obtained relative perfusion images show promise for clinical application, in the clinical material available to us at this moment we find large variations which we expect to be clinically relevant. In the past we have studied myocardial perfusion with CFR methods from the literature such as for example [12]. These methods were demanding with respect to the procedure in the catheteriza-

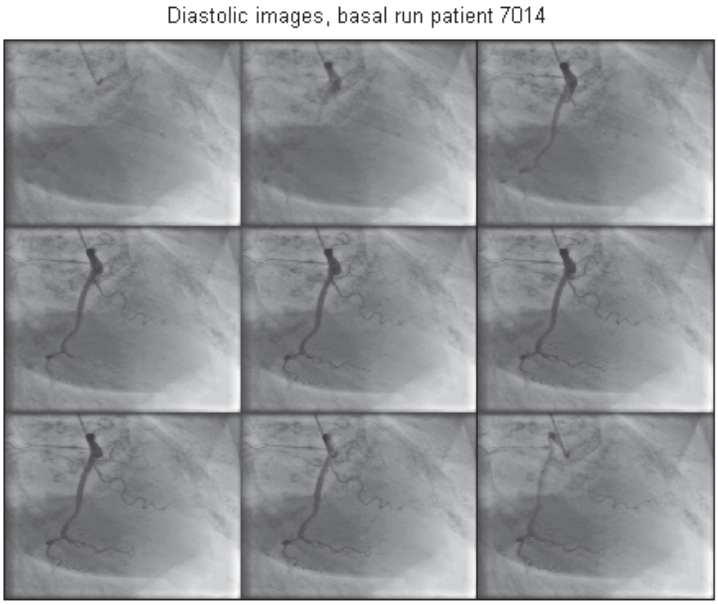

Figure 15.6: The selected basal diastolic images corresponding to Figure 15.5.

tion laboratories. We now use the standard protocol with slightly longer image sequences, only one or two runs, with comparable results. Although our results seem hopeful further clinical evaluation, because of the small series, is needed.

References

[1] K.M. Detre, E. Wright, M.L. Murphy, T. Takaro, "Observer agreement in evaluating coronary angiograms," Circulation 52(6), 979-986 (1975).

[2] L.M. Zir, S.W. Miller, R.E. Dinsmore, J.P. Gilbert, J.W. Hawthorne, "Interobserver variability in coronary angiography," *Circulation* 53(4), 627-632 (1976).

[3] E.J. Topol, S.E. Nissen, "Our preoccupation with coronary luminology," *Circulation* 92(8), 23333-2342 (1995).

[4] J.H.C. Reiber, P.W. Serruys, C.J. Kooijman, W. Wijns, C.J. Slager, J.J. Gerbrands, J.C.H. Schuurbiers, A. den Boer, P.G. Hugenholtz, " Assessment of short-, medium-, and long-term variations in arterial dimensions from computer-assisted quantitation of coronary cineangiograms," *Circulation* 71(2), 280-288 (1985).

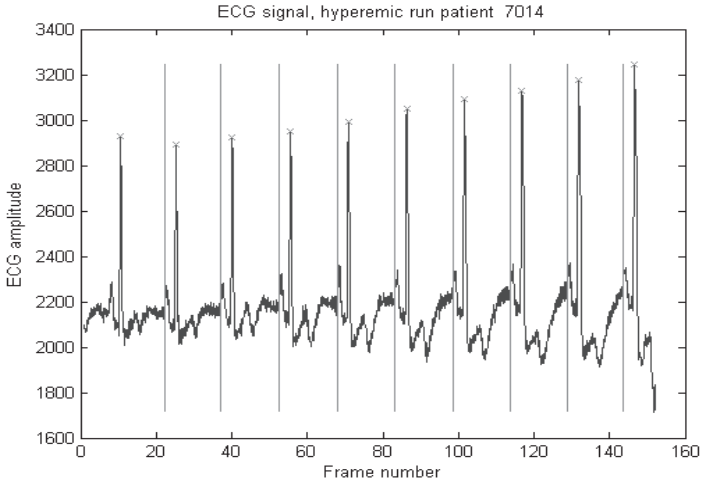

Figure 15.7: The ECG signal of the hyperemic run, indicated are the detected R-peaks and the selected diastolic images.

[5] J.H.C. Reiber, P.W. Serruys, *Quantitative Coronary Arteriography*, Kluwer Academic Publishers, 1991.

[6] R.O. Cannon, P.G. Camici, S.E. Epstein, "Pathophysiological dilemma of syndrome X," *Circulation* 85(3), 883-892 (1992).

[7] R.L. Kirkeeide, K.L. Gould, L. Parsel, "Assessment of coronary stenoses by myocardial perfusion imaging during pharmacologic coronary vasodilation. VII. Validation of coronary flow reserve as a single integrated functional measure of stenosis severity reflecting all its geometric dimensions," *J. Am. Coll. Cardiol.* 7(1), 103-113 (1986).

[8] K.L. Gould, R.L. Kirkeeide, M. Buchi, "Coronary flow reserve as a physiologic measure of stenosis severity," *J. Am. Coll. Cardiol.* 15(2), 459-474 (1990).

[9] F.J. Klocke, R.E. Mates, J.M. Canty, A.K. Ellis, "Coronary pressure-flow relationships, controversial issues and probable implications," *Circ. Res.* 56(3), 310-323 (1985).

[10] K.L. Gould, K. Lipscomb, "Effects of coronary stenoses on coronary flow reserve and resistance," *Am. J. Cardiol.* 34, 48-55 (1974).

[11] J.T. Cusma, E.J. Toggart, J.D. Folts, W.W. Peppler, N.J. Hangiandreou, C.S. Lee, C.A. Mistretta, "Digital subtraction angiographic imaging of coronary floe reserve," *Circulation* 75(2), 461-472 (1987).

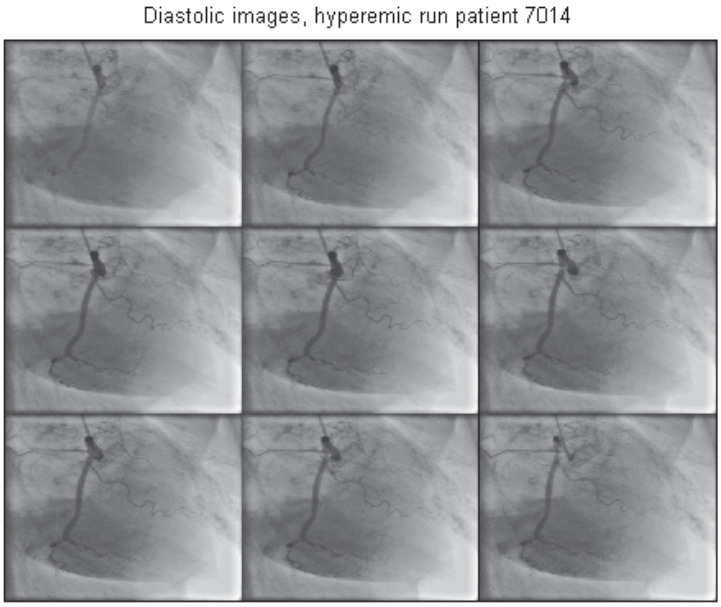

Figure 15.8: The selected basal diastolic images corresponding to Figure 15.7.

[12] R.A. Vogel, "The radiologic assessment of coronary blood flow parameters," *Circulation* 72(3), 460-465 (1985).

[13] V. Legrand, G.B. Mancini, e.r. Bates, J.M. Hodgson, M.D. Gross, R.A. Vogel, "Comparative study of coronary flow reserve, coronary anatomy and results of radionuclide exercise tests in patients with coronary artery disease," *J.Am. Coll. Cardiol.* 8(5), 1022-1032 (1986).

[14] G.B. Mancini, S.B. Simon, M.J. McGillem, M.T. LeFree, H.Z. Friedman, R.A. Vogel, " Automated quantitative coronary arteriography: morphologic and physiologic validation in vivo of a rapid angiographic method," *Circulation* 75(2), 452-460 (1987).

[15] M.J. Kern, A. Lerman, J.-W. Bech, B. de Bruyne, E. Eeckhout, W.F. Fearon, S.T. Higano, M.J. Lim, M. Meuwissen, J.J. Piek, N.H.J. Pijls, M. Siebes, J.A.E. Spaan, "Physiological assessment of coronary artery disease in the cardiac catheterization laboratory: a scientific statement from the American heart association committee on diagnostic and interventional cardiac catheterization, council on clinical cardiology," *Circulation* 114(12), 1321-1341 (2006).

[16] N.H.J. Pijls, B. van Gelder, P. van der Voort, K. Peels, F.A.L.E. Bracke, H.J.R.M. Bonnier, M.I.H. El Gamal, "Fractional flow reserve: a useful in-

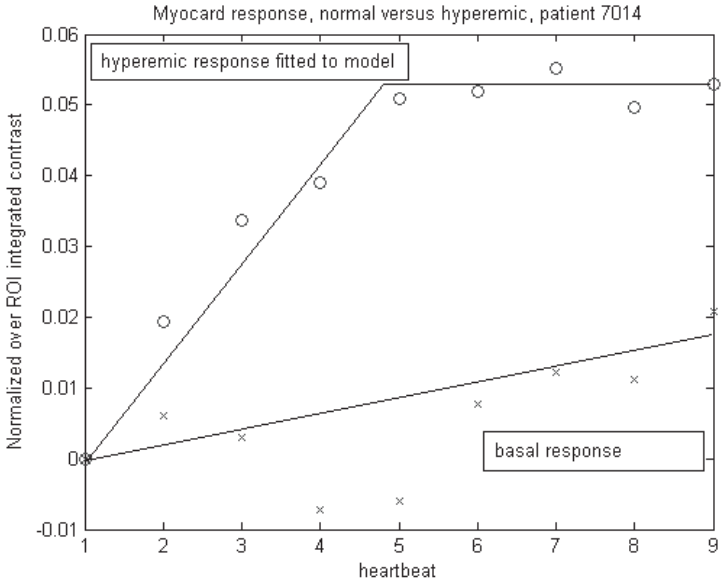

Figure 15.9: The difference in myocard response between basal and hyperemic run as function over time. The slope of the hyperemic run shows about a five times larger flow.

dex to evaluate the influence of an epicardial coronary stenosis on myocardial blood flow," *Circulation* 92(11), 3182-3193 (1995).

[17] S. Molloi, A. Ersahin, J. Tang, J. Hicks, C.Y. Leung, "Quantification of volumetric coronary blood flow with dual energy subtraction angiography," Circulation 93(10), 1919-1927 (1996).

[18] M. Schrijver, *Angiographic image analysis to assess the severity of coronary stenoses*, PhD thesis, University of Twente, The Netherlands, 2002.

[19] G.A. ten Brinke, *Quantitative analysis of angiographic sequences*, MSc thesis, University of Twente, The Netherlands, 2005.

[20] S. Barre, http://barre.nom.fr/medical/dicom2.

[21] F.H. Netter, *Atlas of human anatomy*, 3rd ed., Icon, Teterboro, NJ 2003.

Table 15.1: Selection of results obtained with manual ROI placement and automated parameter extraction.

Patient #	# basal images	# hyperemic images	Hyperemic - basal slope ratio	Hyperemic - basal time - to - peak ratio
6447	121	131	2.3	0.62
6503	151	151	1.07	1.0
6541	133	151	1.09	0.71
6555	124	151	2.4	0.5
6556	97	140	1.35	0.71
6595	151	146	2.2	0.83
7014	151	151	5.45	0.55

Chapter 16

Automated myocardial perfusion from coronary X-ray angiography[1]

The purpose of our study is the evaluation of an algorithm to determine the physiological relevance of a coronary lesion as seen in a coronary angiogram. The aim is to extract as much as possible information from a standard coronary angiogram to decide if an abnormality, percentage of stenosis, as seen in the angiogram, results in physiological impairment of the blood supply of the region nourished by the coronary artery. Coronary angiography, still the golden standard, is used to determine the cause of angina pectoris based on the demonstration of an important stenose in a coronary artery. Dimensions of a lesion such as length and percentage of narrowing can at present easily be calculated by using an automatic computer algorithm such as Quantitative Coronary Angiography (QCA) techniques resulting in just anatomical information ignoring the physiological relevance of the lesion. In our study we analyze myocardial perfusion images in standard coronary angiograms in rest and in artificial hyperemic phases, using a drug *e.g.* papaverine intracoronary. Setting a Region of Interest (ROI) in the angiogram without overlying major vessels makes it possible to calculate contrast differences as a function of time, so called time-density curves, in the basal and hyperemic phases. In minimizing motion artifacts, end diastolic images are selected ECG based in basal and hyperemic phase in an identical ROI in the same angiographic projection. The development of new algorithms for calculating differences in blood supply in the region as set are presented together with the results of a small clinical case study using the standard

[1] presented at Medical Imaging 2010: Computer - Aided Diagnosis, and published in part as: C.J. Storm, C.H. Slump, "Automated myocardial perfusion from coronary X-ray angiography," in *Medical Imaging: Computer - Aided Diagnosis*, M.L. Giger, N. Karssemeijer, eds., *Proc. SPIE*, vol. 7624, 76242S, 2010.

angiographic procedure.

16.1 INTRODUCTION

Coronary angiography is up till now the most important modality to diagnose coronary abnormalities particularly stenoses causing the clinical syndrome angina pectoris. See Fig. 16.1 for an example of a right coronary angiogram (RCA). In clinical cardiology the estimation of the percentage stenosis in a coronary artery is in the standard clinical practice still mostly based on visual assessment leading to large inter and intra observer variability in reading coronary arteriograms [1, 2, 3]. Image analysis using computer assistance does result in a more consistent judgment, however, this approach is mainly based upon static geometric parameters such as length of the stenosis and percentage of diameter and area reduction of a single segment in the stenosed artery [4, 5]. In 70-90% of the coronary angiograms there are stenoses to justify the diagnosis angina pectoris, however, in the 10-30% of the coronary angiograms there are slight or no abnormalities at all in the epicardial vessels although the patients do have real anginal complaints [6]. This group of patients may benefit from additional diagnostic procedures demonstrating disturbances in the micro circulation of the myocardium. These disturbances are mostly caused by the reduction of blood supply based on atherosclerotic changes of the epicardial coronary vessels but not always. In that case secondary to specific heart diseases are affecting the microcirculation such as hypertension and/or diabetes. However, if the disturbances are not secondary to a known clinical syndrome, the syndrome is called syndrome X. The microcirculation of the myocardium is responsible for optimizing the functional capacity of the myocardial cells. The extent of myocardial perfusion to nourish the myocardial cells is regulated on demand and activated by local and general factors: exercise, stress and many others. The imbalance of demand and supply causes complaints such angina pectoris or heart failure.

The anatomical basis of the microcirculation consists of a proximal and distal compartment in which the prearterioles in the proximal compartment play an important role in optimizing the perfusion pressure in the arterioles. These regulation is the combined action of neural (sympathetic), humoral and local vasoactive factors. In contrast the arterioles are sparsely innervated resulting in a regulation mostly depending on local factors in particular the oxygen concentration. That is why these arterioles play a very important role in the regulation of blood flow in the myocardium to ensure equilibrium in supply of nutrients and the washout of waste products. Through this mechanism the coronary flow is regulated in proportion to the need of the myocardium for oxygen, which is closely related to the delivered amount of cardiac work. In the absence of diseased epicardial vessels there is hardly any resistance to the flow in these vessels in contrast to the micro vascular

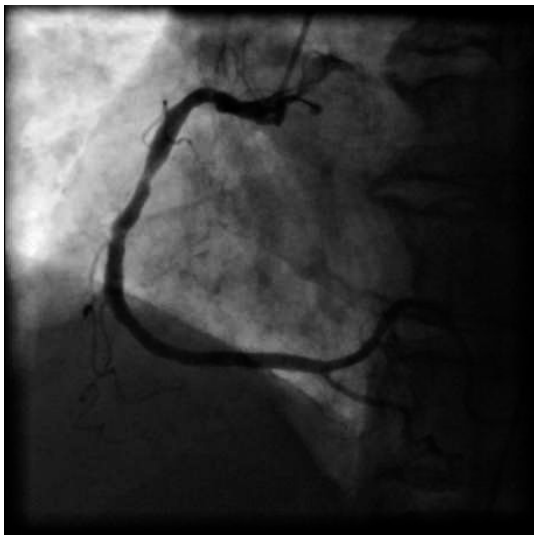

Figure 16.1: Example of an angiogram of a right coronary artery in right anterior oblique view, the apparent stenosis is (visually) estimated to be 50%. In standard practice this is considered too less for interventional follow-up. However, in case the arterioles are maximally dilated, the stenosis can become flow limiting.

component. So the microvascular vessels determine the amount of blood the myocardium will get in a factor three to six times the basal amount depending on the demand. This is called Coronary Flow Reserve (CFR) [7, 8]. Coronary flow reserve depends mostly on the possibility of the arterioles to dilate. Micro vascular dysfunction is mostly a combination of factors: vascular based vessel wall thickening or abnormal reaction on regulating substances, and myocardial such as myocardial wall thickening in hypertension. In case of syndrome X there is no conclusive anatomical substrate in the coronary angiograms to explain a reduced CFR. However, ultrasound studies show a high percentage of vessel wall abnormalities causing a reduced release of vasoactive hormones leading to a decrease in vasodilatation of the arterioles. Diagnostic tests are necessary when multi angulated angiograms, to reduce the chance missing asymmetric lesions, give no critical lumen changes explaining the complaints of the clinical syndrome angina pectoris. Spasm of the epicardial vessels should be excluded by provocative *e.g.* ergonovine intracoronary during angiography. When both procedures are negative micro vascular dysfunction has to be excluded by measuring coronary flow reserve. The CFR is measured by pharmacologic intervention to get maximal vasodilatation, in humans three compounds are used, i.e. intravenous dipyridamole

or adenosine or intracoronary papaverine or adenosine. There are several methods to measure the CFR: invasively or non-invasively. The non-invasive methods are mostly using radioactive materials (nuclear medicine), the invasive techniques consist of mostly expensive catheters for example Doppler catheters to measure flow difference in the epicardial vessels in basal conditions and after pharmacologic interventions. Doppler flow measurement has an extra problem because of epicardial vessel dilatation resulting often in a change of position causing a change of the angle used as cosines in the flow calculations. Quantitative angiography is to our opinion a useful method to evaluate the extent of possible dilatation of the arterioles after pharmacologic intervention as substitute of exertion in an easy way without extra catheters or procedures in connection of a normal standard coronary angiography. This paper is organized as follows. In the next section we describe our approach in detail. Then we describe the data and present results. We finalize with a discussion and conclusions.

16.2 METHODS

16.2.1 CFR

The relation between aortic root pressure and coronary flow is quite complex and has been studied by many authors and this has resulted in a variety of approaches and models [9]. Consensus has been established that the vasodilation of the arterioles regulates the flow through the myocard. The visual or computer assisted assessment of the severity of a stenosis, such as visible in Fig. 16.1, influences the flow only if its resistance is of the same order of magnitude as the resistance by the myocard. Therefore, a more functional, physiological measure is to be preferred over geometric parameters characterizing the severity of a stenosis [10]. The functional CFR measurement provides information about the perfusion of the heart muscle [18]. In a Region-of-Interest (ROI) in the angiogram (without an overlying major blood vessel) the contrast is measured as a function of time (the so-called time-density curve). With CFR the measured local maximum contrast density represents the vascular volume and the measured local contrast arrival time is inversely proportional to flow [11]. The required hyperemic state of exercise can be induced artificially by the intracoronary injection of a vasodilator drug *e.g.* papaverine. In this hyperemic state, contrary to the basal state, the arterioles are maximally dilated, thus the normal increase of the blood flow to the physical limits is set by the sizes of the epicardial coronary arteries and especially the partially occluded segments. The CFR can be visualized in a functional image with the color coded image values proportional to the increase in blood flow in the pertinent part of the heart muscle. Areas with less blood flow in-

crease do show up dark, no essential difference in comparison with the basal state, indicating effects of impaired blood flow due to stenosed segments in the coronary arteries and possible (partial) infarction. Although good results with the CFR method have been reported [12, 13, 14], in clinical practice the procedure is demanding, especially the correction of the background contributions is difficult because of the dynamics of the contracting heart. The requirement is that the two image sequences, basal and hyperemic, should be registered exactly the same. However, movements due to patient respiration cannot be eliminated completely. In order to avoid misregistration artifacts, pacing of the heart together with ECG triggered contrast injection and image acquisition did appear to be mandatory. As the measurement of the absolute CFR is difficult [15], alternatives such as the Relative Coronary Flow Reserve (RCFR) [10] and the Fractional Flow Reserve (FFR) [16] have been developed. Dual energy subtraction [17] has been proposed to overcome the motion artifacts. The main advantage of the FFR method is that all measurements are made during maximum arteriolar vasodilatation. On the other hand the method is not that easy incorporated in daily clinical routine because this method is time consuming and expensive due to the extra required catheter for the intra-coronial flow measurement. In this paper we present in the next section a less demanding approach which is less time-consuming and less demanding in procedure.

16.2.2 Model

In this section we model the integration over a ROI positioned on the myocard in the angiogram. We assume that within the ROI there are no overlying major bloodvessels. The integration *i.e.* the summation of the (log of the) pixel intensities inside the ROI together with the angiogram being a radiographic projection, provides for a 3D volume measurement of the amount of contrast agent contained in the myocard. We assume with neglect of possible diffusion that the injected contrast completely replaces the blood. The myocard can be considered to be a reservoir which holds temporarily the contrast agent for a certain mean transit time $\tau_{transit}$. Let $P(x, y, t)$ denote the pixel intensities at time t as a function of the two spatial coordinates x and y. The angiogram $P(x, y, t)$ is a projection along the z-axis of the 3D distribution of contrast agent which is a function of the spatial coordinates x, y, z and t. The result of the integration is proportional to the concentration contrast material under the ROI. A schematic diagram of the myocard model is shown in Fig. 16.2, the inflow of contrast at the arterial side is $I_{in}(t)$, the outflow $I_{out}(t)$ is at the venal side. The result of the integration over the reservoir is given by

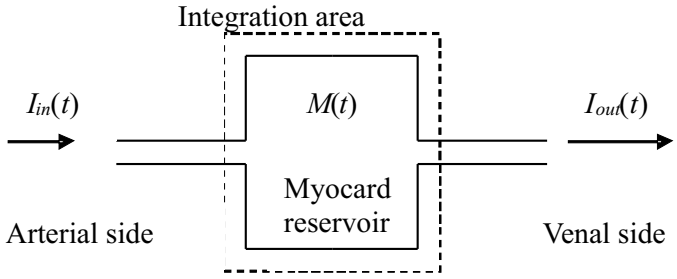

Figure 16.2: Schematic diagram of the ROI integration resulting in the contrast measurement $M(t)$ in the myocard reservoir.

the contrast measurement $M(t)$:

$$M(t) = \begin{cases} 0, & \text{if } t \leq \tau_{inject} \\ \int\int_{ROI} P(x,y,t)dxdy, & \text{if } t > \tau_{inject} \end{cases} \tag{16.1}$$

Conservation of mass leads to the relation between the measured contrast and blood flow:

$$\frac{d}{dt}M(t) = I_{in}(t) - I_{out}(t) \tag{16.2}$$

After a certain time τ_{peak} the contrast concentration saturates as the whole contrast bolus is contained in the myocard. The contrast concentration starts to diminish after the mean transit time $\tau_{transit}$. An idealized contrast curve is shown in Fig. 16.3. According to [11], the rising slope of the $M(t)$ curve of

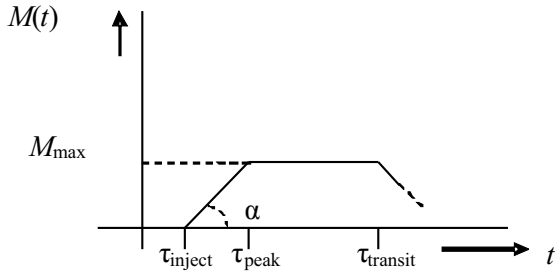

Figure 16.3: The idealized contrast $M(t)$ and the describing parameters. Of special interest is the slope α as it is related to flow.

Fig. 16.3 is proportional to flow. From first principles, we obtain the following

solution to the differential equation (2):

$$M(t) = \left(1 - exp(-\frac{t}{\tau_{rise}})\right) u(t) - \left(1 - exp(-\frac{t - \tau_{transit}}{\tau_{decay}})\right) u(t - \tau_{transit}) \tag{16.3}$$

with $u(t)$ the unit step function. In Fig. 16.10 we show two simulated first-order responses of the myocard to a contrast bolus injection.

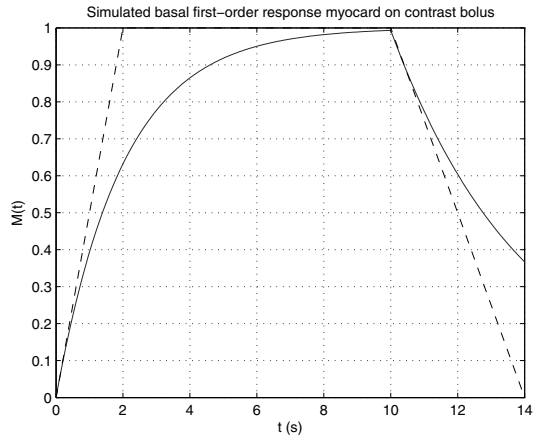

(a) basal state

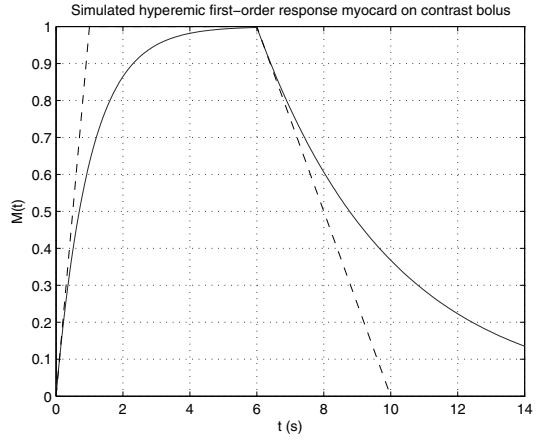

(b) hyperemic state

Figure 16.4: Simulated first-order responses of the myocard on a contrast bolus, basal (a) state with parameters τ_{rise} = 2 s, $\tau_{transit}$ = 10 s and τ_{decay} = 4 s;and hyperemic (b) state with parameters τ_{rise} = 1 s, $\tau_{transit}$ = 6 s and τ_{decay} = 4 s.

In practice, we compare the (ratio) of the rising slope in basal and hyperemic conditions. There is a small time - offset between the moment of injec-

tion and the start of the image sequence. Therefore, we have to synchronize the two runs with respect to each other.

16.2.3 Image Handling

The images analyzed in this paper are acquired with an Axiom Artis dFC single plane C-arm system with a dynamic flat detector for cardiology from Siemens Medical Solutions. The frame rate is 15 frames / s. During the acquisition, the ECG is recorded simultaneously. In this paper we have chosen for the vascular bed of the right coronary artery for reasons of less overlying larger bloodvessels, see *e.g.* Fig. 16.1. The method we propose consists of the following steps: The basal and the hyperemic runs are typically acquired at the end of the patient study. The hyperemic state is evoked by intracoronary injection of 8 mg papaverine and flushed with contrast agent. Overall 6F catheters are used. The image data is archived on CD. With a computer script [19] the Dicom files are converted to 8 bit 512×512 bitmap format for further processing by Matlab. The converted Dicom files are read into Matlab together with the ECG data. From the ECG data the R-peaks are automatically detected and the end-diastolic images are selected in each heartbeat. For this we select the image at *e.g.* 80% of the R-R interval after the previous R-peak. See Fig. 16.10 for an example of an ECG signal with detected R-peaks and the selected diastolic images. Our first image is slightly before the second R - peak after the start of the run. In this way we obtain a set of in the order of 10 - 15 images for the basal and the hyperemic flow situation. See Fig. 16.10 for an example of selected images corresponding to Fig. 16.10. Fig. 16.10 shows the ECG signal of the consecutive hyperemic run, together with the detected R-peaks and the selected end-diastolic images. Fig. 16.10 displays these hyperemic images.

Because we are going to compare the two runs with respect to slope of the time-density curve, we must ensure the same contrast flow situation to start with in both runs. There is a variable time-offset between the start of the image acquisition and the manual injection of the contrast material. Coronary flow is primarily during diastole, so the first images with visible contrast are not necessarily in the same relative heart cycle in the two runs. We then can either manually select a polygon shaped ROI or have the pertinent myocard automatically detected and select the ROI accordingly. For the selection an image is chosen in the middle of the sequence. This is done because both the larger vessels and the myocard are visible and we can manually place the ROI such to avoid to overlay the larger vessels. Fig. 16.9 shows the manual selected ROIs at end - diastolic phase of 18 patients.

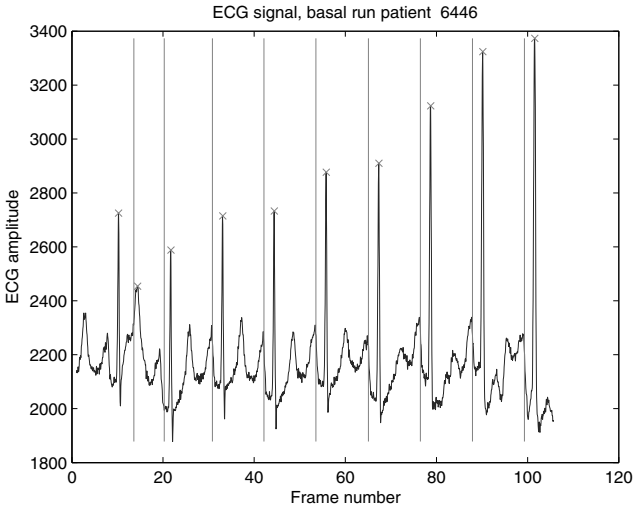

Figure 16.5: Example of a patient ECG signal, indicated are the detected R-peaks and the selected diastolic images.

16.2.4 Automated ROI selection

The automated ROI selection is preferably based on an image near the end of the sequence where the myocard is visible. The image segmentation can be simplified by logarithmic subtraction of a background so-called mask image, *i.e.* an image of the same ECG phase selection, acquired before appearing contrast. In our case applying a threshold to the image histogram after mask subtraction appeared to be sufficient for identifying the ROI. In this way the ROI does not need to be contiguous, major blood vessels are automatically excluded, if the heart beat is regular. Figure 10a shows an enhanced log-subtracted image of patient 6446 from the basal run, the coloring of the myocard is clearly visible, leading to the ROI shown in Fig. 16.10(b). The advantage is that in such an automatic selected ROI only the projected myocardial muscle is taken into account without larger and medium size bloodvessels. On the other hand, the contrast from the vessels is only a minor contribution to the integration over the ROI. The intensity is integrated over the ROI for each of the images at the same ECG phase. Also from the hyperemic run the selected images are measured with the same ROI. The contrast is computed as function over time from both runs, normalized through division by the area of the applied ROI and the comparison between normal and hyperemic run can be made. As the final step, we have to take into account the Automatic Exposure Control (AEC) of the diagnostic X-ray system.

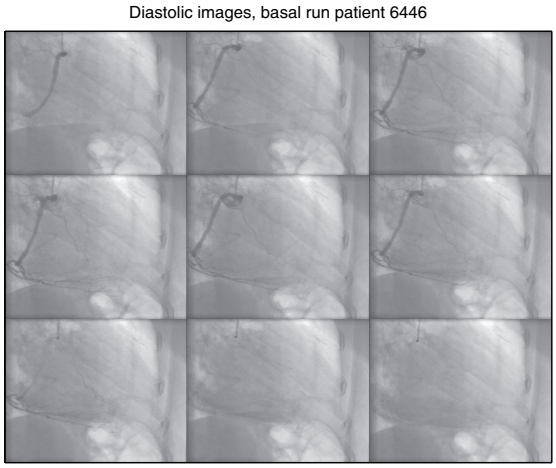

Figure 16.6: The selected basal diastolic images corresponding to Fig. 16.5.

16.2.5 AEC correction

The function of the AEC of a diagnostic X-ray system is to ensure the proper exposure for the consecutive image acquisition. This system component is of crucial importance for obtaining good image quality by setting appropriate values for kVp and mA and s. In the cardio application the X-ray exposures are typically pulsed with duration of 5 - 8 ms at 15 frames / s. There is a wide variation in patient mass and size, the AEC ensures about the same image intensity for each patient. As our purpose is to measure the response of the myocard over time and not the response of the AEC on the changed contrast, we have set up measurements to identify the AEC behavior [21]. The ideal AEC for quantitative measurements would keep the exposure factors constant after the start of the run. We were not able to manually set or overrule the AEC. On the other hand, it was our purpose to keep the standard protocol. Not much literature about AEC in general could be found and also the information from the vendor was not conclusive. From our experiments [21] we conclude that the AEC control loop is steered by the average image intensity over a circle inside the image matrix of 50% diameter. Fortunately the kVp setting appeared not to change; only the mA was adapted in our case with only small contrast dynamics. The appearing image contrast strongly depends on kVp; for changing kVp the quantitative measurements become more complicated. We now have three situations:

1. 1. If the selected myocard ROI is totally outside the AEC control circle, the exposures are not adjusted and the myocard response is adequately

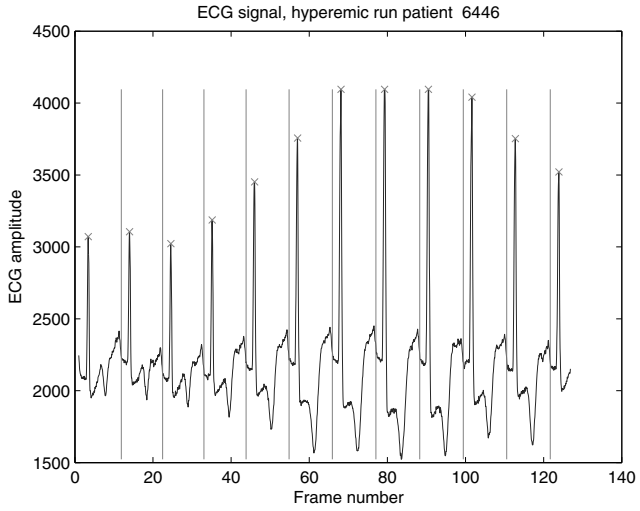

Figure 16.7: The ECG signal of the hyperemic run, indicated are the detected R-peaks and the selected diastolic images.

measured. No correction is needed.

2. 2. If the selected myocard ROI is completely inside the AEC control circle, the system adapts the mA in order to keep the average image intensity constant. The contrast within the myocard ROI with respect to the background intensity inside the AEC control circle is increased this way and we compensate for this effect by a weighting factor. The measured myocard intensity contribution is weighted by the ratio of the average intensity inside the AEC control circle excluding the myocard ROI region before contrast injection and after contrast injection, see Fig. 16.11.

3. 3. If the selected myocard ROI is partly inside and partly outside the AEC control circle, we have only to compensate the contribution from the part inside the circle.

16.3 RESULTS

We have performed the analysis described in the previous section on patient 6446. Fig. 16.12 shows the obtained results for the case of a manually selected ROI. The results with an automated ROI selection are similar. There is hardly any difference is response between basal and hyperemic flow. This

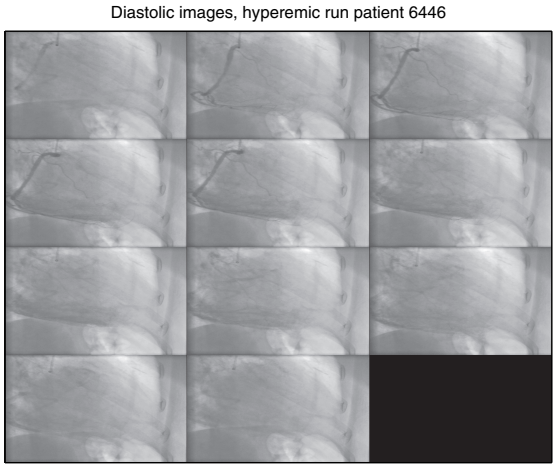

Figure 16.8: The selected hyperemic diastolic images corresponding to Fig. 16.7.

indicates that there is no CFR, apparently the preaterioles are already maximally dilated also in the basal situation. In this case the RCA can be flow limiting and possible should be taken care off. Of patient 6446 also a nuclear medicine SPECT myocard perfusion scan was made. The rest image is shown in Fig. 16.13(a) and the corresponding exercise image is shown in Fig. 16.13(b). The nuclear medicine rest study shows up quite normal; however, the stress study reveals a small ischemic area near the anterior septum. The angiographic findings including the extra papaverine image sequence of the right dominant patient 6446 are confirmed by the nuclear medicine study.

16.4 CONCLUSIONS

Our purpose is in the automated evaluation of the patho-physiological relevance of lesions, stenoses, in the coronary arteries as seen in an angiogram. We aim to extract as much as possible quantitative information about the physiological condition of the heart from standard angiographic image sequences. Coronary angiography is able to reveal the location and the projected diameter and length of the lesion. There is no information about the clinical, pathophysiological consequences of the stenosis. In this paper our aim is to assess the clinical significance of a lesion. We therefore analyze the myocardial perfusion as revealed in standard angiographic image sequences. In [20]20 we have presented the first results of our approach. In the present

Figure 16.9: Manual selected end - diastolic myocardial ROIs of 18 patients.

paper we report a case study about a patient that has been catheterized following the standard protocol and from whom also a scintigraphic perfusion scan was made. The angiographic image sequences consist of 8 bit images with a resolution of 512 $\times$ 512 pixels at a frame rate of 15 images / s. The frame lengths are somewhat longer than usual in order to include the registration of the perfusion. Our approach is simple and can be highly automated, is less time-consuming, less difficult and cheap as compared with other methods, above all there are no extra hazards for the patient.

Time density curves are obtained over the myocardium separated from the overlying major coronary vessels in case a ROI was manually placed. Automatic ROI selection appears also feasible; almost all bloodvessels can be excluded from the ROI. Because of the motion of the coronary arteries and the local myocardium we use the ECG signal to select images at the same (diastolic) phase.

The results depend to some extend on the X-ray exposure control dynamics, *i.e.* we want to measure the response of the vascular bed in the myocardium and not the response of the X-ray exposure control. Preferably we

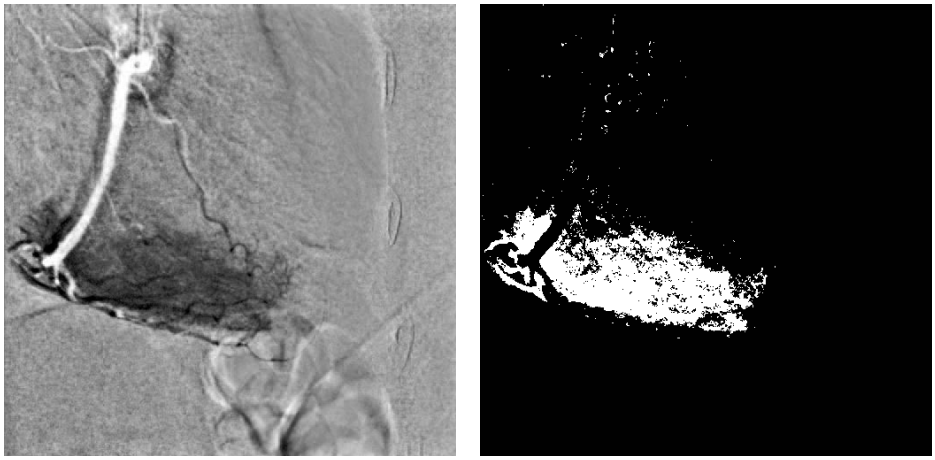

(a) enhanced log - subtracted image (b) resulting binary ROI

Figure 16.10: On the left (a) an enhanced log - subtracted image. *i.e.* image 76 - 19 of the basal run of patient 6446. On the right (b) the resulting binary ROI based on histogram thresholding.

acquire the images with a fixed kVp and mA during the acquisition of the image sequence. This appeared not to be possible, and we have realized a compensation scheme. Because we compare the two flow situations basal and hyperemic which we measure identically, our approach to obtain the relative CFR is rather robust. The obtained relative perfusion images from the case study show no CFR, a conclusion which is confirmed by the nuclear medicine study. This holds promise for clinical application. In the past we have studied myocardial perfusion with CFR methods from the literature such as for example [12]. These methods are demanding with respect to the procedure in the catheterization laboratories. We now use the standard protocol with slightly longer image sequences, only one or two runs, with comparable results. Though the proposed method looks promising, further clinical evaluation with a larger patient series, supported by in vitro experiments, is needed for further improvement and validation.

References

[1] K.M. Detre, E. Wright, M.L. Murphy, T. Takaro, "Observer agreement in evaluating coronary angiograms," Circulation 52(6), 979-986 (1975).

[2] L.M. Zir, S.W. Miller, R.E. Dinsmore, J.P. Gilbert, J.W. Hawthorne, "Interobserver variability in coronary angiography," Circulation 53(4), 627-632 (1976).

[3] E.J. Topol, S.E. Nissen, "Our preoccupation with coronary luminology," Circulation 92(8), 2333-2342 (1995).

[4] J.H.C. Reiber, P.W. Serruys, C.J. Kooijman, W. Wijns, C.J. Slager, J.J. Gerbrands, J.C.H. Schuurbiers, A. den Boer, P.G. Hugenholtz, " Assessment of short-, medium-, and long-term variations in arterial dimensions from computer-assisted quantitation of coronary cineangiograms," Circulation 71(2), 280-288 (1985).

[5] J.H.C. Reiber, P.W. Serruys, *Quantitative Coronary Arteriography*, Kluwer Academic Publishers, 1991.

[6] R.O. Cannon, P.G. Camici, S.E. Epstein, "Pathophysiological dilemma of syndrome X," Circulation 85(3), 883-892 (1992).

[7] R.L. Kirkeeide, K.L. Gould, L. Parsel, "Assessment of coronary stenoses by myocardial perfusion imaging during pharmacologic coronary vasodilation. VII. Validation of coronary flow reserve as a single integrated functional measure of stenosis severity reflecting all its geometric dimensions," J. Am. Coll. Cardiol. 7(1), 103-113 (1986).

[8] K.L. Gould, R.L. Kirkeeide, M. Buchi, "Coronary flow reserve as a physiologic measure of stenosis severity," J. Am. Coll. Cardiol. 15(2), 459-474 (1990).

[9] F.J. Klocke, R.E. Mates, J.M. Canty, A.K. Ellis, "Coronary pressure-flow relationships, controversial issues and probable implications," Circ. Res. 56(3), 310-323 (1985).

[10] K.L. Gould, K. Lipscomb, "Effects of coronary stenoses on coronary flow reserve and resistance," Am. J. Cardiol. 34, 48-55 (1974).

[11] J.T. Cusma, E.J. Toggart, J.D. Folts, W.W. Peppler, N.J. Hangiandreou, C.S. Lee, C.A. Mistretta, "Digital subtraction angiographic imaging of coronary flow reserve," Circulation 75(2), 461-472 (1987).

[12] R.A. Vogel, "The radiologic assessment of coronary blood flow parameters," Circulation 72(3), 460-465 (1985).

[13] V. Legrand, G.B. Mancini, E.R. Bates, J.M. Hodgson, M.D. Gross, R.A. Vogel, "Comparative study of coronary flow reserve, coronary anatomy and results of radionuclide exercise tests in patients with coronary artery disease," J.Am. Coll. Cardiol. 8(5), 1022-1032 (1986).

[14] G.B. Mancini, S.B. Simon, M.J. McGillem, M.T. LeFree, H.Z. Friedman, R.A. Vogel, " Automated quantitative coronary arteriography: morphologic and physiologic validation in vivo of a rapid angiographic method," Circulation 75(2), 452-460 (1987).

[15] M.J. Kern, A. Lerman, J. -W. Bech, B. de Bruyne, E. Eeckhout, W.F. Fearon, S.T. Higano, M.J. Lim, M. Meuwissen, J.J. Piek, N.H.J. Pijls, M. Siebes, J.A.E. Spaan, "Physiological assessment of coronary artery disease in the cardiac catheterization laboratory: a scientific statement from the American heart association committee on diagnostic and interventional cardiac catheterization, council on clinical cardiology," Circulation 114(12), 1321-1341 (2006).

[16] N.H.J. Pijls, B. van Gelder, P. van der Voort, K. Peels, F.A.L.E. Bracke, H.J.R.M. Bonnier, M.I.H. El Gamal, "Fractional flow reserve: a useful index to evaluate the influence of an epicardial coronary stenosis on myocardial blood flow," Circulation 92(11), 3182-3193 (1995).

[17] S. Molloi, A. Ersahin, J. Tang, J. Hicks, C.Y. Leung, "Quantification of volumetric coronary blood flow with dual energy subtraction angiography," Circulation 93(10), 1919-1927 (1996).

[18] M. Schrijver, *Angiographic image analysis to assess the severity of coronary stenoses*, PhD thesis, University of Twente, The Netherlands, 2002.

[19] G.A. ten Brinke, *Quantitative analysis of angiographic sequences*, MSc thesis, University of Twente, The Netherlands, 2005.

[20] C.J. Storm, C.H. Slump, "CAD of myocardial perfusion," Proc. SPIE Medial Imaging: Computer-Aided Diagnosis, vol. 6513, pp. 65132D, 2007.

[21] C.J. Storm, C.H. Slump, "Estimation of X-ray parameters in digital coronary angiography for compensation of myocardial perfusion measurement," Proc. SPIE Medical Imaging: Physics of Medical Imaging, vol. 6913, pp. 6913L-11, 2008.

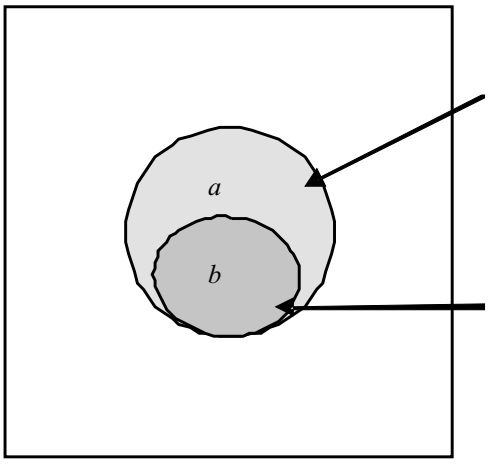

(a) AEC circle a

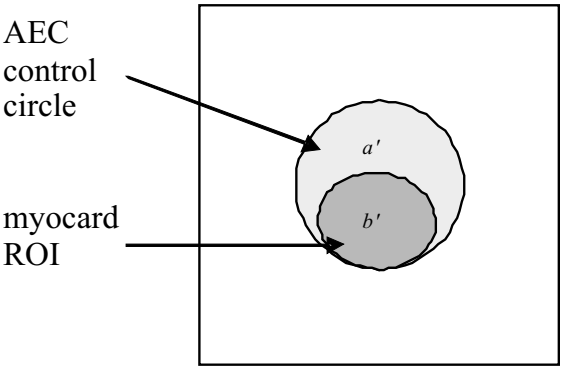

(b) AEC circle b

Figure 16.11: On the left (a) the image matrix with the AEC control circle before contrast injection, average image intensity in the myocard ROI equal to a, average image intensity over the AEC circle excluding the myocard ROI equal to b. On the right (b) the image matrix with the AEC control circle after contrast injection, average image intensity in the myocard ROI equal to a', average image intensity over the AEC circle excluding the myocard ROI equal to b'. Weighting factor to compensate the measured b' equals a/a'.

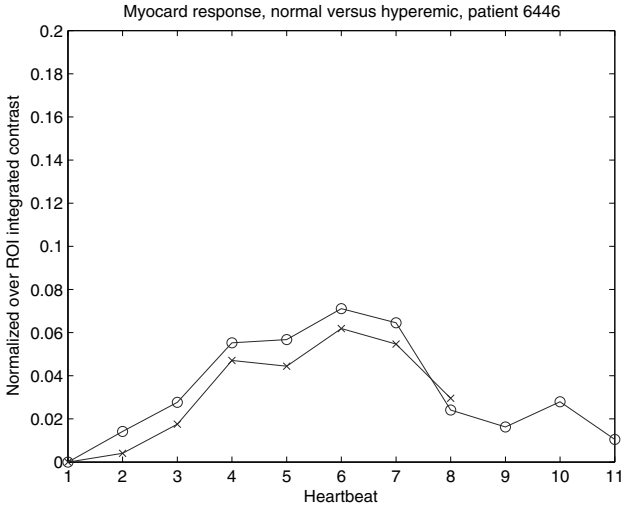

Figure 16.12: The basal ROI integrated time-density indicated with $'x'$ and the hyperemic ROI integrated time-density indicated with $'o'$. There is no difference in myocard response between basal and hyperemic run as function over time, indication no CFR.

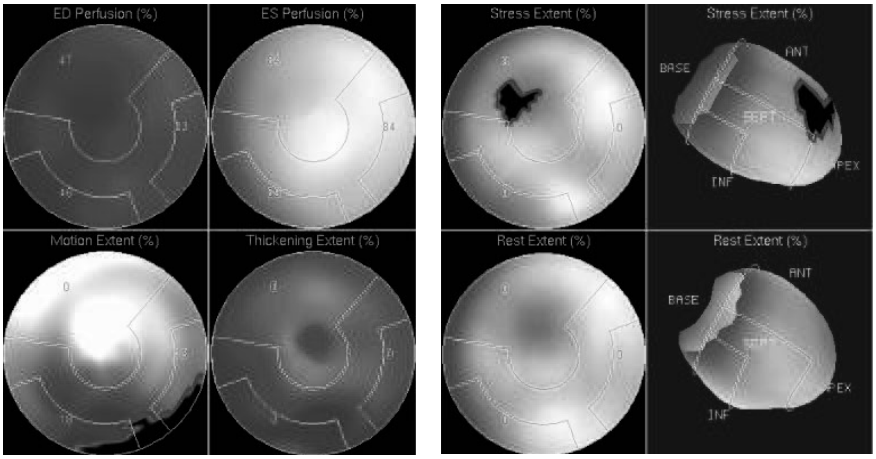

(a) (b)

Figure 16.13: On the left the result of the rest study with 527 MBq Tc-99m of patient 6446; on the right the result of the stress study with 530 MBq Tc-99m.

Chapter 17

Developments in diagnostics of coronary heart disease

Catheter-based direct invasive coronary angiography is until now the gold standard in the diagnostics of coronary heart diseases as it makes blood flow and intracoronary anatomy visible. However, this method has some complications, even in the hands of experts. Complications such as local bleeding at the place where the catheter enters the body, transient rhythm disturbances and anaphylactic reactions are known as minor complications without permanent damage. But there are also major complications, such as nephrotoxicity, cardiogenic shock requiring hospitalization, and even death because of untreatable ventricular rhythm disturbances or renal failure. The catheterization procedure itself, in use since the 1950s in (too?) many hospitals worldwide, requires specialized personnel and well-adapted hardware and software, and it is time-consuming, thus involving high costs. Because of these factors and other less medical important matters, such as hospitalization of the patient for a short stay, a search has started for simpler, less invasive, faster and more patient-friendly methods, aside from the need to work more economically.

Technical development in X-ray imaging hardware and faster computer systems resulted in a new imaging system known as computer tomography (CT). Originally this was called the EMI scan because the scanner was developed at a research facility of Electric and Musical Industries in the UK in 1967 by Godfrey Hounsfield, an electrical engineer. Hounsfield developed the principle of this image reconstruction system by combining applied mathematical techniques that made use of a series of separate X-ray images. These techniques were first published in 1963 by Allan Cormack [1] at Tufts University, Massachusetts, but they were not introduced to clinical practice because of the limited memory capacity of computer systems at that time. Both inventors received the Nobel Prize for Medicine in 1979.

Table 17.1: CT development over time, indicating the number of slices, adapted from [22].

Manufacturer	*Scanner type*	*Number of slices M*	*Year*
EMI	Mark I	2	1972
Siemens	SIRETOM 2000	2	1974
Siemens	SOMATOM SD	2	1977
Imatron	C-100	2	1983
Elscint	Twin	2	1994
GE	LightSpeed	4	1998
Marconi	Mx8000	4	1998
Siemens	SOMATOM Volume Zoom	4	1998
Toshiba	Aquilion	4	1998
GE	LightSpeed 16	16	2001
Philips	IDT 16	16	2001
Siemens	SOMATOM Sensation 16	16	2001
Toshiba	Aquilon	16	2001
GE	VCT 64	64	2004
Philips	Brilliance 40	40	2004
Siemens	SOMATOM Sensation 64	64	2004
Toshiba	Aquilion 64	64	2004
Toshiba	prototype	256	2005
Toshiba	Aquilion 256	256	2007

The first clinical images of a brain, a non-moving object, made by this new CT system were published in 1972. These images were made in Atkinson Morley's Hospital in Wimbledon, UK. The first installation of a CT system in the USA was about the same time at the Mayo Clinic. The procedure of image reconstruction out of thin tomographic images was in those days very slow, as it took several minutes to create one hazy image because of the limited computer capacity, with a matrix of only 80×80 pixels. Since that time, the development of faster computer systems, resulting in shortening of the scan time, and the extension of computer memory capacity have led to the possibility of scanning even moving objects such as the heart. The technical innovation in CT development is shown in Table 17.1.

Parallel to the development in CT scanners, important research was performed in electronic subtraction techniques of X-ray images, first by Sturm [2] in 1964 and Ziedses des Plantes [5] in 1968, see Figure 17.1. However, the time-base instabilities of the electronic image technology at that time made this method of image acquisition impractical and unreliable. This applied principle of electronic subtraction techniques was based on the earlier work

of Ziedses des Plantes, using analogue X-ray images, published in his thesis [4] that he defended in 1934.

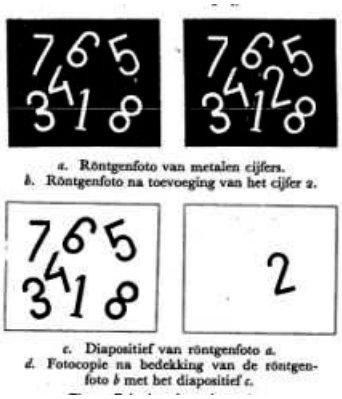

a. Röntgenfoto van metalen cijfers.
b. Röntgenfoto na toevoeging van het cijfer 2.
c. Diapositief van röntgenfoto *a*.
d. Fotocopie na bedekking van de röntgenfoto *b* met het diapositief *c*.

Figure 17.1: Principe of subtraction as published by Ziedses des Plantes [3].

After the introduction of high-fidelity video, image analogue-to-digital conversion of static images usable for electronic subtraction techniques became available. By applying this technique Smith [6] was able to make the first reliable examples of subtraction images of blood vessels; this technique was called digital subtraction angiography (DSA). The first applications of this subtraction technique using tomograms (slices) in clinical angiographic cardiology [7], using a computer tomography (CT), were made with an Electron Beam Computer Tomograph (EBCT), also named fast CT or cine CT, developed in the late 1970s by Boyd et al. at the University of California at San Francisco, see Figure 17.2.

This system consists of an X-ray source composed of a 210-degree arc ring of tungsten targets activated from a magnetically focused beam of electrons fired from an electron gun behind the scanner ring. Images were acquired after intravenous injection of normal contrast agents. Progress in technical CT development was bidirectional, namely via the EBCT system and secondly via the principle of a rotating gantry, the MSCT (Multi Slice Computer Tomograph).

The difference between these two systems is that the EBCT does not involve moving components, but it is bulky. By contrast, the MSCT contains a fast 360-degree rotating X-ray imaging system, which is compact compared to the EBCT system. For practical reasons the MSCT systems are mostly used nowadays. The EBCT system uses a unique electron beam configuration with no moving parts in the imaging chain. This results in the depiction of the heart via 3-D acquisition of multiple parallel tomograms with high spatial and temporal resolution. EBCT offers a resolution below 100 ms, which makes this kind of CT unique for imaging a moving object, such as the beat-

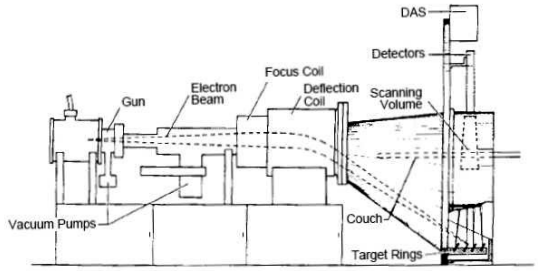

(a) longitudinal axial cross section

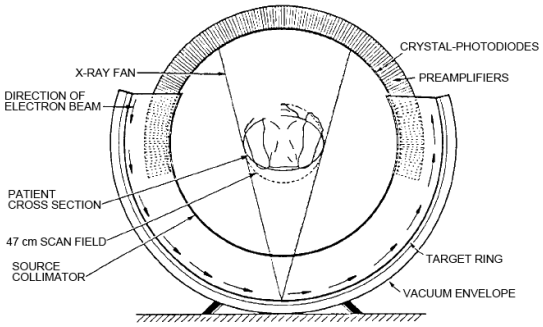

(b) axial cross section

Figure 17.2: Principle of an EBCT system developed in 1979. In this design the X-ray source is electronically steered along the semicircular strip below the patient. X-ray transmission is measured by a fixed array of detectors above the patient. This system has no moving parts.

ing heart, driven by ECG triggers.

Another approach to fast subsecond CT scanning is the dynamic spatial reconstructor (DSR) developed at the Mayo Clinic [23, 24]. The DSR contains 28 X-ray tubes that are mounted equally spaced over a 180 degree arc and also 28 sets of video cameras arranged in the opposing semicircle behind a curved fluorescent screen. The entire assembly rotates continuously about the patient table at 15 rmin to provide a reconstruction every 1/60 s. Any portion of the body can be scanned by appropriately positioning the table. One complete volume (up to 240 cross sections) can be obtained from 28 views recorded in 1/100 of a second and repeated 60 times/s. Special-purpose hardware and software is designed to perform reconstructions and to provide efficient off-line calculations of all dynamic volume images generated, see Figure 17.3. Technical complications have limited this approach to animal studies; also the required dose was too high for application to humans.

The MSCT type of scanner uses a mechanically rotating gantry. Although

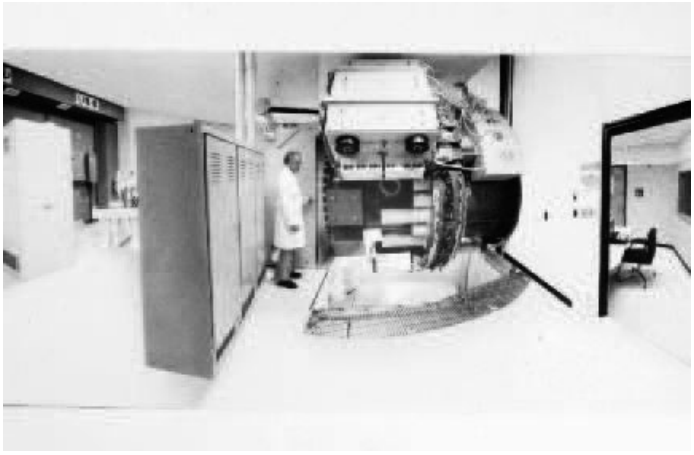

(a) The DSR machine

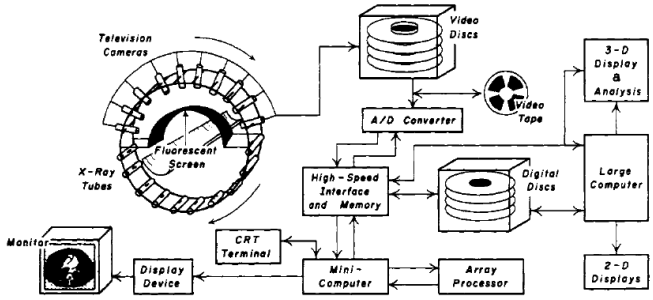

(b) Block diagram of the DSR

Figure 17.3: The dynamic spatial reconstructor, multiple rotating sources and detectors designed so as to have fast enough data acquisition for reconstruction of the beating heart [24].

in practice slightly differing systems are in use dependent on the manufacturer, they all have in common a temporal resolution that is high enough to allow imaging of the beating heart without, or with only slight, motion artifacts. An important restriction in image acquisition is the need for a regular heart rhythm and a heart frequency below 70 beats per minute to obtain more than one image slice per gantry rotation. This restriction is especially important for the older generation of scanners. It can therefore not be applied with patients with a high heart rate or an irregular rhythm such as atrial fibrillation or multiple extra systoles. The temporal resolution of a MSCT scanner is defined by its rotation time. Using MSCT for coronary angiography, the rotation time needs to be below 420 ms, corresponding to a temporal resolution of less than 210 msec. The modern tomography systems mostly in use nowadays have a rotation gantry time of 333 ms, corresponding to a temporal

resolution of approximately 167 ms and acquiring up to 64 slices simultaneously. Although much technical progress has been realized in recent years, especially in hardware and software, the heart rate needs still to be reduced, mostly by intravenous injection or infusion of a beta blocker, to get reliable images. The need to slow down the heart rate is no longer necessary with the 256 slice CT (Toshiba, prototype in 2005, introduced commercially in 2007). By using such a fast CT system it will be possible to scan the whole heart in one heart cycle with slices of 0.5 mm and 13 cm in the z-axis without motion artifacts.

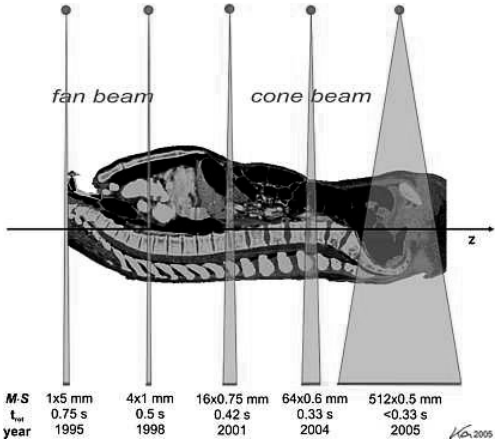

Figure 17.4: Development over time of the CT image acquisition from fan beam to cone beam, number of slices $M \times S$, slice thickness. Adapted from [22].

Another semi-invasive modality to visualize the coronary arteries is magnetic resonance imaging (MRI). The MRI system, not based on radiation but on magnetism, results in no extra radiation burden for the patient. It is used without iodine contrast agents, so it is also usable in patients with bad renal function. MRI images can be generated independent of the heart rate, contrary to CT until now. These properties make MRI suitable for sequential studies in the same patient. The first clinical cardiac study made by MRI using contrast enhancement with Gadolinium (Gd 64), a silvery white, malleable and ductile rare metal with strong paramagnetic properties for intravenous injection, was by McNamara [8] in 1984. Gadolinium is injected as a chelated compound that does not pass the blood-brain barrier and is excreted by the kidneys. Adverse reactions due to the use of gadolinium-enhanced contrast agents occur seldom, although all kinds of allergic reactions are possible. Gadolinium should not be used in case of acute renal failure. However, despite recent advances in technical development, MRI coronary angiography even at 1.5 T(esla) produces in plane only a resolution of around 0.7 mm,

in contrast to 0.3 mm in X-ray conventional coronary angiography.

In the last two decades many single and multicentre studies have been undertaken to discuss the pros and cons of each method and also the limitations of the (MS)CT and MRI diagnostic methods. Both systems give, in addition to diagnostic information on stenoses and occlusions [9], also information about the different textures of coronary plaques. Especially non-calcified lesions can be visualized[10] by CT systems. CT low dense plaques (CTLDP) correspond well to rupture-prone soft plaques as seen with intracoronary ultrasound [11] and coronary angioscopy [12]. Detection of these soft plaques is of prognostic value because these lesions are important in the development of an acute coronary syndrome, contrary to the earlier assumed importance of a severely narrowed lumen [13]. Although MRI and MSCT are both suitable for the detection of lumen narrowing based on calcium deposit in the texture of plaques, MSCT is much faster and relatively inexpensive at this moment. The quality of the MSCT images obtained is better, resulting in a more accurate and reliable diagnosis of coronary atherosclerotic lesions compared to MRI. Thus in clinical use, X-ray techniques are superior to MR angiographic methods.

Another aspect at this moment is the difference in sensitivity and specificity between MRI and CT in clinical use. The sensitivity and specificity of MRI in identifying significant coronary lesions ranges between 30 to 90% and 70 to 95%, respectively [14]. This is a wide variation, not ideal for clinical use, aside from the problems of using MRI in patients that have metallic materials implanted that are sensitive to magnetism. MSCT, because of the improvement in temporal and spatial resolution, has a much better sensitivity, varying between 72 to 95% [15], and a specificity variation between 86 to 98% [16]. MSCT has thus become a more reliable tool in diagnosing coronary lesions. Although noninvasive detection by MSCT of intraluminal narrowing has a higher score compared with MRI, the future in diagnostics will go towards better recognition of the type and character of the lesion and the viability of the myocardium perfused by the abnormal coronary artery. MRI currently scores higher in detection of the character of a lesion (calcium and/or fat), but newer algorithms and hardware are being developed, for use in MSCT systems. Implementation of these newer algorithms in MSCT systems will make these systems very efficient for screening and detection of coronary heart disease, although at this time "classic" more invasive coronary angiography is still needed in patients with doubtful lesions. As such, MSCT can be an effective method to detect abnormalities in the coronaries and can function as the "roadmap" for interventions. This means that MSCT can in the near future be the only appropriate method to exclude coronary heart disease in patients who are suspected to have angina pectoris, especially in an outpatient clinic setting. Sometimes, however, it will necessary

to complete MSCT images by means of other diagnostic methods such as semi-noninvasive nuclear PET scanning, MRI or even invasive intracoronary injections of vasodilatation medication (for example papaverine) to diagnose or exclude a physiologically important abnormality in myocardial perfusion.

Although MSCT has great potential for screening, being fast, reliable and patient-friendly, there are also significant negative aspects in the use of MSCT, especially the radiation burden in frequent use of these systems in the same patient. Next to this radiation burden, the need to use iodine contrast agents to visualize the coronaries makes these systems unsuitable for patients with impaired renal functions or patients allergic to iodine. Besides these problems there is the need for a regular, not too fast heart rhythm, $\leq$ 70 bpm, to prevent motion blur. To slow down the heart rate sometimes requires administration of extra medication by intravenous injection of, in most cases, a beta blocker. This commonly used medication can result in unwanted side effects or interfere with the normal cardiac function of the patient, which can result in an unreliable image of the state of the cardiac function. The newer MSCT systems, which are much faster with 64 slices or higher, can handle a faster heart rate and also a not too fast irregular rhythm (atrial fibrillation, many extra systoles). As such, the need to slow down the heart rate or to start treatment of the rhythm disturbance before carrying out an MSCT examination is not an absolute reason anymore to exclude this patient category.

Another more important problem encountered in the use of MSCT systems is the amount of radiation needed to investigate a patient with potential coronary heart problems compared with the old "method" of invasive coronary angiography. Many investigations have been done in vivo and in vitro (phantoms) to measure the radiation burden on skin and organs such as the female breast, because the mammae are in the direct radiation field during cardiac analysis. The radiation burden for mammae is 10 to 30 times higher in an MSCT cardiac examination than in a regular mammography [17] examination (normally between 0.3 to 2.3 mGy with a mean of 1.1 mGy). The result of all these measurements is that CT scans, also for cardiac use, lead to a very high radiation burden. Estimations of the total radiation burden vary, but the mean radiation burden for MSCT imaging of the coronary system without bypasses is 9.76 $\pm$ 1.84 mSv in a study of 46 patients [18] and 2.69 $\pm$ 1.27 mSv compared to a normal invasive investigation. In patients after coronary bypass surgery, the radiation burden using MSCT was 12.46 $\pm$ 2.23 mSv and using conventional coronary angiography 6.27 $\pm$ 4.04 mSv. The literature shows different radiation burdens, but the overall conclusion is that CT results in a much higher radiation burden compared to conventional coronary angiography. The development of new hardware and software is expected to reduce the difference in radiation burden between conventional coronary angiography and CT coronary angiography in the near future, although with

CT the burden will always be higher. In spite of this extra radiation burden, CT will in the near future be the most important tool in screening for coronary heart diseases, and being more informative than noninvasive methods such as exercise testing or echocardiography [25].

Regular follow-up of patients after a coronary intervention, stenting and/or coronary bypass grafting (CABG) will be the next step in the use of CT, provided that the radiation burden can be diminished, as this is very important for the individual patient. This is a significant issue because, although cardiac CT is just a small fraction of the overall use of computer tomography (more than 62 million scans in the US in 2007, including 5 million in children [19]), the growth of cardiac CT means an extra radiation burden. This enormous increase in numbers (from 3 million in 1980 to > 62 million scans per year in 2007, just in the US) is an important risk factor, especially for young patients, who can develop cancers and or suffer hereditary genetic defects. Epidemiologic studies looking for these risk factors are just beginning [20], so the results will be known in due time, but it is currently estimated that 1.5 to 2.0% of all cancers in the US are attributable to this enormous increase in the use of CT. In 1996, before the CT era [21], the estimates were about 0.4%, so there has been an alarming increase.

Because of this enormous expansion in the use of CT diagnostics, but also in the knowledge of risk factors, it is important to use this form of diagnostics with absolute cautiousness. Reduction of the overall radiation burden, firstly for the individual patient but also for the radiological worker, requires the development of more sophisticated hardware and software. But another, often overlooked, important issue is: is there a real or absolute medical need for this form of diagnostics?

Estimates concerning the absolute need of a CT scan in different medical specialties reveal that as much as 50% of scans, also in children, are unnecessary. This accounts for a substantial part of the radiation burden for all mankind, resulting in extra biological damage but also in enormous economic cost. These facts imply an important task and challenge for the medical world, including cardiology, to consider firstly whether there is a real need for this kind of diagnostic examination, and not just fill in an application form, to exclude the possibility of coronary or other disease. However, if angina pectoris is suspected, CT will in the near future be the method of choice for diagnosis of abnormalities in coronary perfusion, with subsequent therapy. But if there is a need for intervention in the form of angioplasty, the "old" conventional angiographic X-ray machine in the catheterization lab will be still needed.

References

[1] A.M. Cormack, "Representation of a Function by its Line Integrals, with some Radiological Applications," *J. Appl. Phys.* 34, p. 2772, 1963.

[2] E.H. Wood, R.E. Sturm and J.J. Sanders, "Data processing in cardiovascular physiology with particular reference to Roentgen video densitometry," *Proc. Mayo Clin.* 39, pp. 849-865, 1964.

[3] B.G. Ziedses des Plantes, "Toepassing van subtractie bij het röntgenonderzoek van het hart en de grote vaten," *12 December 1959 Ned. T. Geneesk.* 103II.50, pp. 2554-2561, 1959.

[4] B.G. Ziedses des Plantes, *Planigraphie en subtractie*, Thesis Utrecht, Kemink & Zn N.V., Utrecht, 1934.

[5] B.G. Ziedses des Plantes, "The application of the subtraction method to cerebral angiography," *Progress in Brain Research* 30, pp. 181 - 188, 1968.

[6] H.C. Smith, R.E. Sturm and E.H. Wood, "Videodensitometric system for measurement of vessel blood flow, particularly in coronary arteries, in man," *Am. J. Cardiol.* 32(2), pp. 144-150, 1973.

[7] R.G. Gould, "Principles of ultrafast computed tomography: Historical aspects, mechanism, and scanner characteristics," in *Ultrafast computed tomography in cardiac imaging: Principles and practice*, W. Stanford and J.A. Rumberger, editors, pp. 1-6, Mt Kisko, Futura, New York, 1992.

[8] M.T. McNamara, C.B. Higgins, R.L. Ehman, R. Sievers and R.C Brasch, "Acute Myocardial Ischaemia: Magnetic Resonance with Gadolinium DTPA," *Radiology* 153(1), pp. 157-163, 1984.

[9] M. Ehara, J.F. Surmerly, M. Kawai, O. Katoh, T. Matsubaru, M. Terashima et al., "Diagnostic accuracy of 64-slice computed tomography for detecting angiographically significant coronary artery stenosis in an unselected consecutive patient population: Comparison with conventional invasive angiography," *Circ. J.* 70, pp. 564-571, 2006.

[10] F. Inoue, Y. Sato, N. Matsummoto, S. Tani and T. Uchiyama, "Evaluation of plaque texture by means of multislice tomography in patients with acute coronary syndrome and stable angina," *Circ. J.* 68, pp. 840-844, 2004.

[11] S. Achenbach, F. Moselewski, D. Ropers, M. Ferencik, U. Hoffmann, B. MacNeill et al., "Detection of calcified and noncalcified coronary

atherosclerotic plaque by contrast enhanced, submillimeter multidetector spiral computed tomography: A segment based comparison with intravascular ultrasound, *Circulation* 109, pp. 14-17, 2004.

[12] S. Komatsu, N. Hirayama, Y. Omori, Y. Ueda, I. Mizote, Y. Fujisawa et al., "Detection of coronary plaque by Computed Tomography with a novel analysis system, Plaque Map and comparison with intravascular Ultrasound and angioscopy," *Circ. J.* 69, pp. 72-77, 2005.

[13] M.C. Fishbein and R.J. Siegel, "How big are coronary atherosclerotic plaques that rupture?", *Circulation* 94, pp. 2662-2666, 1996.

[14] R.J. van Geuns, H.G. de Bruin, B.J. Rensing et al., "Magnetic resonance imaging of the coronary arteries: clinical results from three dimensional evaluation of a respiratory gated technique," em Heart 82, pp. 515-519, 1999.

[15] K. Nieman, F. Cademartiri, P.A. Lemos, R. Raaijmakers, P.M. Pattynama and P.J. de Feyter, "Reliable non-invasive coronary angiography with fast submillimeter multislice spiral computed tomography," *Circulation* 106, pp. 2051-2054, 2002.

[16] E. Martuscelli, A. Romagnoli, A. Eliseo et al., "Accuracy of thin-slice commuted tomography in the detection of coronary stenoses, *Eur. Heart J.* 25, pp. 1043-1048, 2004.

[17] E.L. Nikoloff and P.Q. Alderson, "A comparative study of thoracic radiation doses from 64-slice cardiac CT," *Br. J. Radiol.* 80(955), pp. 537-544, 2007.

[18] T. Dill, A. Deetjen, O. Ekinci, S. Mölmann, G. Conradi, A. Kluge, C. Weber, H. Nef and C.W. Hamm, "Radiation dose exposure in multi slice computed tomography of the coronaries in comparison with conventional coronary angiography," *Int. J. Cardiol.* 124(3), pp. 307-311, 2008.

[19] D.J. Brenner and E.J. Hall, "Computed tomography - an increasing source of radiation exposure," *N. Eng. J. Med.* 357, pp. 2277-2284, 2007.

[20] J. Giles, "Study warns of avoidable risks of CT scans," *Nature* 431, pp. 391-391, 2004.

[21] A. Berrington de Gonzales and S. Darby, "Risk of cancer from diagnostic X-rays: estimates for the UK and 14 other countries," *Lancet* 363, pp. 345-351, 2004.

[22] W.A. Kalender, *Computed Tomography*, Publicis Corporate Publishing, Erlangen, 2005.

[23] E.L. Ritman, R.A. Robb, S.A. Johnson et al., "Quantitative imaging of the structure and function of the heart, lungs, and circulation," *Mayo Clin. Proc.* 53, pp. 3-11, 1978.

[24] R.A. Robb, E.A. Hoffman, L.J. Sinak et al., "High-speed three-dimensional X-ray computed tomography: The dynamic spatial reconstructor," *Proc. IEEE* 71, pp. 308-319, 1983.

[25] T.W. Galema, *Improved imaging in cardiac patients: echocardiography and CT - coronary angiography*, Thesis Erasmus University Rotterdam, June 2010.

Curriculum Vitae

The author of this thesis was born in Monster in the year 1942. After the primary school he attended the secondary school in The Hague, gymnasium β. Study medicine Leiden University. After graduating he has worked as a military physician (general medicine and contributing to an infant consultation centre) at the airbase Twente in Enschede for more than one year. After this period he started as an assistant not in training (agnio) at the department pulmonary diseases in the Zuider Ziekenhuis Rotterdam. Six month later he switched to the radiology department Erasmus University Rotterdam, Head prof. K. Hoornstra, to become a radiologist. Missing the clinical work he switched, after one year of radiological training, again for a combination clinical work and technology to a speciality combining these two items: cardiology. As part of the training in cardiology he has worked for two years in the department internal medicine, Head dr. J. Bok, community hospital Dordrecht. To complete the training in cardiology, he worked for four years in Rotterdam, cardiology department Erasmus University, Head prof. P.G. Hugenholtz. After registration as cardiologist he joined a recently started cardiology group in the Zuider Ziekenhuis in Rotterdam as the third member, starting up the department non invasive cardiology, pacemaker technology (implantation and follow up) and playing an active role in the extension of the cath lab, next to training of starting assistants. This period ended in August 2004 interrupted by a sabbatical at the Leiden University, prof.dr. A.G.V. Bruschke, being the start and base of this thesis. In September 2004 he was asked to become head of the cardiology department, Ziekenhuis Walcheren in Vlissingen to help in stabilizing and expanding the cardiology department, this period ended December 2007 because of retirement. After his retirement he has worked for some time as locum tenens in the Haven Ziekenhuis in Rotterdam and in the Vlietland Ziekenhuis in Schiedam. At this moment once again as locum tenens in the Sint Franciscus Gasthuis Rotterdam, department of cardiology.

Bibliography

1. Storm C.J., Hagemeijer F., Hugenholtz P.G. Haemodynische bewaking met Swan-Ganz balloncatheters; nut en complicaties, Ned Tijdschr Geneeskd. 1977 Jul9;121(28):1130-5

2. Hagemeijer F., Storm C.J. Fan-shaped shadows due to pulmonary artery catheters: heparin prophylaxis. Br Med J. 1977 Oct29;2(6095):1124

3. Storm C.J., Tjepkema P.L. Amoebenabces van de lever, na perforatie leidend tot harttamponade. Ned Tijdschr Geneeskd. 1983 Jan 1;127(1):15-7

4. Remme W.J., van Hoogenhuyze D.C., Krauss X.H., Hofman A., Kruyssen D.A., Storm C.J. Acute hemodynamic and antiischemic effects of intravenous amiodarone. Am J Cardiol. 1985 Mar 1;55(6):639-44

5. Remme W.J., van Hoogenhuyze D.C., Kruyssen D.A. Krauss X.H., Storm C.J. Amiodarone. Haemodynamic profile during intravenous administration and effect on pacing-induced ischaemia in man. Drugs. 1985 Mar;29 suppl 3;11-22

6. Storm C.J., van de Poel J.A., van de Kemp P.A. Het gedrag van de pacemaker tijdens therapeutische bestraling. Ned Tijdschr Geneeskd. 1985 Jul 20;129(29):1388

7. Beaufort-Krol G.C., van Leeuwen G.H., Storm C.J., Ricardus J.H., Dumas A.M., Schaap G.J. Coxiella burnettii as mogelijke oorzaak van endocarditis bij een 7-jarige jongen. Tijdschr Kindergeneeskd. 1985 Aug; 53(4): 153-7

8. Remme W.J., Krauss X.H., van Hoogenhuyze D.C., Cox P.H., Storm C.J., Kruyssen D.A. Continuous determination of regional myocardial blood flow with intracoronary krypton-81m in coronary artery disease. Am J Cardiol. 1985 Sep 1;56(7):445-51

9. Remme W.J., van den Berg R., Mantel M., Cox P.H., van Hoogenhuyze D.C., Krauss X.H., Storm C.J., Kruyssen D.A. Temporal relation

of changes in regional coronary flow and myocardial lactate and nucleoside metabolism during pacing-induced ischemia. Am J Cardiol. 1986 Dec 1;58(13):1188-94

10. Remme W.J., van Hoogenhuyze D.C., Krauss X.H., Hofman A., Storm C.J., Kruyssen D.A. Dose related coronary and systemic haemodynamic effects of intravenous bepridil in patients with coronary artery disease. Eur Heart J. 1987 Feb;8(2):130-140

11. Beaufort-Krol G.C., Storm C.J. Chronic Q fever endocarditis. J Pediatr. 1987 Feb;110(2):330-1

12. Remme W.J., van Hoogenhuyze D.C., Hofman A., Storm C.J., Krauss X.H., Kruyssen H.A. Acute antiischaemic properties of high dosages of intravenous diltiazem in humans in relation to its coronary and systemic haemodynamic effects. Eur Heart J. 1987 Sep;8(9):965-74

13. Storm C.J., Buis J., Marinus J., van Benthem A.C., Dijk v A., Bruschke A., X-ray videodensitometry vs. intracoronary Doppler flow. Two methods evaluating myocardial perfusion by calculating coronary reserve. Oral presentation Xth CONGRESS OF THE EUROPEAN SOCIETY OF CARDIOLOGY , 1988, Vienna -Austria

14. Remme W.J., Kruyssen D.A., van Hoogenhuyze D.C., Hofman A., Krauss X.H., Storm C.J. Acute hemodynamic and antiischemic properties of intravenous bepridil in coronary artery disease. Am J Cardiol. 1989 Mar 15;(11):670-5

15. Remme W.J., Look M.P., Bootsma M., Kruyssen H.A., Verroste J.M., Krauss X.H., van Hoogenhuyze D.C., Storm C.J. Neurohormonal activation during acute myocardial ischaemia. Effects of ACE inhibitors. Eur Heart J. 1990Apr, 11Suppl B:162-71. Review

16. Storm C.J., van Mechelen R. A severed pacemaker lead in a hepatic vein. Pacing Clin Electrophysiol. 1993 Jun;16(6):1349-53

17. Venneker E.H., Remme W.J., van Hoogenhuyze D.C., Krauss X.H., Bartels G.L., Kruyssen D.A., Storm C.J., van Schelven D. Acute systemic and antiischemic effects of epanol in patients with coronary artery disease. Cardiovasc. Drugs Ther. 1994 Apr;8(2):211-9

18. Remme W.J., Kruyssen D.A., van Hoogenhuyze D.C., Krauss X.H., Bartels G.L., Storm C.J., de Leeuw P.W. Hemodynamic, neurohormonal, and myocardial energetic effects of pimobendan, a novel calcium-sensitizing compound, in patients with mild to moderate heart failure. J Cardiovasc Pharmacol. 1994 Nov;24(5):730-9

19. Van den Broek J.G., Slump C.H., Storm C.J., van Benthem A.C., Buis B. Three-dimensional densitometric reconstruction and visualisation of stenosed coronary segments. Comput Med Imaging Graph. 1995 Mar-Apr;19(2):207-17

20. Remme W.J., van der Ent M., Bartels G.L., van Schelven D., van Hoogenhuyze D.C., Krauss X.H., Kruyssen H.A., Storm C.J. Acute hemodynamic effects and preload-dependent cardiovascular profile of the partial phosphodiesterase inhibitor nanterinone in patients with mild to moderate heart failure. Cardiovasc Drugs Ther. 1996 May;10(2):137-44

21. Csizmadia N.P., Slump C.H., Lubbers A.P., Schrijver M., Storm C.J. Digital densitometric determination of relative coronary flow distributions. Med Biol Eng Comput. 2001 May;32(3):303-9

22. Van Domburg R.T., Sonnenschein K., Nieuwlaat R., Kamp O., Storm C.J., Bax J.J., Simoons M.L. Sustained benefit 20 years after reperfusion therapy in acute myocardial infarction. J Am Cardiol. 2005 Jul5;46(1):15-20

23. Buschman H.P.J., Storm C.J., Duncker D.J., Verdouw P.D., van der Kemp P., van der Aa, H.E. Control of Heart Rate with Vagus Nerve Stimulation. Neuromodulation, Volume 9, Number 3, July 2006, pp 214-220

24. Walpot J., Storm C.J., Bosmans J., Paelinck B.P., Pasteunin W.H., Wielenga J., Klazen C., Hokken R., Sorgedrager J., Teeuwen J. Right atrial inflow obstruction of the inferior vena cava due to atrial aneurysm and ean elongated Eustachian valve. Eur J Echocardiogr. 2008 Nov;9(6):861-4.Epub 2008 Jul 4

25. Storm C.J., van Ombergen A.M. Patiënt met unilateral zwelling in de hals. NTvG 2010 154:A632

List of thesis contributions

- Remme W.J. Metabolic and neurohumoral aspects of acute ischaemia in man. Thesis Erasmus Universiteit Rotterdam 1990
- Bouten C.V.C. Assesment of daily physical activity by registration of body movement. Thesis Technische Universiteit Einhoven 1995
- Van Oosterhout M.F.M. Local myocardial adaptations during chronic ventricular pacing Thesis Universiteit Maastricht 1999
- Schrijver M. Angiographic Image Analysis to assess the severity of coronary stenoses. Thesis Technische Universiteit Twente 2002
- Plasqui G. Daily physical activity, energy expenditure and physical fitness. Assessment and implications. Thesis Universiteit Maastricht 2004

Samenvatting

De medische term angina pectoris als syndroom van beklemming en of pijn in of op de borst ingevoerd door Heberden enkele eeuwen geleden, had toen een onbekend pathologisch (vasculair) substraat. De ontdekking van Röntgen stralen in 1895 door W.C. Röntgen, door hemzelf X stralen genoemd, was het begin van een snelle ontwikkeling in de vasculaire diagnostiek, alsmede de diagnostiek van hartziekten. Deze ontwikkeling werd nog verstrekt door de ontdekking van elektrische activiteit van het hart vastgelegd door een electrocardiograaf (snaar galvanometer) als electrocardiogram (ECG) door Einthoven in 1903. Deze twee nieuwe diagnostische mogelijkheden prikkelden talloze onderzoekers tot verder onderzoek naar de causale oorzaak van het klinisch beeld: angina pectoris. In historisch perspectief gezien werd al heel snel na de ontdekking van de Röntgen stralen begonnen met vaatonderzoek door middel van het opspuiten van het (arteriële) vaatsysteem in een preparaat, in dit geval de menselijke hand, als eerste gepubliceerde casus. Het gebruikte contrast middel om de Röntgen stralen te absorberen was aanvankelijk bijzonder toxisch wat gebruik in de levende mens toen absoluut onmogelijk maakte. Echter toen bleek dat het mogelijk was om een (vaat)systeem af te beelden werden tal van chemische verbindingen met daarin een element met een hoog atoomnummer, noodzakelijk voor de absorptie van de Röntgenstralen, ontwikkeld en klinisch toegepast met sterk wisselend resultaat zowel wat beeldvorming als verdraagzaamheid betrof. Uiteindelijk heeft deze ontwikkeling geleid tot het nu meestal gebruikte contrast middel voor vasculair onderzoek: een anionische jodium verbinding rond een benzeenkern. Deze groep contrastmiddelen is weinig toxisch en is goed injecteerbaar. De mogelijkheid het hart te sonderen tijdens het leven werd voor het eerst aangetoond in 1929 door Forssmann, die onder Röntgen begeleiding een urine katheter opvoerde via zijn eigen arm vene tot in zijn hart. Door dit bewijs, het probleemloos kunnen opvoeren van katheters in de levende mens, ontstond een nieuw vak: cardiovasculaire diagnostiek. Een belangrijk facet bij het ontstaan en verdere uitbouw van deze cardiovasculaire diagnostiek was de ontwikkeling van betere Röntgen apparatuur en beeldvormingsystemen. Aanvankelijk gebruik makend van een simpel direct

oplichtend fosfor scherm met een minimale licht opbrengst, worden tegenwoordig de beelden door middel van complexe beeldvormingketens zichtbaar gemaakt. Dit analoge beeld materiaal werd aanvankelijk opgeslagen meestal als 35 mm film ter archivering, nu na introductie van beelddigitalisatie op een harde schijf. Door de komst van videosystemen kon het nog steeds analoge beeld, naast de film, direct na de procedure bekeken worden en konden eventuele onvolkomenheden direct hersteld worden door middel van aanpassingen in de registratie. Dit betekende dat een volledige herhaling van de procedure, wat tot extra stralenbelasting leidde voor patiënt maar ook voor de radiologische werker, niet meer nodig was. In zeventiger jaren van de vorige eeuw ontstond de mogelijkheid, door innovatieve ontwikkelingen in hardware (computers) en software, om analoge beelden te digitaliseren. Aanvankelijk gebeurde dit door de film achteraf te digitaliseren waardoor de mogelijkheid ontstond de verkregen beelden te bewerken om meer informatie uit deze opgeslagen beelden te verkrijgen. Ontwikkeling van tal van software programma's resulteerde in de mogelijkheid diverse berekeningen uit te voeren zoals o.a. procentuele vernauwingen in vaten en de lengte van een vernauwing. Deze software staat bekend onder de verzamelnaam QCA (Quantitatieve Coronair Angiografie). Verder technische ontwikkeling in hardware heeft geleid tot de mogelijkheid de beelden direct te digitaliseren zodat het mogelijk werd de verkregen beelden vrijwel direct te bewerken door middel van geoptimaliseerde software zodat de (interventie)cardioloog nu direct informatie heeft over voornamelijk afmetingen in het coronair systeem. De op deze manier verkregen gegevens zijn voor therapeutische interventies doorgaans voldoende. Naast deze meest gebruikte mogelijkheden is het ook mogelijk gebleken meer fysiologische informatie te verkrijgen gebruikmakend van digitale bewerkingen uit normaal verkregen filmbeelden. Deze fysiologische gegevens hebben betrekking op myocardiale weefsel doorbloeding onder basale en hyperaemische omstandigheden belangrijk voor de bepaling van vitaliteit van het myocard in het verzorgings gebied van de gefilmde coronair arterie. Deze aanvullende, nuttige, informatie is uit een "normaal" angiogram, waarin alleen een stenose wordt gezien, niet af te leiden. In dit proefschrift wordt de ontwikkeling van de vasculaire coronair diagnostiek vanaf het begin tot op heden beschreven, alsmede de ontwikkeling in contrast vloeistoffen. Voortbouwend op de principes en mogelijkheden om extra (fysiologische) gegevens te verkrijgen uit een normaal coronair angiogram wordt verder in dit proefschrift aanvullend in vitro en in vivo onderzoek beschreven evenals eigen ontwikkeling van software waardoor het mogelijk werd deze aanvullende gegevens (semi)-automatisch te verkrijgen. Tevens wordt de verdere ontwikkeling en innovatie in techniek op hardware- en software gebied beschreven welke geleid heeft tot het concept computer tomografie (CT), gebruikmakend van

Röntgenstralen en subtractie technieken. Deze nieuwe techniek maakt het mogelijk op een semi noninvasieve wijze, met intraveneuze injectie van een contrastmiddel, afbeeldingen van het coronair systeem te verkrijgen evenals myocardiale weefsel karakteristieken. Deze techniek, die op zich wel voordelen heeft ten opzichte van de directe coronair angiografie, zoals kosten besparend en sneller, heeft echter een zeer belangrijk nadeel. Dit belangrijke nadeel is de veel hogere stralenbelasting voor de patiënt, wat deze techniek voor alsnog alleen geschikt maakt voor screening en diagnostiek. Parallel aan de ontwikkeling op CT gebied loopt de ontwikkeling en optimalisering van MRI (Magnetic Resonance Imaging) apparatuur, dit systeem blijkt op een aantal vlakken zelfs beter bruikbaar met betrekking tot coronair afwijkingen en weefsel perfusie dan de CT scanners en heeft het belangrijke voordeel geen Röntgen stralen te gebruiken. Overziend in de tijd zal de toekomst met betrekking tot coronair diagnostiek met name screening zeer waarschijnlijk gaan naar semi non invasief onderzoek CT of MRI. Soms zelfs een combinatie van beide technieken, dit in verband met aanvullend karakter van deze beide technieken. Dit betekent dat de technieken om uit een normaal coronair angiogram fysiologische gegevens te extraheren minder belangrijk zullen worden maar de ontwikkeling van deze angiografische technieken heeft wel duidelijk bijgedragen tot meer begrip van tal van fysiologische processen. Deze nieuwe technieken worden nu ook toegepast in de beeldverwerking bij zowel CT scanners als ook in MRI apparatuur. Echter op therapeutisch vlak, interventies, blijft voorlopig het "ouderwetse" cath lab bestaan met de huidige, maar met misschien nieuwere software ter optimalisering van de beeldvorming wat vooral de Röntgen tijd kan bekorten waardoor de procedure tijd, nodig voor een interventie, korter wordt. Een zeer belangrijk facet, want hoe korter de Röntgen tijd, reductie van stralenbelasting, alsmede procedure tijd, des te minder schadelijk de procedure is voor zowel de vaak jongere radiologische werker alsook voor de patiënt. Een aspect wat zeker in het verleden door gebrekkige kennis over de potentiële risico's van straling weinig aandacht kreeg. Ten onrechte want genetische schade, doorgaans onherstelbaar, of een verhoogde kans op het ontstaan van kanker, dient zo veel mogelijk voorkomen te worden.

Summary

The clinical symptom called angina pectoris as a sign of thoracic discomfort or pain, "invented" by Heberden in the eighteenth century was at that time not ascribed on a pathological (vascular) substrate. The discovery of Röntgen rays by W.C. Röntgen in the year 1895, called by him X-rays, was the starting point of a fast development in diagnostics of vascular (heart) diseases. The growth in these diagnostics, especially in heart disease, was extra intensified after the discovery of the electrocardiogram by Einthoven in 1903. These two new diagnostic possibilities stimulated many researchers to look for the real cause of the clinical symptom: angina pectoris. A short time after the discovery of the X-rays, the first case of a vascular diagnostic investigation, the arterial system of a preparation (a human hand), was published. The contrast agent used at that time was extremely toxic so it was not usable in the living man. However, the demonstration of the possibility to inject contrast agents in a vascular system to make these systems visible resulted in a search for new, less toxic, contrast agents. Before the introduction of the nowadays mostly used contrast agents for intravascular use, anionic iodine molecule bounded to a benzene ring, many chemical molecules were tested all with high atom number elements, because X-ray absorption is atom number dependent. Most of these agents were too toxic or not usable because of the physical properties. The modern contrast agents are hardly toxic and have physical properties as blood and are easy to inject. The possibility to introduce a catheter, without life threatening complications, in the heart of a living man, was demonstrated by Forssmann in 1929 using an urine catheter introduced via a vein of his own arm entering the right side of his heart captured by an X-ray photo, resulted in a new speciality: invasive cardiology. An important aspect in the development of this speciality was the improvement in Röntgen apparatus and imaging systems. This thesis analyzes the history of vascular (coronary) diagnostics from the start till now using X-rays for imaging. Imaging systems started as a simple direct, faint illuminated phosphor screen without storage possibilities are nowadays complex imaging chains and storage systems. Storage initially as 35 mm film but at present after digitizing images are mostly stored at a hard disc. Introduction of video systems

resulted in the possibility to analyse directly, after acquiring, the still analogue images, in doing so it was possible to restore immediately imperfect or incomplete images (films) preventing a repeat of the procedure resulting in less radiation for patient and radiological workers. In seventies of the last century, because of innovative developments in hardware (computers) and software, it became possible to convert analogues images to digital images. Digitations of coronary film, initially done after the clinical procedure, made it possible to get more information from the same film using remodeling of the acquired images than before. This possibility resulted in the development of many software programs to make all kind of calculations such as percentage of stenoses and length of a stenose. These algorithms are known under the name QCA (Quantitative Coronary Angiography). At present because of technical development in hardware and software it is possible to convert the analogues images direct in digital images during acquisition, in doing so all possible and needed calculations of the dimensions of a vessel are directly available to perform the right invention. Next to these calculations of dimensions it appeared possible to obtain from these digital images also more physiological information such as tissue perfusion under basal and hyperaemic situations as a sign of vitality of the myocardium. These techniques, introduced in the seventies of the last century based on subtraction principles, did give important supplementary information about the physiologic importance of a stenose. Based on these principles several new algorithms are developed tested in vitro and in vivo, and are described in this thesis. Development in hardware, computer technology and software resulted in a new type of investigation making use of X - rays and subtraction technique: Computer Tomography (CT). This new technique makes it possible to get on a semi invasive way (intravenous injection of contrast) information of a great part of a coronary vessel but also information about perfusion and tissue characteristics. So at present this new technique, still under development, seems to have an advantage especially with regard to the invasive way of coronary angiography, needing less specialised personnel making the procedure cheaper and faster. However, there is a very important negative aspect in using CT techniques because the much higher radiation burden for the patient to get the comparable information next to the fact that this technique is only suitable for diagnostic screening. Parallel to the development in CT technique another form of diagnostic (cardiac) investigation has been developed: MRI (Magnetic Resonance Imaging). This technique, not using ionising radiation, an important advantage, gives comparable in information as CT on an also semi invasive way, using an intravenous injection of gadolinium as contrast agent. However, at the moment the specificity and sensitivity in detection of abnormalities in the coronaries by CT scans is better in comparison to MRI but MRI is better in detection of tissue characteristics. So in conclusion: in the

future the screening and perhaps diagnostics for coronary heart disease will go to the semi invasive way by CT or MRI, or sometimes combined because of slight differences in information, instead of the "normal" invasive coronary angiography. However, the "old" cath lab will stay in use for therapeutic interventions applying much of the software developed in the last decades to optimize these procedures, less X-ray radiation and a shorter procedure time. A very important facet to reduce the chance on development of cancer and to prevent the often irreparability of genetic damage caused by radiation exposure. Facts, especially, in the past, often neglected because of the insufficient knowledge of the hazards of radiation by the users.

Dankwoord

In een geanimeerd gesprek met nu prof. dr. ir. J.H.C. Reiber, als toeval mijn tafelgenoot, bij een diner in Washington DC tijdens één van de grote Amerikaanse cardiologie congressen in de jaren tachtig van de vorige eeuw, ontstond het idee en de basis van deze thesis. Het gesprek ging over het "normale" analoge coronair angiogram en de omstreeks die tijd beginnende mogelijkheid deze filmbeelden achteraf te digitaliseren om zo bewerkingen en berekeningen te kunnen uitvoeren om mogelijk wat meer klinisch relevante informatie uit deze beelden te kunnen verkrijgen. Tal gesprekken daarna in de "hoogbouw" in Rotterdam hebben mij gestimuleerd om door te gaan met de uitwerking van enkele van deze ideeën over bijvoorbeeld diameter van coronair vaten dat wil zeggen kaliber wisselingen, flowpatronen in normale en vernauwde kransslagaderen en weefsel(myocard) perfusie. Beste Johan hiervoor blijf ik je zeer erkentelijk. Mijn toenmalige maatschap cardiologie in het Zuider Ziekenhuis in Rotterdam had voor elk lid een sabbatical year ingesteld wat mij de mogelijkheid gaf na uitvoerige gesprekken met prof. dr. A.G.V. Bruschke in het Academisch Ziekenhuis in Leiden mijn ideeën, zoals met dr. Reiber besproken, te bespreken waarop prof. Bruschke mij toestond dit op zijn afdeling in praktijk te brengen. Beste Albert hiervoor ben ik je bijzonder erkentelijk. Naast de geboden mogelijkheden op het cath lab met steun en ondersteuning van prof. dr. B. Buis† heb je mij geïntroduceerd in het AMC bij prof.dr.ir. J.A.E. Spaan, om in vitro ervaring met Doppler flow katheters op te doen in een buis systeem, dit ter voorbereiding van deze metingen in vivo tijdens een catheterisatie procedure. Deze Doppler flowmetingen in de coronair vaten werden als vergelijk gebruikt naast de flow berekeningen gebaseerd op Röntgen beelden die in de beginperiode werden verkregen na digitalisatie van analoge filmbeelden op het laboratorium van prof. Reiber, toen benoemd en werkzaam als hoogleraar in Leiden. Mijn dank gaat ook uit naar de medewerkers van prof. Reiber voor hun geduld om mij in te werken en te helpen bij het digitaliseren van de analoge filmbeelden. Naast de techniek van intracoronaire Doppler metingen heeft nog een ander vergelijk protocol gelopen op basis van nucleaire technieken, een protocol in overleg met de afdeling nucleaire geneeskunde prof.dr. E.K.J. Pauwels en zijn staf. Bij deze

in vivo studies zijn de verpleegkundige staf en de medewerkers van het cath lab van bijzonder grote steun geweest maar bovenal de patiënten, die na het vooraf bespreken van het protocol, allen hun medewerking gaven. Van onschatbare waarde in mijn Leidse periode maar ook daarna is Ad van Benthem geweest, gedetacheerd vanuit Philips Medical in Best om het testen van nieuwe Röntgen hard- en software te begeleiden, die zich bijzonder heeft ingespannen de verkregen video beelden op tape te zetten om deze beelden op een later tijdstip te kunnen bewerken aanvankelijk in Best. In Best zijn vele uren besteed aan het uitwerken van deze beelden, het aanpassen van algoritmen etc. hierbij heb ik in het bijzonder steun gehad van mijn promotor, toen nog dr.ir. C.H. Slump en ir. J. Marinus, beiden waren in die tijd werkzaam bij Philips Medical Systems. De toen beschikbare software bleek niet of nauwelijks bruikbaar of zelfs onbetrouwbaar om meer informatie uit de beschikbare beelden te extraheren. In samenspraak met nu prof. Slump, intussen benoemd als hoogleraar TU Twente, werd het plan opgevat nieuwe en/of verbeterde software te gaan ontwikkelen, vaak als afstudeer opdracht, met name voor coronaire flow en perfusie berekeningen. Ten einde de betrouwbaarheid hiervan te testen werd bij de TU Twente, afdeling elektrotechniek van prof. Slump, een fantoom, eerst alleen buizen later zelfs met een imitatie bloeddruk, ontwikkeld waarbij exacte flow gegevens konden worden gemeten. Dit model is met bijzondere toewijding gemaakt door Hennie Kuiper werkzaam daar als technicus. Het evalueren van deze software gebruikmakend van dit fantoom werd in Leiden op het cath lab van de universiteit verricht met hulp van een aantal enthousiaste Twentse afstudeerders in de avonduren na het reguliere catherisatie programma, ook hierbij heeft Ad van Benthem vele avonden opgeofferd voor technisch ondersteuning op Röntgen gebied en archivering van de verkregen beelden. Al deze metingen hebben geleid tot verfijning van bestaande algoritmen als ook nieuwe software en hebben bijgedragen tot een beter begrip van de relatie coronair arterie stenose en de fysiologische betekenis van een dergelijke stenose. Talloze patiënten hebben hun bijdrage geleverd, belangeloos, aan het verder testen en ontwikkelen van deze software tot een redelijk bruikbaar instrument ter beoordeling van de fysiologische betekenis van een vernauwing. Patiënten uit de regio Leiden, Rotterdam en de laatste jaren uit Zeeland hebben aan deze ontwikkeling meegewerkt, zonder hen zou de studie zeker nooit tot een eind zijn gekomen want het klinisch belang voor patiënten heeft altijd centraal gestaan in de ontwikkeling van beter bruikbare informatie opleverende software. Software te gebruiken om een betere, betrouwbare diagnose te kunnen stellen en daardoor een adequaat therapie plan te kunnen voorstellen. Rest mij in het bijzonder prof.dr.ir. C.H. Slump, beste Kees, te bedanken voor het vertrouwen in mij gesteld, om het toch zeker langdurige proces van testen en weer eens testen tot dit

uiteindelijke eind te brengen. Ik had vaak twijfels vanwege en door de trage voortgang, alles moest gebeuren naast ziekenhuis en maatschap gerelateerde besognes, die meestal achteraf niet veel of zelfs niets betekenenden maar wel tijd "vraten", gaf jij mij iedere keer weer opnieuw een duw(tje) om het tot een eind te brengen waarvoor mijn bijzonder oprechte dank. Zonder jouw duwen was het zeker nooit tot een afronding gekomen! Verder wil ik een ieder, studenten TU Twente, cath lab medewerkers, verpleegkundigen, secretaressen, poli-medewerkers, ziekenhuis techneuten enz. enz. maar vooral de patiënten, allen die ooit op enigerlei betrokken waren bij deze in vitro en in vivo (patiënten) onderzoeken, bedanken. Wanneer ik mij ook maar enkele namen zou herinneren en noemen doe alle anderen te kort waarvan ik de naam echt niet meer weet: dus ieder die op enigerlei wijze heeft bijgedragen aan het uiteindelijk resultaat van deze studie, zoals nu eindelijk vastgelegd, in de loop van de tijd heel, heel hartelijk bedankt!

Cock J. Storm
Mijnsheerenland
Oktober 2010